

AGARD-LS-166

AGARD-LS-166

AD-A214 284

AGARD

ADVISORY GROUP FOR AEROSPACE RESEARCH & DEVELOPMENT

7 RUE ANCELLE 92200 NEUILLY SUR SEINE FRANCE

AGARD LECTURE SERIES No.166

Kalman Filter Integration of Modern Guidance and Navigation Systems

DTIC
ELECTE
AUG 01 1989
S D Q D

DISTRIBUTION STATEMENT A

Approved for public release
Distribution Unlimited

NORTH ATLANTIC TREATY ORGANIZATION



DISTRIBUTION AND AVAILABILITY
ON BACK COVER



DEFENSE LOGISTICS AGENCY
DEFENSE TECHNICAL INFORMATION CENTER
CAMERON STATION
ALEXANDRIA, VIRGINIA 22304-6146

IN REPLY
REFER TO

AD-A214 284

DTIC-FDAB (202) 274-6847 (AV) 284-6847

15 Nov 89

AQ 89-1343(a-b)

SUBJECT: Request for Scientific and Technical Report

TO:

1. We have been unable to locate the report referenced below in the Defense Technical Information Center Collection. In accordance with DoDD 3200.12 "DoD Scientific and Technical Information Program" the Defense Technical Information Center is requesting that two copies of the Technical Report cited below be sent to us.

Please return letter
with report.

2. All copies of the report must be suitable for reproduction including a clearly marked distribution statement as described in DoDD 5230.24. (See reverse for categories of distribution statement.) A clearly marked loan copy suitable for reproduction is acceptable.

3. If for any reason you cannot furnish the report, please return the copy of this letter annotating your reason on the reverse side.

4. A franked mailing label for shipping the reports and a DTIC Form 58 to obtain the AD number after processing are enclosed.

FOR THE ADMINISTRATOR:

Sharon Serzan
SHARON SERZAN
Chief, Acquisition Section

2 Encl

1. Franked Label
2. DTIC Form 58

89-1343(a-b)

NATO Advisory Group for Aerospace Research and Development

~~(a) The Organization and Functions of Documentation and Information Centres in Defence and Aerospace Environments~~ AGARD-CP-445 Mar 89

(b) Kalman Filter Integration of Modern Guidance and Navigation Systems AGARD-LS-166 - Jun 89

ds/89-319

00807

DTIC FL-88, Mar 88

PLEASE CHECK THE APPROPRIATE BLOCK BELOW:

☐ _____ copies are being forwarded. Indicate whether Statement A, B, C, D, E, F, or X applies.

☐ DISTRIBUTION STATEMENT A:

APPROVED FOR PUBLIC RELEASE; DISTRIBUTION IS UNLIMITED

☐ DISTRIBUTION STATEMENT B:

DISTRIBUTION AUTHORIZED TO U.S. GOVERNMENT AGENCIES ONLY; (Indicate Reason and Date). OTHER REQUESTS FOR THIS DOCUMENT SHALL BE REFERRED TO (Indicate Controlling DoD Office).

☐ DISTRIBUTION STATEMENT C:

DISTRIBUTION AUTHORIZED TO U.S. GOVERNMENT AGENCIES AND THEIR CONTRACTORS; (Indicate Reason and Date). OTHER REQUESTS FOR THIS DOCUMENT SHALL BE REFERRED TO (Indicate Controlling DoD Office).

☐ DISTRIBUTION STATEMENT D:

DISTRIBUTION AUTHORIZED TO DOD AND U.S. DOD CONTRACTORS ONLY; (Indicate Reason and Date). OTHER REQUESTS SHALL BE REFERRED TO (Indicate Controlling DoD Office).

☐ DISTRIBUTION STATEMENT E:

DISTRIBUTION AUTHORIZED TO DOD COMPONENTS ONLY; (Indicate Reason and Date). OTHER REQUESTS SHALL BE REFERRED TO (Indicate Controlling DoD Office).

☐ DISTRIBUTION STATEMENT F:

FURTHER DISSEMINATION ONLY AS DIRECTED BY (Indicate Controlling DoD Office and Date) or HIGHER DOD AUTHORITY.

☐ DISTRIBUTION STATEMENT X:

DISTRIBUTION AUTHORIZED TO U.S. GOVERNMENT AGENCIES AND PRIVATE INDIVIDUALS OR ENTERPRISES ELIGIBLE TO OBTAIN EXPORT-CONTROLLED TECHNICAL DATA IN ACCORDANCE WITH DOD DIRECTIVE 5238.25, WITHHOLDING OF UNCLASSIFIED TECHNICAL DATA FROM PUBLIC DISCLOSURE, 6 Nov 1984 (Indicate date of determination). CONTROLLING DOD OFFICE IS (Indicate Controlling DoD Office).

☐ This document was previously forwarded to DTIC on _____ (date) and the AD number is _____.

☐ In accordance with the provisions of DoD instructions, the document requested is not supplied because:

☐ It is TOP SECRET.

☐ It is excepted in accordance with DoD instructions pertaining to communications and electronic intelligence.

☐ It is a registered publication.

☐ It is a contract or grant proposal, or an order

☐ It will be published at a later date. (Enter approximate date, if known.)

☐ Other. (Give Reason.)

Print or Type Name

Authorized Signature Date

Telephone Number

NORTH ATLANTIC TREATY ORGANIZATION
ADVISORY GROUP FOR AEROSPACE RESEARCH AND DEVELOPMENT
(ORGANISATION DU TRAITE DE L'ATLANTIQUE NORD)

AGARD Lecture Series No. 166
**KALMAN FILTER INTEGRATION OF MODERN GUIDANCE
AND NAVIGATION SYSTEMS**

Accession For	
NTIS CRA&I	<input checked="checked" type="checkbox"/>
DTIC TAB	<input type="checkbox"/>
Unannounced	<input type="checkbox"/>
Justification	
By	
Distribution /	
Availability Codes	
Dist	Avail and/or Special
A-1	



This material in this publication was assembled to support a Lecture Series under the sponsorship of the Guidance and Control Panel of AGARD and the Consultant and Exchange Programme of AGARD presented on 26—27 June 1989 in Delft, The Netherlands, on 29—30 June 1989 in Neubiberg (near Munich), Germany and on 3—4 July 1989 in London, United Kingdom.

THE MISSION OF AGARD

According to its Charter, the mission of AGARD is to bring together the leading personalities of the NATO nations in the fields of science and technology relating to aerospace for the following purposes:

- Recommending effective ways for the member nations to use their research and development capabilities for the common benefit of the NATO community;
- Providing scientific and technical advice and assistance to the Military Committee in the field of aerospace research and development (with particular regard to its military application);
- Continuously stimulating advances in the aerospace sciences relevant to strengthening the common defence posture;
- Improving the co-operation among member nations in aerospace research and development;
- Exchange of scientific and technical information;
- Providing assistance to member nations for the purpose of increasing their scientific and technical potential;
- Rendering scientific and technical assistance, as requested, to other NATO bodies and to member nations in connection with research and development problems in the aerospace field.

The highest authority within AGARD is the National Delegates Board consisting of officially appointed senior representatives from each member nation. The mission of AGARD is carried out through the Panels which are composed of experts appointed by the National Delegates, the Consultant and Exchange Programme and the Aerospace Applications Studies Programme. The results of AGARD work are reported to the member nations and the NATO Authorities through the AGARD series of publications of which this is one.

Participation in AGARD activities is by invitation only and is normally limited to citizens of the NATO nations.

The content of this publication has been reproduced
directly from material supplied by AGARD or the authors.

Published June 1989

Copyright © AGARD 1989
All Rights Reserved

ISBN 92-835-0514-X



*Printed by Specialised Printing Services Limited
40 Chigwell Lane, Loughton, Essex IG10 3TZ*

THEME

The integration of modern guidance and navigation systems is usually performed with a sub-optimal implementation of the Kalman filter. The most difficult problem is how to develop that sub-optimal implementation when considering system modelling, algorithm design and real hardware non-linearities. This Lecture Series brings together a group of speakers with outstanding practical experience in the design of integrated systems, providing the audience with the principles, insights and mechanisms of real, current-day system synthesis approaches and giving the overall background necessary for synthesizing future practical guidance and navigation systems. Two of the lectures deal with the synthesis of solutions to tracking problems. The remainder of the lectures deal with the integration of avionics systems.

This Lecture Series, sponsored by the Guidance and Control Panel of AGARD, has been implemented by the Consultant and Exchange Programme.

* * *

En règle générale, l'intégration des systèmes modernes de guidage et de navigation est réalisée avec une utilisation sous-optimale du filtre de Kalman. Le problème le plus délicat qui se pose au concepteur est de faire évaluer cette utilisation sous-optimale pour satisfaire aux besoins de la modélisation de systèmes, de la conception de l'algorithme et des non-linéarités du matériel réel. Ce Cycle de Conférences rassemble un groupe de conférenciers ayant une très grande pratique de la conception des systèmes intégrés.

Les auditeurs ont donc l'occasion de se familiariser avec les principes, les mécanismes et les possibilités des méthodes de synthèse de systèmes utilisés aujourd'hui, de prendre connaissance des principes de base de la synthèse de futurs systèmes concrets de guidage et de navigation. Deux des communications présentées traitent de la synthèse des solutions apposées aux problèmes de poursuite. Les autres communications concernent l'intégration des systèmes avioniques.

Ce Cycle de Conférences est présenté dans le cadre du programme des consultants et des échanges, sous l'égide du Panel AGARD du Guidage et du Pilotage.

LIST OF SPEAKERS

Lecture Series Director: Dr George T.Schmidt
The Charles Stark Draper Lab.
MS 2A, 555 Technology Square
Cambridge, MA 02139
USA

AUTHORS/SPEAKERS

Mr David Callender
Navigation Systems Department
Ferranti Defence Systems Ltd.
Silverknowes, Edinburgh EH4 4AD
United Kingdom

Dr Oddvar Hallingstad
Norwegian Defence Research Establishment
Division for Electronics
PO Box 25
N-2007 Kjeller
Norway

Mr Frank Hupke
MBB GmbH
Unternehmensbereich Hubschrauber
und Flugzeuge
PO 80 11 60
8000 München 80
Germany

Dr David F.Liang
Defence Research Establishment Ottawa
Shirley Bay
Ottawa, Ontario K1A 0Z4
Canada

Dr Peter Maybeck
Air Force Institute of Technology
(AFIT/ENG)
Wright-Patterson AFB
Ohio 45433-6583
USA

Mr Pierre Vacher
ONERA-CERT
B.P. 4025
2 Avenue Edouard Belin
31055 Toulouse Cedex
France

CONTENTS

	Page
THEME	iii
LIST OF SPEAKERS	iv
	Reference
INTRODUCTION AND OVERVIEW TO KALMAN FILTER INTEGRATION OF MODERN GUIDANCE AND NAVIGATION SYSTEMS by G.T.Schmidt	1
DESIGN OF A KALMAN FILTER FOR TRANSFER ALIGNMENT by O.Hallingstad	2
DEVELOPMENT OF THE INTEGRATED ALL-WEATHER NAVIGATION SYSTEM FOR TORNADO by F.Hupke and F.Schwegler	3
A HIGH PERFORMANCE AIRBORNE INS/GPS INTEGRATED NAVIGATION SYSTEM by D.I.Callender	4
THE DEVELOPMENT OF MISSION-SPECIFIC ADVANCED INERTIALLY-BASED AVIONICS SYSTEMS by D.F.Liang and D.J.DiFilippo	5
DEVELOPMENT OF A MARINE INTEGRATED NAVIGATION SYSTEM by D.F.Liang and J.C.McMillan	6
ADAPTIVE TRACKING OF MANEUVERING TARGETS BASED ON IR IMAGE DATA by P.S.Maybeck	7
TRAJECTOGRAPHIE PASSIVE PAR AZIMUT; AMELIORATION DE LA QUALITE D'ESTIMATION par P.Vacher, M.Gauvrit, G.Maynard De Lavalette et P.Mennecier	8
BIBLIOGRAPHY	B

INTRODUCTION AND OVERVIEW
TO KALMAN FILTER INTEGRATION OF MODERN GUIDANCE
AND NAVIGATION SYSTEMS, AGARD LS 166

George T. Schmidt
The Charles Stark Draper Laboratory
Cambridge, MA, USA 02139

SUMMARY

The integration of modern guidance and navigation systems is usually performed with a sub-optimal implementation of the Kalman filter. The most difficult problem is how to develop that sub-optimal implementation when considering system modeling, algorithm design, and real hardware non-linearities. This Lecture Series brings together a group of speakers with outstanding practical experience in the design of integrated avionics systems and tracking mechanizations. This will provide the audience with the principles, insights, and mechanisms of real, current-day system synthesis approaches and provide the overall background necessary for synthesizing future practical guidance and navigation systems. This introductory paper will provide a brief overview of the lectures to be presented.

INTRODUCTION

The overall objective of this Lecture Series is to present practical approaches to the integration of complex avionics systems with additional emphasis on tracking problems. To achieve satisfactory system performance, most practical integration approaches have evolved into some form of the Kalman filter, hence the particular title of the Lecture Series.

The development of the Kalman filter theory in the early 1960's was immediately followed by application in the Apollo program and in military systems. [1, 2, 3]. The implementation was in the form of a recursive computer algorithm that was suited for flight computers of that era. Since then, the orders of magnitude improvements in flight computer speed and memory capability have made even larger filter implementations possible. Yet the practical and nonlinear effects for each application must still be resolved to provide satisfactory performance. It is hoped that this Lecture Series, which emphasizes practical approaches, will provide insights into actual theoretical and ad hoc techniques that have led to successful implementations.

This Lecture Series is also a continuation of the AGARD Guidance and Control Panel's involvement in helping to advance the state of the art and technical interchange among members of the Guidance and Control community.

OVERVIEW OF THE LECTURES

Lecture 1:

The first lecture is by Dr. O. Hallingstad of Norway. It is titled "Design of a Kalman Filter for Transfer Alignment." The lecture describes the design philosophy used in the development of the alignment subsystem of the inertial midcourse navigation system for the air-launched Penguin antiship missile adopted for the F-16 fighter aircraft. The desired performance was achieved through a Kalman filter design. The design process and the effort put into simulations during the development are described. Special stress is laid on the deduction of the filter model and its validity testing. Next, a description follows of the interaction between simulations and tests during captive flight testing. Data from captive flight testing are compared with simulation results.

Lecture 2:

Lecture two is titled "Development of the Integrated All-weather Navigation System for Tornado" and is given by Mr. F. Hupke of Germany. The lecture will give a detailed presentation on the following topics: primary development approach, problems encountered and actual solutions implemented, optimization techniques used and modifications required as a result of flight tests of the Tornado navigation system. An abundance of detailed design information will be presented.

Lecture 3:

The third lecture is by Mr. David I. Callender of the U.K. and discusses a high-performance airborne INS-GPS integrated navigation system. The system architecture, and the trade-offs that drive its evolution, are examined for a practical high-accuracy integrated navigation system designed for a number of current requirements including long-duration patrol missions. The system incorporates a 4-gimbal inertial navigator of inherently high stand-alone performance, integrated with a state-of-the-art 5-channel P-code GPS receiver. The system partitioning and interfacing are configured to optimize system accuracy during potentially lengthy periods when a full GPS solution may be unavailable, while providing satisfactory integrity under reversionary conditions. The main Kalman filter takes range and range-rate signals from the GPS and in the primary navigation mode models fourteen INS and two GPS error parameters, while the Kalman filter in the GPS operates independently, to provide a stand-alone navigation solution for integrated system reversionary modes. The system architecture, both in hardware and software allows a high degree of inherent flexibility which may be required to tailor it to various specific applications.

Lecture 4:

The fourth lecture is by Dr. D. Liang of Canada and is titled "The Development of Mission Specific Advanced Inertially Based Avionics Systems." The applications described include an airborne system configured with an inertial system, a synthetic aperture radar, a doppler radar and other sensors that were successfully flight tested. Another application described is a helicopter integrated navigation system. The lecture describes the development of Kalman filters to integrate these avionics configurations including the design objectives, simulation analyses, and some test data.

Lecture 5:

The next lecture is again by Dr. D. Liang of Canada and is titled "Development of a Marine Integrated Navigation System." The lecture will describe this microprocessor based system that can work with a variety of navigation sensors such as Omega, Transit, GPS, etc. It has been successfully tested on both Canadian and U.S. ships. Details of the filter implementation, technical problems, design objectives and some design features unique to this application will be highlighted. Results of sea trial evaluations will be compared to simulation results.

Lecture 6:

Lecture 6 is given by Dr. P. Maybeck of the U.S. and is titled "Adaptive tracking of Maneuvering Targets Based on IR Image Data." Both this lecture and the following lecture are presented at the request of the Guidance and Control Panel to discuss the application of filtering techniques to tracking problems. Dr. Maybeck will address the problem of accurately tracking the azimuth and elevation of a highly maneuverable airborne target using the outputs from a forward-looking infrared sensor. Among the topics he will discuss is how adaptive extended Kalman filters or enhanced correlator/Kalman filter combinations can lead to substantially improved performance over standard correlation trackers. The lecture describes a tracker able to handle "multiple hot-spot" targets.

Lecture 7:

Lecture 7 will be given by Mr. P. Vacher of France. It is titled "Bearings Only Tracking: How to Improve the Estimation Quality." The lecture describes many of the difficulties of target tracking problems such as nonlinearities and maneuvers when using bearings-only tracking whose characteristic feature is poorness of information in terms of observability. Because of these aspects, efficient and robust algorithms must be used. The lecture will describe investigations of recursive and global algorithms as well as leg by leg estimation techniques. Conditioning of the computations, the implementation of the algorithms, and the accuracy of the estimators will all be presented.

CONCLUDING REMARKS

The lecturers participating in this Lecture Series will present the results of many years of practical experience in the design and implementation of integrated systems. The intended result of this Lecture Series is the transfer of knowledge that can lead to newer and better system synthesis approaches and the development of practical guidance and control systems throughout the NATO community.

REFERENCES

1. Leondes, C.T., (editor), Theory and Applications of Kalman Filtering, Agardograph 139, February 1970. (AD704306)
2. Schmidt, G.T., (editor), Practical Aspects of Kalman Filtering Implementation, AGARD Lecture Series No. 82, May 1976. (ADA024377)
3. Schmidt, S.F., "The Kalman Filter: Its Recognition and Development for Aerospace Applications," AIAA Journal of Guidance and Control, Vol. 4, No. 1, pp. 4-7, Jan.-Feb. 1981.

①

COMPONENT PART NOTICE

THIS PAPER IS A COMPONENT PART OF THE FOLLOWING COMPILATION REPORT:

TITLE: Kalman Filter Integration of Modern Guidance and Navigation Systems.

TO ORDER THE COMPLETE COMPILATION REPORT, USE AD-A214 284.

THE COMPONENT PART IS PROVIDED HERE TO ALLOW USERS ACCESS TO INDIVIDUALLY AUTHORED SECTIONS OF PROCEEDING, ANNALS, SYMPOSIA, ETC. HOWEVER, THE COMPONENT SHOULD BE CONSIDERED WITHIN THE CONTEXT OF THE OVERALL COMPILATION REPORT AND NOT AS A STAND-ALONE TECHNICAL REPORT.

THE FOLLOWING COMPONENT PART NUMBERS COMPRISE THE COMPILATION REPORT:

AD#: P005 817 thru AD#: P005 822

AD#: _____ AD#: _____

AD#: _____ AD#: _____

Accession For	
NTIS GRA&I	<input checked="" type="checkbox"/>
DTIC TAB	<input type="checkbox"/>
Unannounced	<input type="checkbox"/>
Justification	
By _____	
Distribution/	
Availability Codes	
Dist	Avail and/or Special
A-1	

DTIC
ELECTE
NOV 16 1989
S E D

This document has been approved
for public release and sale in
distribution is unlimited.

DTIC FORM 463
MAR 85

OPI: DTIC-TID

DESIGN OF A KALMAN FILTER FOR TRANSFER ALIGNMENT

by
Dr. Oddvar Hallingstad
Norwegian Defence Research Establishment (NDRE)
P.box 25, N-2007 Kjeller
NORWAY

SUMMARY

The Norwegian Defence Research Establishment (NDRE) has been involved in the development of several inertially based integrated navigation systems. In all of these systems, the Kalman filter has been the sensor integrator. During the last years one of the main efforts has been on the development of the navigation system for the air launched Penguin Mk3 missile.

Low cost inertial navigation systems (INS) are extensively applied in missile midcourse guidance. The launch platform is generally equipped with a high quality INS, and there is a need for some means to transfer this performance to the missile INS. This is done by transfer alignment (TA) before launch. This alignment may in general be achieved by angle, position, velocity or acceleration matching (alone or in combination).

This paper describes the design philosophy used in the development of the alignment subsystem of the inertial midcourse navigation system for the air launched Penguin antiship missile adopted for the F-16 fighter aircraft. The desired performance was achieved through a three level Kalman filter (KF) design process. On the first level we assume that our system is linear and then we design the KF. On the second level we deal with the design of the preprocessor which make the linear assumptions on level one valid. The last level deals with the field testing of the missile navigation system which is the final test of the validity of the design procedure.

LIST OF SYMBOLS AND ABBREVIATIONS

The notation used in this article is based on reference [10].

g	Free fall acceleration	T	KF update time interval
IMU	Inertial measurement unit	(·)	Vector or matrix belonging to the system truth model.
INS	Inertial navigation system	(·) ^d	Vector or matrix belonging to the filter design model.
MINS	Master INS (aircraft)	(·) ^m	Vector belonging to the MINS.
SINS	Slave INS (missile)	(·) ^s	Vector belonging to the SINS.
KF	Kalman filter	(·) _t	Time t
TA	Transfer alignment		
x, y, z	The three body axes		
X, Y, Z	The three navigation frame axes		

1 INTRODUCTION

The F-16/Penguin is an anti sea invasion weapon system with a high performance missile designed to take optimum advantage of the confined Norwegian coastal waters. To protect the aircraft and missile and avoid missile impact on land the missile has a high navigation accuracy independent of both aircraft and missile trajectories. The heart of this system is the missile INS, a relatively low cost semi strapdown INS (the roll axis is gimballed) based on two two-axes gyroscopes and three accelerometers with a turn-on to turn-on accuracy of the order of deg/h and mg (milli g), respectively.

The missile has to be able to fly a variety of attack profiles in order both to avoid and to make use of the mountainous Norwegian coastal terrain. One of several attack sequences is illustrated in figure 1. The missile will in typical operational scenarios experience heavy manoeuvres, both high g turns and linear accelerations in 3 dimensions, both immediately before launch and in free flight. This puts heavy demands on the inertial midcourse navigation system and the prelaunch initialisation procedure. In this paper, the main topic will be the design of this prelaunch initialisation procedure.

The original transfer alignment (TA) problem was to estimate the mechanical misalignment between the case axes of two IMUs. Since our IMUs have been turned into full fledged inertial navigation systems (INSs), it turns out that the TA problem may be formulated as an ordinary navigation system update problem. Because the MINS is order of magnitudes more accurate than the SINS, the output from the MINS may be considered error free. Thus the original TA problem has been transformed into the navigation problem: Estimate the velocities and the misalignments in the SINS using the velocity

AD-P005 817

outputs from the MINS as measurements of the true velocities. The Kalman filter (KF) is used to solve this problem. The reason why we use velocities instead of positions as measurements to the KF will be discussed in subsection 3.1.2.

In section 2 we will describe the transfer alignment problem in more detail and discuss the design objectives and the design procedure for a Kalman filter meeting the specifications. The design procedure consists of three levels. On the first level we assume that our system is linear and then we design the KF (section 3). On the second level we will in section 4 discuss the design of the preprocessor which make the linear assumptions on level one valid. The last level discussed in section 5, deals with field testing of the missile navigation system. This is the final test of the validity of the design procedure.

2 TRANSFER ALIGNMENT

2.1 System Description

The alignment is done by matching the outputs from the F-16 INS and the missile INS by means of a KF. The design objectives and procedure for the KF are given in the next sections. The KF transfer alignment algorithm is implemented in the software for a Motorola 68000 based microcomputer in the Penguin/F-16 adapter. The adapter fits between the standard F-16 pylon and the missile.

Figure 2 shows a physical block diagram of the main components in the TA system. The INS in the F-16 aircraft is a gimbaled 3 axes platform while the INS in the missile is a semistrapdown platform (the roll axis is gimbaled). The accuracy of MINS is several magnitudes better than the SINS implying that the MINS may be considered error free for TA purposes.

The accelerations and angular velocities sensed by the two platforms differ due to the spatial separation and the nonrigid body connecting them. This nonrigid body is susceptible to both mechanical deformations and vibrations.

The available navigation data on the F-16 1553B and the missile buses are updated with 50 Hz. This is obviously too much for a KF. So there must be some form of averaging of the measurements. The time lags for the data from the two sources are also different.

2.2 Design Objectives and Constraints

The most important design criteria was that the missile INS alignment should not impose heavy restrictions on the normal operation of the aircraft. That is, there should be no added restrictions on g loads imposed by the alignment subsystem, and of particular importance, the alignment should not impose restrictions on aircraft manoeuvres during the launch sequence. In addition, the alignment subsystem should not require any changes on the aircraft. Some of the design objectives and constraints for the KF are :

- The navigation accuracy (position and attitude) should meet the specifications at the target.
- The alignment time must be shorter than the requirements.
- The filter should only utilize the readily available velocity and attitude data on the F-16 1553B data bus.
- The computation load and memory requirements have to fit into the available Motorola 68000 based micro computer in the missile adapter.
- The filter has to be robust. I.e. unexpected large or unknown error sources should not cause major performance degradation.
- The filter may be turned on at any time and then stay on even during long missions.

2.3 Design Procedure

Designing a KF for TA meeting the design objectives given in the previous section may be done using the following three level iterative procedure :

Level 1 : Kalman filter design

On this level we assume that the system equations have been linearised so that the KF may be applied. This assumption depends on the success of the preprocessor design on level 2. The design is assisted by a covariance analyses simulation program.

1. Put the problem into a KF framework.
2. Decide whether an optimal KF may do the job (disregarding computation load and memory requirements) or not.
3. Eliminate states from the optimal KF arriving at a suboptimal filter.
4. Tune the suboptimal filter.

5. Perform a sensitivity analysis to determine the robustness of the suboptimal filter. Repeat from 2 if necessary.

Level 2 : Preprocessor design

The purpose of the preprocessor is to interface the KF designed on level 1 to the physical system. The design is made using a Monte Carlo simulation program where the main nonlinear aspects of the physical system are implemented.

1. Decide how to perform level arm compensation and calculation of the KF measurements.
2. Determine the discretisation algorithm of the timevariant matrices used by the KF and based on output from the SINS.
3. Determine the KF update frequency.
4. Design a supervisor which detect abnormal situations, i.e. hardware failures, out-layers and abnormal signal statistics.
5. Perform a Monte Carlo simulation incorporating the KF from level 1.
6. Repeat from 1 if necessary. If the KF is inadequate repeat level 1.

Level 3 : Field testing

Both level 1 and level 2 designs were based on simulation programs. On level 3 the algorithms found on the previous two levels are implemented in the alignment unit and tested in the physical system. The test results are analysed using a post flight simulation program.

1. Implement the algorithms in the alignment unit hardware.
2. Perform captive flight tests.
3. Perform missile test firing
5. Analyse the test results using the post flight simulation program or if necessary the Monte Carlo simulation program and the covariance simulation program.
6. Repeat the level 1 and 2 design if necessary.

3 KALMAN FILTER DESIGN

We will in this section show how to deduce the KF part of the alignment algorithm. The KF design is based on several assumptions which will be tested in section 4 and 5. The design objectives and constraints given in subsection 2.2 may for the KF design in this section be taken care of as follows :

- If all the assumptions for a KF are valid it will be optimal, implying that the navigation accuracy at the target and the alignment time cannot be made better by any other estimation method. Therefore, test of the optimal KF will tell whether these requirements are achievable or not.
- The optimal KF design will pose unacceptable computation load and memory requirements. We have to design a suboptimal KF. The deduction and test of this suboptimal KF that preserve the optimality is therefore the main concern in this section. The computation load will be reduced by eliminating states, simplifying the matrix structure and by updating the KF with a much lower frequency than the measurement frequency (section 4).

3.1 System Truth Model

We will in this subsection present the system truth model and its properties. The system truth model is the best, most complete mathematical model that can be developed. For our KF design purpose it is linear and serves both as a starting point for the suboptimal filter design and as a reference for achievable alignment accuracy.

3.1.1 Nonlinear Model

A block diagram of the main components in the physical TA system is shown in figure 2. A mathematical model of the process part would consist of the following models (as our Monte Carlo simulation program does) :

1. A trajectory generator which calculates the linear and angular acceleration inputs to the MINS and SINS ($\vec{a}^n, \vec{\omega}^n, \vec{a}^s, \vec{\omega}^s$). The generator may be designed in many different ways. In our Monte Carlo simulation program we first specify a trajectory (curve) consisting of line and circle segments in the computation frame. Then we specify the tangential acceleration involved. The model of the aircraft is fairly simple because we specify that the normal component of the acceleration is always normal to a plane through the wings of the aircraft. The actual linear (\vec{a}^m) and angular

$(\vec{\omega})$ accelerations for the MINS may then be calculated. The input $(\vec{a}', \vec{\omega}')$ to the SINS is calculated by adding the level arm effect $(\vec{\omega} \times \vec{r})$ and the output from a vibration model to \vec{a}' and $\vec{\omega}'$.

2. A model of the gyros and accelerometers in the aircraft gimballed inertial platform and the navigation equations implemented in the MINS. In most of our Monte Carlo simulations we were only interested in relative navigation errors. Thus, we used the positions and attitudes given in the trajectory generator directly.
3. A model of the gyros and the accelerometers in the missile semistrapdown inertial platform and the navigation equations implemented in the SINS. The SINS's navigation equations used the quaternion algorithm.

The common way to apply the KF to a nonlinear system is by using an extended Kalman filter (EKF) where one has to implement nonlinear models of the dynamics and the sensor equations in the computer. The transfer alignment problem may also be solved using an EKF. But the nonlinear dynamic equations mentioned above would be too much for a real time application. Instead, one makes a linear error model of the difference between the outputs from the MINS and SINS. This will be done in subsection 3.2. As a matter of fact also this error modelling procedure may be interpreted as making an EKF. In this case the SINS is interpreted as the dynamic nonlinear model of the true aircraft dynamic. That is, the nonlinear aircraft dynamic equations are solved on a combined analog-digital computer (the SINS) and the SINS is reset by the KF error estimates. It is this feedback which makes the filter an EKF and not a linearised KF in this interpretation.

3.1.2 Linearisation

The KF is an algorithm which is optimal only for linear gaussian systems, but most of the real world problems are nonlinear (including our TA problem). A main question is therefore how to linearise the process in figure 2 in order to make the KF algorithm applicable. We make the following assumptions:

1. The MINS is considered error free because its accuracy is several orders of magnitude better than the SINS. The navigation data from the MINS are consequently taken as true positions, velocities and angles. For filter design purposes only the relative estimation errors are of interest. The absolute navigation error may be obtained by calculating the RMS of the relative navigation error and the absolute navigation error in the F-16 INS.
2. The preprocessor (discussed in the next section) compensates exactly for the spatial separation of the two platforms by compensating for the level arm effect $(\vec{\omega} \times \vec{r})$ and averaging out any vibration differences. Thus, we assume that the two platforms are sensing the same linear and angular accelerations.
3. We assume that an initial coarse alignment has been done, making the axes misalignment so small that a linear error model is valid.
4. In order to keep the misalignments small the SINS will be reset by the KF error estimates. That is, the SINS will be in closed loop during alignment.

These assumptions render the linear TA truth model given in figure 3. The validity of the assumptions will be tested by Monte Carlo simulations and field tests. Thus, the difference between the MINS and SINS measurements may be modelled by a linear time variant stochastic model of the form (the linear truth model):

$$\dot{\underline{x}}'(t) = F'(t)\underline{x}'(t) + G'(t)\underline{w}'(t)$$

with a discrete measurement model:

$$\underline{z}'_k = H'_k \underline{x}'_k + \underline{v}'_k$$

Table 3-1 shows an example of a system truth model and state variables. The three position states are not included. But they are needed for evaluation purposes as the alignment has to be evaluated according to the position and level errors at the target. Consequently, the position states are included in the simulation programs but not in the implemented KF.

No. of States	Description	Abbreviation	Initial values (1- σ)
3	Relative velocity error (X,Y,Z)	V	0.4 m/s
3	Relative attitude error (X,Y,Z)	E	16 mrad
3	Gyro coloured noise (x,y,z)	GYCN	2 deg/h (30 s)
3	Gyro bias (x,y,z)	GYB	6 deg/h
3	Gyro scale factor (x,y,z)	GYSF	0.20 %
4	Gyro mass unbalance (x,z)	GYMU	6 deg/h/g
3	Accelerometer bias (x,y,z)	ACB	2 mg
3	Accelerometer scale factor (x,y,z)	ACSF	0.26 %
6	Accelerometer nonorthogonality (x,y,z)	ACNO	0.4 mrad
1	Relative azimuth measurement bias	AMB	16 mrad

Table 3-1 System truth model, state variables

The initial error truth model of inertial platforms are easily set up by using the accelerometer and gyro models from the producer in addition to information of the actual mechanisation. But this initial truth model contains up to 100 state variables. We arrived at the state vector in Table 3-1 by sensitivity simulations. The initial model was excited by different trajectories and only the states showing the greatest response was kept in the system truth model in table 3-1.

The readily available measurements to the alignment filter are velocity and azimuth differences between the MINS and the SINS. The purpose of the azimuth measurement is to prevent azimuth unstability during nonmanoeuvring periods. Due to deficiencies in the down channel (Z-axis) of the F-16 inertial navigation system the Z-axis velocity difference is not used for the time being. The system truth measurement model is given in table 3-2.

No. of meas.	Type of measurement noise	Abbreviation	1- σ values
3	White velocity meas. noise (X,Y,Z)	VMN	0.4 m/s
1	White azimuth meas. noise	AMN	8 mrad

Table 3-2 System truth measurement model

Table 3-2 shows that we intend to use velocity and not position as measurement. In an INS the position is only an integration of the velocity. Position may therefore not contain more information about the errors in the SINS than the velocity does, see reference [11]. Because the computation load for a KF is proportional to n^3 where n is the no of states in the KF, we decided not to use position as measurement to the KF. Further, due to our inaccurate SINS (compared to the MINS) we assume the MINS to be error free. The position outputs from the MINS are therefore used to update the position of the SINS directly.

Using positions as measurements to the KF would have the following advantage : The errors due to unmodelled kinematical motion of the SINS relative to the MINS would be more averaged than using velocities, allowing a longer KF update interval. But the simulations show that altogether we are better off using only velocities.

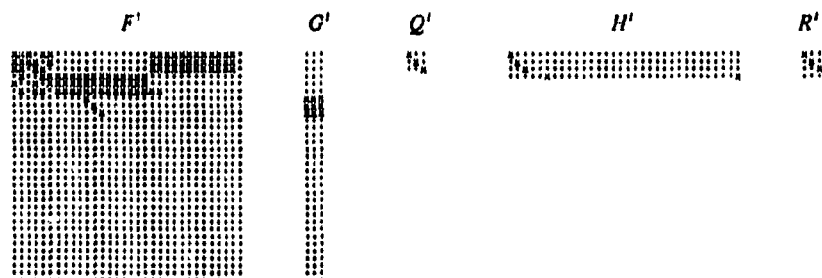


Table 3-3 Truth Model Matrix Structure

Table 3-3 shows the truth model matrix structure. A nonzero element is marked by 'x' and a zero element by '.'. The matrices are sparse due to all the bias states. The nonzero system matrix (F') elements are of three main categories :

1. Elements depending on the specific force measurements (output from the accelerometers). These elements are large and manoeuvre dependant (depending on linear accelerations).
2. Elements coupling the component errors into velocity and level error states. These elements are elements in coordinate transformation matrices from the platform gyro and accelerometer frames to the navigation frame. These elements are attitude dependant.
3. The rest of the nonzero elements (like the Coriolis coupling)

Our simulation programs utilises the structure by dividing the matrices into submatrices and eliminating multiplication with a zero submatrix.

3.1.3 Optimal KF

The alignment time and navigation accuracy at the target depends on the prelaunch aircraft manoeuvres. Fortunately, the simulations of a KF based on the system truth model show that all these requirements are fulfilled if the aircraft make only a minor prelaunch turn. This indicates that normal aircraft manoeuvres will be sufficient. The optimal prelaunch manoeuvre would be the free flight trajectory of the missile. Because then all the error sources of the SINS would have been excited also during alignment and estimated. But also a normal mission shows usually more than sufficient manoeuvres. In addition to aligning the reference axes, the alignment procedure will also to a certain extent calibrate the inertial sensors' bias and scale factors.

In order to calculate the navigation and alignment accuracy the aircraft and missile trajectories have to be defined. To simplify the problem somewhat, this paper will consider two stylistic situations of a minimum alignment and a complete alignment.

Minimum alignment time is the time required for the alignment filter to estimate pitch and roll attitude errors. This does not include warm up, power on test, and initial coarse alignment. Minimum alignment is defined as an alignment where there has been no manoeuvres to make the azimuth error observable. This information is available for the pilot as status information on the F-16 stores control panel.

Complete alignment requires that an aircraft manoeuvre has made the azimuth attitude error and other manoeuvre dependent accelerometer and gyro errors observable. In addition, the alignment time has to be long enough so that the estimates of attitude and gyro biases have stabilized.

Figure 6 shows the trajectory used in the generation of the error budget in figure 4. This trajectory is sufficient for a complete alignment.

Figure 4 shows the error budget for the position and level error states at the target. In the figure we have combined the effect from all three axes for each kind of error. This is not done in the original simulation and we are there able to distinguish between the axes. The dominating error sources for the position errors (given the trajectory in figure 6) are the gyro coloured noises (GYCN) and the velocity measurement noises (VMN). The GYCNs are nonobservable due to a 30 s correlation time. The VMNs are also dominating because we assume them to be large due to nonmodelled vibration noise.

For the level errors the dominating error sources are the GYCN, the gyro scale factor (GYSF) and the gyro mass unbalance (GYMU). The GYMU is not observable for nonmanoeuvring cases. For our trajectory we are not able to separate it from the gyro bias.

An analysis of the error equations with respect to observability gives the following results :

- Azimuth error is observable through the velocity measurements given a manoeuvre in the horizontal plane. The level errors are also observable without manoeuvres due to the free fall acceleration g .
- Because the roll angle is always zero, the y-gyro coloured noise, bias and scale factor are not observable through the azimuth measurement. But they may be estimated through velocity measurements due to the level error to velocity couplings.
- In order to estimate the accelerometer scale factors and nonorthogonality and the gyro mass unbalance the aircraft must have manoeuvres.

3.2 Filter Design Model

The optimal KF tested in the previous section satisfied the accuracy requirements at the target. But a 32 state KF would be too much for the available micro computer. Hence, in this subsection we will try to reduce the computer demand by eliminating states, simplifying the system matrices and discretisation algorithm.

3.2.1 State Elimination

The computation load of a KF may be decreased by :

- Eliminating state variables in the filter model.
- Replacing coloured noise state variables by bias states (time update of bias states is not necessary).
- Simplifying the discrete error model used for time update calculations.

The candidates for elimination are nonobservable states and states which give a small contribution to the total navigation error at the target. Nonobservable states may eventually be replaced by an observable linear combination. The effect of state eliminations and other simplifications should always be checked by a full covariance simulation. Simulations of different trajectories suggested that the following states may be eliminated from the list in table 3-1 :

- 6 accelerometer nonorthogonality states because their influence on the navigation accuracy is small for the majority of manoeuvres.
- 3 gyro coloured noise states because their observability is low (30 s correlation time) and their main effect of keeping the KF gains up may be replaced by white process noise on the velocity and angular levels. Elimination of these coloured noise states is also important because it leads to a significant reduction of KF time update computation time.
- 1 x-gyro scale factor because the SINS is roll stabilized.
- 4 gyro mass unbalances because their effect on the navigation accuracy is neglectable (the effect is manoeuvre dependent).

The number of states in the filter model is now 18 versus 32 in the system truth model (disregarding the three position state variables which will not be implemented in the final filter). The last 12 state variables are modelled as biases which will give an insignificant contribution to the time update computation load. The total computation load is now acceptable.

The problem with the present filter model is that the KF gains for the bias states will approach zero. This may imply filter divergence due to all the unmodelled states. Figure 5 shows the true alignment accuracy for the X-axis in the missile platform as calculated by the covariance simulation program. The divergence problem will be addressed in subsection 3.3.

3.2.2 Matrix Simplification

In section 3.1.2 we discussed the structure of the linear truth model. Many of the couplings shown are of minor importance in an INS like ours because of the large component errors. Therefore, we eliminate all the couplings due to Coriolis-accelerations and error in the calculation of the g-vector. These simplifications will also speed up the on line calculation of the elements in the design model matrices. The structure of the design model is shown in table 3-4. Notice the introduction of white process noise on the velocity and angular levels.

F^d	G^d	Q^d	H^d	R^d

Table 3-4 Design Model Structure

3.2.3 Discretisation

The connection between the matrices in the linear, timevariant, continuous stochastic differential equation

$$\dot{\underline{x}}^d(t) = F^d(t)\underline{x}^d + G^d \underline{w}^d$$

and the discrete difference equation

$$\underline{x}_{k+1}^d = \Phi_k^d \underline{x}_k^d + \Gamma_k^d \underline{w}_k^d$$

is given by :

$$\Phi^d(t, t_k) = F^d(t) \Phi^d(t, t_k) \quad \Phi^d(t_k, t_k) = I$$

$$\Gamma_1^d Q_1^d (\Gamma_1^d)^T = \int_{t_0}^{t_1} \Phi^d(t_1, \tau) G^d Q^d (G^d)^T (\Phi^d(t_1, \tau))^T d\tau$$

We will comment on the calculation of these matrices for long intervals in subsection 4.2. If the interval is short enough, we may calculate the matrices by Taylor series expansion. As table 3-5 shows, the F^d -matrix is nilpotent and the Taylor series for F^d is :

$$\Phi_1^d = I + F^d T + \frac{1}{2} (F^d T)^2$$

An approximate solution of the integral for $\Gamma_1^d Q_1^d (\Gamma_1^d)^T$ is easily found by using the formula for the Φ_1^d -matrix. As table 3-5 shows the structure of these matrices is sparse.

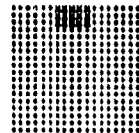
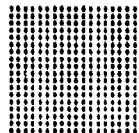
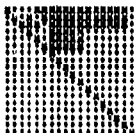
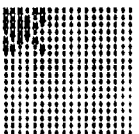
$(F^d)^2$	$(F^d)^3$	Φ_1^d	$\Gamma_1^d Q_1^d (\Gamma_1^d)^T$
			

Table 3-5 Design Model Discretisation

3.3 Filter Tuning

As shown in figure 5, a simple elimination of state variables gives a divergent KF. We have therefore introduced fictitious process noise in order to keep the KF gains at an acceptable level. The computation burden is kept low by introducing white noise only to the velocity and error angle equations in the filter design model. In addition we want to make the filter robust. This is done by making the a priori covariances for the design model larger than the nominal values. The filter performance degradation due to these conservative design filter values is small for nominal values in the truth model.

Figure 5 shows the tuned alignment accuracy for the X-axis of the platform. The true estimation error is now not distinguishable from the optimal estimation error. A similar comparison of KF gains shows that the tuned filter has almost optimal gains. The sensitivity of the tuned filter model to changes in the process model was investigated by the covariance simulation program. The following cases were examined :

- Initial velocity and level errors an order of magnitude greater than nominal.
- Unexpected bias shifts in the y- and z-gyros.
- Many different alignment manoeuvres including the extremes : no manoeuvres at all and very violent manoeuvre.
- Long term stability.

The conclusions from all these simulations were that :

1. The tuned KF satisfies the accuracy requirements with only modest demands on the alignment manoeuvres
2. The suboptimal KF gives almost the same position and attitude accuracies at the target as the optimal KF. Also the important KF gains are almost identical to the optimal case. This is achieved by introducing fictitious process noise on the attitude rate error level.
3. The filter is robust due to relative large a priori covariances
4. The calculation time for the KF time and measurement updates is fast due to an UD-algorithm utilising the matrix structures.

The results of these simulations, and also evaluation through Monte Carlo simulations and experience from captive flight testing, led to the final tuned filter model in table 3-6.

No. of States	Description	Abbreviations
3	Relative velocity error (X,Y,Z)	V
3	Relative attitude error (X,Y,Z)	E
3	Gyro bias (x,y,z)	GYB
2	Gyro scale factor (x,y,z)	GYSF
3	Accelerometer bias (x,y,z)	ACB
3	Accelerometer scale factor (x,y,z)	ABSF
1	Relative azimuth measurement bias	AMB

Table 3-6 Tuned filter model, state variables

3.4 UD-factorisation algorithms

The UD-factorisation algorithm (reference 2) was used both in the simulation programs and the implemented KF. The use of numerical stable algorithms is a necessity in covariance simulation programs due to the high dimension of the augmented state vector. In the real time implementation the conventional covariance equations would probably have been sufficient. But since the computation burden is almost equal to the UD-algorithms the latter were chosen.

The UD-algorithms were simplified in order to utilize the special structure of the equations at hand (this kind of simplifications is much easier to do to covariance equations). Especially the elimination of the gyro coloured noise states were important in keeping the computation load small.

Notice, that the UD-algorithm has to use both Γ_i^d and Q_i^d in the update equations. This is done by Cholesky factorisation algorithm.

4 PREPROCESSOR DESIGN

The KF designed in section 3 satisfied the design requirements. But the KF was designed making several assumptions about the preprocessor function. The simulations in that section did not account for those assumptions. In this section, we will show how the preprocessor is designed and give some results of the Monte Carlo simulations. This simulation program accounts both for the most important nonlinear effects and the difference between the INS output frequencies and the KF update frequency. The preprocessor main structure is given in figure 7.

4.1 Kalman Filter Measurements

The accelerations and angular velocities sensed by the two platforms differ due to the spatial separation and the nonrigid body connecting them. The nonrigid body is susceptible to mechanical deformations and vibrations. Thus, the velocity measurements from the SINS have to be corrected for the level arm effect and the vibrations. Since we cannot update the KF with 50 Hz, we calculate the average effect of the level arm over one KF update time interval and correct the average velocity measurements from the SINS before we form the difference with the averaged velocity measurements from the MINS. This averaging leads to a reduction in the measurement noise and averages the high frequency vibrations. But it could lead to stability problems due to the new correlation between process and measurement noise. Fortunately, simulations show that this added correlation is too small to make any problem for our KF.

4.2 Time Variant Matrices

The most correct way to calculate Φ_i^d and $\Gamma_i^d Q_i^d (\Gamma_i^d)^T$ is by using a sub interval, ΔT given by the INS measurement frequency. The Φ_i^d -matrix is then given by

$$\Phi_i^d = \Phi_i(\Delta T) \Phi_i(\Delta T) \dots \Phi_i(\Delta T)$$

where $\Phi_i(\Delta T)$ is calculated by the formula in subsection 3.2.3 and using the most recent acceleration measurements in the calculations. Because the computation load would be too great, we first calculate the average F -matrix for the KF time update interval and then calculate Φ_i^d according to the formula given in subsection 3.2.3. Simulations verify that this is satisfactory for our system.

4.3 Kalman Filter Update Frequency

In order to check the robustness of the KF for the chosen KF update frequency, T , we run the Monte Carlo simulation program with update intervals from $T/2$ to $4T$. The simulations showed no significant difference in the estimation errors. The chosen update frequency, measurement calculation and matrix calculation methods are therefore judged to be healthy.

4.4 Error Checks

In the application of KFs to real systems it is of vital importance to realize that abnormal situations will arise. Hence, some kind of error detection and status indication has to be built into the system. The tests to be implemented may be foreseen to a certain extent, but due to the hardware dependence, field tests have to be done. The final test limits are determined through a close interplay between simulations and field tests. This interplay will be discussed in the next section, but the actual tests will be presented here.

The KF assumes that the measurement statistics are given. Due to hardware deficiencies, outliers which violates these statistics have to be expected. These outliers are eliminated by using a 3- σ test on the innovation process.

The azimuth angle is observed through velocity changes in the horizontal plan. During periods with small velocity changes (manoeuvres) the azimuth angle is nonobservable through the velocity measurements, but the azimuth angle measurement maintains the accuracy by relying on the aircraft INS and assuming no relative rotation of the two body axes. The azimuth measurement is not used when the manoeuvres exceed a given limit. However, during manoeuvres the missile and aircraft axes may move relatively to each other creating a new permanent offset. This is modelled by reinitialisation of the azimuth measurement bias.

Due to hardware failures the KF may diverge. Such divergence may be detected by monitoring and checking the calculated variances in the KF and the mean and standard deviation of the innovation processes.

The component estimates (gyros and accelerometers) are checked and error flags are set if the estimates exceeds certain limits, thus indicating component failure.

The alignment accuracy depends on the alignment time and manoeuvres. The KF covariances and the mean and standard deviation of the innovation processes are used to calculate a performance index. This index tells the pilot if a manoeuvre may enhance the alignment or not.

4.5 Monte Carlo Simulation

The performance of the navigation system has been evaluated using both covariance and Monte Carlo simulations. Monte Carlo simulations involve multiple runs of a simulation including all known noise and error sources to establish accumulated statistical properties of selected state variables as a function of time. And, as opposed to a covariance analysis, a Monte Carlo simulation has no inherent restrictions to the implementation of the models involved. E.g. there is no need for a linearised model for the generation of the measurements to the suboptimal KF. Computer cost is the major disadvantage of the Monte Carlo validation technique.

We have done a lot of Monte Carlo (MC) simulations in order to verify the KF design from section 3 and the preprocessor design in this section. All of the simulations show close agreement with the covariance simulations. The differences are well within the statistical limits (based on 100 MC runs). In addition to covariance calculations the MC program may also calculate the mean values. Also these simulations give values within the statistical limits.

The alignment is close to optimum. It is very robust, and there is little to be gained by expanding it.

5 FIELD TEST RESULTS

5.1 Captive Flight Tests

The flights have not been planned specifically for evaluating the navigation system, but rather as rehearsals for the actual missile firing. Alignment times have varied. Most of them have represented complete alignment, and only a few have had minimum alignment (see subsection 3.1.3 for definition). 43 tests have been evaluated, none of which have been identical.

The position error has been calculated by integrating the velocity difference between the aircraft and the missile INS, with corrections for relative movements. The navigation error has been well within specifications and in close agreement with predicted performance from simulations. A few of the 43 tests were close to minimum alignments.

5.2 Missile Test Firings

A number of missiles has been launched during the engineering development and technical evaluation phases. It has been difficult to isolate the missile INS error from test range instrumentation errors, F-16 fire control errors, and F-16 INS errors, however, the missile firings indicate a close agreement with computer simulations and captive flight testing.

5.3 Deficiencies and Errors

Initially our most serious problem was telemetry dropouts. Especially it was difficult to receive reliable data during aircraft manoeuvres. The situation was gradually improved during the test period. Among improvements were better aircraft tracking equipment on the ground and merging of data from more than one telemetry receiver antenna. On the software side a lot of effort had to be put into program modifications in order to handle data dropouts and unreliable data. Heavy restrictions on the flight trajectories were imposed by telemetry coverage and general air safety restrictions in the test area. In fact, the captive flight testing was an integrated part of the normal fighter pilot training in southern Norway. Our testing should not interfere with the normal operation of this airfield. A telemetry pod on the F-16 aircraft itself would have spared us a lot of problems. This was not available at that time, however, today this is an integrated part of the test equipment.

Our next serious problem turned out to be the weather. When finally the aircraft, the missile, and the telemetry and data reduction system, all, from a technically point of view, were ready for testing; wind, ice and snow quite a few times turned out to be the final reason for the cancellation of the take off. After all, our aircraft was not on alert, and the pilot had to follow peacetime general air safety precautions. However, we had to adapt to this situation as well. Through simulations we realised that a lot could be done by just taxiing on the runway. Especially, the identification of quite a few time tag errors was done by data from F-16 pirouettes on the runway. The fighter pilots did not actually love the test trajectory when a test engineer again and again ordered a 720 degrees pirouette just to have another look at his KF states.

The captive flight test period gave us, as mentioned, new knowledge about system behaviour. However, due to concurrent effort in testing, simulation, and new algorithm development it turned out to be very easy to identify these deficiencies when they appeared and to make appropriate software changes. Two examples were changes necessary for the compensation of relative motion on the azimuth measurement and changes to the use of this measurement, a result of new knowledge about how the pilot operated the aircraft and how the missile was mounted to the aircraft, respectively. Another example is the fact that manoeuvres early in the fine alignment period with relatively low constant g loads introduce delays in the alignment. Minor changes had to be introduced in the setting of status information on the stores control panel display. And in general, as expected, several test limits and the initial uncertainties of a few filter states had to be slightly adjusted. However, our major problems were due to true errors as listed below.

The time tag and KF prefilter software, or the synchronization of missile and aircraft data, the major part programmed in assembly and fix point arithmetic, turned out to include a lot of errors. All of them had to be identified and removed to achieve a reliable alignment performance. The most difficult time tag error to identify was one which caused altitude information to be put into the least significant bits on the F-16 time tag. This error was identified and removed when we realised that the delay caused by time tag was a function of aircraft altitude.

Incorrect sign on different terms in the missile INS software was another problem. All of these errors were, except for one, identified and corrected before or early in the captive flight test period. The one left over, due to inconsistencies in the documentation, was an incorrect sign in one of the terms for compensation of the movement over the Earth. This error was in some instances equivalent to a gyro bias of more than 10 the nominal value, and the alignment filter decomposed this error as different component errors as a function of aircraft manoeuvres. We finally identified this error by code inspection when telemetry data had told us that the error was a function of velocity and heading in level flight. On reflection, this particular error, and maybe some of the time tag problems, may have been sorted out by simulations before the captive flight testing started. This was, at the time, not possible mainly because the INS navigation software, the alignment software, and the time tag software all were, with a few exceptions, tested independently by different people. A closer integration during testing may have been a wiser approach. However, of particular importance is the fact that the simulation software eventually had to be designed by the same people implementing the necessary real time system software; thus, more effort put into simulation, with the same resources for the total job, may have delayed the captive flight testing. We had to decide on a priority. We had prepared for open loop testing of the

alignment filter, testing without actually updating the INS with error estimates. However, open loop testing turned out to be of little practical use as the INS diverged too fast for the isolation of the relatively small error effects. To sum up, our experience is that it is easy, through inspection of KF behaviour, to tell if the system behaviour is different from expected. However, to isolate the error source is very difficult and a time consuming iteration between testing and detailed software code inspection in a lot of different subsystems. When the source finally is identified the necessary modifications are fast and easily included in the stage of development described here.

6 CONCLUSIONS

The alignment subsystem imposes no additional restrictions on the operation of the F-16 fighter aircraft. There is no need for a particular alignment trajectory, and, the fighter pilot may switch on the alignment at any time, e.g. when he is checking other subsystems on the ground before the mission. From the KF design approach a high performance, highly reliable and robust missile midcourse inertial navigation system emerged. Navigation accuracy is well within specifications. The reasons for the success were in the first place the effort put into simulations both during alignment filter development and during the captive flight testing, and secondly the extent of data collected during testing for performance analyses. If we should have done the job over again, we would have put even more effort into the simulations, the telemetry system and the post processing of telemetry data. Finally, the transfer alignment unit was possible to test and evaluate through relatively inexpensive captive flight testing.

ACKNOWLEDGEMENTS

Many members of the guidance and control group at NDRE have been involved in the design, implementation and testing of the missile navigation system and the Kalman filter. Particularly, I am in debt to J. Bardal, H. Gulbrandsen and K. Rose who have done much of the work described in this paper.

REFERENCES

1. Gelb, A. (ed.), Applied Optimal Estimation, M.I.T. Press, Cambridge, Mass., 1974.
2. Thornton C.L. and Bierman G.J., "UDU" Covariance Factorization for Kalman Filtering", Control and Dynamic Systems, Vol. 16, Academic Press.
3. Bar-Itzhack, I.Y. and Porat, B., "Azimuth Observability Enhancement During Inertial Navigation System In-Flight Alignment", Journal of Guidance and Control, Vol. 3, July-Aug. 1980, pp. 337-344.
4. Porat, P. and Bar-Itzhack, I.Y., "Effect of Acceleration Switching During In-Flight Alignment", Journal of Guidance and Control, Vol. 4, July-Aug. 1981, pp. 385-389.
5. Sutherland A.A. Jr. and Gelb A., "The Kalman Filter in Transfer Alignment of Airborne Inertial Guidance Systems", NWC TP 4653, Naval Weapons Centre China Lake, October 1968.
6. Baziw J. and Leondes C.T., "In-Flight Alignment and Calibration of Inertial Measurement Units - Part I: General Formulation", IEEE Trans. Aerosp. Electron. Sys., Vol. AES-8, No. 4, July 1972.
7. Baziw J. and Leondes C.T., "In-Flight Alignment and Calibration of Inertial Measurement Units - Part II: Experimental Results", IEEE Trans. Aerosp. Electron. Sys., Vol. AES-8, No. 4, July 1972.
8. Kraemer J.W., Roessler J.J. and Bradin D.M., "In-Flight Alignment/Calibration Techniques for Unaided Tactical Guidance", NAECON 1978 RECORD, pp. 705-711, May 1978.
9. Kortüm W., "Design and Analysis of Low-Order Filters Applied to the Alignment of Inertial Platforms", AGARD lecture series No. 82 on Practical Aspects of Kalman Filtering Implementation, March 1976.
10. Maybeck P.S., "Stochastic Models, Estimation, and Control", Volume 1, Academic Press, 1979.
11. Farrell J.L., "Transfer Alignment for Precision Pointing Applications", NAECON 1979 RECORD, pp. 1033-1039.

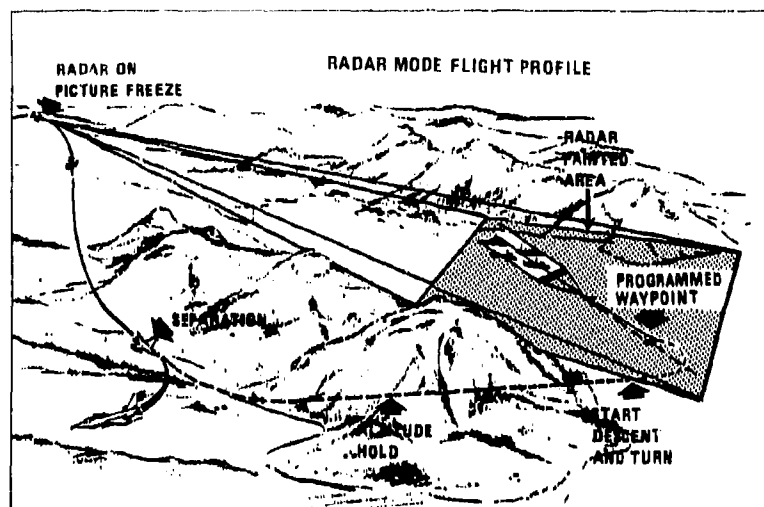


Figure 1 Radar Delivery Mode

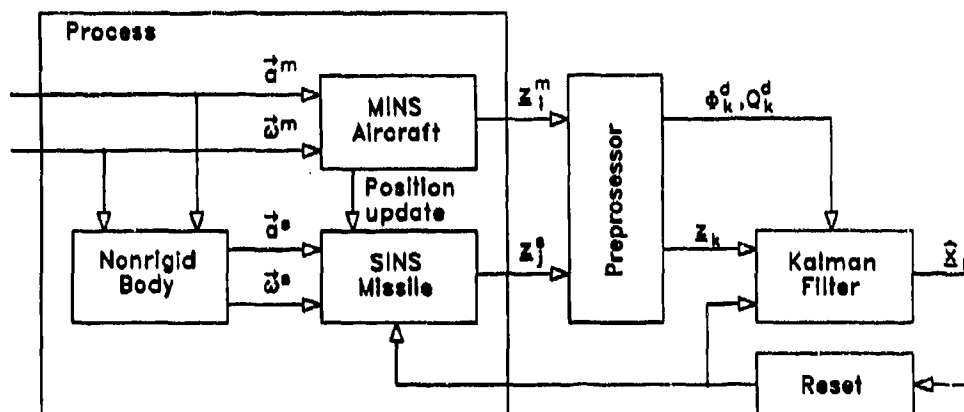


Figure 2 Physical System Block Diagram

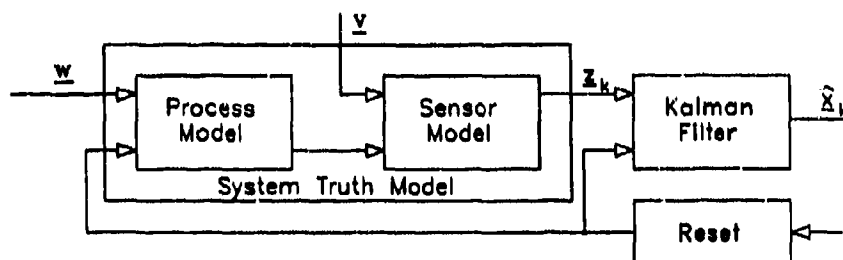


Figure 3 Linear Transfer Alignment Model

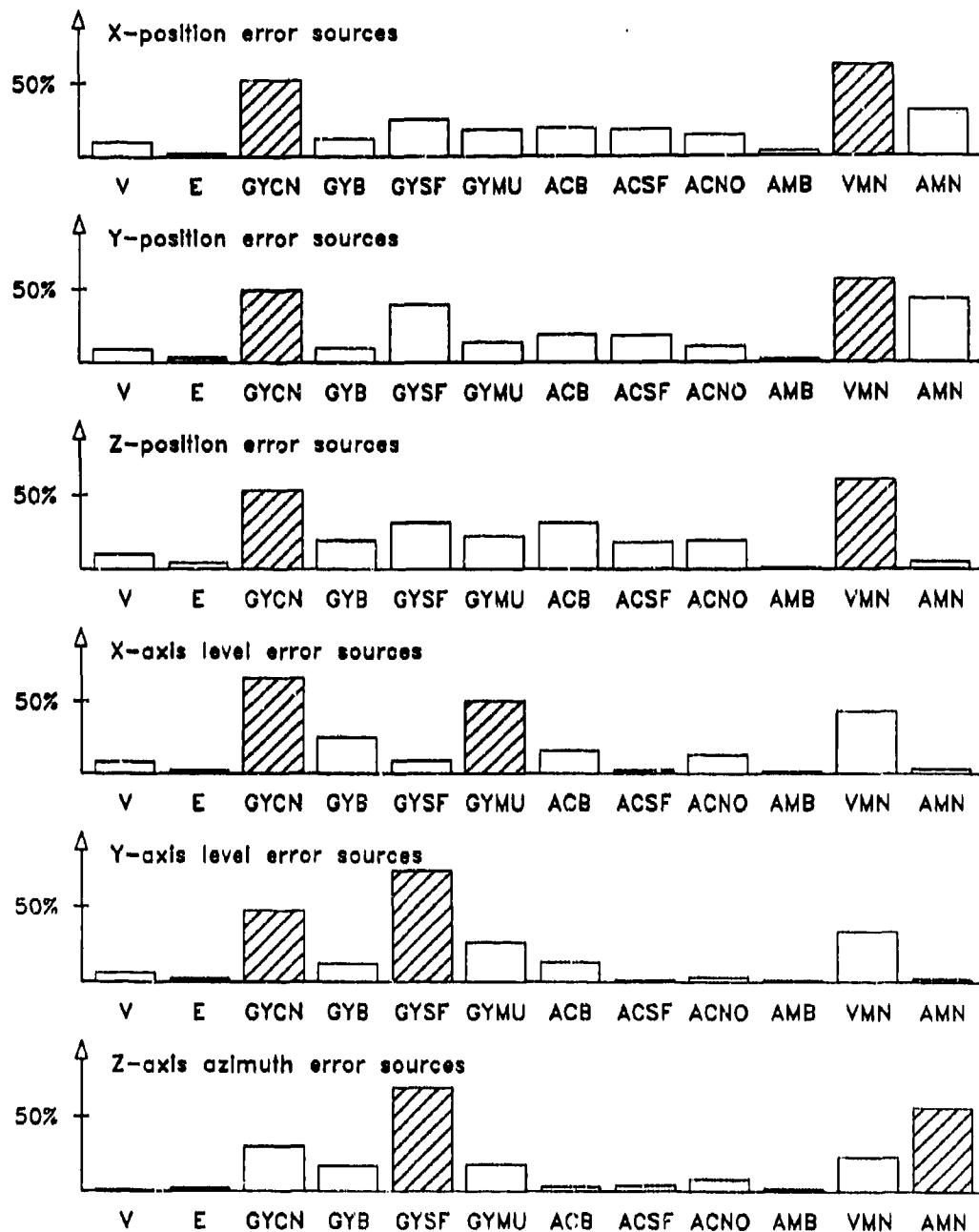
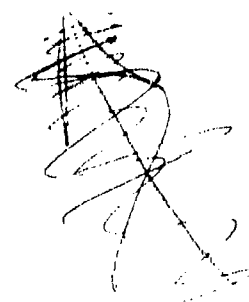


Figure 4 Optimal System Error Budget at the Target



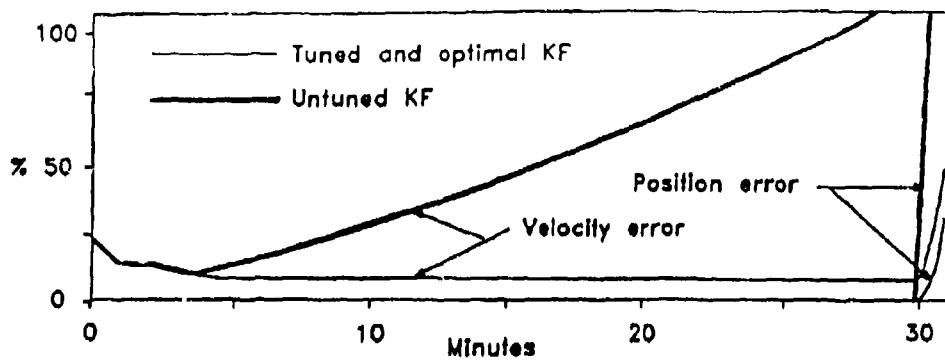


Figure 5 True SD for Optimal, Untuned and Tuned KF

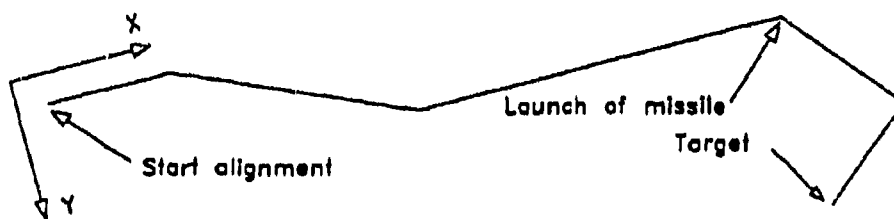


Figure 6 Sample Trajectory in the X-Y Plain

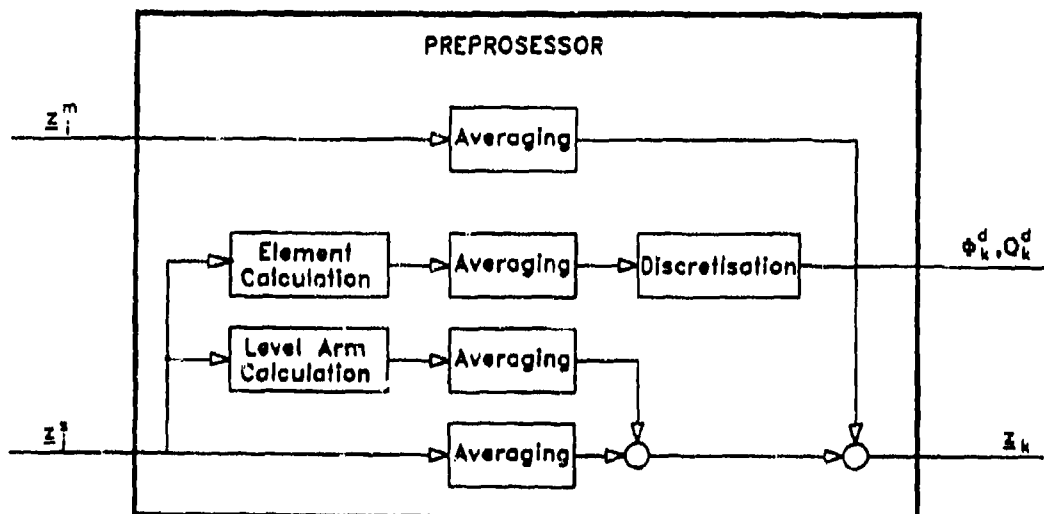


Figure 7 Preprocessor Block Diagram

①

COMPONENT PART NOTICE

THIS PAPER IS A COMPONENT PART OF THE FOLLOWING COMPILATION REPORT:

TITLE: Kalman Filter Integration of Modern Guidance and Navigation Systems.

TO ORDER THE COMPLETE COMPILATION REPORT, USE AD-A214 284.

THE COMPONENT PART IS PROVIDED HERE TO ALLOW USERS ACCESS TO INDIVIDUALLY AUTHORED SECTIONS OF PROCEEDING, ANNALS, SYMPOSIA, ETC. HOWEVER, THE COMPONENT SHOULD BE CONSIDERED WITHIN THE CONTEXT OF THE OVERALL COMPILATION REPORT AND NOT AS A STAND-ALONE TECHNICAL REPORT.

THE FOLLOWING COMPONENT PART NUMBERS COMPRISE THE COMPILATION REPORT:

AD#: P005 817 thru AD#: P005 822

AD#: _____ AD#: _____

AD#: _____ AD#: _____

Accession For	
NTIS GRA&I	<input checked="" type="checkbox"/>
DTIC TAB	<input type="checkbox"/>
Unannounced	<input type="checkbox"/>
Justification	
By _____	
Distribution/	
Availability Codes	
Dist	Avail and/or Special
A-1	

DTIC
ELECTE
NOV 16 1989
S E D

This document has been approved
for public release and sale its
distribution is unlimited.

AD-P005 818

Development of the Integrated All-Weather Navigation System for Tornado

by

Frank Hupke / Dr. Florian Schwegler
 Messerschmitt-Bölkow-Blohm GmbH
 Abt. FE 311/FE 303
 Postfach 80 11 60
 D8000 München 80
 West Germany

Summary

The integrated navigation system for the Tornado weapon system has now been in service for almost 10 years. A detailed presentation will be given on the following topics: primary development approach, problems encountered in development and solutions, side developments that were not implemented for various reasons, methods used for optimization, and modifications of the filter as revisions of the Tornado navigation system were performed.

Abbreviations

A/C	aircraft
BAMS	binary angle measurement system
CPU	Central Processor Unit
GPS	Global Positioning System
INS	Inertial Navigation System
KF	Kalman Filter
LSB	Least significant Bit
OFF	Operational Flight Program
S/W	Software
SWR	Software Requirements
TRN	Terrain Referenced Navigation

1. Introduction

This paper deals with the development and maintenance of a Navigation Kalman Filter starting with the time of definition and realisation up to the time of optimisation and modification. It will present chronologically most of the problems encountered during the KF lifecycle. Most of the information concerning the KF development in the time before in-service release was already subject of an AGARD lecture in 1977 (1) and is partially repeated for completeness. The KF development was conducted at various places in the U.K and F.R.G. (involved parties: ESQ, EASAMS, MBB and with IABG, RAE, and DFVLR as consultants). The authors were involved from 1979/1973 onwards respectively.

A specific feature of this navigation KF is its long lifetime which raises some special problems concerning maintenance. To get an idea of timescales up to now the main milestones in Tornado navigation KF lifecycle are given in table 1.

The Tornado weapon system will be in service well into 2000's thus the navigation KF has not yet passed its mid life point and some major modifications of KF are in sight.

2. Basic Design

The structure of the navigation KF depends very much on the navigation subsystem architecture and this is essentially determined by the defense tasks to be performed with the Tornado weapon system.

For example, a mission must be able to be conducted using the Terrain Following capability. For successful completion accurate preflight planning and high navigation accuracy are necessary to meet flight path profile. This can only be fulfilled by simultaneous use of several navigation sensors and an optimal navigation state estimator, the Kalman Filter.

Major Milestones	Year
Time of definition	1971 (Start)
Development Flight test and optimisation	1974 (Start)
In-service Flight Release	1979
Introduction of Standfix	1981
Modification of KF for integration of a Terrain Referenced Navigation (TRN)	>1989

Table 1 - Major Milestones in Navigation KF Lifecycle

An Inertial platform and a Doppler radar were selected as the main navigational sensors to provide input data to a KF implemented in the A/C central computer. For update of the navigation state by measurement of fixpoints, the on board ground mapping radar in various modes, radio navigation and some visual aids are used (On-top overflying, Head Up Display).

The next decision to be made was whether to use the filter in a closed or open loop. In a closed loop the filter corrections (e.g. velocity errors, tilt angles) are fed back to the inertial platform. In an open loop the filter corrections are added to the inertial platform output for further use in the overall system.

The closed loop mechanisation has some advantages with respect to INS alignment not only on ground but also inflight. But for reasons of system integrity really two independent closed loop systems are necessary. The open loop mechanisation exhibits higher integrity and lower development risk (see Table 2).

Having just one computer and with offers of fairly well developed integral INS an open loop mechanisation was selected.

With the determination of the navigation subsystem components the basic structure of Kalman Filter is defined.

The KF contains eleven states - nine for the Inertial Navigation System and two for the Doppler. This was a compromise between computing requirements and specified performance partly based on supplier data. Later it turned out that a 12-state would have been better although the present system easily meets specification. The elements of the KF state vector are now:

Inertial Navigation system:

Position errors in latitude and longitude
North/east velocity errors

Tilt angle around three axes
North/east gyro drift

(augmenting states)

Doppler:

Along heading scale factor error (augmenting state)
Azimuth misalignment angle (augmenting state)

The equations governing the error behaviour of the INS follow text books (Ref.2).

Assuming strong exponentially correlated disturbances the Doppler errors were represented by the output of a first order linear system with large time constant. This assumption led to workable results.

Additional to the essential KF equations determined by the physics of the sensors further equations were added reflecting the crew interactions with the KF. This completed the requirements for the navigation KF software which was written down in a software requirement paper (SWR) as working paper for the programmers and initiated the S/W development phase.

Item	Open loop	Closed loop
Redundancy	For A/C computer failure pure IN still available	Really effective with two closed loop systems
Development risk	Lower because of better Off Line development	Off Line development and optimisation less straight forward
Computer load	Slightly more	Smaller because of dropping time propagation of state vector
Alignment	No advantage	Quicker on ground and better performance when entering NAV mode, Possible inflight

Table 2 Closed/open loop - Tradeoffs

3. KF Software Development

This development was carried out in two areas, the generation of the on-board computer program and a 'Fortran World' (see also table 3). The 'Fortran World' consisted mainly of three items:

- The System Model (F1)

A very detailed system simulation consisting of equipment models, flight path simulation and a model of the Kalman Filter.

- Software Proving (F2)

Test software used to verify that the onboard computer does the same thing as the simulation program.

- Off Line Analysis (F3)

Software using recorded 'real' sensor data together with reference data (from tracking ground radars) for optimisation and performance analysis/demonstration.

The real KF program was developed for the A/C central computer, i.e the main processor in the Integrated Avionic System of Tornado. This computer had a 16-bit wordlength for commands and data (now more than 32 bits) and a store which grew up from 16k words at the beginning to 224k words today. Together with the operational flight program (OFP) it is the "heart" of the avionic system. The navigation software package including the KF is only a part of the operational flight program (around 2 - 3 k words). The program language is a dedicated Assembler.

No really exciting problems were encountered during the Assembler KF development. The calculations with KF relevant matrices (covariance -, gain matrix etc.) were supported by a 'Software Floating Point Routine'.

The System Model:

The origins are now lost. What was available in 1973 after a change in staff consisted of:

- A large IN and Doppler simulation with error statistics based on supplier data but unfortunately not very well documented. A simulation run took around 5 hours to generate sensor data for approximately two hours flight time on the available general purpose computer and to write them onto a tape.
- A KF model which accepted this tape and produced a considerable amount of paper (print outs of matrices and graphs of all sorts). Again, system-noise figures were based on supplier data.
A large quantity of such outputs indicated that performance would be met for the first one and a half hours of flight (most of the graphs had been cut off at this time) but for the remaining time performance got worse.
- A two inch paper dealing with IN error modeling and KF theory.

With this state of affairs and dedicated flight trials due to start in less than a year we decided to stop work on the system model and to concentrate on the following two items:

- Testing of the MC program fully knowing that modifications would be required in the future.
- Preparation of S/W to evaluate real sensor data recordings (Off Line Analysis, see paragraph 5)

During the preparation of test cases for the MC some design errors/deficiencies were detected:

- As known after linearisation the state transition matrix Φ contains Δt only in first order (system matrix $A * \Delta t$). One might think that dropping Δt^2 in P-Matrix propagation would reduce numerical problems. But the result was disastrous and this approximation was cancelled.
- The incorporation of Doppler information into the KF with measurement every 10 sec. requires presmoothing. Initially this was a low pass filter with a time constant of a few seconds but a straight forward summing over a fixed time interval is numerically more accurate and saves computer time.

Test Data	FORTRAN KF	ASSEMBLER KF
	F1	A1
Simulated Sensor Data: pseudorealistic behaviour	Zero order optimisation Performance Prediction Confidence checks	Was planned but time schedule did not permit, con- sidered to be inefficient
	FA2	
Synthetic data (step inputs)	Software proving Debugging of the Assembler program Solving numeric difficulties using the FORTRAN KF as a test standard	
	F3	A3
Recorded Flight Data + external reference	structural and numeric optimisation of the KF Assessment of sensors and system performance with and without position aiding	Only necessary if step FA2 shows sig- nificant differences between the two pro- grams, but a good confidence check.
	F4	A4
Inflight Data + external reference	Not applicable in this project, might be possible in other applications	Official proving of navigational subsystem system performance Cross check with F3

Table 3 KF Software Development Stages

- An unsuitable choice of measurement plane for some position fixes where the measurement prediction is no longer a linear combination of the state variables at short measurement ranges.
- There was a sign error in the equations for the Doppler. Unfortunately this error was masked by a quite small time constant in the Doppler error model and the effect of this error became only evident after 1 1/2 hour.

At this development stage the importance of good documentation became very evident.

The main effort of the development program was now concentrated on the next two development phases (Table 3) software proving (development stage 2) and off-line analyses (development stage 3) of recorded sensor data which were available before the filter became airborne.

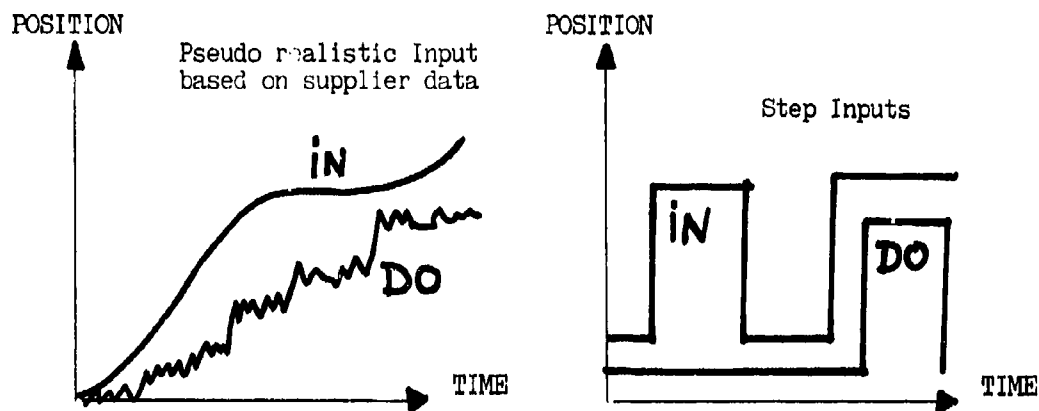


Figure 1 - Synthetic Test Data

4. KF Development Stage 2 - Software Proving

The next task was to prove if the Assembler KF fulfils the KF software requirements i.e. that it performs the required functions with the necessary accuracy. Hereto, the FORTRAN KF was used as a reference tool. Inputting identical test data (step inputs see figure 1) into both programs and comparing the output data turned out to be an effective test method. In spite of previous individual debugging of both programs, differences in the output were found due to program flow errors, wrong setting of constants (e.g. meter/feet, value of LSB, BAMS etc.) and misinterpretation of the KF SWR. The ratio of errors found clearly indicated the need for i) a higher language to be used in the development of avionic systems and ii) a tool supported design documentation.

One test method was found quite useful in the early test stages: Setting individual constants in both programs to values quite different from the design in such a way that they have a pronounced effect when the KF is driven with a standard set of input data (with this method the Doppler sign error, paragraph 3, was detected). Further differences between the programs were due to the number representation in A/C central computer (floating point with 16 bit mantissa). Numerical improvements were achieved with a proper choice of the Doppler pre-smoothing filter and suitable KF iteration rate (initially to high).

Errors	Assembler	Fortran
Program Flow	30 %	50 %
Constants	70 %	50 %
Errors found	<div style="border-top: 1px solid black; border-bottom: 1px solid black; display: inline-block; width: 100px;"></div>	<div style="border-top: 1px solid black; border-bottom: 1px solid black; display: inline-block; width: 100px;"></div>
	Fortran	1

Table 4 Error Statistic Assembler/FORTTRAN

5. KF Development Stage 3 - Off Line Analysis

With the availability of flight data the KF was adapted to meet real world requirements. Suitable preprocessed flight data were fed together with position and velocity reference data (derived from Tracking Radar Data, Decca in the first phase) into a ground based computer to rerun a flight several times with different versions of the KF.

There are some important advantages in evaluating flights on a general purpose computer rather than on the real A/C central computer:

- 1) After some preprocessing of sensor data it is possible to "rerun" a flight in a couple of minutes rather than hours in real time.
- 2) Modification of program and constants necessary to obtain the desired performance are performed much quicker and safer.
- 3) Easy access to peripheral - Printer, plotter, tape units and disks.

This method was applied mainly to adjust the System noise, the initial covariance matrix and the measurement monitoring.

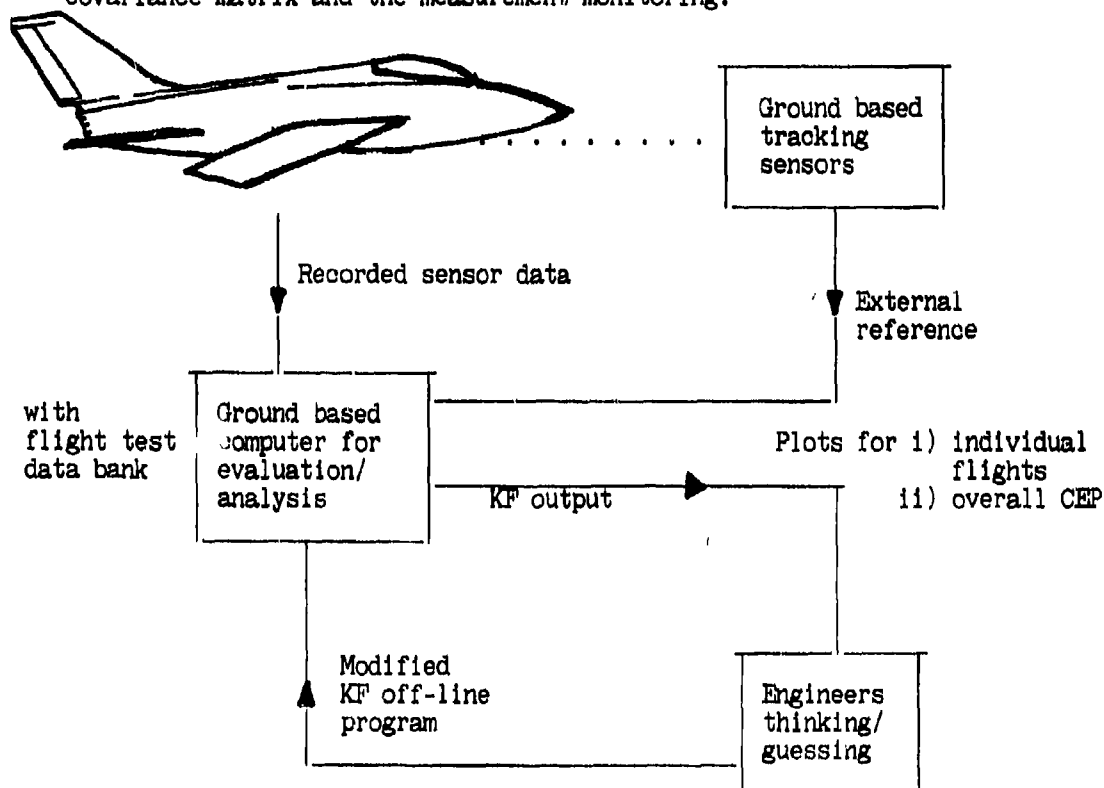


Figure 2 KF OFF-Line model development Loop

5.1 Measurement Monitoring:

Before a measurement is processed by the KF it is checked if it lies within the area enclosed by an $X\%$ ellipsoid made up by system plus measurement uncertainty.

For the case where it lies outside, the measurement is disregarded (this was modified in a later KF version, see below). This measurement monitoring prevents 'KF corruption' by 'unreasonable' measurement results.

For example, it may happen that the crew updates the A/C position by measurement of ranges to a fixpoint but for some reason the object identified

... be this fixpoint is totally wrong and would generate a big measurement difference and therefore would probably not be accepted by the measurement monitor.

There were no specific theoretical models available for determining the monitor thresholds and so they were derived empirically.

There are two types of measurement monitoring incorporated in the OFP.

- The Doppler-IN velocity monitor is fully computerized (i.e. not under crew's control) using a value much below the 30 threshold one finds in many applications. If Doppler data have been continuously rejected for a certain time a warning is given to the navigator on a synthetic display.
- When a position fix is performed the measurement error and the monitor check result 'Accept' or 'Reject' is displayed on that synthetic display. For the development and first production versions of KF the fix data were only processed if monitor and navigator agreed that results are reasonable. The navigator could not override the monitor if it rejected the fix.
In those days, this hard limit against the philosophy that final judgement should rest with the man not the machine was confirmed by industry flight test experience.

The quality of a fix and thus its weight depends on the sensors used and the ranges involved. But also the crew's estimation of fix quality could be considered when determining the weight factor. It was intended to investigate a possible KF improvement with respect to this item at a later stage; above all industry awaited customer's experience which should be taken into considerations (see paragraph 7.1 ' Position Fix Weight ').

Apart from measurement monitoring, some navigation sensor monitoring (especially for the Doppler) is also useful in preventing the processing of 'unreasonable' sensor data. One of these software monitors detects transients of Doppler caused by sudden changes in soil reflectivity caused by ground, calm water and rough water alternating using air data computer information. Another one detects Doppler malfunction by calculating the variances of the Doppler radar velocities in the direction of the three radar beams.

These monitors could be used to suppress Doppler data processing by the KF or to reduce weighting factors.

Today, Doppler data is not used by the KF if the Doppler data status is bad or certain bank and inclination limits are exceeded.

5.2 Initial Covariance Matrix and Systemnoise:

There were two methods applied to determine the Initial Covariance Matrix and the system noise. The first was an analytic one and the second was a rather empiric one which consisted basically in looking at results and trying modifications with a limited amount of analytic work.

The latter, a "magic number" approach yielded quicker and better results throughout. Graphical representation plays an important role in such an empirical approach. For detailed investigations we found it better to display true IN errors (i.e IN data minus tracking radar data) and their estimates (KF output) versus time rather than INS errors and residual errors.

If a large number of flights is evaluated it is convenient to have the net result in the form of a CEP curve for position and velocity versus time together with an indication of their statistical significance (Fig.4 and 2). Flights stored in a data bank may be rerun under different conditions, the Doppler may be switched off and position fixes of different accuracy may be simulated.

To prove the benefits of having a Kalman Navigation filter and that it is working properly comparison has to be made with simpler mechanisations. In our case a suitably smoothed Doppler/IN Mix (deterministic model) with

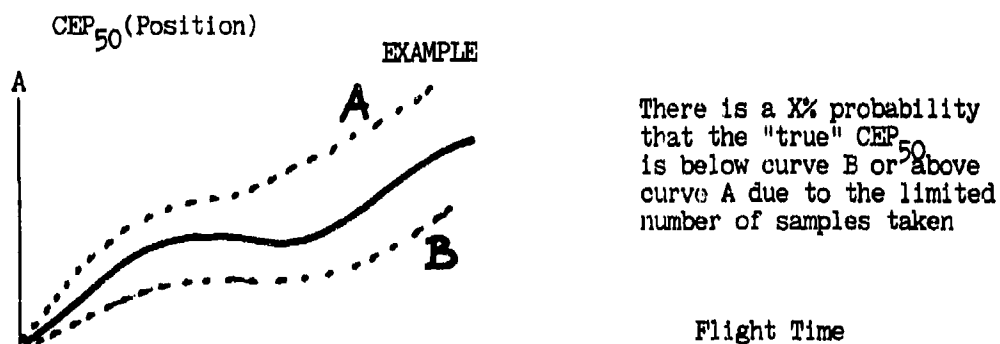


Figure 3 - KF Performance Representation

straight resets of position after position fixes. Results showed the significant superiority of the KF over such simpler mechanisations. In the course of optimisation, the system noise was not only numerically significantly changed from the initial values provided by the suppliers but also the structure changed and this is summarized in table 6 and 7.

SYSTEM NOISE

INERTIAL NAVIGATOR				DOPPLER
Level Gyro Drift	Attitude	Velocity	Position	- Scaling - Misalignment
N hour low pass filter driven by white noise	Only contribution for the vertical tilt	zero	zero	- N minutes low pass filter driven by white noise - Nil

Table 6 - System Noise Elements at the beginning of development

At the beginning, system noise elements for position, velocity, level attitude, and Doppler misalignment were set to zero (Table 6).

During development, time dependent terms and contributions after completion of a turn were introduced to system noise improving KF performance. It was effective to describe also Doppler misalignment by a first order low pass and assuming an appropriate non-vanishing system noise component (Table 7). All these corrections seemed to be suitable to compensate non-linear effects.

	INERTIAL NAVIGATOR			DOPPLER	
	Level Gyro Drift	Attitude	Velocities	Scale error	Misalignment
White noise driving low pass	0			0	0
A+B*time		0			
After com- pletion of a turn		0	0		0

Table 7 - System Noise at the end of development

5.3 A Numerical Problem with Covariance Matrix after Position Fixing

A special numerical problem with KF occurred in a development stage when flight test data were available from a Buccaneer fitted with IN, Doppler, and the A/C central computer. This A/C was flying in the UK. At the same time the first Tornado prototype flying in Germany did not show this KF misbehavior which was found to occur after a significant flighttime over water followed by position updates using an oilrig in the North Sea.

Inflight recordings indicated anomalies in the covariance matrix after this update, although up to this time the filter had performed quite well. The problem was tackled from two sides, driving the real computer on a ground-based rig with similar profiles to those encountered in flight and by using the Fortran reference program.

As numerics were supposed to play a role, the computer used to run the Fortran program was modified to perform the four basic operations as if it had a floating point number representation with a 16 bit mantissa.

The greater flexibility of this general purpose computer provided the source for the problem faster than investigations with the 'real' machine:

A position fix has great influence on the covariance matrix in reducing it. Flying some time over water, where the Doppler is weighted little, increases the covariance matrix while building up quite small asymmetries.

As running a complete flight profile in the modified general purpose computer took only a couple of minutes, a solution to the problem by simply forcing symmetry could be demonstrated over a number of different flight-profiles. The symmetry was simply achieved by averaging the P-matrix off diagonal terms before measurement updating.

Numerical results with 16 bit mantissa plus forced symmetry were practically identical to 24 bit calculations with or without forced symmetry of the covariance matrix.

With the solution to hand it took only a week to continue trials with a software modification (this included flight release paperwork and approval by responsible offices in Germany).

Today a possibility exists to enhance numerical stability of the KF by the use of the floating point processor in the recent A/C central computer (224K). Today, the 'software floating point' routine (16 bit mantissa) is still applied to numeric calculations. The use of the floating point processor (23 bit mantissa) would require some rearrangements in the A/C computer tasking controller and would also affect slightly other S/W functions (e.g weapon aiming etc.).

	16 bit	24 bit Mantissa
without forced symmetry	instable	stable
with	stable	stable

Table 5 Stability of Co-variance matrix

The customer is aware of this situation but is avoiding any modification of the KF at this time. But at least, with the integration of additional navigation sensors (see paragraph 8) the use of the floating point processor for KF calculations will become necessary.

6. KF Side-Development

During development and also after the first in-service flight release of the OFP, some questions arose concerning KF structure and real sensor behaviour. With the access to sensor data and the availability of the KF off-line program, it was possible to find adequate answers. But, nevertheless, the results of the following investigations were not incorporated in the production version of the Tornado KF.

6.1 Azimuth Drift Filter

This modification of the Tornado navigation KF replaces the Doppler along heading scale factor error modelling with an error modelling of the azimuth gyro drift. The equation for the tilt vertical axis was slightly changed by adding this IN azimuth gyro drift (change of system matrix); minor adaptations were also made accordingly for system noise and initial co-variance matrix.

Results indicated that such a filter would have an advantage over the existing one for longer times of flight. However, the activities were stopped by the customer who was not convinced on effectiveness. From today's viewpoint a 12-state KF (Doppler along heading and azimuth gyro drift) is also discussable but during the initial phase this alternative was not considered due to core/time implications.

Nevertheless, some provisions are implemented in the S/W today and the option is still there to introduce this filter if in the future longer missions than currently planned are necessary and then it would play a more significant role. The selection of the appropriate filter could be under the control of the crew.

6.2 On-line Doppler data monitoring to improve navigation over sea

Flight trials (TORNADO/Buccaneer) over sea showed a poor performance for Doppler/IN aided navigation but this might be expected due to the laws of physics for Doppler radar. On the basis of these trials the original weighting factor in the KF measurement noise matrix for sea was modified. Another attempt to reduce Doppler malfunction was to use wind information derived from the Air Data Computer and Doppler/IN. When over sea a fraction of wind could be attributed to water surface motion (strongly non linear) and compensated (i.e correction of measured Doppler velocities). Nothing has been done in this area but inspection of some data RAE Farnborough has

been carried out.

Another problem was in the manually setting of the Doppler into the land or sea mode, found by industry air crews. Some investigations were made on how to put up a warning if the setting into the appropriate mode was forgotten. Industry proposed a warning based on i) stored geography and ii) a "Terrain roughness" filter. For the first, there are many possible solutions but these are not relevant here; the latter one uses the "higher frequency content" of the difference of pressure height and radar altitude. However the customer did not support these ideas.

We engineers always try to do a perfect job; the navy thoughts might be little different, ships etc. are moving anyhow, and they might think what is the benefit of perfect navigation which steers me to a place where the ship might be. We have the feeling that there is room for further improvements here.

6.3 Navigation Updates on Straight Lines (Baseline Fix)

Something else that we have investigated in detail is fixing on "straight lines" - e.g. little bits of motorways, power lines etc. - which can be easily incorporated in the filter and which would work well as simulations on a modified KF off-line program demonstrated. A remaining problem is the user interface to define the 'straight lines', e.g. as two points or one point and a direction.

However again this did not meet the operators requirement; as it seems that the Services have built up catalogues of 3D fixpoints covering their potential operating scenarios.

6.4 IN Gyro Drift Storage

Another way to improve KF performance would seem to be the storage of the IN gyro drifts in the A/C central computer at the end of a flight. These stored data (or a suitable fraction) can then be used as start values for KF initialisation for the next flight provided the same IN equipment is still fitted. We did not investigate this approach further because we had not enough recorded data from flights which were tracked and had a sufficient number of different IN equipments.

7. KF Development Stage 5 - Modifications of KF in production S/W loads

The off-line analysis method applied during the development stages also turned out to be powerful after in-service release. Some comments from the customer concerning the navigation performance made us investigate modifications of the production KF. In some cases, it was sufficient to rerun the modified KF model fed with "old" flight test data from earlier flights. Once, encouraged by results of these simulations, experimental changes of Assembler KF were defined, coded and tested on rigs and aircraft. The Fortran KF also provided reference data for the validation of the Assembler KF (Table 8).

Test Data	FORTAN KF	ASSEMBLER KF
	F5	A5
Recorded Flight Data + external references (or from data bank)	Analysis of modifications Use as reference for S/W validation	Change due to new requirements as re- sult from F5

Table 8 KF software development after In-service Release

7.1 Position Fix Weight (Double Accept)

Position fix weighting factors were never optimised, this optimisation would require some task. What we (industry) have investigated in this area is the system accuracy attainable using well defined targets (offsets): corner reflectors, significantly marked objects etc. We do have some data relating to fixpoints like bridges, cross roads, etc. but these data too have no real significance with respect to the real operating scenario as our testcrews know the areas too well.

When it turned out that the KF with just Doppler/IN (no Position fix) was meeting specification values, for Doppler/IN **PLUS** Position fixes every 20 min., the customer lost interest in an optimisation of Position Fix weighting values.

The problem on how to take into account operator's estimation for fix quality when determining fix weight factor was solved in a simple and radical way. The navigator was enabled to override a KF fix reject in which case the S/W only updates the two KF state elements containing the position error while the co-variance matrix remains unaffected.

Thus today, the customer is quite happy with the navigation performance and resists any changes in this area. On the same line is the requirement to apply fully target measurement corrections for weapon aiming calculations but to leave navigation performance (i.e. KF) unchanged.

7.2 Standfix

Crews reported that when making a position fix immediately before take-off, a significant navigation error was present due to IN drifts.

On the ground Doppler is not engaged and position fixes to compensate errors due to IN drifts can be performed only when the aircraft is positioned at certain well surveyed points.

Figure 4 shows typical IN velocity/heading behaviour with the A/C moving or at rest.

IN velocity /heading output



Figure 4. - Typical IN velocity/heading output behaviour on ground

When a human being considers this curve it is evident when the aircraft is at rest and when it is moving. A piece of S/W is also capable of interpreting whether aircraft is stationary or not. This subroutine - we called it standdetector - monitors smoothness (i.e. gradient) of IN velocity and heading output to generate the logical 'aircraft stationary Yes/No'. It is easy to define adequate measurement matrix and measurement noise matrix for

the steady aircraft state. Thus as long as the stand detector states steady aircraft a 'Standfix' is performed every 10 seconds i.e a 'zero velocity fix' with measurement noise. This mechanisation leads to a remarkable improvement of the navigation system on ground carried over into approximately one hour of flight, depending on circumstances. There was only one small problem with the Stand detector after a rapid IN alignment. However an update of the Stand detector parameters cured this problem.

8. KF Future Development

Today, the current navigation KF has an excellent performance which is confirmed by the national airforces. Nevertheless, the crews still attempt to achieve the best navigation state with the current system by finding the optimal ground procedure when aligning the navigation subsystem. Looking at the most likely developments of the TORNADO navigation subsystem some non trivial impacts on the navigation KF are expected. New navigation systems under consideration for integration into the TORNADO navigation subsystem are Terrain Referenced Navigation (among others e.g. LATAN, TER-PROM etc.) and the Global Positioning System. None have really been integrated into the KF up to the present.

8.1 Terrain Referenced Navigation (TRN)

The Terrain Referenced Navigation system provides A/C position and velocity based on stored terrain data and height sensor input. IN position input is used as the start value for internal calculations. The TRN also provides proper weighting factors of its output parameters. Two possible integration stages are in discussion: first, integration of TRN without affecting existing navigation KF and second, integration of TRN supplying the navigation KF with TRN position and velocities. The KF part estimating position fix errors can be used for processing of the TRN inputs with minor modifications. The problem is to adjust TRN measurement noise and to determine the iteration time of TRN input to KF. The Off-Line Analysis method (Paragraph 4., Figure 2) is a suitable tool to do this job.

8.2 Global Positioning System (GPS)

GPS is a possible candidat for enhancing the TORNADO integrated navigation system. Again, determination of measurement noise (for position and velocity) and the iteration KF input rate will be the problem. But at this time no deeper investigations have been made in this area.

9. Conclusions

For the development phase it is reasonable to make ample allowance for the structure of the system noise at the start of all developments involving Kalman filter.

The central A/C computer program was updated with these system noise changes before it became airborne. Since then off-line analysis of flight data has continued and only minor changes have been incorporated in the navigation filter meanwhile.

Off line analysis has provided useful information on equipment deficiencies such as the Doppler scaling error, the existence of which the supplier was a little reluctant to admit., IN gyrodrifts and misalignment. Correlating the state vector estimates from flights flown with different equipments is a great help in the analysis of weakly or non-observable states (such as Doppler misalignment and an INS heading output bias).

The following points of major importance emerge from the experience gained during the development and optimisation of this navigation filter:

- The need for good documentation to enable the transfer of knowledge to the follow-on responsible engineers.
- The usefulness of data bank derived from flight test data in connection with flexible evaluation programs for the evaluation and optimisation of existing systems and design of new ones.
- A fair dialogue with operators about their experiences in order to satisfy real operational requirements.
- Tight control of the onboard computer software is a fairly complex and time consuming task, especially with programs written in Assembler.

References

- 1) H.F.Schwegler, " Development of the Integrated All-Weather Navigation System for Tornado (MRCA) " in Applications of Advances in Navigation to Guidance and Control, AGARD Conferences Proceedings No.220, Stuttgart 1977,
- 2) Kenneth R.Britting, " Inertial Navigation System Analysis ", Wiley Interscience 1971
- 3) Peter S. Maybeck, " Stochastic Models, Estimation, And Control " Vol. 1, Mathematic in Science And Engineering, 1979, Academic Press, Inc.
- 4) A short course on KALMAN FILTER THEORY AND APPLICATION, 1971 presented by THE ANALYTIC SCIENCES CORPORATION
6 Jacob Way,
Reading, Massachusetts 01867

①

COMPONENT PART NOTICE

THIS PAPER IS A COMPONENT PART OF THE FOLLOWING COMPILATION REPORT:

TITLE: Kalman Filter Integration of Modern Guidance and Navigation Systems.

TO ORDER THE COMPLETE COMPILATION REPORT, USE AD-A214 284.

THE COMPONENT PART IS PROVIDED HERE TO ALLOW USERS ACCESS TO INDIVIDUALLY AUTHORED SECTIONS OF PROCEEDING, ANNALS, SYMPOSIA, ETC. HOWEVER, THE COMPONENT SHOULD BE CONSIDERED WITHIN THE CONTEXT OF THE OVERALL COMPILATION REPORT AND NOT AS A STAND-ALONE TECHNICAL REPORT.

THE FOLLOWING COMPONENT PART NUMBERS COMPRISE THE COMPILATION REPORT:

AD#: P005 817 thru AD#: P005 822

AD#: _____ AD#: _____

AD#: _____ AD#: _____

Accession For	
NTIS GRA&I	<input checked="" type="checkbox"/>
DTIC TAB	<input type="checkbox"/>
Unannounced	<input type="checkbox"/>
Justification	
By _____	
Distribution/	
Availability Codes	
Dist	Avail and/or Special
A-1	

DTIC
ELECTE
NOV 16 1989
S E D

This document has been approved
for public release and sales
distribution is unlimited.

A HIGH PERFORMANCE AIRBORNE INS/GPS INTEGRATED NAVIGATION SYSTEM

David I. Callender
Navigation Systems Department
Ferranti Defence Systems Ltd
Silverknowes,
Edinburgh EH4 4AD
UK

ABSTRACT

The system architecture and the trade-offs that drive its evolution are examined for a practical high-performance Integrated Navigation System designed for a number of current requirements. The system incorporates a 4 gimbal inertial navigator of inherently high stand-alone performance, integrated with a state-of-the-art 5 channel P-code GPS receiver. The system partitioning and interfacing are configured to optimise system accuracy during potentially lengthy periods when a full GPS solution may be unavailable, while providing satisfactory integrity under reversionary conditions. The main Kalman Filter takes pseudo-range and range rate measurements from the GPS rather than position and velocity and in the primary navigation mode models INS and GPS error parameters. The Kalman Filter in the GPS receiver operates independently to provide the desired reversionary capability.

The system architecture, both in hardware and software, allows a high degree of inherent flexibility which is required to tailor the Integrated Navigation System to a wide variety of specific applications.

INTRODUCTION

There is a growing requirement for modern navigation systems to provide high accuracy navigation data on a continuous basis. Data of this consistency is not available from a single navigation system but must be derived from the integration of data from several sensors. This paper describes the design considerations for a high performance INS/GPS Integrated Navigation System. A hardware configuration is given which forms the basis of a flexible integration system that can be easily adapted for a wide variety of applications.

SYSTEM REQUIREMENTS

The Integrated Navigation System to be described is required to provide the following functions throughout long duration flights:-

- a) Navigation data of an accuracy and consistency not available from a single navigation system.
- b) Effective navigation on the failure of any single navigation sensor or during the loss of GPS data due to manoeuvring, jamming or GPS control or space segment failure.
- c) High accuracy autonomous Inertial Navigation System performance when no other sensors are available.
- d) Warning that any sensor is failing or has failed, from the detection of degraded sensor performance to a gross sensor failure.
- e) Comprehensive validity checks on all the sensor data. This includes comparison of the INS data with GPS and the comparison of the pseudo-ranges and range rates between the satellites being tracked.
- f) In-flight calibration of the sensors to eliminate the need for routine ground calibration.

The primary sensors for the Integrated Navigation System are an Inertial Navigation System, a GPS receiver and antenna system and an Air Data Computer. Secondary sensors which may be used under reversionary conditions are Omega, Radar Altimeter and Gyro Magnetic Compass. Using these sensors, the Integrated Navigation System provides the best possible position, velocity, attitude and heading information to the rest of the aircraft systems.

How do these requirements affect the characteristics required from the Inertial Navigation System and the GPS Receiver? These are the only sensors that are considered in depth for this system since the Air Data Computer and the secondary sensors are already part of the aircraft fit in many applications.

AD-P005 819

GPS RECEIVER SUB-SYSTEM REQUIREMENTS

The navigation requirements for most future military aircraft are such that dual frequency precision code GPS receivers must be used. However, applications range from transport aircraft to high agility fighters and it might be considered that in low dynamic cases a simplified 2 channel multiplexed receiver could be used to reduce cost. Unfortunately multiplexing a receiver channel reduces the signal-to-noise ratio by up to 6 db since only part of the available signal information is being used. This results in a reduction in the jamming resistance and the ability to track satellites in conditions of low signal strength. These are important aspects in many military applications and effectively eliminate the use of a multiplexed receiver. Thus a 5 channel receiver is used, with the additional advantage that since each satellite in use is being tracked continuously, such a receiver can withstand higher dynamics in the absence of rate-aiding data.

The receiver should be capable of using rate-aiding data to compensate for antenna motion. Depending on the receiver design and the type of jammer, this can give a small improvement in the anti-jamming performance by allowing the tracking loop bandwidths to be reduced to reject the jammer without losing lock under dynamic conditions.

If the GPS is to be used in a jamming environment, the use of an Adaptive Antenna and Antenna Control Unit should be considered. A typical antenna array is capable of steering multiple nulls independently to reduce antenna sensitivity in the direction of jamming signals, either from external sources or from other transmitters on the aircraft operating at frequencies close to L1 or L2. The use of an adaptive antenna system is very application specific and is not considered further in this paper.

From these considerations, the GPS receiver should be a 5 channel P-code receiver. Rate-aiding data is required to prevent loss of lock of the receiver during high dynamic manoeuvring and to improve its jamming resistance.

INERTIAL NAVIGATION SYSTEM PERFORMANCE

The Integrated System provides very high accuracy position and velocity data at all times. When GPS is available, the integrated system outputs have the long term accuracy of the GPS with the superior short term characteristics of the INS. The accuracy is largely independent of the quality of the INS since the Kalman Filter is continually re-estimating the corrections required by the inertial system. However, when GPS data is unavailable due to either jamming, non-availability of satellites or a failure of some part of the GPS sub-system, the Kalman Filter can only propagate the state estimates existing prior to the loss of the GPS data. The inertial system error sources must therefore be stable in-run to ensure that these estimates remain valid when no update measurements are available.

The most extreme case occurs when no GPS data is available at any time during the flight, in which case the Integrated Navigation System performance will be that of the Inertial Navigation System. In order to meet the stand-alone accuracy requirement for the INS, the error sources must be stable from run-to-run so that calibrations obtained from a previous flight when GPS was available may be used. If they are not sufficiently stable then some pre-flight calibration procedure must be carried out in order for the INS to meet the autonomous accuracy requirement. The particular error sources and their stability and effect on INS performance are discussed later.

Secondly, sensors such as the Omega do not greatly affect the INS accuracy requirements. Omega typically has an accuracy of 2000 m CEP while the uncalibrated INS may have an error growth rate of $800\%t$ m CEP where t is the navigate time in hours. The INS will therefore be the better position sensor for the first 2.5 hours of flight. The Omega position information is not accurate enough to allow the inertial instrument errors to be estimated and so a reduced Kalman filter is run which only models the INS position, velocity and tilt errors.

From these considerations, the Inertial Navigation System must be capable of highly accurate stand-alone performance and must therefore have stable instrument error sources. The type of currently available INS that best meets these requirements for high position and velocity accuracy is a gimbaled system using conventional floated rate integrating gyros or dry tuned gyros.

INERTIAL NAVIGATION SYSTEM DESCRIPTION

The Inertial Navigation Unit used in this Integrated Navigation System is a Ferranti FIN 1041 INS (figure 1) which is a high accuracy derivative of the FIN 1012 system currently in service on the Nimrod maritime reconnaissance aircraft. The FIN 1041 is a conventional gimbaled inertial system which uses floated rate-integrating gyros. It consists of two major sub-assemblies, namely the Inertial Platform and the Electronic Card Bank.



FIGURE 1 FIN 1041 INERTIAL NAVIGATION SYSTEM

The Inertial Platform is a 4 gimbal fully aerobatic platform originally designed for use in a highly dynamic aircraft. It is mounted on stiff anti-vibration mounts which provide some isolation from external shocks without significantly degrading the quality of the attitude outputs. The platform contains 3 Ferranti type 125 floated gyros which have a high sensitivity and low in-run variability under stable operating conditions. This is important in order to maintain the navigation performance when other sensors are not available.

The accelerometers are Ferranti type FA2Fs which are viscous damped, pendulous force feed-back instruments. Again they are highly sensitive and have good bias stability.

Both the gyros and the accelerometers are operated at a constant temperature to obtain the correct sensitivity and to minimise the in-run variability. The whole platform is mounted in an environmental system which is controlled so that the instrument cluster is held at nominally 55 deg C. After the transients due to initial heating of the platform from ambient to operating temperature have settled out, the cluster is maintained to within 0.1 deg C of the nominal temperature.

The Electronic Card Bank contains the platform electronics, an analogue-to-digital convertor, a synchro-to-digital convertor, a computer, the input/output interfaces and the power supply modules.

The platform electronics consist of the gyro spin-motor supply, accelerometer and gyro analogue interfaces, the gimbal servos and the accelerometer and gyro interfaces with the computer.

The computer is a Ferranti F-DISC 2 card computer with a floating point co-processor. It is a micro-programmed machine which is orientated towards real-time control applications.

The FIN 1041 interfaces with the other units within the Integrated Navigation System via a MIL-STD-1553B dual redundant data bus. The 1553B interface card is capable of acting either as a bus controller or a remote terminal. The mode of operation is intended to be selected by a discrete signal but it could equally well be controlled by the dynamic bus control commands supported by 1553B.

There are also direct interfaces with other systems already fitted on the aircraft such as discrete 'INS Good' and 'INS Fail' outputs and 3 wire synchro outputs of attitude and heading.

The power supply modules generate all the internal supplies required by the INS from the aircraft 28 V dc supply. They are state-of-the-art designs using integrated magnetics to reduce the volume and weight and to increase the efficiency. They are switched mode units operating at a frequency of 250 kHz with an average efficiency of 85%. This contributes towards the low INS power consumption of 150 W compared with 280 W for the older FIN 1012 system from which the FIN 1041 is derived.

Both the card bank and the inertial platform require forced air cooling. The platform air flow is regulated by the computer as part of the servo loop which controls the

instrument temperature. The card bank air flows through heat exchangers that remove heat from the cards by cold-wall cooling. The cards have integral heat planes which conduct the heat to the cold walls. They also reduce thermal stresses by distributing the heat evenly across the card.

Many functions that were implemented in hardware in the older FIN 1012 system are now carried out in software. This results in a reduced card count which in turn gives a lower power consumption and improved reliability. The increased reliance on software also makes the system very flexible, allowing major functional changes to be made with little or no impact on the hardware.

The software is modular and is written in CORAL 66. Functions implemented by the software include INS mode control, digital alignment algorithms, the wander-angle navigation solution, 3rd order baro-inertial height loop, instrument error compensation, calibration routines, 1553B interface control and built-in-test (BIT).

INS OPERATING MODES

The Inertial Navigation System has 2 principal modes of operation, which are:-

- a) Align, which levels the platform and carries out gyrocompassing and drift estimation.
- b) Navigate, which provides 3 dimensional outputs of position, velocity and attitude.

Prior to the alignment, the platform is heated up to its operating temperature. At the same time, initial position and altitude data may be entered, although it is not necessary to do this before the start of the alignment.

The alignment is implemented in software and consists of two stages. These are coarse levelling, during which the gyros are run up and the platform is levelled by driving the gimbals to null the pitch and roll synchro outputs, and fine levelling and gyro compassing, where the platform is gyro stabilised and is further levelled by the digital alignment process. (see figure 2).

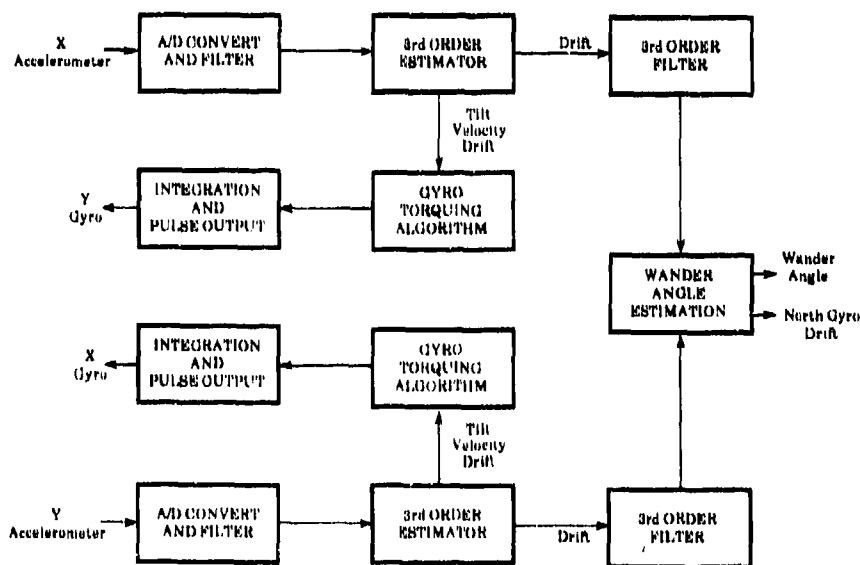


FIGURE 2: DIGITAL ALIGNMENT BLOCK DIAGRAM

The digital alignment is implemented using two third-order estimators which provide tilt, velocity and drift estimates in both level axes. These estimates are applied to the torquing algorithms which drive the gyros until the platform is level. In addition, the X and Y drift estimates are passed to two third-order filters before being used to estimate the wander angle. The alignment estimation also produces an estimate of the north gyro drift error which is then resolved back through the wander angle and applied to the X and Y gyros to compensate for run-to-run drift errors. If the alignment time extends beyond 40 minutes, assessment of the azimuth gyro drift is started. This measures the changes in the wander angle over a period of time and is completed 90 minutes after the start of the alignment. This allows the gyro drifts to be calibrated to provide the best autonomous performance if it is known that no other sensors will be available during a flight.

The navigation equations implement a local vertical wander angle solution which gives the INS a world-wide navigation capability. The vertical channel is a conventional third-order baro-inertial height loop which requires an external source of height data to bound the inertial errors.

INSTRUMENT ERROR COMPENSATION AND CALIBRATION

The instrument error compensation is also carried out by the software. The trim parameters are held in a PROM associated with the Inertial Platform. At present some 160 parameters are trimmed but there is the capacity available for up to 8000 trim parameters. The principle instrument trims are listed in table 1 together with those associated with the synchros and the platform interface. The heading and attitude dependent trims are stored as look-up tables (LUT).

GYRO	ACCELEROMETER	SYNCHRO	ELECTRONICS
Drift	Bias	Attitude Dependent Trims (LUT)	Acc. Switch Rectification
Scale Factor	Scale Factor		Gyro Switch Rectification
Spin Axis MU			
Input Axis MU			
Misalignment			
S.F. Temp. Coefficient			
Heading Dependent Trims (LUT)			

TABLE 1: PIN 1041 TRIM PARAMETERS

In addition to digital error compensation routines, there are also extensive calibration routines for use during ground test to measure the instrument parameters. Most of the routines are self-contained and fully automatic but some, such as the measurement of transient instrument errors, require external equipment and some operator intervention.

INS/GPS INTEGRATION

The primary integration is that between the Inertial Navigation System and the GPS receiver. The INS produces continuous information with no short term interruptions but with errors that grow slowly with time in ways which can be well modelled. The GPS on the other hand produces accurate position and velocity information which does not degrade with time but which can be interrupted. By combining these sensors, a continuously available integrated solution is produced with an accuracy comparable to that of GPS even when the GPS is unavailable for periods up to 15-20 minutes. The degradation of performance if the GPS is unavailable for longer periods depends on how well the INS has been calibrated.

The integration is required to be of a very high accuracy and this is best achieved by calibration of those inertial error sources which vary significantly either on a run-to-run basis or by long term drifting over a period of months or years. The GPS cannot be relied upon to be continuously accurate during every flight due to airframe masking, jamming or poor satellite geometry. The calibration of the inertial instruments enables the integrated solution to propagate through such periods with minimum degradation.

USE OF PSEUDO-RANGE AND RANGE RATE DATA

There are several advantages in using GPS pseudo-range and range rate data rather than position and velocity. Firstly, measurements can still be used when there are too few satellites visible to allow the GPS receiver to calculate a full navigation solution. Secondly, data from as many satellites as the receiver is tracking is available to the integration filter whereas data from only 4 is used in the GPS position calculation. Therefore, more information is available to the integration filter during times of good GPS coverage allowing a better calibration of the INS error sources. Thirdly, significant GPS position output changes of the order of 40 m can occur after a satellite constellation change. This is again a result of only using 4 satellites in the GPS navigation solution. Finally, the use of pseudo-range and range rate data permits more comprehensive validity checking of the GPS data. It is possible for a satellite to have a fault but for the fault condition not to be reflected by the SV health word for several hours. It is therefore vital that independent consistency checks are carried out on the GPS data at all times.

However, the pseudo-ranges are not corrected for GPS user equipment clock errors such as bias and drift and these states must therefore be estimated by the integration filter if pseudo-range data is to be used.

USE OF INS AND GPS MEASUREMENTS

The Integrated Navigation System described in this paper uses INS position and velocity data together with pseudo-range data from the GPS receiver (figure 3). In order to make use of the GPS data, the position and velocity of each satellite at the time of the GPS measurement is also required.

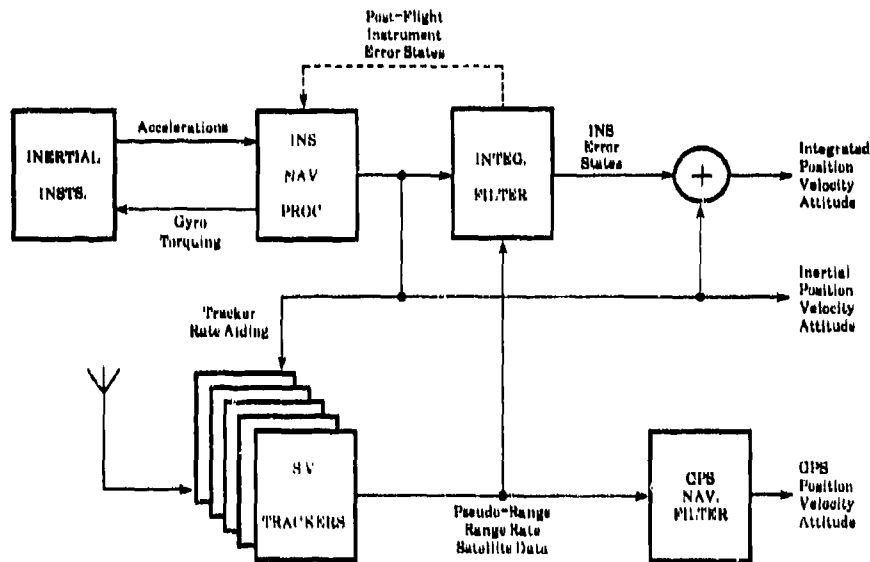


FIGURE 3: HORIZONTAL INTEGRATION BLOCK DIAGRAM

The Kalman filter uses the differences between the INS and the GPS measurements as its input. However, the INS outputs are in geographic axes while the GPS satellite data is in Earth Centred Earth Fixed (ECEF) coordinates. The data must therefore be transformed to a common frame of reference in order to calculate line-of-sight distances and velocities and so the INS data is transformed from geographic axes to ECEF.

Position errors are derived by first calculating the line-of-sight distance from the INS to the satellite. This is then corrected for the lever arm distance between the INS and the GPS antenna before being subtracted from the pseudo-range measurement to leave a range error along the LOS to the satellite. This process is repeated for each of the satellites being tracked by the receiver.

The velocity errors are dealt with in the same way by calculating the line-of-sight velocity between the INS and the satellite and subtracting it from the range rate corrected for antenna motion. Again this is repeated for each satellite being tracked.

The best estimates of position and velocity are produced by adding the current estimates of the position and velocity errors to the latest inertial position and velocity outputs. Similarly, the heading error is added to the inertial heading output to give the integrated heading output. Because the Kalman filter is modelling position, velocity and tilt error states which only change slowly with time, delays in the corrections caused by data validity checking and filtering do not matter, provided that they are much less than the Schuler period of the INS. This also means that it is not necessary for the filter to cycle at a high rate.

DATA SYNCHRONISATION

The calculation of errors between the INS and the GPS pre-supposes that the measurements from each of them were made at the same point in time. This is not usually the case. The GPS measurements which are made every second are not synchronised with the INS data outputs which occur every 20 - 50 ms. The usual method

of synchronising the data is to time tag it using free-running clocks in each unit which are periodically synchronised to keep the time difference between them within acceptable limits.

What are the acceptable limits ? Some of the INU error sources give rise to velocity errors of the order of 0.1 ft/s rms. Therefore the errors in the velocity measurement introduced by correcting for lack of data synchronisation should be less than this value, for example 0.05 ft/s.

Velocity errors due to lack of clock synchronisation are introduced during periods of acceleration. In order to keep the errors less than 0.05 ft/s during an acceleration of 2g, the timing error between the clocks must be less than 0.8 mS. The clock in the INS is a crystal oscillator which can have a bias of up to 50 ppm with respect to the nominal frequency. This bias also varies with temperature. The time tag clock in the GPS receiver may have similar characteristics, depending on the receiver design. Hence for a difference between the clocks of 100 ppm, they need to be synchronised every 8 seconds to keep the difference to less than 0.8 mS.

RATE AIDING OF THE GPS RECEIVER

Rate aiding of the GPS receiver can improve its anti-jamming performance by reducing the bandwidth of the code tracking loop. It also reduces the satellite acquisition time since the receiver has apriori knowledge of the antenna velocity and therefore the expected Doppler shift of the carrier frequency.

The antenna must be compensated both for linear motion and for lever arm effects, where aircraft angular rates result in a velocity at the antenna. The effectiveness of the corrections is determined both by the accuracy of the data and its latency. To prevent velocity errors of less than 1 ft/s occurring during a 2g acceleration, the velocity latency must be kept below 15 mS. Angular rate data can have a latency of up to 200 mS for a small lever arm and moderate angular accelerations before the velocity error reaches 1 ft/s. These requirements are easily achieved by time tagging the data to allow the GPS receiver to calculate its age and correct it for aircraft accelerations if necessary.

DATA VALIDATION

Both the INS and GPS data must be rigorously tested to ensure that no spurious measurements are fed to the Kalman filter. These tests should be independent of the integrated navigation solution and also of other sensors. A basic check is to test that successive samples of data do not imply rates of change that exceed the maximum aircraft dynamics. For example, if two successive velocity measurements implied an aircraft acceleration of 6g and the INS is fitted to a large transport aircraft then one of the measurements is likely to be in error, or else the aircraft is in a situation where the navigation accuracy is unlikely to be of much concern.

The GPS receiver is able to provide a considerable amount of information to assist with data integrity checking. The GPS data can be checked by monitoring the satellite health word, the predicted User Range Accuracy (URA) word, cross checking data from one satellite against data from the others and also by comparing successive measurements. The test is similar to that used for the INS but allowance is made for the noisy nature of the GPS data.

In general, the accept/reject limits should be made too tight rather than too open. Measurements are bad until proven good and it is preferable to reject good measurements rather than risk accepting bad ones.

INS HORIZONTAL ERROR STATES

Since the Kalman Filter is required to calibrate the Inertial Navigation System, the error states to be modelled must be determined. The filter provides position, velocity and tilt corrections to the INS outputs. Considering the horizontal axes only, this requires two position, two velocity and three tilt states. The two horizontal tilts are acceleration error terms while the Z tilt is the heading error.

The instrument parameters which need to be modelled include those which have significant run-to-run variability or long term drift. Further, the calibration algorithms themselves are not perfect and therefore some error sources, while not varying with time, may have significant calibration errors which are worth modelling.

The effect of these error sources on the performance of the INS must also be determined. This has been done by using a simulation program which excites an error model of the INS with flight profile data and generates the position, velocity and tilt errors contributed by the different instrument parameters. The typical values for these parameters are found from the population statistics of the instruments and from a knowledge of the calibration algorithms and their likely errors. The instrument variabilities and their effect on INS performance are shown in tables 2 and 3. The

figures in table 3 are taken from the simulation results of a single typical sortie profile rather than from a Monte Carlo simulation run and so should be treated with caution.

ERROR SOURCE	RUN-TO-RUN VARIABILITY	CALIBRATION ACCURACY	RESULTANT ERROR
Gyro Drift (X, Y)	0.002°/hr	0.002°/hr	0.003°/hr
Gyro Drift (Z)	0.02°/hr	0.007°/hr	0.021°/hr
Gyro Scale Factor	0.007%	0.015%	0.017%
Spin Axis MU	0.03°/hr/g	0.03°/hr/g	0.04°/hr/g
Input Axis MU	0.01°/hr/g	0.03°/hr/g	0.03°/hr/g
Misalignment	None	1 arc min	1 arc min
Accelerometer Bias	N/A (See Below)	N/A (See Below)	N/A (See Below)
Acc. Scale Factor	0.015%	0.007%	0.015%

TABLE 2 : INSTRUMENT VARIABILITY (1 SIGMA)

ERROR SOURCE	RADIAL VELOCITY AT 8 Hrs. (ft/s)
X Gyro Drift	0.42
Y Gyro Drift	0.37
Z Gyro Drift	0.85
X Gyro Scale Factor	0.07
Y Gyro Scale Factor	0.15
X Spin Axis Mass Unbalance	0.23
X Input Axis Mass Unbalance	0.06
Y Spin Axis Mass Unbalance	0.08
Y Input Axis Mass Unbalance	0.17
X Acc. Scale Factor	0.20
Y Acc. Scale Factor	0.08

TABLE 3 : EFFECT OF INSTRUMENT ERRORS ON PERFORMANCE

From the table, it can be seen that the gyro drift run-to-run variability contributes the most to the error in navigation performance and therefore all three gyro drifts are modelled. Next are the gyro mass unbalances of which the spin axis unbalance is the less stable. Here the measurement uncertainty is also large which makes both terms worth modelling. Simulation work is continuing to determine whether the input axis unbalances should be included, but until the results are available it is only intended to model the spin axis unbalances because of their greater variability.

Both the gyro and accelerometer scale factor errors are of the same order of magnitude and produce similar velocity error contributions. Of the two, the accelerometer scale factor errors have a larger long term drift than the gyro scale factors and are therefore the terms that are modelled.

Run-to-run accelerometer bias errors are not modelled because they are effectively cancelled out in the navigate mode by tilt errors in the platform which are introduced during the alignment. The fraction of earth's rate which is sensed by the level axis gyros due to the tilt is modelled out by the gyro drift states. It should be noted that a strap-down INS is very sensitive to accelerometer bias effects and they need to be modelled if this type of system is used.

OTHER FILTER STATES, NOISE AND COVARIANCES

This results in 14 states being modelled, which are summarized in table 4. In addition to the INS error states, two GPS clock states are modelled to estimate the clock bias and drift in the GPS receiver thus giving a total of 16 states. This is well within the capabilities of the chosen computer. Indeed, expansion to 30 states is possible but it is not considered desirable to introduce extra states unless they can be easily distinguished, have a good physical meaning and have error statistics that are well understood. It is also undesirable to have too many states because the memory requirements increase with the square of the number of states while the computation

time increase with the cube. Therefore a 30 state filter would require approximately four times the memory and take eight times longer to cycle than a 16 state filter.

INU ERRORS	INSTRUMENT ERRORS	GPS ERRORS
Latitude Error	X Gyro Drift	Clock Bias
Longitude Error	Y Gyro Drift	Clock Drift
North Velocity Error	Z Gyro Drift	
East Velocity Error	X Spin Axis MU	
X Tilt Error	Y Spin Axis MU	
Y Tilt Error	X Acc. Scale Factor	
Holding Error	Y Acc. Scale Factor	

TABLE 4: KALMAN FILTER ERROR STATES

The initial covariances used by the filter reflect the maximum likely magnitude of the specific parameters. In general it is safer to make these values too large, which may result in a slower settling of the state estimates, rather than too small which can lead to filter instability. The initial instrument covariances are determined from the instrument statistics and should be derived from both the instrument variability and the calibration accuracy.

Initial covariances of the other states are dependent on INS characteristics such as the alignment mechanisation and velocity quantisation. Position covariance is determined by likely accuracy of the initial position data (with due allowance for surveying errors, insertion of incorrect data and so on).

The unmodelled instrument errors are treated as terms which modify the process noise. They may be driven by the aircraft dynamics; for example, an unmodelled mass unbalance can be driven by the horizontal acceleration to increase the process noise of a tilt during aircraft manoeuvres. Similarly, uncompensated external errors, such as gravity anomaly effects, require the process noise to be set to a higher value than that calculated from system considerations alone, resulting in reduced state estimation accuracy.

Measurement noise of such quantities as INS position and velocity depend on the quantisation of the data, its latency and the resolution and jitter of the time tagging data, since uncorrected delays in the data introduce greater measurement uncertainty.

FEEDBACK OF ERROR STATES

This is a loosely coupled system in the sense that there is no feed-back of the state estimates to the INS to ensure data integrity in the event of filter failure. If bad data is used by the filter thus corrupting the state estimates, the INU performance is unaffected.

However, instrument error states are fed back to the INS post-flight and are applied as corrections to the trims for the next flight. The amount by which the corrections are permitted to update the trims is determined by such factors as the length of time for which good GPS data was available during the flight, the covariances associated with the state estimates at the end of the flight and the length of time since the last calibration or update. This allows the INS to track any long term drift of the instrument parameters and ensures that the best possible trims are always used.

KALMAN FILTER IMPLEMENTATION

The Kalman filter uses the errors between the INS position and velocity and the GPS pseudo-ranges and range rates as the inputs for the measurement updates.

Sub-system error models are updated in discrete time. Calculation of the transition matrix has been carefully optimised to allow for significant periods of propagation with no measurements. A modified error state vector is used which avoids the use of vehicle acceleration in the transition matrix thus increasing the accuracy for a given update rate. The relative scalings of the state vector parameters have been carefully chosen in order to reduce the sensitivity to numerical errors throughout the algorithms.

The filter measurement and time updates are carried out using the U,D Covariance Factorisation method which provides excellent numerical stability at a relatively low additional computational cost compared with the conventional Kalman-Bucy algorithms. This method has been successfully used in many modelling studies and in real-time implementations in a variety of systems.

For time-critical systems, the coding of the U,D time update (Modified Gram-Schmidt algorithm) has been given the most attention as it is by far the dominant contribution to the computing time budget. In relation to real-time, this budget is of course directly proportional to the chosen iteration rate. Hence in a situation where GPS measurements are available at a high rate, it may be necessary to use measurement averaging. To allow for longer time period averaging, the measurement update algorithm is modified to take account of the dominant transition matrix terms. This is a conservative approach which provides more flexibility in the choice of update rate and allows the reduction of measurement error correlation.

Covariance matrix elements are computed from the U,D factors in order to assess the filter convergence. Since this is a time-intensive process, it is computed at a lower rate. Covariance estimates are also used as inputs to the algorithm which carries out the post-flight update of the inertial error compensations.

FILTER CYCLE RATE CONSIDERATIONS

The filter cycle rate is also influenced by other factors such as sensor data correlation times and computational loading. The INS position and velocity errors are correlated over long periods of time. In contrast, the GPS position and velocity outputs can have correlation times of several seconds because of the filtering introduced by the GPS Kalman filter in the navigation processor. However, the correlation times for the GPS pseudo-range and range rate measurements are less than 1 second and this is another good reason for considering the use of pseudo-range and range rate data instead of GPS position and velocity.

Time updates of the state vector do not present a great computational burden and the update rate is therefore principally determined by the accuracy requirements and the linearity of the model for the given aircraft dynamics. For high dynamics, the filter should be updated more frequently than for a low dynamic application.

The covariance matrix should be updated at least once between measurement updates. Since the computational burden is high, it is updated as infrequently as possible, the minimum rate again being determined by the accuracy requirements and the aircraft dynamics.

The measurement update rate depends on the computer loading, which is high, and the correlation times of the sensor errors and the error covariances. There is little point in the cycle time being much less than a certain value because updates contain little new information due to correlation of the sensor data. Conversely if the error covariances are large, the filter should be cycled more rapidly to improve the error estimates. Unless a variable update rate is used, the cycle time will be a compromise between these requirements.

VERTICAL CHANNEL INTEGRATION

The vertical channel integration is carried out independently of the horizontal integration. This is because the inertial errors for a local level system separate naturally into sources affecting the horizontal and vertical channels. Also, barometric and radar altimeter data only relate to the vertical channel. Finally, as has already been mentioned, the memory and computational requirements are reduced by running two smaller filters rather than a single large one.

The vertical channel integration optimises the outputs of vertical velocity and height by combining GPS pseudo-range and range rate errors with INS vertical acceleration, baro height and radar altitude in a seven state filter (figure 4), the states of which are listed in table 5. The Z accelerometer bias state also absorbs the accelerometer scale factor error and this needs to be considered when modifying the noise assumptions during periods of vertical acceleration of the aircraft. This state also absorbs the vertical component of gravity anomaly which will not be compensated in the INS. The presence of this must be borne in mind when determining the vertical acceleration statistics.

INU ERRORS	BAROMETRIC ERRORS	GPS ERRORS
Z Accelerometer Bias	Baro Bias	Clock Bias
Z Velocity Error	Baro Scale Factor	Clock Drift
Baro/Inertial Height Error		

TABLE 5 : VERTICAL CHANNEL ERROR STATES

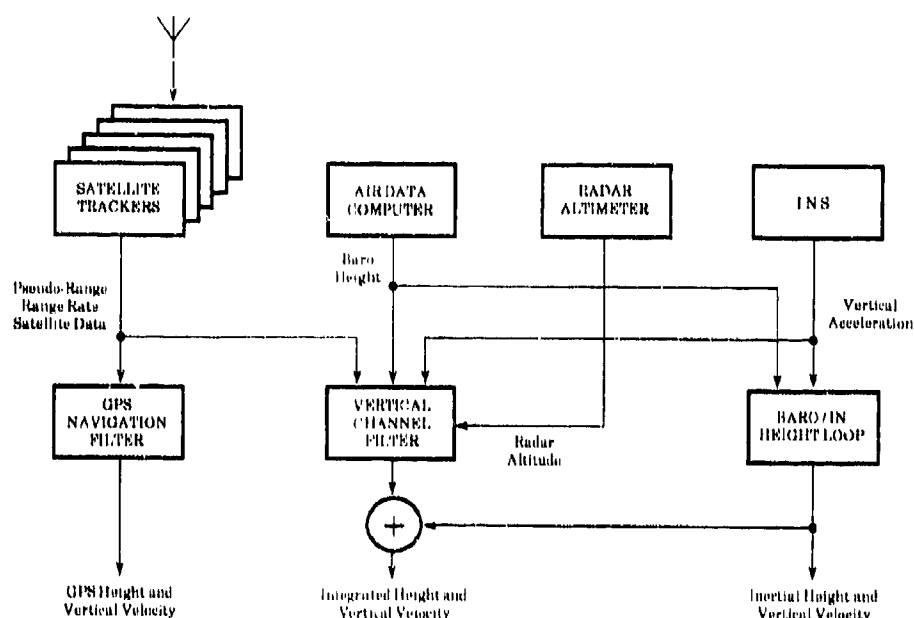


FIGURE 4: VERTICAL INTEGRATION BLOCK DIAGRAM

The barometric bias and scale factor states are intended to determine the atmospheric corrections of the day. Integrated vertical velocity and height errors are produced by adding the error estimates to the inertial vertical velocity and baro/inertial height since these have the best short term characteristics.

The GPS clock states modelled by the vertical channel filter will not necessarily be the same as those estimated by the horizontal integration filter because different components of the GPS data have been used in each case. The estimates of the two filters are combined to form single estimates of the clock bias and drift by using techniques applicable to federated filters (references 1 and 2). The covariances from the two filters are also combined to give single values for the bias and drift covariances in a similar manner.

PERFORMANCE MONITORING

The integration process generates data which allows the performance of some of the sensors to be monitored. For example, the state estimates and covariances of the inertial instrument errors can be compared over several flights and if excessive variability or trending is observed, the operator can be informed that the relevant instrument is producing degraded performance. The INS can therefore be replaced before a hard instrument failure occurs, thus preventing an in-flight failure of the inertial navigation function.

Similarly, if the GPS clock state estimates are outside set limits a possible failure of the GPS receiver or the use of inaccurate satellite data is indicated.

Excessive errors due to unmodelled error sources can be detected but not necessarily identified by comparing the sensor outputs with the integrated solution. Any large differences or high rates of change of differences can be flagged up, although they should be treated with caution since the faulty sensor may have contributed to the integrated solution against which it and the other sensors are being compared.

The sensors should also be self-monitoring so that although they may not be able to monitor their own performance, they can monitor environmental conditions or operator actions that may degrade it. Typical parameters that are monitored are power supply input voltage, component temperatures and cooling air temperature and flow rate (if required). If any of these parameters go outside set limits, the operator is warned that degraded performance may occur.

Additional data is stored after each flight to assist in the analysis of possible sensor failures. This includes such quantities as the length of time for which GPS was available, the satellites used, BIT information and INS alignment time and quality.

INTEGRATED NAVIGATION SYSTEM - PHYSICAL CONFIGURATION

Having determined the sensor and computational requirements of the Integrated Navigation System, the physical partitioning of the functions must be considered. There are several options which are feasible, ranging from a single box solution, where a single processor carries out the INS navigation functions, the GPS navigation filter and the horizontal and vertical integration filters (figure 5) to a multiple LRU solution (see figure 6). In this configuration, each function is implemented within a separate box which is capable of operating independently of the other units.

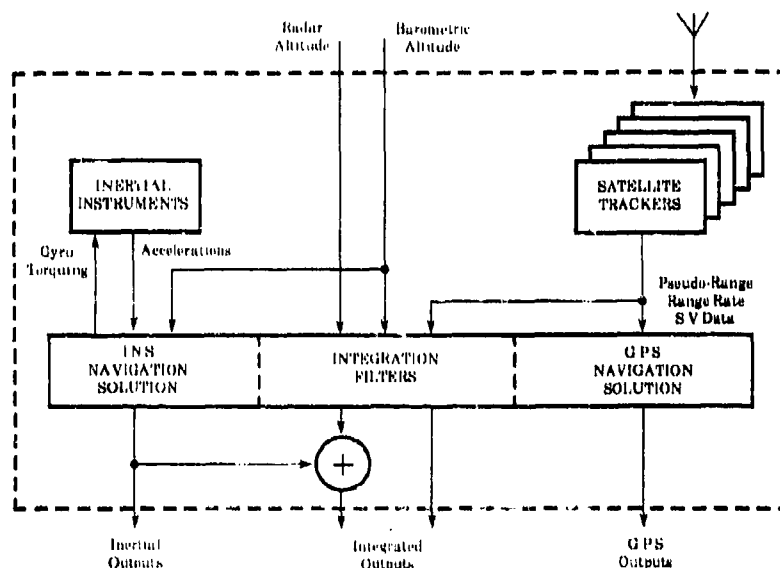


FIGURE 5: SINGLE LRU IMPLEMENTATION

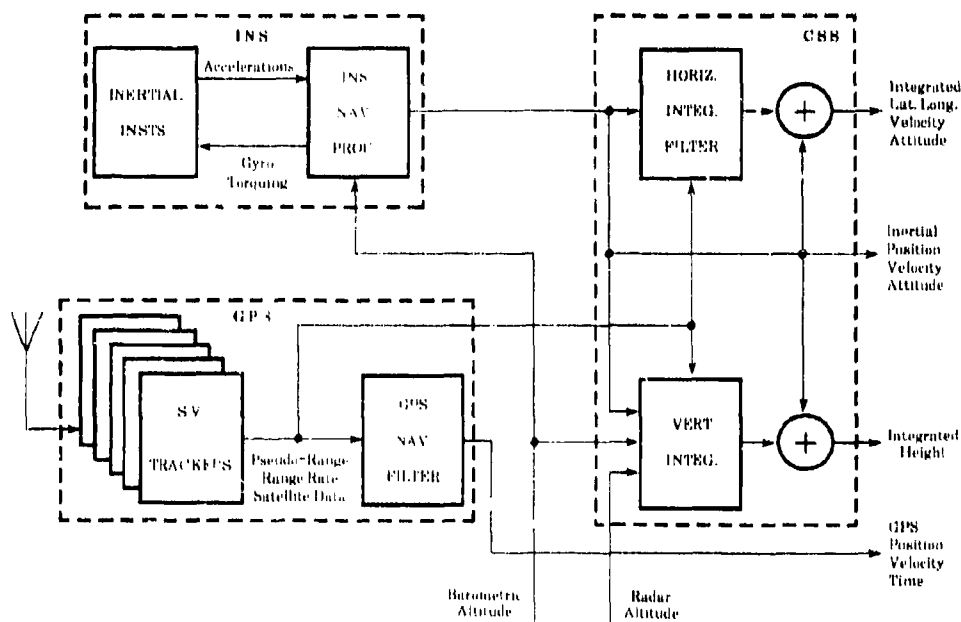


FIGURE 6: MULTIPLE LRU CONFIGURATION

Some factors that drive the system configuration are Integrated System redundancy and reversion, available installation space, spare computing capacity requirements and total power consumption.

For example, a single box solution requires the minimum of installation and has the lowest power consumption but it has very poor redundancy or reversionary characteristics because of its reliance on a common computer and common power supplies. The failure of either of these will cause the loss of all navigation data from the INS, the GPS and the integration filters.

At the other extreme, the multiple LRU solution is more expensive to install and has a higher power consumption but the redundancy is very good because each of the functions is capable of operating independently of the others. Any one of the INS, the GPS or the Computation Sub-System, in which the integration filters are implemented, can fail and navigation data is still available from the remaining sensor or sensors, although possibly with degraded accuracy.

The Ferranti approach to the Integrated Navigation System configuration is a combination of these solutions. Since the system is required to output navigation data from both the integration filters and from each of the sensors, the INU and the GPS must be capable of operating independently of each other and of the integration filters. This dictates that separate LRUs are used. However, the installation costs are reduced by combining two units within a single box (figure 7).

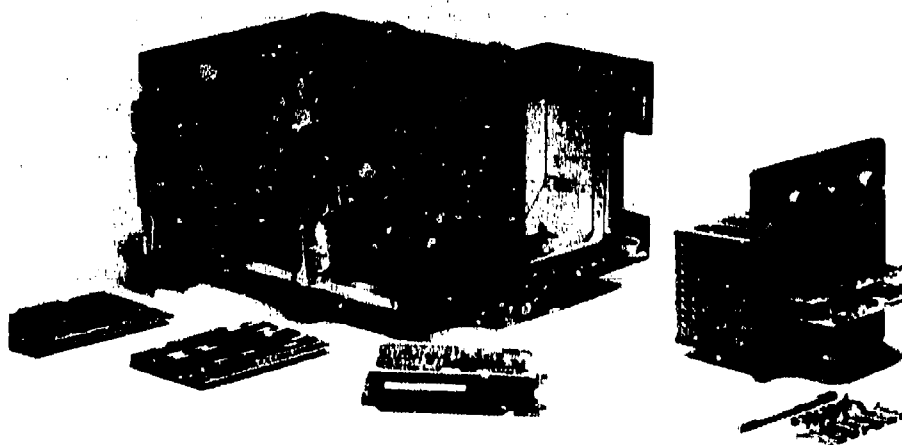


FIGURE 7 EXPLODED VIEW OF THE FIN 1041

This is achieved by designing the FIN 1041 INS as an updated version of the FIN 1012 system. The new cards and power supply modules fit into the space previously occupied by the cards. This leaves a large volume in the INS box where the old power supply was fitted for the installation of additional electronics, in this case the Computation Sub-System (CSS).

The CSS has its own power supply and communicates with the INS via the 1553B data bus, as it does with the other elements of the system. It is also a convenient unit in which to fit any aircraft-specific interfaces such as ARINC 429 links for the Omega and analogue drives for a Horizontal Situation Indicator (HSI) or for an autopilot. Spare computing capacity is also available to perform such tasks as steering, automatic route flying, flight management and system control functions.

HARDWARE CONFIGURATION

The final system configuration is shown in figure 8. The primary bus control is implemented in the Computation Sub-System (CSS), with the secondary bus control in the

INS. This allows other INSs and GPS receivers to be used with the minimum of modification. Of course, if any INS other than the FIN 1041 is used, the CSS must be repackaged for separate installation, resulting in a more expensive system.

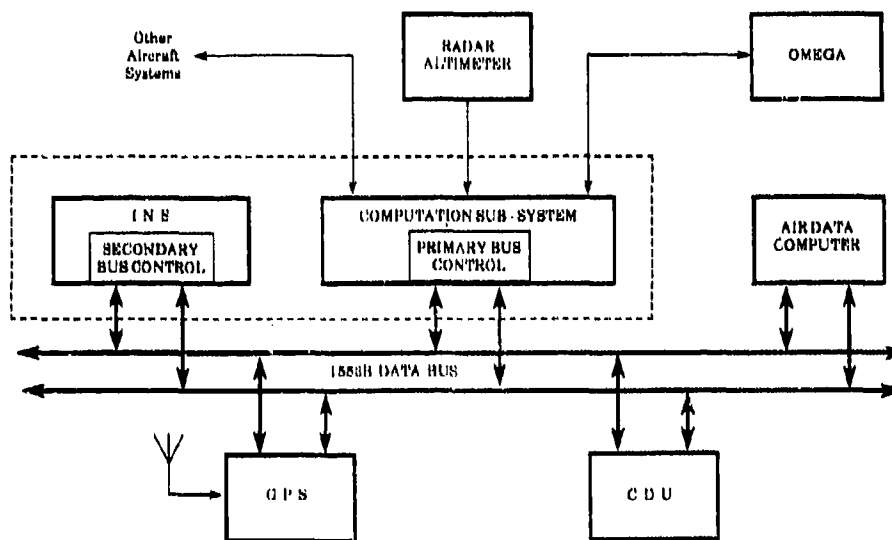


FIG.8: INTEGRATED NAVIGATION SYSTEM CONFIGURATION

The CSS can easily be tailored to interface with a variety of aircraft systems without affecting the rest of the integrated navigation system. This makes it attractive for the retrofit market where it is required to interface with existing avionics.

The CSS can also form the basis of a navigation system update to aircraft already fitted with an INS. The only hardware changes required are those for specific interfaces and so this forms the basis of a low risk system with minimum development requirements. However, extensive changes may be required to the integration filter software, depending on the type of INS, its mechanisation and its instrument statistics. For example, a strap-down Ring Laser Gyro system has a different transition matrix and different instrument errors from a gimbaled floated gyro INS, and these changes may take a considerable time to develop and prove. Even so, the risk is reduced because the basic filter and measurement pre-processing and validation software remains unchanged.

SUMMARY

This paper describes some of the factors affecting the design of a high performance INS/GPS Integrated Navigation System. The need for high accuracy even in the absence of mixing aids requires the use of a high quality Inertial Navigation System. In order to maintain the INS performance and eliminate the need for routine ground calibration, the INS is calibrated in flight when GPS data is available. The choice of the instrument errors to be modelled depends both on the inertial instrument statistics and on the effect of particular error sources on the performance of the INS. This is determined by simulation of the error sources, the likely magnitude of which are calculated from the instrument statistics. From the results the instrument parameters to be modelled are selected.

In order to calibrate these errors, GPS data with the minimum processing delays and the minimum correlation is required. The pseudo-range and range rate measurements are therefore used rather than the GPS position and velocity outputs. The INS position and velocity errors derived from the GPS data are processed by a Kalman filter to produce estimates of the INS and instrument errors.

Before the INS and GPS data can be used to calculate the errors, the INS data must be corrected so that it refers to the GPS measurement time to within less than 1 ms. This tight timing synchronisation is required because the inertial instrument errors are being calibrated to provide the best possible integrated navigation performance when GPS is unavailable for prolonged periods.

Once the data has been synchronised, it must then be validated to prevent incorrect measurements from being used by the Kalman filter. This prevents the corruption of the instrument error estimates which would otherwise degrade the integrated navigation performance, especially if the GPS became unavailable at the same time. Some possible validity checks for both the INS and the GPS are described.

The Kalman filter is optimised for long periods of propagation without measurement updates. The measurement and time updates use the U,D Covariance Factorisation method for numerical stability.

The instrument error states are not fed back to the INS in order to prevent degradation of the INS performance in the event of corruption of the state estimates due to the use of bad measurements.

The state estimates are retained until the next flight when they are used to update the INS instrument error corrections. This permits the tracking of long-term changes of the instrument characteristics.

The vertical channel integration is carried out in a separate filter to reduce the memory and computational requirements. GPS data is combined with INU vertical acceleration, barometric altitude and radar altitude to provide corrections to the INS vertical velocity and height and also estimates of the barometric bias and scale factor errors.

The outputs of the Kalman filter are also used to assess some aspects of the sensor performance and allow soft failures to be detected in the INS instruments and the GPS receiver. Additional data recorded by the integrated system assists in the assessment of possible sensor failures thus reducing the mean-time-to-repair of the overall system.

The hardware configuration is determined largely by the redundancy requirements as well as the need for each sensor to produce navigation outputs independently of the others. This results in a multi-MRU system with very good reversionary characteristics. It uses a 1553B bus for data transfer within the Integrated Navigation System and can interface with a wide variety of other aircraft systems.

The elements developed for this Integrated Navigation System provide the basis for a flexible system which is capable of considerable expansion via the 1553B data bus and which can be tailored to suit a broad range of integration and navigation functions.

REFERENCES

1. Carlson, N.A. "Federated Square Root Filter For Decentralized Parallel Processes" Proc NAECON, May 1987.
2. Carlson, N.A. "Distributed Filtering" ION-GPS-88, September 1988.
3. Bierman, G.J. "Factorization Methods For Discrete Sequential Estimation", 1977.

ACKNOWLEDGEMENTS

Several people helped with the writing of this paper, in particular G Gordon and I Morrison who contributed material on the Kalman Filter and the INS software.

①

COMPONENT PART NOTICE

THIS PAPER IS A COMPONENT PART OF THE FOLLOWING COMPILATION REPORT:

TITLE: Kalman Filter Integration of Modern Guidance and Navigation Systems.

TO ORDER THE COMPLETE COMPILATION REPORT, USE AD-A214 284.

THE COMPONENT PART IS PROVIDED HERE TO ALLOW USERS ACCESS TO INDIVIDUALLY AUTHORED SECTIONS OF PROCEEDING, ANNALS, SYMPOSIA, ETC. HOWEVER, THE COMPONENT SHOULD BE CONSIDERED WITHIN THE CONTEXT OF THE OVERALL COMPILATION REPORT AND NOT AS A STAND-ALONE TECHNICAL REPORT.

THE FOLLOWING COMPONENT PART NUMBERS COMPRISE THE COMPILATION REPORT:

AD#: P005 817 thru AD#: P005 822

AD#: _____ AD#: _____

AD#: _____ AD#: _____

Accession For	
NTIS GRA&I	<input checked="" type="checkbox"/>
DTIC TAB	<input type="checkbox"/>
Unannounced	<input type="checkbox"/>
Justification	
By _____	
Distribution/	
Availability Codes	
Dist	Avail and/or Special
A-1	

DTIC
ELECTE
NOV 16 1989
S E D

This document has been approved
for public release and sale
distribution is unlimited.

The Development of Mission-Specific Advanced Inertially-Based Avionics Systems

D.F. Liang, Head, Electromagnetics Section
D.J. DiFilippo, Project Scientist
Defence Research Establishment Ottawa

Shirley Bay
Ottawa, Canada K1A 0Z4

SUMMARY

The Defence Research Establishment Ottawa has been involved in the development of several mission-specific airborne inertially based multi-sensor integrated avionics systems.

More specifically, DREO has successfully completed the Phase II development and flight trial evaluation of an airborne Synthetic Aperture Radar Motion Compensation System (SARMCS). To achieve high resolution, high contrast and low geometric distortion in synthetic aperture radar imagery, it is necessary to apply accurate motion compensation to the radar returns. The hardware configuration consists of a ring laser gyro inertial navigation system, a doppler radar, a baroaltimeter and a specially designed strapped-down Motion Compensation Inertial Measurement Subsystem (MCIMS).

The Department of National Defence is also undertaking a program to develop and flight test a Helicopter Integrated Navigation System (HINS) which can satisfy the operational requirements of Canadian New Shipborne Aircraft (NSA). The roles of this maritime helicopter include search and rescue, Anti-Surface Surveillance and Targeting (ASST), Anti-Submarine Warfare (ASW), and Anti-Ship Missile Defence (ASMD).

This lecture will describe the development of appropriate Kalman filters to integrate the selected avionics configurations. Design objectives, configuration definition, simulation analysis and some flight test data are presented.

1.0 INTRODUCTION

Modern avionics systems are becoming increasingly sophisticated as the demands for better mission performance and the scope of applications continue to escalate. These mission requirements are being imposed in a cost/weight/performance conscious environment. The Defence Research Establishment Ottawa (DREO) has been involved in the development of several mission-specific airborne inertially-based multi-sensor integrated avionics systems. In this paper, we will specifically describe how DREO has applied the Kalman filtering technology to the development of a Helicopter Integrated Navigation System (HINS)* and an airborne Synthetic Aperture Radar Motion Compensation System (SARMCS).

Even though these two projects apply essentially the same technology and utilise similar sensors, the mission requirements are drastically different. In the case of the SARMCS, there was initially significant doubt that the mission objectives could ever be satisfied with the state-of-the-art technology, given the extremely stringent accuracy requirements specified. Therefore, the Phase I Feasibility Study first focussed on the analysis of performance accuracy requirements and error budget determination, followed by a system configuration design and simulation. Even with the successful completion of the Phase I study, it was still uncertain that the extremely encouraging simulation results could actually be achieved in a realistic flight environment. In order to verify the feasibility of the design objectives before a much larger amount of resources was committed, a Phase II Post Flight Evaluation Analysis Program was carried out in advance of the Phase III Real-time Prototype System Development. Even though this lengthened the overall development schedule, it was felt necessary in view of the risk involved.

In the case of the HINS project, there were available various types of off-the-shelf navigation subsystems, so that a large number of equipment configurations could be designed to possibly meet the specified mission requirements. In this case, the typical approach is to use previous experience in selecting two or three candidate configurations in an ad hoc manner. This has the potential danger of eliminating good alternatives early in the project, possibly resulting in a suboptimal configuration. Thus, DND (Department of National Defence) decided to utilise a significant portion of the navigation system development time to simulate and study a number of potential configurations with the aim of identifying, developing and testing an integrated navigation system which best satisfied the requirements established for the project.

The HINS approach to achieve this aim was to have the project divided in two phases. In the Phase I System Definition and Design, extensive work was initially directed towards the collection of data describing potential navigation equipment for the maritime warfare helicopter. This data base was used in an Integrated System Evaluation Program (ISEP) to generate a large number of navigation system sensor configurations. From these, several configurations were selected as candidates for a more detailed simulation study. Performance assessments of the candidate configurations were conducted using Monte Carlo and covariance analysis techniques. At the end of Phase I, a preferred configuration

* HINS is a registered Trade Mark of the Canadian Department of National Defence

AD-P005 820

was recommended for subsequent Phase II development. In the Phase II ADM Development, which is still ongoing, the objective is to realize the Phase I recommended system design by constructing and developing through ground and flight testing a HINS Advanced Development Model (ADM). The system software developed in the Phase I study is to be further refined before implementation in a MILSPEC qualified processor. All the necessary interfaces between the processor, operator and sensors are to be developed including the operator interface control, area navigation, data display and fault detection, isolation and reconfiguration functions. The resulting system will be subjected to an extensive series of ground and flight tests for the validation of its development design.

2.0 SYNTHETIC APERTURE RADAR MOTION COMPENSATION REQUIREMENTS AND SYSTEM DESIGN

To attain high quality airborne imagery for the AN/APS-506 radar, it is essential that very accurate motion compensation be applied to the radar returns to account for deviations of the radar phase center from a smooth reference path, chosen a priori. The main task of the SARMCBS is to determine spurious high frequency deviations from the desired motion along the reference path; these displacements are used by the SAR processor to adjust the relative alignment and phase of the radar returns, after which it removes low frequency (quadratic) errors by autofocusing, which amounts to fitting a quadratic phase adjustment to the radar returns across the synthetic aperture to maximize a specified measure of image contrast.

2.1 Motion Compensation Requirements

There are two main modes of SAR operation. In spotlight mode, the antenna is aimed at the designated target (Figure 1) or specified coordinates, and wide bandwidth radar pulses are emitted. In the strip-mapping mode, the orientation of the radar boresight is held constant approximately at right angles (Figure 2) to the nominal flight path, thus illuminating a swath to the side of the aircraft.

For airborne SAR processing, the ideal situation is that the radar antenna, mounted on the aircraft, moves along a straight line in space, transmitting and receiving pulses at equally spaced intervals along this path, which forms the synthetic aperture. However, in general, the actual path of the antenna will deviate from the nominal path due to aircraft turbulence, autopilot inaccuracies, etc. These spurious motions, if uncompensated, can severely degrade the SAR image. The function of the motion compensation system is to sense the antenna motion, and compute the deviations between the actual path and the nominal path. This information is then used to correct the phase of the radar returns so that, ultimately, as far as the radar processor is concerned, the pulses look like they were emitted at these ideal points along the nominal track.

2.2 Performance Accuracy Requirements

Since this project is in support of the development of a SAR radar capability, the performance requirement for motion compensation has been specified in terms of power spectral density (PSD) of the tolerable error in measurement of the displacement of the antenna phase center along the radar line-of-sight (LOS) (Figure 3). The displacement error spectrum has been divided into two components. The portion of the PSD below A Hz lies in the "Don't-Care Region". This contains the components of the displacement error which have characteristic times longer than the maximum aperture time of T seconds (A Hz = $1/T$ seconds). Displacement error components having frequencies above A Hz must be controlled by the motion compensation system. An estimate of the RMS magnitude of the allowable displacement error measured over the scene is:

$$\delta r = 0.33 \text{ mm (RMS).}$$

This is the residual displacement error along the LOS to the target not including contributions from constant and linear components of displacement error, which have no effect on image quality, or quadratic components which are removed by the autofocusing.

The displacement error components above A Hz affect the contrast of the SAR image while those below A Hz degrade resolution and produce geometric distortions of the image. Although the lower frequency components within the "Don't-Care" region may affect the SAR image quality, this error component is to be controlled through the autofocusing algorithm. Therefore the SARMC project only considers error sources above the A Hz region. It should be emphasized that during the early phase of the design study, it was felt that the performance requirement of the order of a millimeter would not likely be achieved in a practical situation as there are a large number of practical design variables which could easily overwhelm this level of accuracy requirement.

2.3 Analysis of Error Sources

In view of the extremely stringent accuracy requirement, primary design consideration was concentrated on estimating the magnitude of the contribution of major system error sources to the residual LOS displacement error. The following error sources were considered:

uncompensated phase center motion due to antenna pointing errors

- . computational and related errors arising from the imperfect solution of the strapdown motion compensation equations
- . gyro and accelerometer errors of the strapdown IMU
- . attitude errors of the strapdown navigator

The analysis indicated that the principal sources of error in computing the LOS displacement are the mislevels of the strapdown navigator, the error in determining the initial depression angle of the target LOS, computational errors in navigation and targetting algorithms, error in the measured relative azimuth of the strapdown IMU and the radar antenna boresight, and errors in the accelerometers and gyros. From the results obtained for the required aperture under conditions of medium turbulence, the error budget of Table 1 was drawn up.

Table 1: ERROR BUDGET

Error Source	Max. Contribution to RMS (mm)	%
1. Sensor errors		
-accelerometer	0.02	0
-gyro	0.09	8
RMS TOTAL (sensors)	0.09	8
2. Computational errors	0.10	9
3. S/D heading error	0.02	0
4. S/D mislevels	0.18	30
5. S/D azimuth alignment	0.05	2
6. Azimuth angle encoder	0.05	2
7. Interpolation errors	0.10	9
8. Initial depression angle	0.15	20
9. Contingency	0.15	20
RMS TOTAL (all)	0.33	100

2.4 SARMCS System Configuration

The SARMCS instrumentation that was designed and installed on board the National Aeronautical Establishment (NAE) Convair 580 aircraft for Phase II is shown in Figure 4. The system configuration consists of:

- a) a ring laser gyro inertial navigation system, denoted the master INS, which is located about three metres from the aircraft center of gravity,
- b) a Doppler radar employing a strapdown three-beam lambda configuration,
- c) a specially designed strapdown inertial measurement unit, denoted as MCIMS (Motion Compensation Inertial Measurement Subsystem), which is located about 50 centimetres from the SAR antenna phase centre,
- d) air data sensors including a static air pressure transducer along with an air temperature probe to determine barometric altitude.

The simplified block diagram of Figure 5 shows the SARMCS functions. All of the blocks within the dotted line are software modules which together comprise the motion compensation processor. The primary sensor is the MCIMS which accurately measures rotational and translational motions. This unit is mounted on the SAR antenna in the nose of the aircraft to provide as direct a measurement as possible of the antenna motion. The raw measurements from the strapdown unit are processed in a strapdown navigator algorithm to yield antenna position, velocity and attitude. This information is then used in a targetting algorithm to generate motion corrections for the radar returns. These include, in addition to phase corrections, adjustments to the radar pulse repetition frequency and range gate slewing to account for aircraft motion. The air data is used to compute baroaltitude which is needed to stabilize the vertical channel in the strapdown navigator. Outputs from a Doppler velocity sensor and a master inertial navigation system on board the aircraft are fed into a Kalman filter algorithm along with outputs from the strapdown navigator. The Kalman filter optimally integrates this information and estimates the errors in the various sensors. The net effect is a transfer of alignment from a Doppler-damped master INS to the strapdown navigator. The error estimates for the strapdown navigator are fed back into the strapdown algorithm and used there to correct the relevant parameters. This error control scheme utilizing the Kalman filter is designed to prevent a build-up of long-term levelling errors commonly referred to as tilts in the strapdown platform which, as indicated in Table 1, are important contributors to motion compensation errors.

2.5 SARMCS Simulation Software

The SARMCS simulation software is divided into 3 separate packages:

- a. The Data Synthesis Package generates realistic synthetic data from the system error models which include
 - . strapdown IMU model
 - . Master INS model
 - . Doppler radar model
 - . Atmospheric pressure and temperature models
- b. The Data Processing Package can process both synthetic and real sensor data. It implements the motion compensation processor of Figure 5, which includes
 - . strapdown navigation and sensor compensation algorithms
 - . barometric altitude algorithm
 - . Kalman filter
 - . targetting algorithms
- c. The Evaluation Package evaluates the performance of the processing package by comparing computed master and strapdown navigator positions, velocities and attitudes with corresponding accurate reference data generated by the Synthesis Package.

2.6 Kalman Filter Design

A baseline 35 state Kalman filter was developed to indicate the best level of achievable performance. The filter is mechanized using Bierman's U-D factorized formulation [1]. The filter structure is implemented in such a way that arbitrary subsets of the full error state vector may be selected for a particular run by specifying values for input parameter tables. Similarly any subset of measurements may be selected. This results in a very flexible design tool. An error control routine uses position, velocity and misalignment error state values to correct position, velocity and attitude estimates of the strapdown navigator after each filter update, unless the update occurs during a SAR window. The corresponding error states are zeroed after executing error control.

The complete set of error states is specified in Table 2. The measurements used to obtain the baseline filter simulation results presented in the next section are given in Table 3. Additional measurements were mechanized, namely: master/strapdown velocity matching, as well as 2-dimensional versions of all the position and velocity matching measurements, constructed in the level components of the wander azimuth coordinates.

2.7 Sub-Optimal Kalman Filter Design

For practical implementation, a suboptimal 21 state Kalman filter was designed. The error state vector is described in Table 4.

The error dynamics of the system states in subvectors x_m and x_s are modelled in the Kalman filter using the general propagation equations for a ϕ angle (true frame) inertial error formulation [2] resolved in a wander azimuth frame. The augmenting states in x_{m1} , x_{d1} , and x_{s1} , which represent time-correlated errors in the various instruments, are modelled as first-order Markov processes.

The modelling of relative strapdown (S/D) system errors instead of absolute S/D system errors in the state vector is a design decision that is motivated by several considerations. First, from a theoretical viewpoint, this is an appropriate choice because measurements constructed by comparing information from two systems with the same error dynamics only allow observability of the relative error between the two systems. A practical motivation for modelling relative S/D errors is that for this case where S/D instrument errors are expected to be much larger than master INS instrument errors, it can be shown that the estimation of x_m and x_{s1} is essentially decoupled from the estimation of x_{m1} , x_{d1} and x_{d1} , in the sense that no significant correlation develops between these two sets of subvectors during Kalman filter operation. This behaviour is mathematically equivalent to having two independent Kalman filters, one of which accomplishes transfer-of-alignment from the master to the S/D platform while the other performs Doppler-damping of master errors. This is a robust configuration in that the effects of slight mismodelling of the lower quality S/D IMU in the Kalman filter cannot feed back through the velocity matching measurements to corrupt the estimation of master system errors.

One feature of the SARMCS Kalman filter that noticeably distinguishes it from a navigation-type Kalman filter is the absence of measurements that bound the inertial position error. This is a direct consequence of tailoring the Kalman filter for the specific task of performing accurate S/D platform alignment. The presence of S/D position errors have only a relatively weak effect on the buildup of

platform misalignments and velocity errors, so there is no need to accurately estimate them in the SARMCS. In fact, S/D position states are dropped altogether; the use of the ϕ angle error formulation for the Kalman filter inertial error models conveniently allows this to be done without impacting on the filter's ability to estimate S/D velocity errors and platform misalignments from the velocity matching measurements.

It is worthy to note that the choice of augmenting states in the SARMCS Kalman filter is based primarily on the criterion of observability. The states in x_{mi} , x_d and x_{gi} represent only those significant instrument errors that are separately observable with the given measurements.

2.7.1 Measurement Modelling

The Kalman filter processes a set of four measurements every 10 seconds to update the state vector and associated error covariance matrix. Two master-Doppler velocity matching measurements are formed from the x and y components of the following vector velocity difference, coordinatized in the aircraft body frame:

$$V_{md} = V_m - V_d + \omega \times L_{md} \quad (1)$$

where V_m is master indicated velocity, V_d is Doppler indicated velocity, ω is aircraft angular rate and L_{md} is the lever arm from the master INS to the Doppler antenna. The other two measurements are master-S/D velocity matching measurements calculated as the x and y components of the following vector velocity difference, coordinatized in the wander azimuth frame:

$$V_{ms} = V_m - V_s + \omega \times L_{ms} \quad (2)$$

where V_s is S/D indicated velocity, L_{ms} is the lever arm from the master INS to the antenna-mounted IMU and V_m and ω are as defined for (1). The Kalman filter measurement model is derived by perturbing (1) and (2) and expressing the results in terms of the modelled error states.

3.0 SARMCS SIMULATION AND FLIGHT TEST VERIFICATION

The mission profile for the simulation is shown in Figure 6. It is consistent with the flight tolerance limits of the CV 580 research aircraft. It involves an initial climb to an altitude of 1000 metres, followed by a racetrack manoeuvre after 10 minutes and an s-turn 20 minutes after takeoff. This is followed by a period of nominally straight and level flight during which 23 SAR apertures are simulated. About 1 hour after takeoff, a second s-turn is carried out to control the strapdown navigator heading error. This is followed by another section of straight and level flight during which 9 more SAR apertures are simulated. All simulation results are obtained using the baseline Kalman filter design unless otherwise stated.

3.1 Simulation Results

Figures 7 to 9 show the north velocity, roll and heading errors of the strapdown navigator, together with RMS values computed from the Kalman filter error covariance. The pitch error has similar characteristics to those of the roll error. Notice that the 1σ bound of the roll error conforms well with the single run error trace. In Figure 9, the heading error RMS is reduced to the level of master heading error after the second s-turn.

Figures 10 and 11 show the LOS displacement error before and after autofocusing. The performance is well within the stated requirements.

Simulation results indicating the performance of the suboptimal 21 state filter are shown in Figure 12. This plot depicts the roll errors of the strapdown navigator, as well as the filter predicted 1σ value. From comparison of Figure 12 to Figure 8, the performance of the two filters is quite similar except for brief periods during aircraft manoeuvres.

3.2 Flight Testing Philosophy

The philosophy for flight testing the SARMCS system involves validating the correct operation of subsystem configurations which increase in complexity until the complete configuration is attained. This type of approach provides a systematic method for detecting and isolating unexpected error sources in the hardware and/or software functions. There are five sequential steps in this flight test plan:

- 1) evaluate the performance of the Master/baro subsystem.
- 2) evaluate the performance of the MCINS/baro subsystem,

- 3) evaluate the performance of the Master/Doppler/baro/ subsystem,
- 4) evaluate the performance of the Master/Doppler/baro/MCIMS subsystem,
- 5) evaluate the performance of the full SARMCS with all SARMCS sensors utilized.

In the first four steps, the subsystems are tested to verify that their velocity accuracies are consistent with expected values predicted by the earlier simulations. A flight reference system (FRS) is used to provide the "truth" data for evaluation of these subsystems. The FRS employs an extended Kalman filter which optimally integrates precision microwave ranges from a Del Norte Triponder system with information from an LTN-91 inertial navigation system. For the FRS, three ground transponders are positioned at surveyed locations. They provide a rectangular coverage area of width 45 kilometres and length 130 kilometres within which at least two ranges with good geometry are received by the aircraft. Under these conditions, the FRS provides continuous aircraft velocity information accurate to 0.1 metres/second and position information accurate to 10 metres. This accuracy is sufficient for evaluating these subsystems since velocity errors in the order of 1 metre/second are expected.

After it has been verified that the various subconfigurations are operating properly, the final step involves testing the full SARMCS configuration by applying motion corrections computed by the SARMCS system to spotlight SAR data. The extent to which the SAR image is enhanced is the ultimate indication of the performance of the SARMCS.

3.3 Flight Test Results

Currently, neither motion compensation nor SAR processing are implemented in real-time. Instead, the radar data, recorded on high density digital tape, and the raw navigation data, recorded on computer compatible tape, are processed in a ground-based facility. As a first step in the processing, motion compensation vectors are generated and applied to the radar data, and then the actual SAR processing is done.

Figures 13 to 16 indicate the performance of the SARMCS using the suboptimal Kalman filter. Figure 13 shows the motion compensated SAR image of essentially a point scatterer. The target is a satellite receiving station's 10 meter reflector-type antenna, equipped with a dual frequency S/X-band feed. The X-band feed was short circuited in order to provide a strong reflection from the antenna. In this type of display, the vertical scale is signal amplitude, one horizontal scale is distance along the radar line-of-sight, and the other horizontal scale is distance perpendicular to the radar line-of-sight. Theoretically, the SAR image for a point target should be one sharp peak, which is fairly close to what is being achieved in this image.

Figure 14 shows the same radar data but processed without motion compensation. Here, it is apparent that the effect of spurious uncompensated aircraft motion is to cause energy from the main peak to spill out into side lobes. The implication of this for a more typical image containing many point targets is that weaker targets in the vicinity of stronger ones might be completely obscured by this sidelobe energy; in optical terms, the resulting image would be described as having poor contrast.

Figure 15 shows a motion-compensated SAR strip map image taken of the Sudbury area in northern Ontario. The strip is about 650 metres wide and 1500 metres long. The area is near the nickel smelter in Sudbury that refines the ore from the surrounding mines. The dim lines are roads, and the brighter ones are railway tracks. The very bright lines are pipes that lead into a cluster of five circular storage tanks; the radar reflection off the circular edge of one of the tanks can be clearly seen in the image.

Again, Figure 16 shows the same piece of radar data but processed without motion corrections. The image is initially focused but then starts to smear out as the aircraft deviates from the nominal straight line track. In this case, the deviation is a result of a 2 degree change in aircraft heading. The pipelines can barely be distinguished in this image.

4.0 MINS MISSION REQUIREMENTS AND SYSTEM DESIGN

The roles of the military maritime helicopter include anti-submarine warfare (ASW), anti-surface ship targeting (ASST) and weapons delivery, ocean surveillance, and search and rescue. Many of the missions must be carried out at ultra-low altitudes under all weather and visibility conditions. The increased range, speed and accuracy of modern weapon systems impose stringent accuracy and reliability requirements upon the aircraft navigation system. To enhance mission success in a hostile environment, the flight crew needs to operate weapon systems, target acquisition and designation systems, radar detection, night vision systems and, perhaps, engage in air-to-air combat. The traditional manual dead reckoning task can no longer provide the required performance accuracy and would unnecessarily distract the flight crew from performing mission critical functions.

4.1 Mission Requirements

For the ASW mission the helicopter navigation system must maintain stable and accurate tactical plots over long periods of time. In the anti-surface ship targetting role, high orders of absolute and relative navigational accuracy are vital to rapid and successful action. There are further complicating factors as well. Operations must often take place under radio silence and shore-based or satellite navigation aids may be destroyed or jammed during wartime. The small crew of the helicopter must not be burdened with monitoring the functioning of, or updating, the navigation system. Consideration of these factors has led to the following minimum operational accuracy requirements:

I. Radial Position Error (95%):

- with external aids* 2.0 nautical miles (nm)**
- without external aids 1.5 nm/hr

II. Radial Velocity Error (95%):

- with external aids* 3.0 ft/sec**
- without external aids 4.0 ft/sec

III. Attitude Error (95%): 0.5 deg

IV. Heading Error (95%): 0.5 deg

*External aids are those systems such as Omega, Loran and the Global Positioning System (GPS) which rely upon transmitters which are located external to the aircraft and may be unavailable during wartime. INS, Doppler and Radar are representative of internal or self-contained aids.

** It is recognized that these performance levels can be exceeded by a large margin if, as expected, GPS is part of the HINS.

4.2 Mission Profiles

For the design of an advanced integrated navigation system, it is important to define the mission operational environment, since integrated system performance to some extent depends on the constraints and requirements of the navigation sensors in each stage of the mission.

Two representative mission profiles for the maritime helicopter have been developed for use during the HINS simulation studies. The first profile is typical of an ASW sonobuoy mission while the second represents an ASW convoy screening mission. The HINS flight test program would seek to follow flight profiles similar to these.

4.2.1 ASW Sonobuoy Mission (see Figures 17 and 18)

(1) Mission Alert: (10 minutes)

-aircraft power turned on, helicopter-destroyer at speed of 18 knots. A contact is detected by the ship sensors at a range of 90 nm and a bearing of 90 degrees to the ship's course.

(2) Launch and Climb: (10 minutes)

-climb at a rate of 800-1000 ft/min. to a cruise altitude of 5000 ft.
 -airspeed during climb 90-100 knots.
 -course 235 degrees.

(3) Enroute/Cruise: (45 minutes)

-course 235 degrees.
 -speed 140 knots, alt 5000 ft., distance flown 100-110 nm.

(4) Sonobuoy Pattern Drop: (25 minutes)

-drop altitude 5000', speed 90 kts.

-rate 1/2 turns (1.5 deg/sec), 15 deg bank angle.

-eight sonobuoys, 5 nm spacing.

(5) Orbit/Sonobuoy Monitor: (40 minutes)

-orbit altitude at 5000 ft., speed 70 kts, circular or racetrack pattern, may alternate direction.

-10 nm long orbits, 15 minute circuits.

(6) Localize/Additional Sonobuoy Drop: (15 minutes)

-contact passes between sonobuoys A and B.

-helicopter descends to 500 ft at 1000 ft/min, flies 7 nm downrange and inserts two additional sonobuoys at C and D.

-orbit at 500 ft for 10 minutes to monitor sonobuoys A, B, C and D.

(7) Magnetic Anomaly Detector (MAD) Run: (10 minutes)

-use MAD to obtain a precise fix on the target by flying 1000 ft diameter ovals at 200 ft alt, always flying in the same direction.

-speed 90 kts, rate 1 turns (3 deg/sec), 22 degrees of bank.

-straight and level re-fly over high probability area.

(8) Attack: (5 minutes)

-helicopter descends to 150 ft and releases torpedo.

(9) Transit Back to Ship: (50 minutes)

-climb to 5000 ft.

-transit speed 140 kts.

4.2.2. Convoy Screening Mission (see Figure 19)

The maritime helicopter provides close-in ASW screening support to task force operation in open ocean. Dipping sonar is used to search a moving sector formed by a 60 deg arc some 9-12 miles in front of the ships.

(1) Mission Alert: (10 minutes)

- aircraft power on.

(2) Launch/Climb/Enroute: (7 minutes)

-climb to 150 ft, transit 10 nm to the search sector and begin first sonar dip at point A.

-transit speed of 140 knots.

(3A) Sonar Dipping: (15 minute cycle)

-this dipping sequence is repeated continuously for the duration of the 4 hr mission, with sonar dip pts. at A, B and C within the sector.

-cruise velocity between dips is 90 kts.

-cruise altitude between dips is 150 ft.

(3B) Dipping Operation:

(a) - 700 to 1000 ft before dip point helicopter turns into wind with rate 1/2 turn. 15 deg bank, slows to 70 kts and descends to 150 ft altitude

(b) - transition to the hover at 50 ft altitude (max power setting, max vibration).

- lower sonar, hover at 50 ft for approximately 6 minutes.

(c) - retract sonar, move to next dip point at 70 kts and 150 ft altitude.

(4) Repeat Sonar Dipping Cycle 3B(b) and 3B(c) above

(5) Return to Ship: (10 minutes)

- velocity 140 kts.

4.3 Candidate Configuration Selection

A wide variety of types and brands of navigation sensors can contribute to meeting the mission requirements of maritime helicopters. The following list of generic navigation subsystems is considered to have merit in the HINS application:

Global Positioning System (GPS),
Inertial Navigation System (INS),
Attitude and Heading Reference System (AHRS),
Doppler Radar,
TACAN,
Omega,
Air Data System,
Strapdown Magnetometer,
Loran,
Radar Altimeter.

In order to make an intelligent selection of a preferred HINS configuration, much information about candidate subsystems is required for evaluation. Amongst the characteristics for which information was sought are:

- i) Performance (navigation parameter, accuracy, error characteristics)
- ii) Cost
- iii) Reliability (mean time between failure)
- iv) Weight, volume and power
- v) Commonality with in-service equipment
- vi) Suitability for helicopter environment

Other characteristics such as maintainability, logistics commonality with in-service equipment and helicopter suitability are being considered on a continuing basis throughout the study.

4.3.1 Evaluations Using Integrated System Evaluation Program (ISEP)

A computer-aided procedure called ISEP was developed during Phase I to systematically develop candidate configurations. ISEP generates a manageable number of configurations, lists the system characteristics and calculates the predicted performance of the integrated system. The many candidate configurations can then be quickly reviewed by the designer and a subset selected for detailed simulation and analysis. A block diagram representation of ISEP is shown in Figure 20. The simplified error models for all the sensors considered are described in Table 5. ISEP uses a simplified set of sensor error models in a covariance analysis routine to generate performance predictions for the HINS configurations. For example, initially simplified INS and AHRS error models were used to coarsely represent the error characteristics of medium accuracy INS and AHRS type subsystems, respectively.

One of the aims of the HINS Phase I project is to determine the optimum sensor configuration which satisfies the performance requirements. This does not necessarily mean that the optimum configuration will consist of those sensors which provide the highest level of accuracy. The trade-off of system accuracy with cost, reliability, weight and size must be considered during the equipment selection process. For example, in the selection of either an INS or AHRS, the ISEP can be effectively used to determine whether an AHRS can satisfy the mission requirements or the improved accuracy to be gained from using a more accurate INS is justified in light of the associated cost, reliability and weight penalty. In addition, due to the lower cost of running the ISEP than that of a detailed generalized covariance analysis program, it is possible to use ISEP to identify critical design elements that require special attention during the detailed simulation and analysis portion of the project.

Some of the issues which can be initially addressed using ISEP are

- i) the benefits of doppler aiding,
- ii) the effects of initialization errors,
- iii) mission profile sensitivity, and
- iv) the benefit of external aiding.

There are five main sets of data which ISEP requires to generate the candidate configurations:

- a) Mission requirements - performance specifications
- b) Sensor characteristics - cost, MTBF, weight, etc.
- c) Mission profiles - used to generate trajectories

- d) Sensor error models
- e) Selection criteria - weight or volume limits, etc.

4.3.2. ISEP Evaluation Results

The ISEP output data for a sample candidate configuration is shown in Table 6. The candidate HINS performance was evaluated by ISEP for both the aided mode of operation (externally referenced sensors such as GPS or Omega were contributing to the solution) and the unaided mode. It should be noted that unaided mode performance was evaluated assuming the availability and use of the Doppler velocity sensor.

The figure of merit for the unaided performance is the least squares fit of the radial position error rate in nautical miles per hour (95%). The figures of merit for the aided performance are the maximum and average radial position error in nautical miles (95%). In all cases the calculated figures of merit are for two dimensional (level axes only) position errors.

The ISEP simulation results are of course dependent on the types of sensor error models and mission profiles considered. There was significant uncertainty regarding how closely the performance predictions using these simplified models match the true performance of the system under consideration. Therefore, it was felt necessary to generate pessimistic as well as optimistic ISEP performance results in addition to the nominal results. In this simplified performance evaluation, the Doppler and Omega errors are represented by three different sets of parameters as shown in Table 7 to provide us with the envelope of performance results. The pessimistic values were chosen to represent reduced-order suboptimal filter design and the use of poorer quality sensors. The optimistic values were selected to represent the limit of achievable performance.

In addition, it was found that the performance results of both the unaided and aided configurations depend very much on the condition of initial alignment. Therefore, three sets of initialization conditions were assumed (Table 8) to represent the ground fine alignment, shipboard fine alignment and in-air alignment. The initial conditions specified for shipboard fine alignment assumed much poorer initial velocity and position accuracy figures than those specified for ground fine alignment.

As a whole, the ISEP results indicate that all configurations considered can fully satisfy the weight and cost objectives, and it is unlikely that the Omega subsystem could provide accurate enough external references to meet the maritime warfare helicopter performance requirements. Based on the ISEP results, a decision was made to proceed with the selection of GPS and totally discard Omega from further design consideration.

In reviewing the ISEP results it was clear that the performance results of an integrated system using AHRS depends heavily on the mission profiles, initialization conditions and the extent of GPS availability. This implies that the filter design of an AHRS/Doppler/GPS integrated system should be subject to much more stringent performance and sensitivity analyses than the design of the INS/Doppler/GPS integrated system. In order to have a more complete Phase I study and to ascertain the selection of the best integration configuration for HINS, it was felt necessary to proceed with more detailed covariance analysis and Monte Carlo simulations on two candidate configurations. They are categorized as medium and high options, roughly based upon their cost and performance as follows:

Medium Option Configuration

AHRS/Doppler/GPS

High Option Configuration

INS/Doppler/GPS

5.0 SIMULATION ANALYSIS AND RECOMMENDATION

5.1 Simulation and Performance Analysis

To properly analyze the performance of various candidate configurations, a versatile simulation package was developed. Since the fidelity and performance prediction of these configurations are of prime importance, a substantial portion of this development project was expended generating complete and accurate error models. These activities are described as follows:

- a) Generate the navigation sensor error models.
- b) Develop the integration algorithms to blend the sensor outputs.
- c) Generate a set of mission profiles to be used for trajectory generation.
- d) Develop control and display software.
- e) Develop diagnostic software to detect sensor failure.

In the detailed simulation analysis both covariance analysis and Monte Carlo simulation software were used. Covariance analysis software is effective for the design of integration filters because it provides ensemble statistical data. Because ensemble statistics are the outputs, covariance analysis can (in many circumstances) reduce the need for computationally intensive Monte Carlo simulations. This statistical information can be used to assess candidate Kalman filter designs and to project the performance of a particular navigation system configuration. Covariance analysis is very useful for assessing the effects of mismatch between the filter design model and the "real world" or truth model. In addition, it can be readily used to establish error contribution tables and error budgets which let the filter designer focus in on the major error contributors.

However, Monte Carlo simulation also has its place in the design of suboptimal Kalman filters. Simulation can be particularly effective in assessing the effect of nonlinearities which are difficult to address in the covariance analysis framework. Also, certain types of mismatches between the Kalman filter model and the truth model are more conveniently addressed with the simulation program than with the covariance program. An example of this is the sensitivity assessment of the effect of sea current correlation time mismatch.

Another area in which the Monte Carlo simulation has been of more use than the covariance analysis program has been in the investigation of the effects of unmodeled manoeuvre-dependent sensor errors. Specifically, the AHRS based HINS simulation made apparent undesired responses of the filter's sensor error states to disturbances, caused by unmodelled sensor errors. Finally, covariance analysis software will never be able to replace the function of simulation software for final checkout of Kalman filter code.

Detailed simulation and error models for all the relevant navigation equipment and environmental disturbances (wind, sea currents) have been developed for the performance evaluation and sensitivity analysis. Table 9 presents a summary of typical error models and performance parameters for several navigation subsystems and sensors.

Figure 21 shows the 95% percentile radial position, velocity and relative velocity errors of the F3 RLG and DTG AHRS configuration with GPS for the sonobuoy mission. With all sensors/subsystems fully operational, the performance of the two configurations are essentially the same, both satisfying all HINS performance goals. This is because GPS dominates the navigation solution providing a highly accurate reference for control of system position, velocity and altitude errors.

Figure 22 compares the radial position errors of the RLG and AHRS configurations without GPS for the entire sonobuoy mission. As would be expected, the performance of the RLG based system is clearly superior to the AHRS configuration, with an 95 percentile error rate limited to 0.9 nm/hr over the entire mission primarily due to the superior performance of the RLG. The difference in performance of the two configurations is most pronounced in the first hour, in which the helicopter normally flies a constant heading while transiting to the area to be investigated. Here, the 95 percentile error rate of the AHRS based system is approximately 5.2 nm/hr. The position error is reduced dramatically, from 4.2 nm to 2.8 nm, after completion of the transit leg following execution of a turn into the search area.

Figure 23 shows the radial position and relative velocity errors of the RLG and AHRS system. The performance of the AHRS based configuration is only slightly worse than that of the RLG based HINS, because both systems obtain substantial calibration during the period in which GPS is available, and subsequent to the outage, doppler velocity data is heavily relied upon to produce the indicated performance.

5.2 Recommended ADM Configurations

Based on the evaluation of many more detailed simulation results, the system configuration of Figure 24 is recommended for subsequent Phase II development. The main hardware items in the HINS ADM are:

- Honeywell H 423 F3 INS
- Rockwell-Collins 3A 5-channel p-code receiver
- Canadian Marconi AN/APN-235 4-beam Doppler Velocity Sensor (DVS)
- Pacer Air Data Sensor (ADS)
- Develco 9200 C strapdown magnetometer
- JET 204 L Vertical Gyro (VG)
- DY-4 M68020 Navigation Computer

As shown in Figure 24, the navigation bus interfaces the primary sensors (INS, GPS, DVS) with the navigation computer system (NCS), which contains the Integrated Navigation Software. The ADS and VG interface directly to the NCS via an AHINC 429 interface, and the magnetometer via an analog interface. The Control Computer System (CCS), which serves as a smart interface between the NCS and the Control Display Unit (CDU), is connected to the NCS by a second 1553 B data bus. It should be noted that the back-up VG and magnetometer can be replaced by a low cost AHRS.

The principal reasons for recommendation of the SNU 84-1 F³ RLG INS over the DTG AHRS are its reliability and its performance. Greater MTBF for the RLG INS is expected to make the life cycle cost difference between the INS HINS and the AHRS HINS smaller than the acquisition cost difference. Furthermore, the MTBF advantage of the RLG INS will improve the operational readiness of the HINS-equipped ASW helicopter.

The performance advantage of the RLG INS based HINS is important only in degraded operational modes (Figure 25). However, it is considered likely that the HINS will be required to operate without Doppler radar under certain conditions. In this situation, if GPS becomes unavailable for any reason, the INS based HINS will provide much better navigation accuracy than the AHRS based HINS.

Disadvantages of the RLG INS based HINS are its greater weight and volume, and its larger acquisition cost. Should the approximately 25-30 lbs weight difference of the two inertial measurement units become critical for HINS, then the AHRS based HINS might be the best choice. A similar comment applies to the volume difference between the two subsystems.

The cost difference issue is more complex, in part because of the effect of MTBF on life cycle cost. However, another factor to be considered is production quantity. Due to the relatively small number of inertial measurement units that would be purchased for HINS, there are substantial cost advantages to be gained using navigation equipment that has other high volume applications. The SNU 84-1 RLG INS is expected to achieve very large (compared to HINS) production quantities, which would be beneficial in terms of HINS costs.

A Doppler radar velocity sensor has been recommended for HINS rather than a Doppler navigation system. The Doppler velocity sensor meets all basic requirements of the HINS application. Although purchase of the navigation system version for HINS would have some benefits, they do not appear to outweigh the cost and weight penalties.

A 3-channel P-code GPS receiver for HINS was recommended, which will provide highly accurate position and velocity data (nominally 50 ft (RMS) and 0.3 ft/s (RMS) respectively). These data are used by the Kalman filter to align the inertial sensors for enhanced free-inertial operation should GPS fail or be unavailable at some point in a mission.

An 18-state Kalman filter design has been recommended for the INS-based HINS. A filter of this size appears to be a good compromise between performance and airborne processing capabilities. The state variables are:

- . x,y position errors (wander azimuth)
- . x,y velocity errors (wander azimuth)
- . x,y,z platform misalignments (wander azimuth)
- . x,y accelerometer biases (body)
- . x,y,z gyro biases (body)
- . DVS x scale factor error
- . DVS z boresight error
- . north, east sea currents
- . north, east winds

The measurements used in this filter are:

- . 3-D DVS velocity
- . 2-D GPS position
- . 2-D GPS velocity
- . 2-D ADS velocity
- . 2-D operator entered position
- . 2-D SINS velocity

The Doppler measurements are corrected for wind blown water motion based on operator entered surface wind velocity, by a means similar to that of [3]. The default mode of operation of this filter is for over-water use. A transition to over-land flight is indicated by an Over Land/Water discrete and appropriate changes to the filter made.

The measurements are constructed in a prefilter which runs at 1 Hz. Every ten prefilter cycles the averaged measurements are sent to the Kalman filter. The corrections produced by this filter are suitably modified and used either in correction of the outputs of the INS in open-loop operation, or in resetting the INS in in-motion alignment or in closed-loop navigation.

6.0 CONCLUSIONS

In this lecture, we have presented two distinct mission-specific inertially-based integrated navigation system development projects. In the SARMCS, we have shown how a high-risk development project can be best handled with careful attention to detailed assessment of key error sources and with a well-planned sequence of steps in the development and flight test evaluation plan. In the HINS, we have dedicated significant development effort in modelling, simulation and trade-off studies. The

performance of the candidate configurations were carefully evaluated through Monte Carlo and covariance analysis with specific attention to mission profiles. The future prospect for the SARMCS looks very promising. The SARMCS development, as well as the entire SAR spotlight mode development project, is on schedule to be completed in time for the CP-140 long range patrol aircraft radar update in the mid-1990's. The HINS is expected to be installed on all Canadian NSA helicopters. This technology not only can be used to produce a modern high performance robust navigation system for Military Marine helicopters, but also is flexible enough for application to other integrated navigation requirements.

REFERENCES

1. G.J. Bierman, Factorization Methods for Discrete Sequential Estimation, New York: Academic Press, 1977.
2. D.O. Benson, "A Comparison of Two Approaches to Pure Inertial and Doppler-Inertial Error Analysis," IEEE Trans. on Aerospace and Electronics Systems Vol. AES-11, No 4, July 1975, pp. 447-455.
3. M. Kayton and W.R. Fried, ed., Avionics Navigation Systems, John Wiley and Sons, 1969, p. 265.

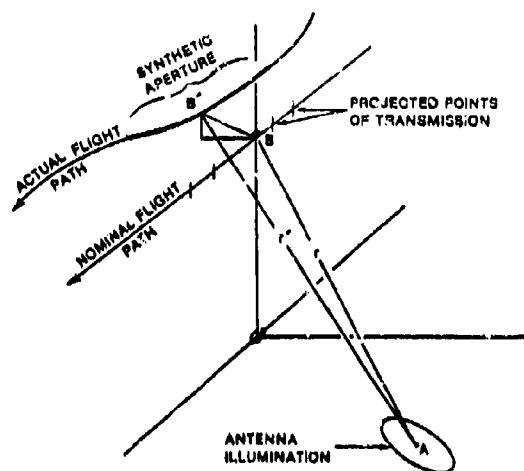


FIGURE 1: SPOTLIGHT SAR GEOMETRY

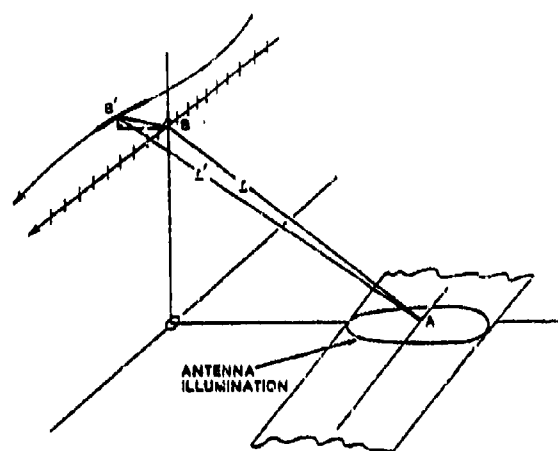


FIGURE 2: STRIPMAPPING SAR GEOMETRY

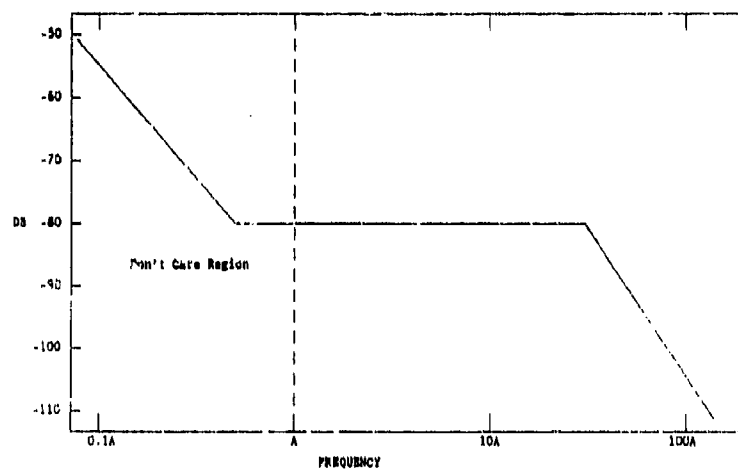
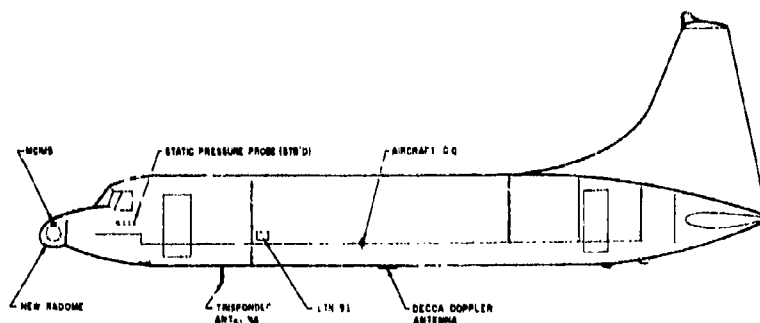
FIGURE 3. NORMALIZED POWER SPECTRAL DENSITY OF TOLERABLE ANTENNA
PHASE CENTRE DISPLACEMENT ERROR

FIGURE 4: LOCATION OF SARMC INSTRUMENTATION ON THE NAE CONVAIR 580.

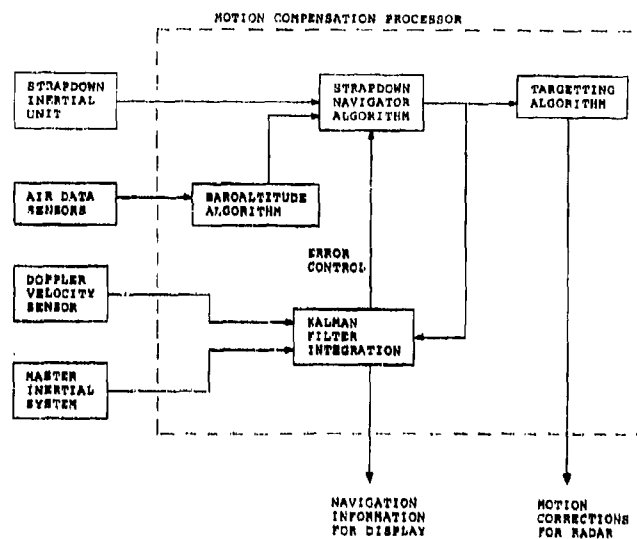


FIGURE 5: BLOCK DIAGRAM OF SARMC SYSTEM.

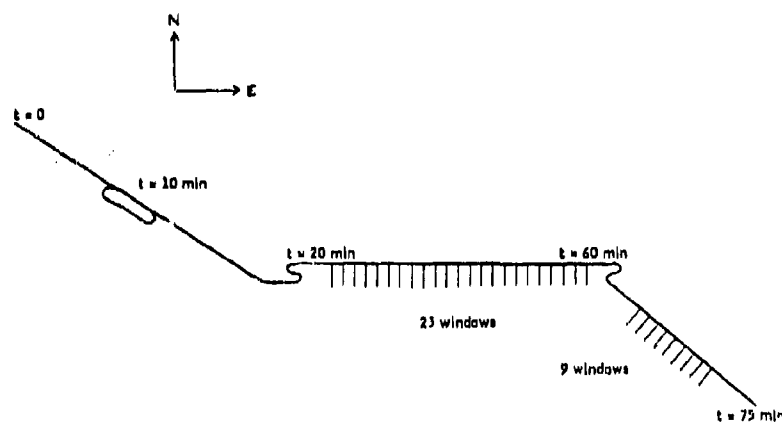


FIG. 6: SAR MISSION PROFILE

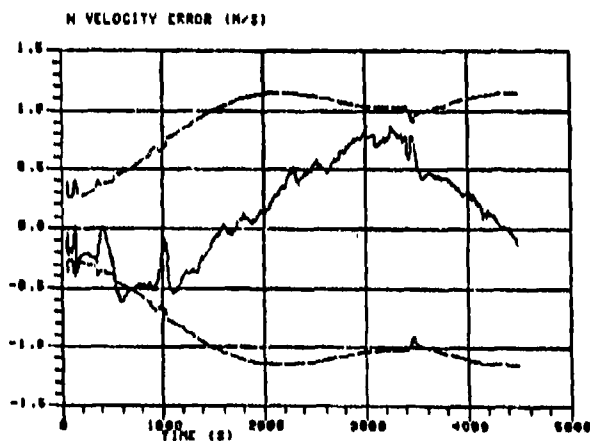


FIG. 7: NORTH VELOCITY ERROR & RMS FOR STRAPDOWN NAVIGATOR

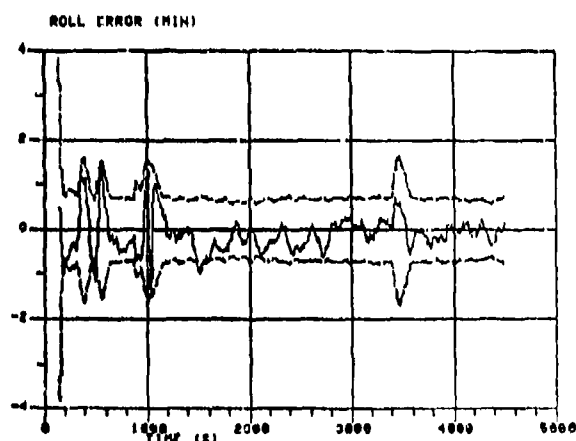


FIG. 8: ROLL ERROR & RMS FOR STRAPDOWN NAVIGATOR

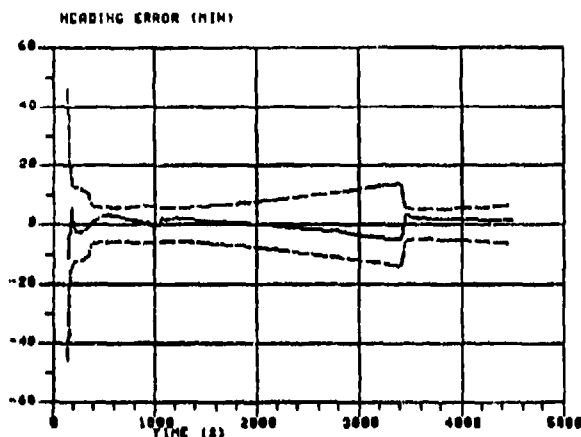


FIG. 9: HEADING ERROR & RMS FOR STRAPDOWN NAVIGATOR

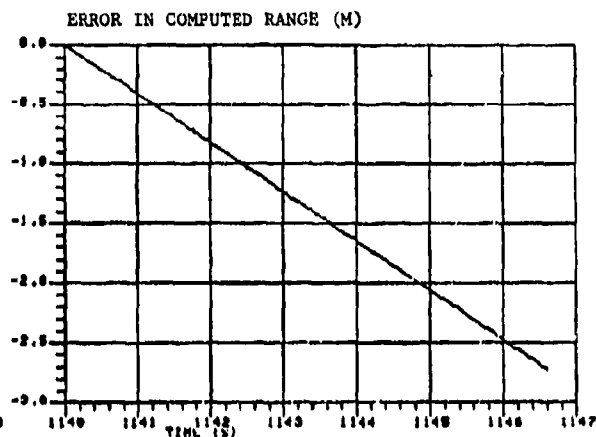


FIG. 10: LOS DISPLACEMENT ERROR BEFORE AUTOFOCUSING

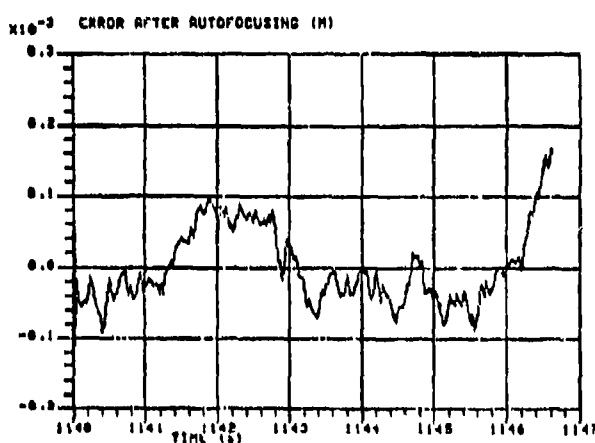


FIG. 11: LOS DISPLACEMENT ERROR AFTER AUTOFOCUSING

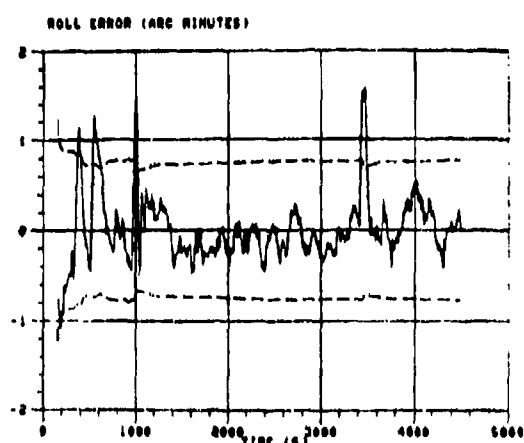


FIG. 12: STRAPDOWN NAVIGATOR ROLL ERROR AND RMS FOR 21 STATE KALMAN FILTER

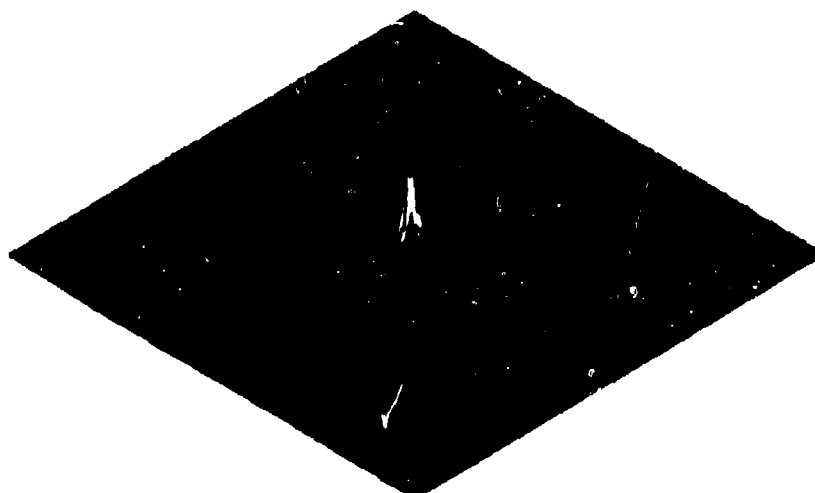


FIGURE 13: MOTION-COMPENSATED TWO-DIMENSIONAL IMPULSE RESPONSE OF THE RADAR

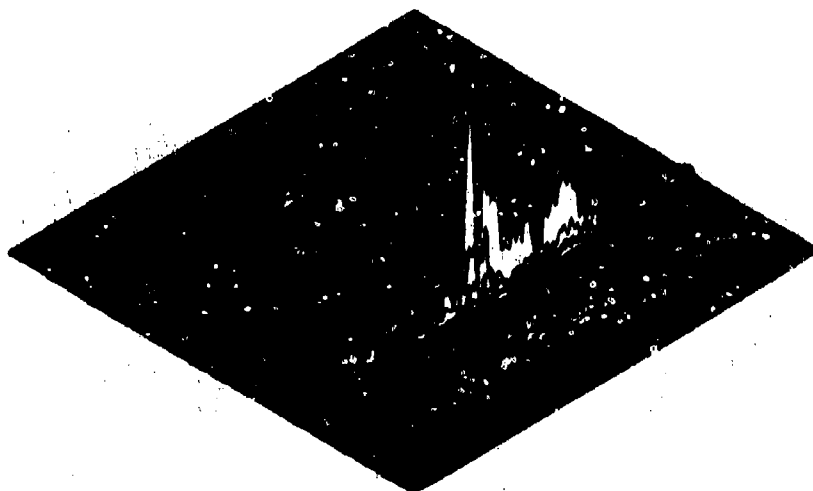


FIGURE 14: UNCOMPENSATED TWO-DIMENSIONAL IMPULSE RESPONSE OF THE RADAR

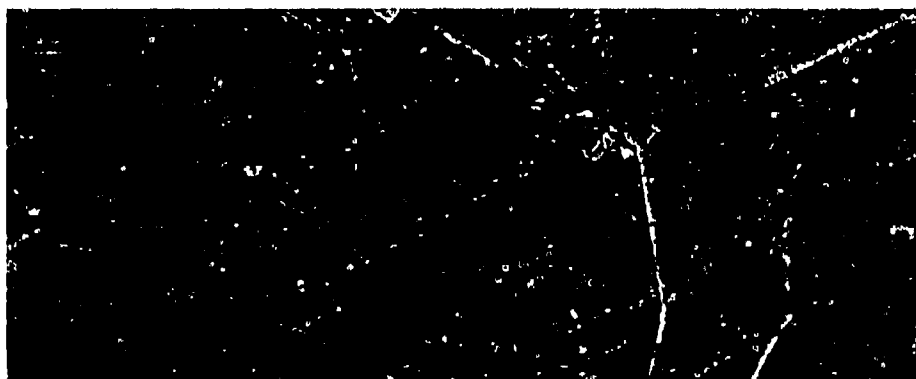


FIGURE 15: MOTION-COMPENSATED SAR STRIP-MAP IMAGE

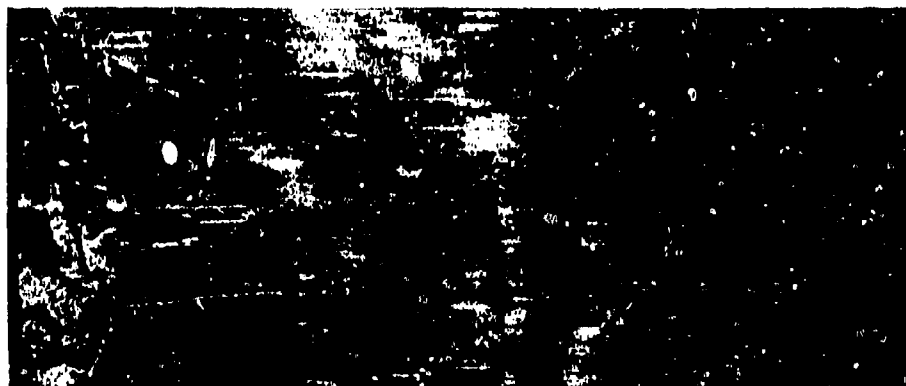


FIGURE 16: UNCOMPENSATED SAR STRIP-MAP IMAGE

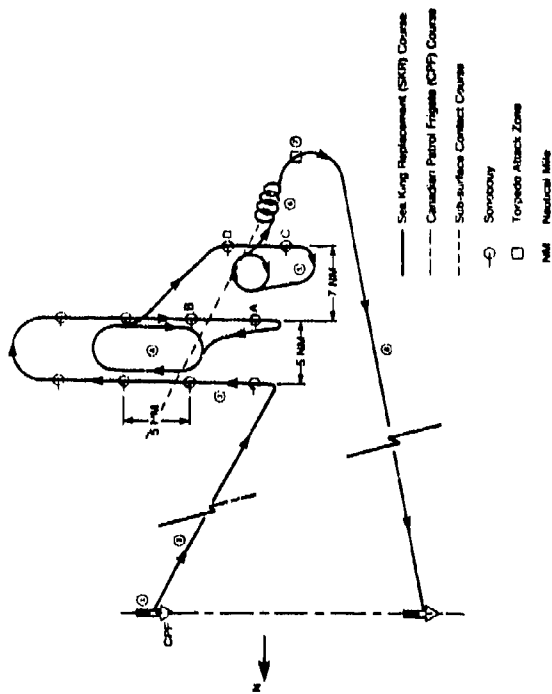


FIGURE 17: PLAN VIEW OF SONOBUOY MISSION

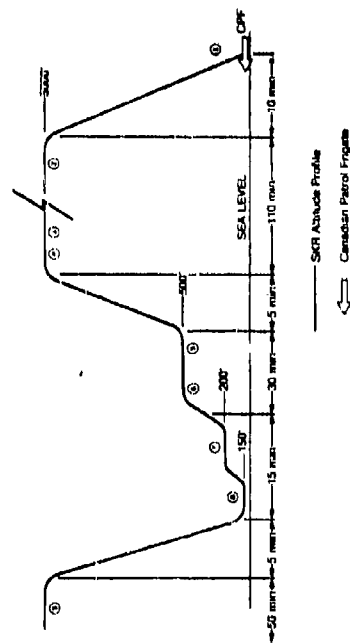


FIGURE 18: ALTITUDE PROFILE FOR SONOBUOY MISSION

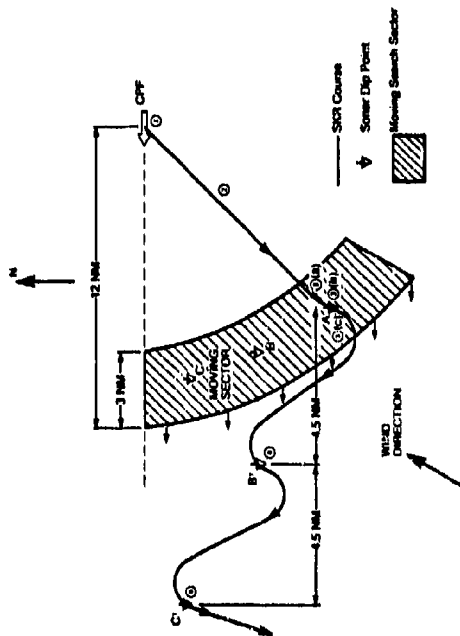


FIGURE 19: PLAN VIEW OF CONVOY SCREENING MISSION

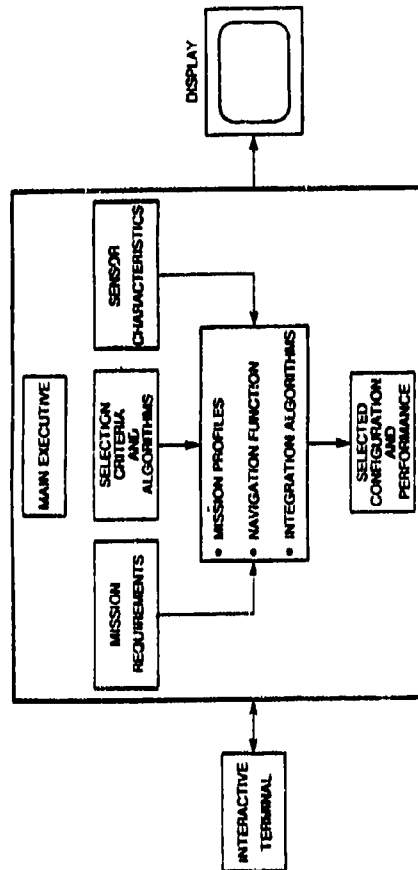
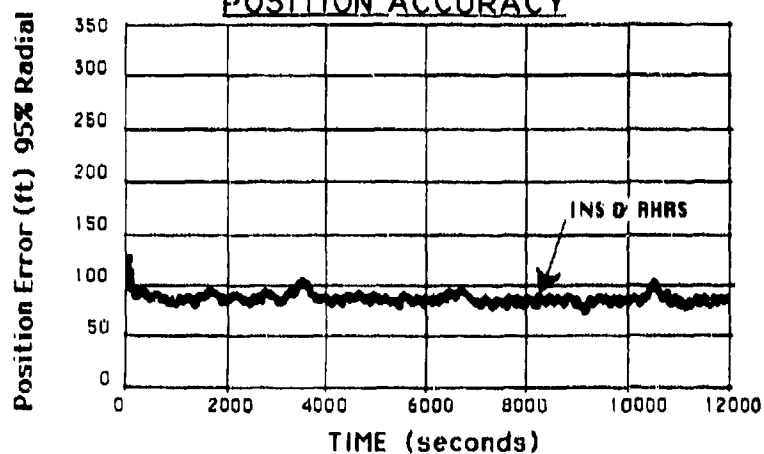


FIGURE 20: INTEGRATED SYSTEM EVALUATION PROGRAM (ISEP)

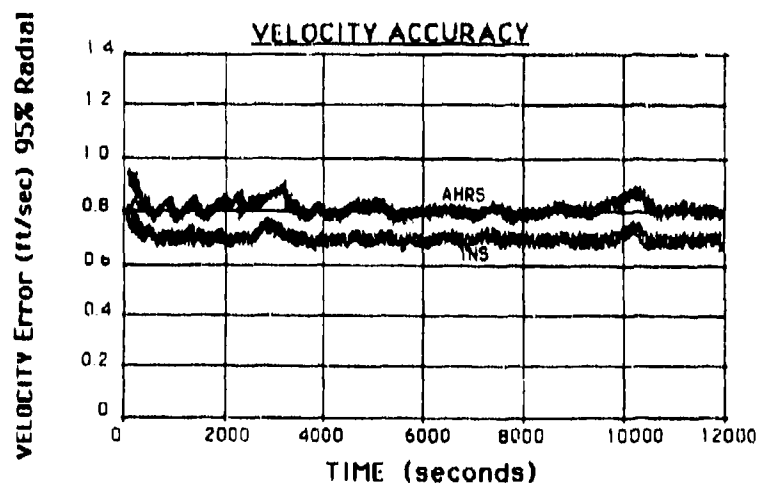
FIGURE 21
INS & AHRS CONFIGURATIONS (WITH GPS)

Figures of Merit (R95% values)	Units	AHRS	INS
Mean Radial Position Error	feet	80	80
Mean Radial Velocity Error	ft/sec	0.8	0.7
Mean Relative Velocity Error	ft/sec	0.8	0.8

POSITION ACCURACY



VELOCITY ACCURACY



RELATIVE VELOCITY ACCURACY

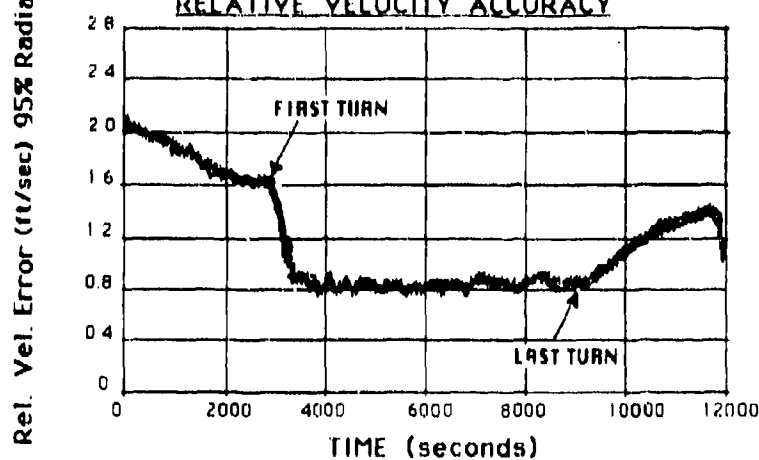


FIGURE 22
INS & AHRS CONFIGURATIONS
 (with out GPS for entire mission)

Figures of Merit (R95% values)	Units	AHRS	INS
Radial Position Error Rate	nm/hr	1.1	0.9
Mean Radial Velocity Error (3000 - 9000 sec)	ft/sec	4.2	3.3
Mean Relative Velocity Error (3000 - 9000 sec)	ft/sec	1.4	1.1

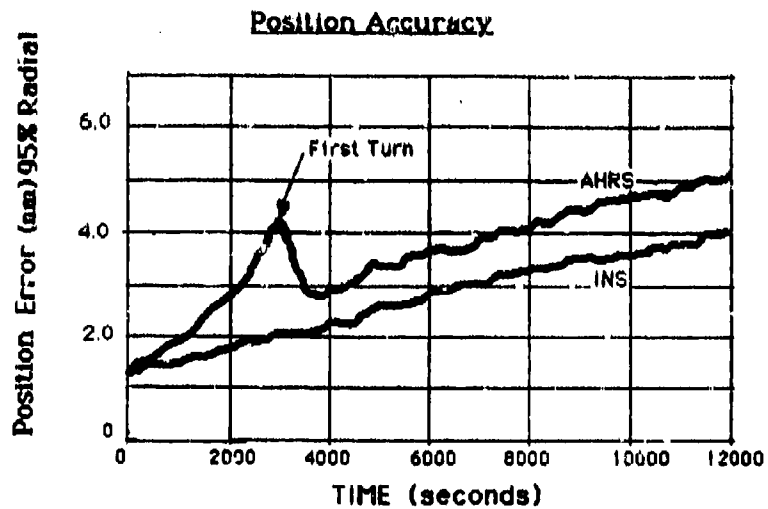
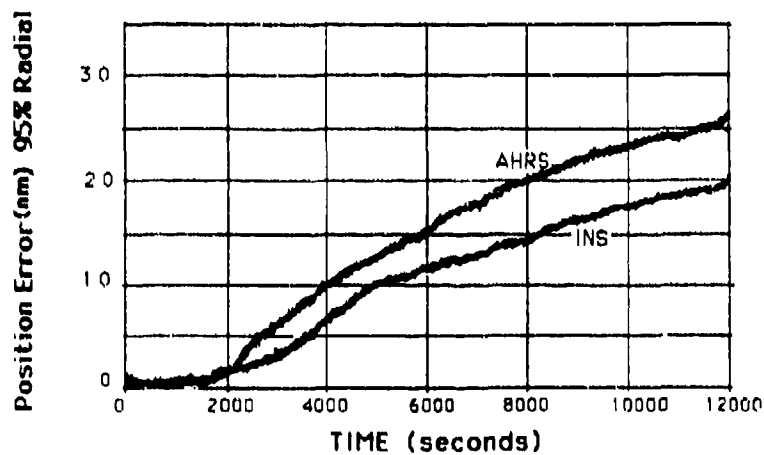


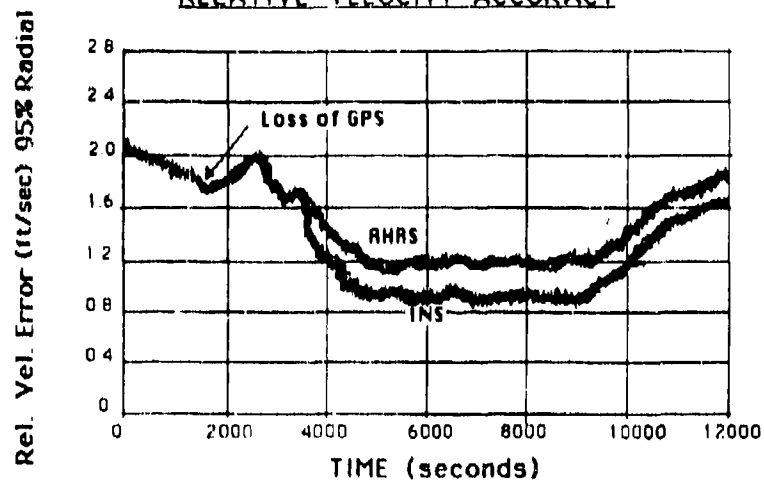
FIGURE 23
INS & AHRS CONFIGURATIONS
 (WITH GPS OUTAGE AT 1800 SEC)

Figures of Merit (R95% values)	Units	AHRS	INS
Radial Position Error Rate (1800 - 12000 sec)	nm/hr	1.0	0.8
Mean Radial Velocity Error (3000 - 9000 sec)	ft/sec	4.0	2.8
Mean Relative Velocity Error (3000 - 9000 sec)	ft/sec	1.2	0.9

POSITION ACCURACY



RELATIVE VELOCITY ACCURACY



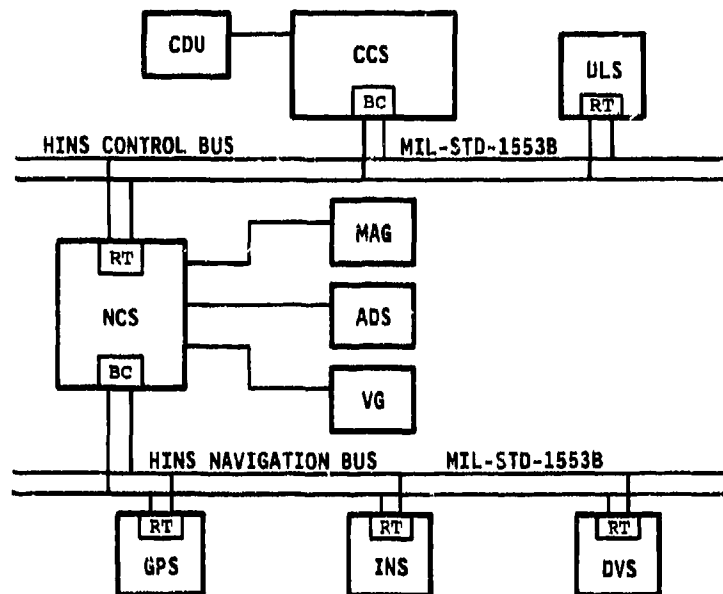


FIGURE 24: HINS ADM ARCHITECTURE

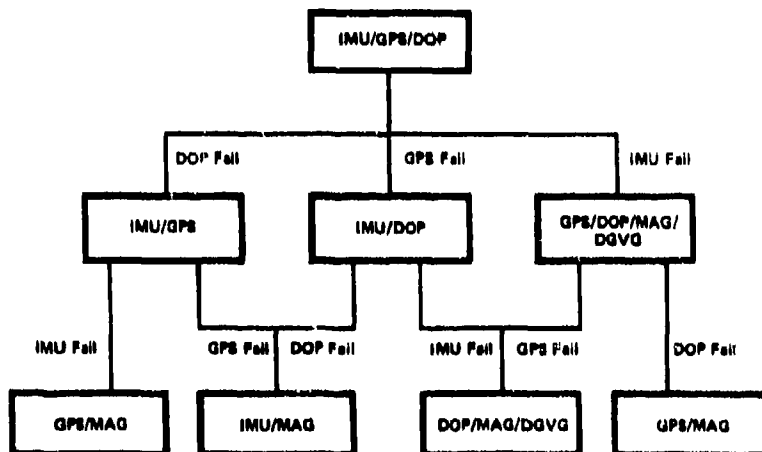


FIGURE 25: HINS FAILURE RECONFIGURATION

Table 2: Kalman Filter Error States

Type of Error State	Description
master inertial	x,y,z position errors ¹ x,y,z velocity errors ¹ x,y,z platform misalignment angles ¹
S/D inertial	x,y,z position errors ² x,y,z velocity errors ² x,y,z platform misalignment angles ²
master exponentially correlated	1 accelerometer bias ¹ x,y,z gyro biases ¹
S/D exponentially correlated	x,y,z accelerometer biases ¹ x,y,z gyro biases ¹
baro & Doppler exponentially correlated	baro altimeter bias ¹ x,y sea bias states ¹ x Doppler scale factor error ¹ y,z Doppler boresight errors ¹ Doppler carrier drift
master w. a. coords.	
¹ strapdown w. a. coords.	
² strapdown body coords.	
³ aircraft body coords.	

Table 3: Error Measurements

1. Master-Doppler velocity matching (Doppler beam coord.)	$c_d^b [c_d^b v_m^b - v_d^b + v_{md}^b]$ where v_m^b is computed master velocity (w.a. coord.), v_d^b is Doppler velocity (aircraft body coord.), v_{md}^b is aircraft angular rate, v_{md}^b is the lever arm from the master INS to the Doppler radar, and c_d^b and c_d^b are the master w.a.-to-body and body-to-Doppler beam direction cosine matrices, respectively.
2. Master-strapdown position matching (body coord.)	$c_g^b (p_m^b - p_s^b) - l_{ms}^b$ where p_m^b and p_s^b are master and strapdown geographic positions, respectively, l_{ms}^b is the lever arm from master to strapdown and c_g^b is the geographic-to-body DCM.
3. Master-baro position matching (master w.a. coord.)	$h_m - h_b$ where h_m and h_b are master and barometric altitude, respectively.

Table 4: Suboptimal Filter Error States

Sub-vector	Description	Frame
x_a	x,y master position errors ¹ x,y master velocity errors ¹ x,y,z master platform misalignments ¹	U.A. U.A. U.A.
x_{ai}	x,y master accelerometer biases	A/C ²
x_d	Doppler forward scale factor error Doppler azimuth boresight error x,y sea biases	A/C A/C U.A.
x_s	x,y S/D velocity errors (relative to master) x,y,z S/D platform misalignments (relative to master)	U.A. U.A.
x_{sg}	x,y,z S/D gyro biases	S/D ³

¹Wander azimuth frame:x,y-level,z-vertical²Aircraft frame:x-forward,y-right wing,z-down³S/D IMU body frame:x-forward,y-transverse,z-down

TABLE 5 - ISEP SIMPLIFIED ERROR MODELS

SENSOR	DESCRIPTION	PER AXIS RMS (1σ)	CORRELATED TIME/DISTANCE
GPS	3 Dimensional Position Fix Errors 3 Dimensional Velocity Fix Errors	50 ft 0.3 ft/sec	
OMEGA	2 Orthogonal Position Errors	0.8 - 1.1 nm	1.3 - 4 hrs
MAGNETOMETER	Heading Bias Error Heading Random Error	1° 0.1°	
LORAN	2 Position Errors	0.2 nm	
TACAN	Correlated Range Error Uncorrelated Noise Correlated Bearing Error Uncorrelated Bearing Noise	0.1 nm 100 ft 1° 0.1°	0.5 hr 0.02 hr
DOPPLER	2-Axis Total Velocity Error Effects Uncorrelated Error	0.5 - 1.5% 0.25 - 1.5%	0.5 - 3 hrs
RADAR ALTIMETER	Uncorrelated Error	2-5%	
AHRS	Gyro Drift Accelerometer Drift	0.5°/hr 500 μg	0.5 - 3 hrs 0.5 - 3 hrs
INS	Gyro Drift Gyro Random Walk Accelerometer Drift	0.0036°/hr 0.0016°/hr 35 μg	0.5 - 3 hrs 0.5 - 3 hrs
WIND	Correlated Error Random Fluctuation	50 ft/sec 5 ft/sec	1 hr

TABLE 6 - ISEP OUTPUT DATA

MANUFACT MODEL NO.	TYPE CANADIAN	COST MTBF	VOLUME WEIGHT	POWER MS1551B	MEASURE 1 VALUE 1	MEASURE 2 VALUE 2	MEASURE 3 VALUE 3
Littton LIN-90	INS yes	105000 5000	.702 44.000	W110 No	g/b-d/shr .010	rw-d/shr .005	ach-mfg 85.00
Marconi Mar-2Ch	GPS yes	50000 Est 1500	.647 UK	W250 Yes	vap-ft 45.00	v-ft/sec .3000	
Honeywell APN-194	Red-Alt No	11000 4500	.052 4.400	W20 No	alt-ft 4.00		
Marconi APN-227	Dop-Rad Yes	50000 2900	.383 35.000	VA65 Yes	vx-ft .170	vy-ft .170	vz-ft .100
Marconi M-143	Air-Data UK	N/A 3000	.452 11.200	W30 N/A	alt-ft 25.00	as-knots 15.00	
Develco D-9200C	Mag-Net No	1700 0	.005 .380	W1.3 No	alt-deg 1.00		
Total Cost = \$211,700 (\$US 83) Canadian Content = 94% Total Volume = 2,215 cu-ft Total Weight = 95.0 lbs System MTBF (series Model) = 898.1 hrs							
Mission Performance (95% radial position error)							
Unaided Performance = 1.0987 nm/hr							
Aided Performance (max) = 0.03640 nm							
Aided Performance (avg) = 0.00940 nm							

TABLE 7 - OMEGA AND DOPPLER SIMPLIFIED ERROR MODELS

	PESSIMISTIC		NOMINAL		OPTIMISTIC	
	PER AXIS RMS	CORRELATED TIME	PER AXIS RMS	COR. TIME	PER AXIS RMS	COR. TIME
Doppler Cor. Noise	1.5%	0.25 Hour	1.0%	0.5 Hour	0.5%	1.0 Hour
Doppler Uncor. Noise	1.0%		0.5%		0.25%	
Omega Cor. Noise	1.2 nm	1.3 Hour	1.0 nm	2.0 Hour	0.8 nm	4.0 Hour
Omega Uncor. Noise	400 M		300 M		200 M	

TABLE 8 - INITIALIZATION CONDITION

		GROUND FINE ALIGNMENT	SHIPBOARD FINE ALIGNMENT	IN-AIR ALIGNMENT
INS	ATTITUDE	0.1 mrad	0.1 mrad	10 mrad
	AZIMUTH	1 mrad	1 mrad	20 mrad
	VELOCITY	0.2 ft/sec	1.5 ft/sec	5 ft/sec
	POSITION	0.2 nm	0.54 nm	1 nm
AHRS	ATTITUDE	0.5 mrad	0.5 mrad	10 mrad
	AZIMUTH	1 mrad	1 mrad	20 mrad
	VELOCITY	0.2 ft/sec	1.5 ft/sec	30 ft/sec
	POSITION	0.2 nm	0.54 nm	1 nm

TABLE 9 - COVARIANCE ANALYSIS TRUTH MODEL

Subsystem	Error Type	Model	Standard Deviation
AHRS	Level Gyro Bias	Gauss Markov $\tau = 10$ hr	0.2 deg/hr
	Vertical Gyro Bias	Gauss Markov $\tau = 10$ hr	0.2 deg/hr
	Gyro Misalignment	Gauss Markov $\tau = 10$ hr	20 arc sec
	Gyro Scale Factor	Gauss Markov $\tau = 10$ hr	180 ppm
	Gyro Random Walk	Random Walk	0.0004 deg/ $\sqrt{\text{hr}}$
	Level Gyro g-sensitive	Gauss Markov $\tau = 10$ hr	0.2 deg/hr/g
	Vertical Gyro g-sensitive	Gauss Markov $\tau = 10$ hr	0.2 deg/hr/g
	Level Gyro g ² -sensitive	Gauss Markov $\tau = 10$ hr	0.1 deg/hr/g ²
	Vertical Gyro g ² -sensitive	Gauss Markov $\tau = 10$ hr	0.1 deg/hr/g ²
	Level Accelerometer Bias	Gauss Markov $\tau = 10$ hr	100 micro-g
	Vertical Accelerometer Bias	Gauss Markov $\tau = 10$ hr	100 micro-g
	Accelerometer Misalignment	Gauss Markov $\tau = 10$ hr	20 arc sec
	Accelerometer Scale Factor	Gauss Markov $\tau = 10$ hr	200 ppm
INS	Level Gyro Bias	Gauss Markov $\tau = 100$ hr	0.008 deg/hr
	Vertical Gyro Bias	Gauss Markov $\tau = 100$ hr	0.01 deg/hr
	Gyro Misalignment	Gauss Markov $\tau = 100$ hr	5 arc sec
	Gyro Scale Factor	Gauss Markov $\tau = 100$ hr	5 ppm
	Gyro Random Walk	Random Walk	0.008 deg/ $\sqrt{\text{hr}}$
	Level Accelerometer Bias	Gauss Markov $\tau = 10$ hr	40 micro-g
	Vertical Accelerometer Bias	Gauss Markov $\tau = 10$ hr	100 micro-g
	Accelerometer Misalignment	Gauss Markov $\tau = 10$ hr	5 arc sec
	Accelerometer Scale Factor	Gauss Markov $\tau = 10$ hr	200 ppm
GPS	Position	Gauss Markov $\tau = 1.0$ hr	30.0 ft
	Random Position	Uncorrelated	3.0 ft
	Velocity	Uncorrelated	0.3 ft/sec
DOPPLER RADAR	Speed Offset	Gauss Markov $\tau = 10$ hr	0.1 knot
	Scale Factor	Gauss Markov $\tau = 10$ hr	0.15 percent
	Bore Sight	Gauss Markov $\tau = 10$ hr	1.0 degree
	Fluctuation	Uncorrelated	0.008 $\frac{\text{knot}^2}{\text{knot} \frac{\text{rad}}{\text{sec}}}$
	Sea Current	Gauss Markov $\tau = 1.0$ hr	1.0 knot
MAGNETO- METER	Bias	Gauss Markov $\tau = 1.0$ hr	1.0 degree
	One Cycle	Gauss Markov $\tau = 10$ hr	0.7 degree
	Two Cycle	Gauss Markov $\tau = 10$ hr	0.7 degree
	Random	Uncorrelated	0.1 degree
TACAN	Bearing Bias	Gauss Markov $\tau = 0.25$ hr	1.4 degree
	Random Bearing	Uncorrelated	0.1 degree
	Range Bias	Gauss Markov $\tau = 1.0$ hr	0.14 nm
	Random Range	Uncorrelated	0.1 nm
AIR-DATA	Altitude	Gauss Markov $d = 250$ nm	600 ft
	Rapidly Varying Wind	Uncorrelated	2 knots
	Slightly Varying Wind	Gauss Markov $d = 60$ nm	5 knots
OMEGA	Phase Bias	Gauss Markov $d = 1800$ nm	10 centi-cycles
	Periodic Error	24 hr Correlated Process	2.5 centi-cycles
	Short Correlated Error	Gauss Markov $\tau = 0.75$ hr	2.5 centi-cycles
	Random Error	Uncorrelated	4 centi-cycles

①

COMPONENT PART NOTICE

THIS PAPER IS A COMPONENT PART OF THE FOLLOWING COMPILATION REPORT:

TITLE: Kalman Filter Integration of Modern Guidance and Navigation Systems.

TO ORDER THE COMPLETE COMPILATION REPORT, USE AD-A214 284.

THE COMPONENT PART IS PROVIDED HERE TO ALLOW USERS ACCESS TO INDIVIDUALLY AUTHORED SECTIONS OF PROCEEDING, ANNALS, SYMPOSIA, ETC. HOWEVER, THE COMPONENT SHOULD BE CONSIDERED WITHIN THE CONTEXT OF THE OVERALL COMPILATION REPORT AND NOT AS A STAND-ALONE TECHNICAL REPORT.

THE FOLLOWING COMPONENT PART NUMBERS COMPRISE THE COMPILATION REPORT:

AD#: P005 817 thru AD#: P005 822

AD#: _____ AD#: _____

AD#: _____ AD#: _____

Accession For	
NTIS GRA&I	<input checked="" type="checkbox"/>
DTIC TAB	<input type="checkbox"/>
Unannounced	<input type="checkbox"/>
Justification	
By _____	
Distribution/	
Availability Codes	
Dist	Avail and/or Special
A-1	

DTIC
ELECTE
NOV 16 1989
S E D

This document has been approved
for public release and using the
distribution is unlimited.

DEVELOPMENT OF A MARINE INTEGRATED NAVIGATION SYSTEM

by

D.F. Liang, Head, Electromagnetics Section

J.C. McMillan, Group Leader, System Design

Defence Research Establishment Ottawa

Ottawa, Ontario

Canada K1A 0Z4

SUMMARY

Startling advances in electronics and computer technologies over the last two decades have significantly altered the scope of military operations, weapon systems and some of the required supporting services. The increased range, speed and accuracy of modern weapon systems impose stringent accuracy and reliability requirements upon the navigation systems of military platforms.

Over the last few years, DREO has been involved in the development of a microprocessor-based Marine Integrated Navigation System (MINS). The present version of the MINS can work with a variety of types and brands of navigation sensors such as Omega, Transit, GPS, Loran C, speedlog and gyrocompass as well as operator-entered position or sextant measurements. It has been successfully tested on both Canadian and US navy vessels and it is due to be installed on almost all of Her Majesty's Canadian ships in 1988.

This lecture will describe the application of Kalman filter design to "optimally" and synergistically combine the diverse types of navigation sensor information. Technical problems, design objectives and some design features unique to this application are highlighted. Results of sea trial evaluations are compared to simulation results. Integrated system design guidelines and "road maps" derived from the Canadian experience are also presented.

1.0 INTRODUCTION

The Canadian Maritime Command has successfully deployed on almost all Canadian Naval Vessels a Kalman filter based multi-sensor Marine Integrated Navigation System (MINS)*. The MINS concept and system design were developed at the Defence Research Establishment Ottawa [1] over the period 1980-1988. Extensive sea trial evaluations were conducted by DREO in 1983, 1984, 1987 and 1988 as well as by U.S. Naval Air Development Center from 1985 to 1987. The design objectives have been verified: MINS does enhance the navigation accuracy, operational reliability and position reporting efficiency of marine vessels that are equipped with a variety of types and brands of navigation sensors such as Omega, Transit, GPS, Loran C, speedlog and gyrocompass as well as operator entered position or sextant measurements.

2.0 SYSTEM DESCRIPTION

The current production version of the MINS (AN/SYN-501) is shown in Figure 1 in block diagram form, along with the sensor input that it can integrate. The MINS processor is a Motorola 68020/68881 with about one half megabyte of memory. Figure 2 shows the plasma display unit, the keypad unit and the central electronics unit.

3.0 SCOPE OF THIS PRESENTATION

This presentation will describe the design of a Kalman filter to "optimally" and synergistically combine the diverse types of navigation sensor information. Results of sea trial evaluations are compared to simulation results. Design guidelines and a "road map for designers" will also be presented.

In the simulation analysis phase, the integrated navigation system data processing algorithm was implemented on a general purpose computer, with "measurement" data numerically simulated using statistical error models to represent the navigation sensor errors. This allows complete control of the testing conditions and facilitates the rapid and efficient evaluation of the filter performance characteristics for a large number of different test voyages.

4.0 SIMULATED TRUTH MODELS

In the initial study phase before any real sea-trial data becomes available, it is important to establish detailed mathematical models of the navigation system error behavior. Analytical and simulation results obtained will therefore be relative to the models adopted.

* MINS is a Trade Mark of the Canadian Department of National Defence

AD-P005 821

In order to properly analyse the performance of various integrated navigation systems, a versatile simulation package was developed. Briefly, the computer program does the following:

- a) simulates a ship scenario (true velocity and position).
- b) generates sensor measurements with appropriate error characteristics.
- c) integrates the dead reckoning (DR) measurements to obtain the DR position every 4 seconds.
- d) obtains an Omega-based position fix every 20 seconds.
- e) obtains a Loran-C position fix every 20 seconds.
- f) obtains a Transit position fix when available, dead reckoning between fixes.
- g) processes these same measurements with the Kalman filter integration algorithms of different state size and
- h) compares the results of c) to g) above with the true values of a) to evaluate the absolute and relative performance of the Kalman filters vis-a-vis the conventional reset method.

This section briefly presents the simulation algorithms for generation of the ship's true position and velocity, the computation of navigation information based on the DR measurements, and a description of individual subsystem errors.

4.1 Ship's True Position and Velocity

The ship's true north and east velocity components are computed using

$$\begin{aligned} V_N &= S \cos \theta + V_{NC} \\ V_E &= S \sin \theta + V_{EC} \end{aligned} \quad (1)$$

where S and θ are the ship's water speed and heading, and V_{NC} , V_{EC} are the north and east ocean current components.

The ship's true position is determined by integrating this velocity, or in the discrete case by the update equation,

$$\begin{bmatrix} \text{LAT} \\ \text{LONG} \end{bmatrix}_{t+\Delta t} = \begin{bmatrix} \text{LAT} \\ \text{LONG} \end{bmatrix}_t + \begin{bmatrix} V_N/R_N \\ V_E/R_E \cos(\text{LAT}) \end{bmatrix}_t \Delta t \quad (2)$$

where R_N and R_E are the north and east radii of curvature of the WGS-84 ellipsoid. The accuracy of this representation will be acceptable if Δt is sufficiently small.

4.2 DR Position and Velocity

Simulation of the DR position estimate is based on equations (1) and (2) except that the ocean current is not known and the measured speed and heading are corrupted with Markov errors. The DR position is simulated by

$$\begin{bmatrix} V_{N1} \\ V_{E1} \end{bmatrix} = \begin{bmatrix} (S + dS) \cos(\theta + d\theta) \\ (S + dS) \sin(\theta + d\theta) \end{bmatrix} \quad (3)$$

$$\begin{bmatrix} \text{LAT1} \\ \text{LONG1} \end{bmatrix}_{t+\Delta t} = \begin{bmatrix} \text{LAT1} \\ \text{LONG1} \end{bmatrix}_t + \begin{bmatrix} V_{N1}/R_{N1} \\ V_{E1}/R_{E1} \cos(\text{LAT1}) \end{bmatrix}_t \Delta t \quad (4)$$

Comparing equations (1) and (2) to equations (3) and (4), it can be seen that the dominant sources of error in the DR position and velocity estimates are the ocean current components, speed log error and gyrocompass heading error. With the gyros and speedlogs typically used on major vessels, the contribution of the heading error is relatively insignificant. Since the heading error is also nonlinear it was decided that the benefit in accounting for this error source explicitly would be marginal and that it could be absorbed into the ocean current error model.

Ocean current is quite random, correlated both in time and space. Therefore each component can be modelled as a first order Markov process with autocorrelation time constant T_C . The speedlog is assumed to be water tracking rather than bottom tracking. This error is also randomly varying, normally zero mean and bounded. Therefore it is modelled as a first order Markov process with auto-correlation time constant T_S . The spectral densities (q_S , q_C) of the corresponding white noise processes (W_S , W_C) are related to their mean-squared values (R_S , R_C) of the respective error state

$$\begin{aligned} q_S &= 2R_S/T_S \\ q_C &= 2R_C/T_C \end{aligned} \quad (5)$$

Since the ship's latitude and longitude are the primary quantities of interest, 2 states are used to represent the error of the DR latitude and longitude. The filter estimates of these two error states can then be used to remove the error from the DR position estimate.

4.3 Omega Errors

Omega is a hyperbolic system that utilizes lines of position based on phase difference measurements from at least three transmitters. It operates in the 10 to 14 KHz band and, since each station has a range of 13,000 Km, only eight stations are sufficient to provide world-wide coverage.

Diurnal changes in the ionospheric propagation characteristics and the inhomogeneity of the earth's magnetic field and surface conductivity cause anomalous variations in the Omega phase measurements. These deterministic errors can be partially compensated for by using phase propagation correction (PPC) tables. However, there remain four major random components of residual error. The statistical properties of this residual error have been studied in detail by various groups and it is generally agreed that when PPC tables have been used, the remaining phase error at the Omega receiver has an autocorrelation function of the form

$$\psi(\tau) = A^2 e^{-\sqrt{T_1}|\tau|} + B^2 e^{-\sqrt{T_2}|\tau|} + C^2 e^{-\sqrt{T_1}|\tau|} \cos(\omega\tau) \quad (6)$$

where auto-correlation times T_1 and T_2 are respectively 180,000 and 4800 seconds, ω is the earth rate and A,B,C are respectively 1520, 500 and 850 metres. This phase error can therefore be adequately described by the sum of three stochastic processes: two first order Markov processes and a periodic process with a period of 24 hours. Since the periodic process is second order, a total of four states are required to properly model each Omega phase error. Determining three independent Omega lines of position (LOPs) requires reception of Omega signals from 4 distinct stations. Therefore a total of 16 Omega error states are required to represent these Omega errors.

4.4 Loran C Errors

The Loran C position fixing system computes lines of position by measuring the difference in time of arrival of pulse signals from master-slave pairs of transmitters. Each Loran C chain consists of a master and two or more slave stations, transmitting synchronized pulse trains on a carrier frequency of 100 KHz with a nominal bandwidth of 10 KHz. Very stable ground wave transmission from the transmitters can produce lines of position with an accuracy of about 400 m at distances up to approximately 1600 Km, when all known deterministic corrections have been made (secondary and additional secondary phase factors, SPP and ASF), and there is no geometric dilution of precision (GDOP = 1).

Under normal operating conditions the major errors which affect the determination of the time difference are anomalies in ground conductivity, which in turn affect the propagation velocity, and similar anomalies in the surface index of refraction. Additional errors are due to receiver noise and atmospheric perturbations. Of course all of these errors are magnified by the GDOP.

Loran C also has a discontinuous error component known as cycle selection error, which is handled by the prefilter. Therefore the filter will see a continuous, bounded and zero-mean error, which is modelled as a first order Markov process.

4.5 Satnav Errors

Satnav, also known as Transit or the Navy Navigation Satellite System, presently consists of 6 satellites in near circular polar orbits at about 1075 Km altitude with 107 minute period. A position fix can be obtained only when a satellite passes over the horizon with a maximum elevation angle between about 5° and 80°. At mid latitudes this happens on the average about once an hour. The position fix is obtained by processing the satellite signal received throughout the pass and therefore the ship's motion during the pass must be known and compensated for. The receiver requires velocity input not only to compensate for the changing position of the ship, but also because the basic positioning measurement is the Doppler shift in the signal from the satellite. The Doppler shift is of course affected by the ship's velocity and, in fact, it is the inaccuracy of this velocity estimate that accounts for the largest part of the Satnav position fix error.

The exact relationship between the velocity and height error input and the position error output is described in Reference [2]. Aside from the known effect of velocity and height input errors, the Transit errors are largely random, zero mean, and independent of each other, and are treated by the MINS filter purely as measurement noise.

During the long intervals between position fixes, the Satnav receiver can only dead reckon, with the ensuing degradation of accuracy.

4.6 GPS Errors

The GPS constellation currently provides about 8 hours per day of useful two dimensional coverage in the test area used for MINS evaluation. GPS satellites are in much higher orbits than Transit, broadcasting at higher frequencies, and pseudo ranging rather than Doppler fixing is used. These and other factors make GPS a much more accurate system. Reference [3] gives a good description of the GPS system and equipment.

GPS position error, even from a C/A code receiver, is generally significantly smaller than that from any other sensors used by MINS. These GPS position measurements have zero mean, bounded errors, which are nominally continuous. Because they are not observable however, these errors are treated by the filter simply as measurement noise. The expected magnitude of this error depends primarily on whether the receiver is of P or C/A code, and on the geometric dilution of precision, which is generally provided by the receiver.

5.0 KALMAN FILTER DESIGN

The dynamics of the error state vector \underline{x} are mathematically described by the system model

$$\dot{\underline{x}} = \underline{F}(\underline{x}) + \underline{W} \quad (7)$$

where \underline{W} is a zero-mean Gaussian white noise process. There are many possible suboptimal filter models that could be derived from simplified truth models. The major problem in Kalman filter design is to determine which error states can be ignored or grouped together to reduce the size of the filter (and hence the computational burden), without significant performance degradation.

As described in Section 4.3, each of the four Omega errors requires a total of 4 error states, whereas the Loran-C requires only one state per time difference error and none are required for both the Satnav and GPS. Therefore reduction of the state size must concentrate on the selection of Omega error states. The actual MINS design can dynamically reconfigure the state vector to model from zero to five phase errors depending on the number of Omega stations being used. But for this section, we will first illustrate the filter design based on four Omega stations and three Loran C stations (for 2 time differences) but no Satnav and GPS. This we will call the MINS-A design. The MINS-B design extended the MINS-A to incorporate GPS and Satnav through the modification of the measurement equation.

Table 1 shows the 24 states used for the "truth" system model, along with several suboptimal error models that were used in the design analysis and simulation. Here, there are 3 different Omega error model representations using 8 states, 12 states and the full 16 states.

5.1 Stochastic Error Models

5.1.1 DR Error Model

Each suboptimal system model neglects the gyrocompass heading error. Partial compensation is achieved by increasing the expected ocean current error to absorb some of this unmodelled error. These DR error states, together with the latitude and longitude errors ($d\lambda, dL$), propagate independently of the Omega and Loran-C errors, according to the linear state equation,

$$\frac{d}{dt} \begin{bmatrix} \Delta\lambda \\ \Delta L \\ S \\ V_{NC} \\ V_{EC} \end{bmatrix} = \begin{bmatrix} 0 & 0 & \cos\theta & 1 & 0 \\ 0 & 0 & \sin\theta & 0 & 1 \\ 0 & 0 & -\beta_s & 0 & 0 \\ 0 & 0 & 0 & -\beta_c & 0 \\ 0 & 0 & 0 & 0 & -\beta_c \end{bmatrix} \begin{bmatrix} \Delta\lambda \\ \Delta L \\ S \\ V_{NC} \\ V_{EC} \end{bmatrix} + \underline{W}_A \quad (8)$$

where θ is the ship's heading and

$$\beta_s = 1/T_s$$

$$\beta_c = 1/T_c$$

The magnitude of the driving noise for this zero-mean Gaussian white (ZMGW) noise process is described by a simple diagonal matrix with elements:

$$Q = \text{diag} [0 \ 0 \ q_a \ q_c \ q_c]$$

where q_a and q_c are already defined in equation (5).

5.1.2 Omega Error Model

The 4 states required to model each Omega phase error propagate according to

$$\frac{d}{dt} \begin{bmatrix} \text{BIAS} \\ \text{MARKOV} \\ \text{PERIODIC} \\ P_2 \end{bmatrix} = \begin{bmatrix} -1/T_1 & 0 & 0 & 0 \\ 0 & -1/T_2 & 0 & 0 \\ 0 & 0 & 0 & 0 \\ 0 & 0 & -\alpha^2 & -2/T_1 \end{bmatrix} \begin{bmatrix} \text{BIAS} \\ \text{MARKOV} \\ \text{PERIODIC} \\ P_2 \end{bmatrix} + \underline{W}_B \quad (9)$$

where \underline{W}_B is a zero mean Gaussian white (ZMGW) noise process, and P_2 is the extra state needed to model the periodic error. T_1 and T_2 are the Markov process correlation times and α is a constant. Here the strongly correlated Markov process is referred to as a bias to distinguish it from the more weakly correlated one (i.e. $T_1 \gg T_2$).

The 21-state DR-OMEGA filter models 4 Omega phase errors according to equation (9), for a total of 16 Omega states.

Since an Omega line of position error is the difference between two independent phase errors, the statistical properties of the LOP error will be basically the same as that of a phase error. By modelling the three LOP errors instead of the four phase errors, the 17-state DR-OMEGA filter requires only 12 states to represent the Omega errors. The four Omega error states for each LOP error propagate according to equation (9) where the driving noise \underline{W}_B is the difference between two uncorrelated zero-mean Gaussian white processes, one for each Omega signal used to determine the LOP.

The 13-state DR-OMEGA filter models 4 OMEGA phase errors, as the 21-state filter does, but uses only two states for each phase error, for a total of 8 Omega error states. This was accomplished by omitting the periodic states and adjusting the parameters of the weakly correlated Markov processes to maintain the correct mean values and correlation times. The phase error of each Omega signal is therefore modelled by the following two Markov processes.

$$\frac{d}{dt} \begin{bmatrix} \text{BIAS} \\ \text{MARKOV} \end{bmatrix} = \begin{bmatrix} -1/T_1 & 0 \\ 0 & -1/T_3 \end{bmatrix} \begin{bmatrix} \text{BIAS} \\ \text{MARKOV} \end{bmatrix} + \underline{W}_C \quad (10)$$

where T_1 and T_3 are the correlation time constants.

5.1.3 Loran-C Error Model

The Loran-C master-slave time difference errors are each modelled as a single independent Markov process, and therefore propagate according to

$$\frac{d}{dt} [\text{LORAN}] = [-1/T_4][\text{LORAN}] + \underline{W}_L \quad (11)$$

where T_4 is the correlation time and \underline{W}_L is the ZMGW driving noise process.

5.2 Measurement Model

The measurement model describes the relationship between the inputs to the Kalman filter, \underline{z} , called measurements, and the state vector \underline{x} that is to be determined from these inputs. For linear systems this is generally of the form

$$\underline{z}(t) = H(t)\underline{x}(t) + \underline{v}(t) \quad (12)$$

where \underline{v} is the measurement noise vector and $H(t)$ is the measurement matrix. The same measurement vector was chosen for each of the filters. It consists of three Omega measurements, two Loran measurements, two Satnav measurements and four GPS measurements.

5.2.1 Omega Measurements

Each of the three Omega measurements is the difference between an LOP as measured by the Omega receiver (with PPCs) and the corresponding LOP as geometrically calculated from the DR position estimate and the known locations of the Omega broadcasting stations. This measurement is related to the 17-state vector (which models LOP errors rather than station errors) according to

$$\begin{bmatrix} z_1 \\ z_2 \\ z_3 \end{bmatrix} = \begin{bmatrix} (\cos\psi_{11} - \cos\psi_{j1}) & (\sin\psi_{11} - \sin\psi_{j1}) & 000 & 1110 & 0000 & 0000 \\ (\cos\psi_{12} - \cos\psi_{j2}) & (\sin\psi_{12} - \sin\psi_{j2}) & 000 & 0000 & 1110 & 0000 \\ (\cos\psi_{13} - \cos\psi_{j3}) & (\sin\psi_{13} - \sin\psi_{j3}) & 000 & 0000 & 0000 & 1110 \end{bmatrix} \underline{x} + \underline{v} \quad (13)$$

where the ψ 's are the bearings from the ship to the Omega stations, and the LOP used in measurement z_k is defined by the phase difference between the signals from Omega stations i_k and j_k [4]. The measurement noise \underline{v} is assumed to be zero-mean Gaussian white noise with covariance matrix R .

The measurement equations for the 21-state and 13-state filters (which model station errors rather than LOP errors) are similar to equation (13) but are more dependent on the choice of Omega stations for the three LOP's. For example if LOP₁ uses stations i and $i + 1$ then the 13-state measurement equation is

$$\begin{bmatrix} z_1 \\ z_2 \\ z_3 \end{bmatrix} = \begin{bmatrix} (\cos\psi_2 - \cos\psi_1) & (\sin\psi_2 - \sin\psi_1) & 0 & 0 & 0 & 1 & 1 & -1 & -1 & 0 & 0 & 0 & 0 \\ (\cos\psi_3 - \cos\psi_2) & (\sin\psi_3 - \sin\psi_2) & 0 & 0 & 0 & 0 & 0 & 1 & 1 & -1 & -1 & 0 & 0 \\ (\cos\psi_4 - \cos\psi_3) & (\sin\psi_4 - \sin\psi_3) & 0 & 0 & 0 & 0 & 0 & 0 & 0 & 1 & 1 & -1 & -1 \end{bmatrix} \underline{x} + \underline{v} \quad (14)$$

The 21-state measurement equations is basically the same as the 13-state, but with each (1 1) replaced by (1110) and each (-1-1) replaced by (-1-1-1 0).

5.2.2 Loran C Measurements

Having defined the above DR-Omega filter design, we now want to extend the design to the DR-Omega-Loran C filter. As can be seen later in Section 6.0, the selected DR-Omega filter design is based on the 13-state filter. Therefore with two additional states to account for the Loran-C error, we have a 15-state design. Each of the two Loran measurements is the difference between a master-slave time delay as measured by the Loran receiver (with SPF and ASF corrections) and the corresponding time delay as calculated from the DR position estimate and the known Loran station locations and coding delays. These measurements are independent of the Omega measurements, and are related to the 15-state vector through the measurement equation

$$\begin{bmatrix} z_4 \\ z_5 \end{bmatrix} = \begin{bmatrix} (\cos\psi_M - \cos\psi_{s1}) & (\sin\psi_M - \sin\psi_{s1}) & 0 \dots 010 \\ (\cos\psi_M - \cos\psi_{s2}) & (\sin\psi_M - \sin\psi_{s2}) & 0 \dots 001 \end{bmatrix} \underline{x} + \underline{v} \quad (15)$$

where ψ_{s1} is the bearing from the ship to the Loran slave station i and ψ_M is the bearing to the Loran master station. The measurement noise vector \underline{v} is ZMGW.

5.2.3 Transit Measurements

The Transit position measurement is related to the 15-state vector by:

$$\begin{bmatrix} z_6 \\ z_7 \end{bmatrix} = \begin{bmatrix} 1 & 0 & F\cos\theta + G\sin\theta & F & G & 0 & 0 & 0 & 0 & 0 & 0 & 0 & 0 & 0 & 0 \\ 0 & 1 & J\cos\theta + K\sin\theta & J & K & 0 & 0 & 0 & 0 & 0 & 0 & 0 & 0 & 0 & 0 \end{bmatrix} \underline{x} + \underline{v} \quad (16)$$

Since Transit provides position directly, the first two columns of the Transit measurement matrix relating the north and east position errors to the Transit measurement errors form an identity matrix. The columns 3 to 5 relate the state vector estimate of dead reckoning velocity error (speedlog error, north and east ocean current) to the Transit fix position error. This sensitivity arises because a Transit position fix is based on Doppler measurements from a satellite. These Doppler measurements of course must be compensated by subtracting the "known" ship's velocity relative to the earth, and this is done using the MINS supplied velocity estimate. An error in MINS velocity therefore produces an error in the transit position fix. The details of the relationship are derived in Reference [2] which gives an algorithm for evaluating the coefficients F, G, J and K . These are functions of the receiver location, the satellite's maximum elevation angle, the satellite's direction of travel (north-to-south or south-to-north) and the direction to the satellite subpoint at maximum elevation (east or west of the receiver).

Unlike the other radio aids Transit is not a "real time" system, since Doppler data must be collected over the roughly 20 minutes of an entire satellite pass, and then batch processed to obtain a position. Therefore the Transit position must be extrapolated from the time at which the position fix is valid, called the fix mark, (near the centre of the satellite pass), to the end of the pass, when the data becomes available. When the DR is used to extrapolate, this also introduces an error sensitivity to the velocity error states.

5.2.4 GPS Measurements

The GPS position and velocity measurements are related to the state vector by:

$$\begin{bmatrix} z_8 \\ z_9 \\ z_{10} \\ z_{11} \end{bmatrix} = \begin{bmatrix} 1 & 0 & 0 & 0 & 0 & 0 & 0 & 0 & 0 & 0 & 0 & 0 \\ 0 & 1 & 0 & 0 & 0 & 0 & 0 & 0 & 0 & 0 & 0 & 0 \\ 0 & 0 & \cos\theta & 1 & 0 & 0 & 0 & 0 & 0 & 0 & 0 & 0 \\ 0 & 0 & \sin\theta & 0 & 1 & 0 & 0 & 0 & 0 & 0 & 0 & 0 \end{bmatrix} \underline{x} + \underline{v} \quad (17)$$

The (GPS - predicted) measurement errors are position and velocity errors, which are modelled directly by the state vector, making the GPS measurement submatrix simply a geometric relationship. The third column simply resolves the speedlog error into its north and east components, which are added to the north and east ocean current components respectively.

5.2.5 Operator Position Fix

The operator entered position fix is the simplest of all, being just a latitude and longitude measurement, so its measurement equation is as follows:

$$\begin{bmatrix} z_{12} \\ z_{13} \end{bmatrix} = \begin{bmatrix} 1 & 0 & 0 & 0 & 0 & 0 & 0 & 0 & 0 & 0 & 0 & 0 \\ 0 & 1 & 0 & 0 & 0 & 0 & 0 & 0 & 0 & 0 & 0 & 0 \end{bmatrix} \underline{x} + \underline{v} \quad (18)$$

5.2.6 Celestial Fix

The celestial fix is the elevation angle of a celestial object. The position error on the earth's surface due to an angular error of size θ in this measurement is in the direction of the celestial object's azimuth γ , of magnitude equal to the arc length on the earth's surface subtended by the same angle θ at the earth's centre. Thus the angular error (in radians) must be multiplied by the earth's radius R , and the resolved into north and east components by the azimuth γ . Thus the celestial fix measurement matrix block is as follows:

$$[z_{14}] = [R \cos \gamma \sin \gamma \ 0 \ 0 \ 0 \ 0 \ 0 \ 0 \ 0 \ 0 \ 0 \ 0] \underline{x} + \underline{v} \quad (19)$$

5.3 Discrete Kalman Filter Implementation

Using the most efficient 15-state Kalman filter design as an example, the continuous differential form of the MINS state propagation model can be explicitly shown as:

$$\dot{\underline{x}} = \begin{bmatrix} A & 0 & 0 \\ 0 & B & 0 \\ 0 & 0 & C \end{bmatrix} \underline{x} + \underline{w} \quad (20)$$

$$A = \begin{bmatrix} 0 & 0 & \cos\theta & 1 & 0 \\ 0 & 0 & \sin\theta & 0 & 1 \\ 0 & 0 & \beta_b & 0 & 0 \\ 0 & 0 & 0 & -\beta_c & 0 \\ 0 & 0 & 0 & 0 & -\beta_c \end{bmatrix} \quad B = \begin{bmatrix} -\beta_b & 0 & 0 & 0 & 0 & 0 & 0 & 0 \\ 0 & -\beta_m & 0 & 0 & 0 & 0 & 0 & 0 \\ 0 & 0 & -\beta_b & 0 & 0 & 0 & 0 & 0 \\ 0 & 0 & 0 & -\beta_m & 0 & 0 & 0 & 0 \\ 0 & 0 & 0 & 0 & -\beta_b & 0 & 0 & 0 \\ 0 & 0 & 0 & 0 & 0 & -\beta_m & 0 & 0 \\ 0 & 0 & 0 & 0 & 0 & 0 & -\beta_b & 0 \\ 0 & 0 & 0 & 0 & 0 & 0 & 0 & -\beta_m \end{bmatrix}$$

$$C = \begin{bmatrix} -\beta_L & 0 \\ 0 & -\beta_L \end{bmatrix}$$

where A, B, and C are respectively the system dynamic matrices for the DR, Omega and Loran-C errors.

Formulating the Kalman filters for implementation on a digital computer requires that the continuous state space model defined by equation (7) be converted to the equivalent discrete model of the form:

$$X(t + \Delta t) = \phi(\Delta t, t) X(t) + W(\Delta t) \quad (21)$$

where the discrete noise vector $W(\Delta t)$ is not the same as the continuous noise process W of equation (7). The discrete driving noise covariance matrix $Q(\Delta t)$ is

$$Q(\Delta t) = \int_t^{t+\Delta t} \phi(\Delta t, \tau) Q(\tau) \phi^T(\Delta t, \tau) d\tau \quad (22)$$

The transition matrix ϕ is required by the MINS filter to extrapolate both the state vector estimate and its covariance matrix according to the standard Kalman filter equations. In the stationary case (where F is independent of time), or for small Δt , ϕ is related to the system dynamics matrix F as follows:

$$\phi(\Delta t, t) = e^{F(t)\Delta t} \quad (23)$$

The only nondiagonal block of the transition matrix ϕ is for the DR states. Exponentiating the DR block of $F\Delta t$ can be done exactly, using eigenvectors as in Reference [4], which yields:

$$\phi_{DR} = \begin{bmatrix} 1 & 0 & A \cos \theta & B & 0 \\ 0 & 1 & A \sin \theta & 0 & B \\ 0 & 0 & e^{-\Delta t/\tau_s} & 0 & 0 \\ 0 & 0 & 0 & e^{-\Delta t/\tau_s} & 0 \\ 0 & 0 & 0 & 0 & e^{-\Delta t/\tau_s} \end{bmatrix} \quad (24)$$

where

$$\begin{aligned} A &= \tau_s \left(1 - e^{-\Delta t/\tau_s} \right) \\ B &= \tau_c \left(1 - e^{-\Delta t/\tau_c} \right) \end{aligned} \quad (25)$$

The dependence of this DR matrix on the ship's heading θ makes this a non-stationary system. The variable components of ϕ are however strictly bounded, and the only consequence is that the propagation period Δt should be kept small enough that $\sin \theta$ and $\cos \theta$ do not change significantly over a single propagation period.

The Omega and Loran-C blocks are found by exponentiating the corresponding diagonal blocks of ϕ , which yields simply diagonal elements:

$$\phi_i = e^{-\Delta t/\tau_i} \quad i = b, m, L \quad (26)$$

6.0 MINS-A SIMULATION RESULTS

Extensive simulations were performed, first to give an indication of the expected performance of an "optimal" filter, and then to find the suboptimal filter with the best accuracy-efficiency characteristics.

As described in Section 4.3, the Omega errors require 4 states per station for optimal filtering, whereas the Loran-C requires only one per LOP and none are required for both the GPS and Satnav. Therefore reduction of the state size must concentrate on the Omega errors. Monte Carlo simulation was used to compare filter performance of 3 different Omega error models: 8, 12 and full 16 states (for 4 stations). It should be noted that in this phase of design trade-off study, the speed log error state was deleted, therefore the simulation study was based on the 12, 16 and 20 state filter designs rather than the 13, 17 and 21 state filters.

6.1 Monte Carlo Simulation of One-Day Voyages

To obtain a meaningful indication of the performance capability of these integration schemes, a large number of 24 hour voyages were simulated. Measurements were generated using the "real world" error model, and processed by the 12-state and 16-state filter algorithms and by the conventional reset algorithm (simply resetting the DR position to the Omega position every few hours). Some of the results are shown in Table 2 which lists the RMS position errors, in metres, for each voyage, and also lists the ratio by which the filter errors are smaller than the reset errors. This table clearly

demonstrates the ability of both filters to consistently produce a significantly more accurate position estimate than the conventional method; even though both filters processed exactly the same measurement inputs used by the conventional reset method. The ratio of the RMS radial position errors show that both filters reduce the position error by a factor of between 2 and 6. The overall improvement ratio for the RMS position error is approximately 4 to 1 for both filters.

Another result that was observed but not listed in this table, is that the position errors of both filters were less than 3 Km at all times during each of these simulation runs, whereas the error using the conventional method was at times greater than 12 Km. This indicates that the "worst case" position error can also be effectively reduced by a factor of about 4 by implementing one of these filters.

Table 3 presents the RMS velocity errors of both the filters and the conventional reset technique, for simulated voyages identical to those of Table 2. Here the velocity errors are also consistently smaller than the conventional reset method. However the range of improvement ratio for both filters is between 1.3 and 1.6, which is considerably smaller than the improvement achieved for position errors. This agrees well with theoretical expectation since Omega measurements only provide additional position information and therefore the synergistic integration of the DR and Omega can improve the accuracy of the position to a much greater extent than the velocity.

To further illustrate and compare the performance behaviour of the two filters with that of the conventional reset technique, the RMS radial position obtained from the 12-voyage averages are presented in Figure 3. From these it is obvious that the position error for the DR is the most severe and tends to grow with the passing of time; accumulating a position error of 15 Km for a journey of 28 hours. The position error for the conventional reset technique also has the same tendency to drift in the time interval between resets. When the reset is performed, the position error is corrected down to the 3-Km accuracy level of the Omega measurement. On the other hand, both filters consistently display stable error behaviour. Their position errors are bounded to about 1 Km and they do not display any time-dependent error growth characteristics after the first few hours of operation.

From Figure 3 it can also be observed that there is no significant difference between the performance of the 16-state and the 12-state filters. This is rather significant, since the 12-state filter is computationally 1.7 times more efficient than the 16-state filter, yet it can perform almost as well as the 16-state filter.

6.2 Monte Carlo Simulation of Four-Day Voyages

In order to further investigate the long-term performance capability of these integration schemes, 12 simulation runs of 4-day voyages were performed. We decided to compare the most efficient algorithm, using 12 states, to the "most optimal" algorithm, using 20-states. The resulting RMS position errors are listed in Table 4, where we can see that the 12 and 20-state filters can be expected to have RMS position errors of about 2.1 and 2.0 Km respectively over a 4-day voyage. This is an improvement in accuracy over the conventional method by a factor of about 2 to 1 for both filters, with the 20-state filter being only slightly better.

The 12-voyage average position errors are illustrated in Figure 4, where the stability of the two filter algorithms can be clearly seen. It should be noticed from Figure 4 that the slight error growth rate seen in Figure 3 for the 12-state filter practically disappears after the first day. The results of a typical simulation run are illustrated in Figure 5.

6.3 Sensitivity Analysis

In Sections 6.1 and 6.2 all performance results presented were based upon numerical simulations that assumed perfect a priori knowledge of subsystem error characteristics and the operational environment. However, considering the variety of operational environments the naval vessels will encounter, it is impossible to use one error model representation to characterize all the true operational system error behaviour. Therefore it is important to systematically examine the performance of these filters under abnormal conditions, when there are serious discrepancies between the prior statistics assumed by the filters and the error characteristics of the true operational environment. For this, extensive sensitivity analysis was conducted to evaluate the performance of the conventional reset technique and the 12-and 16-state filters under abnormal conditions. Conditions used were such that each significant error source statistic was either increased or decreased by a factor of three, while all other error statistics remained unchanged at their normal values. The 20-state filter was not included in these tests because cost considerations and the results of Section 6.2 indicate that it is not the best candidate for eventual implementation.

The results of this study are presented in Table 5, where for brevity each position error represents the RMS over two simulated runs. It is apparent that both filters respond in a very similar manner to each of the abnormal conditions. The improvement ratio of the filter position errors over those of the conventional reset method is within the range of 3.1 to 6.3 under all of these conditions. It should be noted that the absolute error of the filter position estimates was most seriously degraded when the Omega phase error was three times larger than the assumed nominal value. Here the RMS position errors of the filters and the conventional reset are 2,930 meters for the 16-state filter, 3,289 meters for the 12-state filter and 10,428 meters for reset.

For this worst case under abnormal conditions, the simulation results in terms of position error versus time are illustrated in Figure 6. Here it should be kept in mind that not only does this represent the use of Omega measurements three times less accurate than normal, but also that the filters were designed using nominal error parameters. Furthermore, even though there is such a discrepancy between the error models used to generate the abnormal measurements and the nominal error model used to design the filters, the 12-state and 16-state filters remained amazingly stable and are consistently superior to the conventional reset method over a very broad range of possible operational error conditions.

7.0 MINS-B SIMULATIONS

Once the MINS-A filter was selected, extensive Monte Carlo simulations were also performed to predict the performance characteristics of MINS-B, which is MINS-A with added Satnav and Loran-C. Simulation analysis for MINS-B with GPS was not performed because the accuracy would be essentially slaved to the GPS performance. For these tests 15 voyages were simulated, each with a duration of 24 hours. This was repeated for all possible subsets of the selected sensors. The RMS position accuracy results are summarized in Table 6. Although we expect these results to be slightly optimistic, they should accurately reflect the improvement achievable when comparing raw sensor performance to MINS-B performance.

The most interesting RMS time histories are illustrated in Figures 7 to 11, where each curve represents the RMS of 15 simulated voyages. Here we can see that MINS-B can always be expected to give a significantly more accurate position estimate than would be obtained from any of the raw measurements that MINS-B is given.

Of particular interest is the performance of MINS-B with just Satnav and Omega, seen in Figure 11, because these are both global systems. Individually, Satnav and Omega, with dead reckoning of course, each have a navigational accuracy of the order of 2 Km. Optimally integrated by MINS-B this error can be reduced by a factor of about 3, yielding a global navigation capability with accuracy comparable to Loran-C.

8.0 SEA TRIAL RESULTS

In between 1982 and 1988, several sea trials were conducted by DRKO to verify the accuracy and operability of the system. The U.S. Naval Air Development Centre (NADC) also conducted sea trials under the Foreign Weapons Evaluation Program, with the XDM in 1985-1987 on the USS Reasoner in the Pacific and on the Vanguard in the Atlantic. Table 7 summarizes the results of all Canadian sea trials. The results show general agreement between simulation and sea trials. The apparent exceptions are due to unusually large Loran cycle selection errors in 1983 and exceptionally poor Omega geometry in 1984. Each of these trials embody about a week of data, with precise reference data provided by shore based transponders such as Syledis and Maxiran. The exception is the 1987 sea trial (the first trial to use GPS), for which only about 16 hours of Syledis reference data was available.

Out of the large data set of 1987 sea trials, several reruns were conducted in the lab with various subsystems disabled to evaluate the degraded mode performance. These results are presented in Table 8 and Figures 12-13.

It is noteworthy to see Figures 14-16, where typical radial time histories are presented together with the 95% estimated error probability (EEP). It is evident that in most cases the MINS EEP does provide a very good statistical indication of MINS's performance accuracy under diverse operational conditions. Aside from providing useful information to the navigator this EEP also furnishes strong evidence that the filter error models have been properly fine tuned, which is most important especially in any suboptimal filter design.

9.0 DESIGNER DEWARE

Based on our integrated system design experience, we would like to offer the following tips to the designer:

- a. Be generous on size of truth model.
- b. Minimise filter states.
- c. Be precise on noise level of truth model.
- d. Be pessimistic on noise level of filter model.
- e. Implement easily modifiable computational algorithms (Don't take short cuts too early).
- f. Potential causes of divergency:

- Numerical error (negative diag. P)
- Programming error
- Nonlinearity
- Unmodelled error
- Optimistic noise level
- Incorrect model.

10. DESIGNER'S ROAD MAP

For the designer, a simple easy to understand road map is offered for reference:

- a. Determine system truth error model.
- b. Determine true measurement model.
- c. Determine filter error model.
- d. Determine noise model and statistics.
- e. Determine initial conditions, noise and error variance.
- f. Simulate truth model and physical environments.
- g. Verify truth model simulation (How realistic?).
- h. Verify simulation tool: set all error sources to zero to verify that there are no unintended system errors when system output is compared to the input, or/and significantly increase system errors, verify that the output errors are reasonable and behave as expected.
- i. Implement filter algorithm (could waste lots of time if this is done before #h).
- j. Review filter results.
- k. Tuning: good agreement between state estimate error and covariance, and between measurement residual and residual variance (through Monte Carlo and covariance analysis).
- l. Determine achievable optimal performance.
- m. Robustness test (filter should perform well with increased noise level of truth model).
- n. Filter sub-optimization (reduction of filter states to improve efficiency while increasing other noise levels to absorb unmodelled errors).
- o. Substitute simulated data by real data whenever possible.
- p. Conduct controlled test of partial operation.
- q. Redesign or retune the filter if necessary.

11. CONCLUSION

This paper has presented the complete design, development and performance testing of a Kalman filter based integrated navigation system. Lessons learned from the development of this and other integrated systems have also been summarized to assist the integrated system designer so that practical development work can be completed with minimum risk.

REFERENCES

1. D.F. Liang and J.C. McMillan et al, "Low Cost Integrated Marine Navigation System", Navigation Journal of the Institute of Navigation, Vol. 30, No. 4, Winter 1983-84.
2. J.C. McMillan, "A Deterministic Transit Error Model for Optimal Integration", DREO Report in progress 1988.
3. GPS Special Issue, Navigation, Journal of the Institute of Navigation, Vol. 25, No. 2, 1978.
4. J.C. McMillan, "A Kalman Filter for Marine Navigation", M. Phil thesis U. of Waterloo, 1980.

Table 1. System Error States

ERROR SOURCE	ERROR STATES					
	TRUTH MODEL	DR AND OMEGA			DR, OMEGA & LORAN	
		21-STATE	17-STATE	13-STATE	15-STATE	17-STATE*
SPEEDLOG	1	1	1	1	1	1
GYROCOMPASS	1	2	2	2	2	2
OCEAN CURRENT	2					
DR POSITION	2	2	2	2	2	2
OMEGA PHASE						
BIAS	4	4	3	4	4	5
MARKOV	4	4	3	4	4	5
PERIODIC	8	8	6			
LORAN-C	2				2	2
TOTAL NO OF STATES	24	21	17	13	15	17

* this models one extra Omega station

Table 2. RMS Radial Position Errors (metres)

VOYAGE NUMBER	RESET	16-STATE FILTER		12-STATE FILTER	
	RMS ERROR	RMS ERROR	IMPROVEMENT RATIO	RMS ERROR	IMPROVEMENT RATIO
1	3,996	1,107	3.9	985	4.1
2	5,083	1,020	5.0	1,235	4.1
3	4,356	1,148	3.8	1,106	3.9
4	3,842	1,041	3.7	1,180	3.3
5	3,627	1,438	2.5	1,205	3.0
6	4,030	1,307	3.1	1,375	2.9
7	2,841	1,359	2.1	1,290	2.2
8	3,645	1,303	2.8	1,253	2.9
9	5,093	1,404	3.6	1,556	3.3
10	7,152	1,206	5.9	1,342	5.3
11	5,029	860	5.9	1,031	4.9
12	3,607	883	4.1	882	4.4
WORST CASE	7,152	1,438		1,556	
TOTAL RMS	4,488	1,181	3.8	1,213	3.7

Table 3. RMS Velocity Errors (metres/second)

VOYAGE NUMBER	RESET	16-STATE FILTER		12-STATE FILTER	
	RMS ERROR	RMS ERROR	IMPROVEMENT RATIO	RMS ERROR	IMPROVEMENT RATIO
1	.6057	.4018	1.62	.3984	1.63
2	.6033	.4062	1.49	.4072	1.48
3	.6077	.4012	1.51	.4021	1.51
4	.5817	.3977	1.46	.3940	1.48
5	.5965	.3912	1.52	.3989	1.50
6	.5631	.4250	1.32	.4166	1.35
7	.5000	.3980	1.26	.3901	1.28
8	.6023	.4237	1.42	.4209	1.43
9	.5332	.3943	1.35	.3921	1.36
10	.5296	.3972	1.33	.3908	1.36
11	.5725	.3989	1.44	.3909	1.46
12	.6102	.4179	1.46	.4160	1.47
WORST CASE	.6507	.4250		.4209	
TOTAL RMS	.5806	.4046	1.43	.4016	1.45

Table 4. RMS Radial Position Errors (metres)

VOYAGE NUMBER	RESET	20-STATE FILTER		12-STATE FILTER	
	RMS ERROR	RMS ERROR	IMPROVEMENT RATIO	RMS ERROR	IMPROVEMENT RATIO
1	3,576	1,574	2.3	1,636	2.2
2	5,053	2,393	2.1	2,534	2.0
3	3,895	1,670	2.3	1,787	2.2
4	3,784	1,612	2.3	1,723	2.2
5	3,695	2,334	1.6	2,286	1.6
6	3,807	1,991	1.9	2,101	1.8
7	3,329	1,853	1.8	1,879	1.8
8	3,234	2,629	1.2	2,627	1.2
9	4,509	1,779	2.5	2,062	2.2
10	6,194	1,969	3.1	2,057	3.0
11	4,645	1,635	2.8	1,766	2.6
12	3,953	2,364	1.7	2,472	1.6
WORST CASE	6,194	2,629		2,627	
TOTAL RMS	4,217	2,014	2.1	2,102	2.0

Table 5. Abnormal Conditions, RMS Position Errors (metres)

ERROR CONDITION	RESET	16-STATE FILTER		12-STATE FILTER	
	RMS ERROR	RMS ERROR	IMPROVEMENT RATIO	RMS ERROR	IMPROVEMENT RATIO
NORMAL CONDITION	4,107	1,096	3.7	1,144	3.6
DR VELOCITY ERROR					
LARGE*	8,309	1,670	5.0	1,319	6.3
SMALL*	3,470	1,016	3.4	1,102	3.1
MEASUREMENT NOISE					
LARGE*	4,037	1,253	3.2	1,213	3.3
SMALL*	4,103	1,063	3.9	1,133	3.6
OMEGA PHASE ERROR					
LARGE*	10,428	2,930	3.6	3,289	3.2
SMALL*	2,762	590	4.7	463	6.0
DR CORR. TIME					
LARGE*	4,206	1,224	3.4	1,187	3.5
SMALL*	3,845	1,037	3.7	1,122	3.4

* 3 TIMES NORMAL
+ 1/3 TIMES NORMAL

Table 6. MINS-B RMS Radial Position Errors (metres)

SOURCE	ERROR
DR	8,780
OMEGA	2,060
SATNAV	1,700
LORAN-C	770
MINS-B (OMEGA)	1,598
MINS-B (SATNAV)	1,638
MINS-B (LORAN)	632
MINS-B (OM + SAT)	675
MINS-B (OM + LOR)	475
MINS-B (SAT + LOR)	503
MINS-B (OM + SAT + LOR)	368

Table 7. Summary of MINS Trial Results

	1982 SIMULATED		1983 SEA TRIAL		1984 SEA TRIAL		1987 SEA TRIAL **		1988 SEA TRIAL	
	68%	95%	68%	95%	68%	95%	68%	95%	68%	95%
MINS	370	640	254	433	380	1975	138	211	120	248
Loran-C	770	1330	3445*	5428	335	2720	204	325	190	304
Transit/DR	1700	2940	1533	3035	1575	3555	1008	2441	1106	2795
Omega	2060	3560	2209	3501	>50K +	>50K	5214	34748	3374	17032
DR	8780	15190	6775	9268	7540	16520	7910	13891	6868	11889
GPS/DR	NA	NA	NA	NA	NA	NA	668	1973	2666	7297

Samples:	600	1596	19,900	22,391
Duration (hours):	50	133	111	124
Reference system:	Maxiran	Syledis	Loran/Syledis	Syledis

NOTES:

* In 1983 Loran-C suffered from cycle selection errors.

+ In 1984 only 2 Omega LOPs were available, and their geometry was poor.

** The 1987 MINS & Loran-C results are based on the small set of Syledis reference data (1,700 samples over 15 hours) while the rest of the 1987 results are based on the full 111 hours of Loran-C data.

Table 8. 1987 Sea Trial Reruns (vs. Syledis).

68% RMS 95%	SENSORS USED
MINS RERUNS:	
66 86 184	GYRO/Log/Loran/GPS/Transit/
71 91 187	GYRO/Log/Loran/GPS/Transit/Q
128 120 256	GYRO/Log/Loran/GPS/ /
130 132 252	GYRO/Log/Loran/ /Transit/
144 142 261	GYRO/Log/Loran/ /Transit/Q
167 152 323	GYRO/Log/Loran/GPS/ /Q
207 206 330	GYRO/Log/Loran/ / /
218 252 506	GYRO/Log/Loran/ / /Q
247 356 752	GYRO/Log/ /GPS/Transit/
371 427 849	GYRO/Log/ /GPS/Transit/Q
544 553 1051	GYRO/Log/ / /Transit/
233 619 1712	GYRO/Log/ /GPS/ /
554 621 1257	GYRO/Log/ / /Transit/Q
1353 1243 2354	GYRO/Log/ /GPS/ /Q
3278 3402 7193	GYRO/Log/ / / /Q
5672 4915 6411	GYRO/Log/ / / /
102 103 188	GYRO/ /Loran/GPS/Transit/
120 133 291	GYRO/ /Loran/GPS/Transit/Q
180 161 338	GYRO/ /Loran/GPS/ /Q
195 192 348	GYRO/ /Loran/ /Transit/Q
1250 1324 2897	GYRO/ / /GPS/Transit/Q
MINS REALTIME:	
138 125 211	GYRO/Log/Loran/GPS/Transit/
SUBSYSTEMS:	
5672 4928 6411	DR
8641 70411 >100K	Omega
571 608 1205	Transit/DR
668 1127 1973	GPS/DR
204 198 325	Loran-C

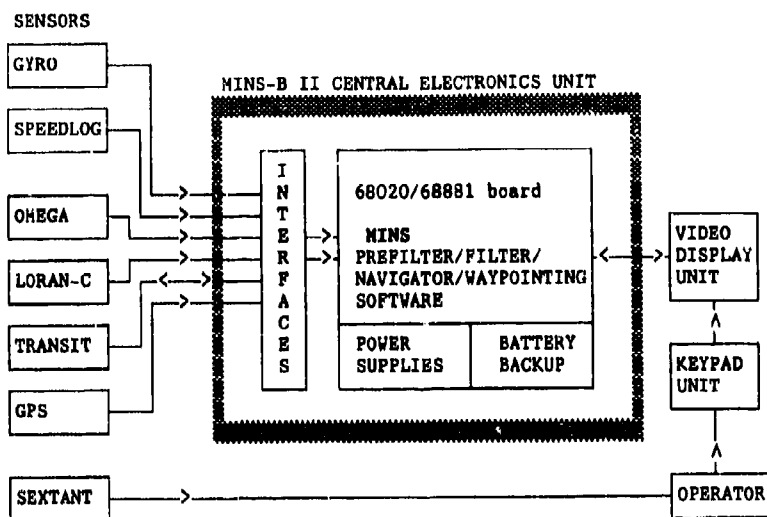


FIGURE 1. MINS BLOCK DIAGRAM

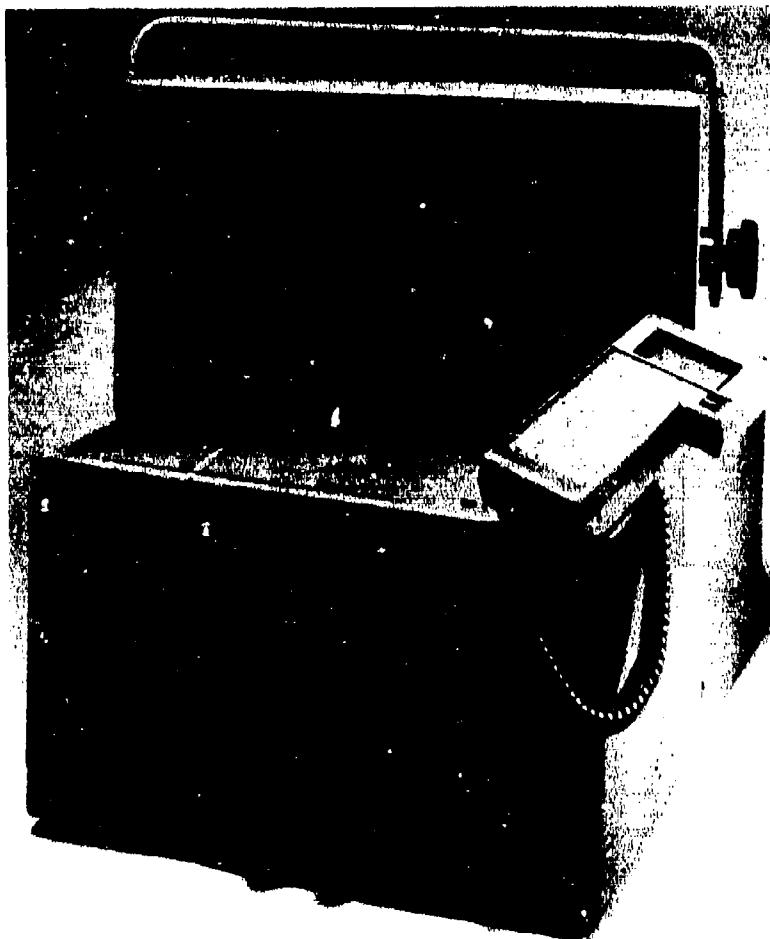


FIGURE 2. MINS-B PRODUCTION SYSTEM

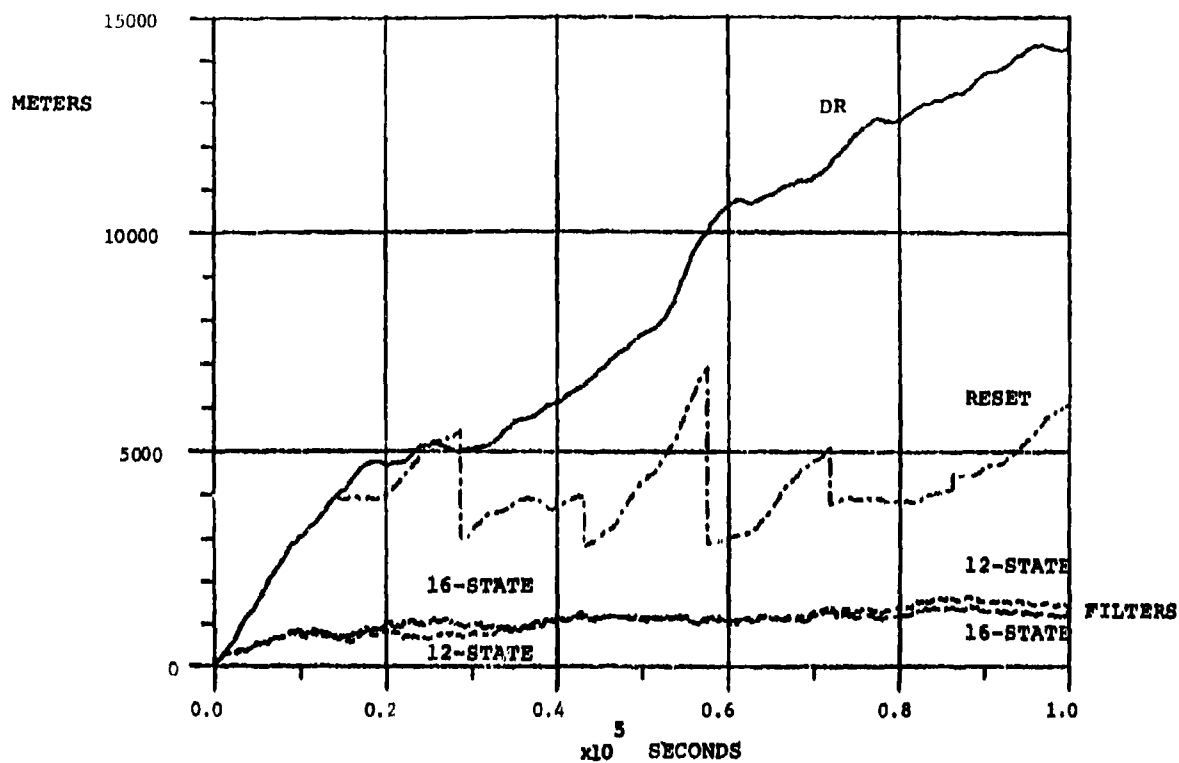


FIGURE 3. RMS RADIAL ERRORS UNDER NORMAL CONDITIONS

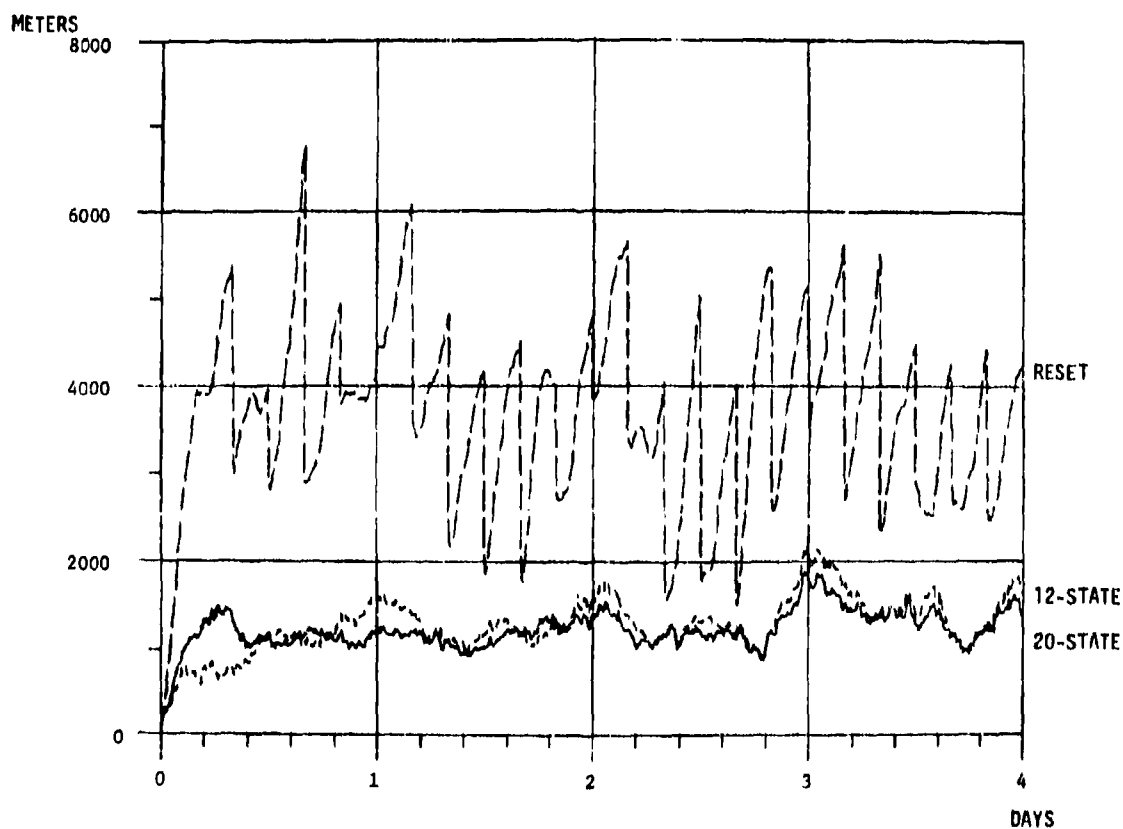


FIGURE 4. RADIAL POSITION ERRORS; 12 AND 20-STATE FILTERS

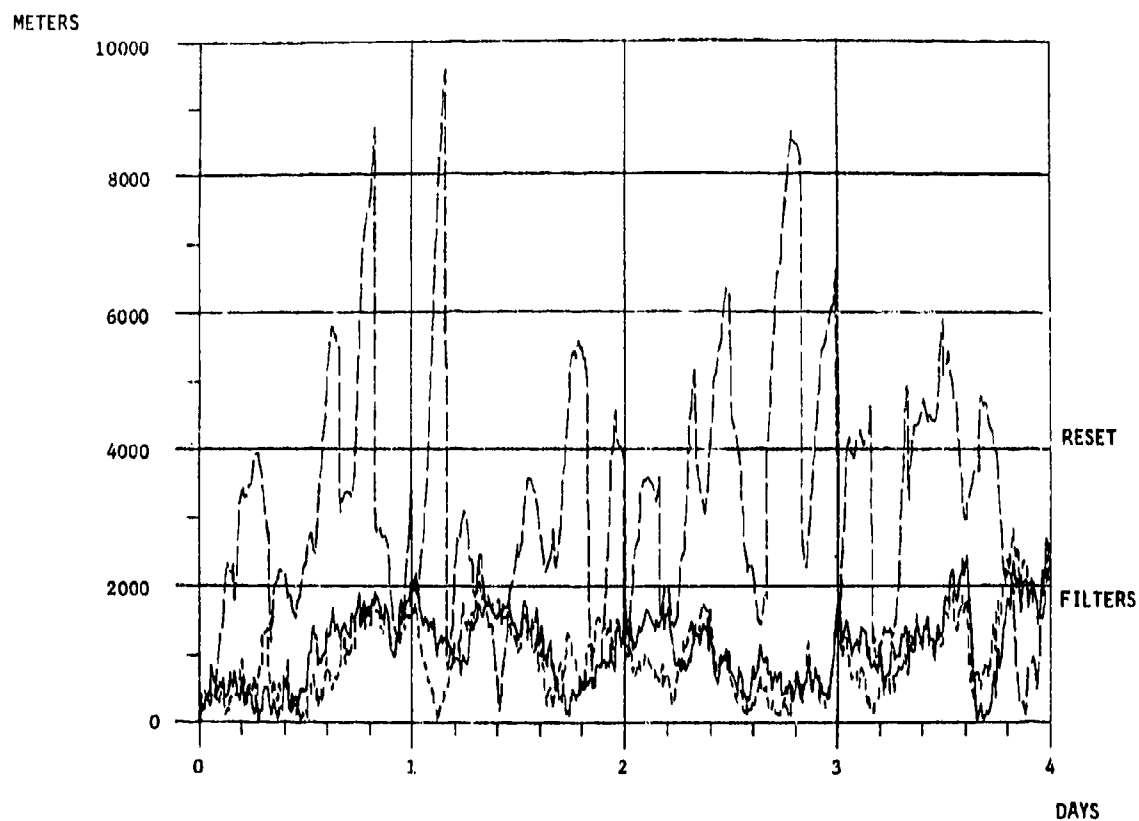


FIGURE 5. TYPICAL RADIAL ERRORS

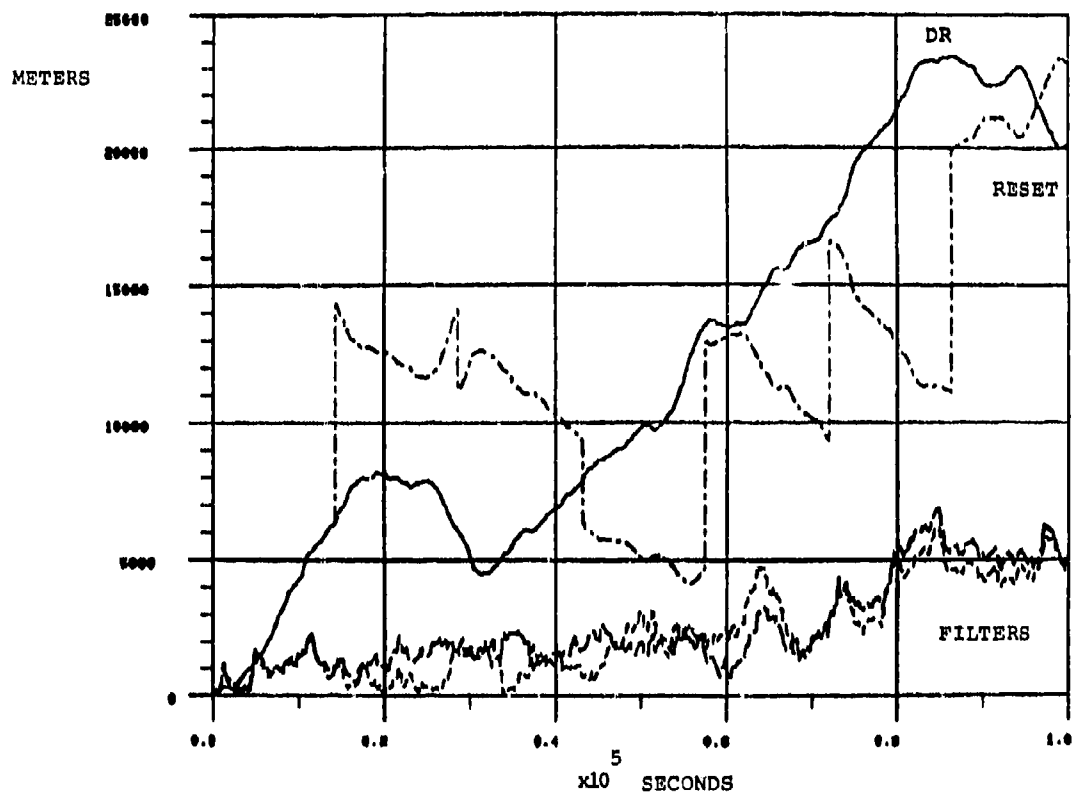


FIGURE 6. RADIAL ERRORS UNDER WORST ABNORMAL CONDITIONS

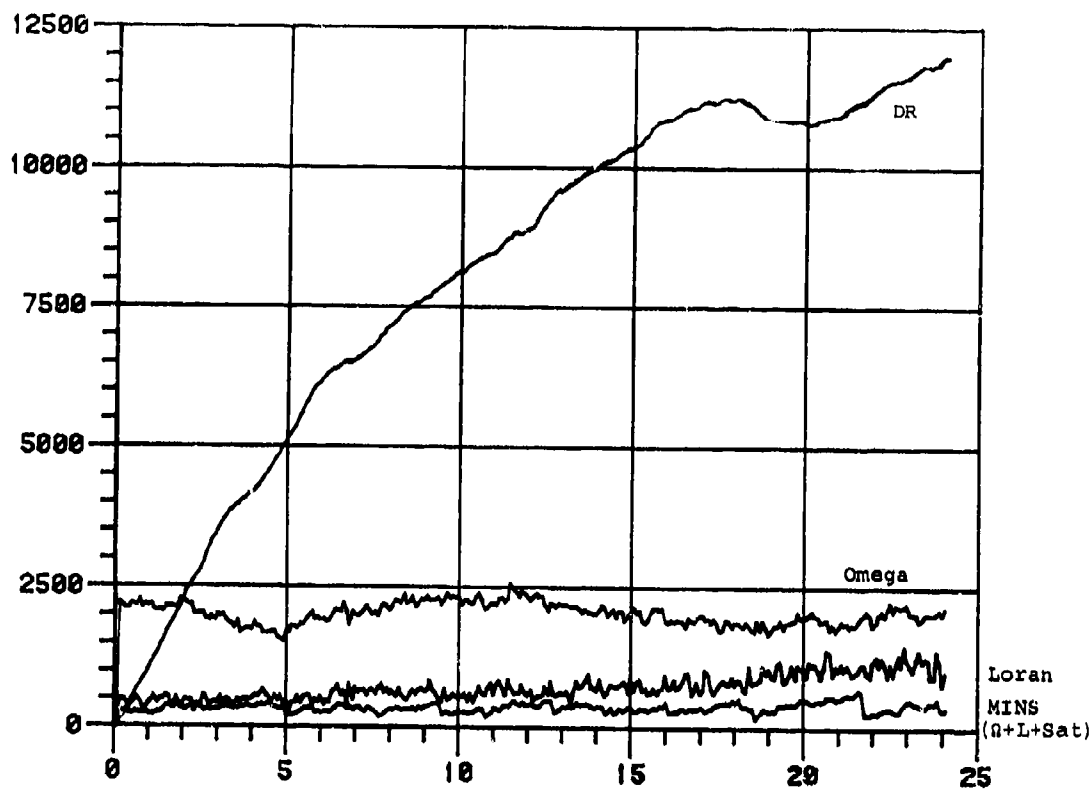


FIGURE 7. 15 VOYAGE RMS RADIAL POSITION ERRORS

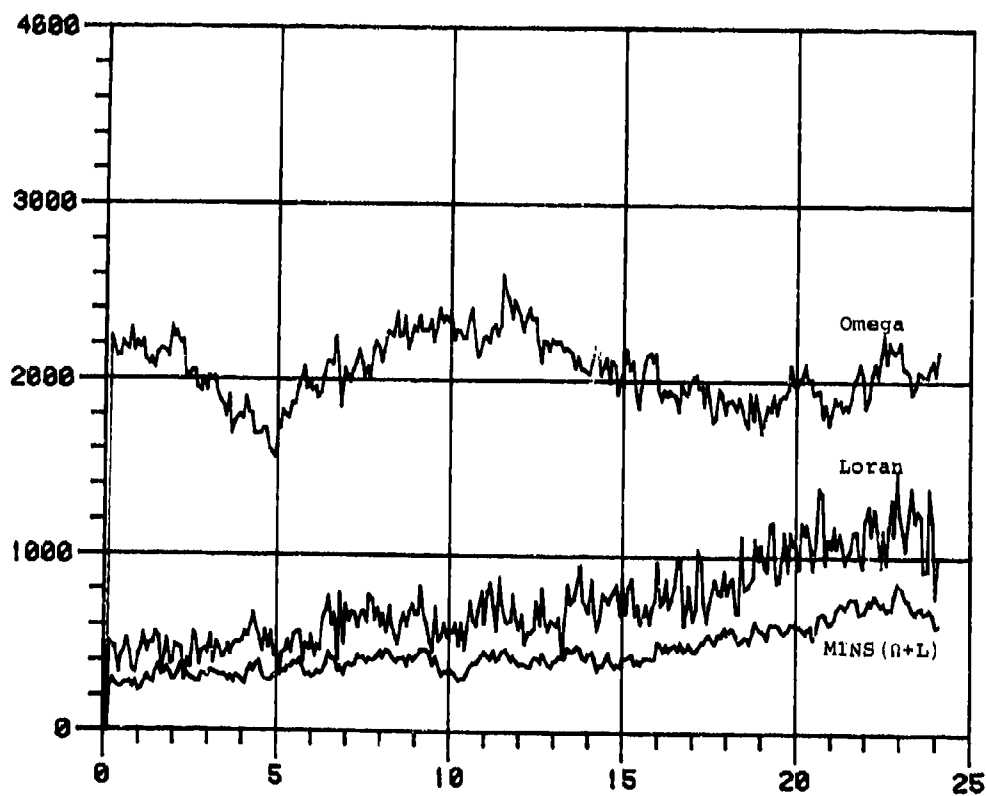


FIGURE 8. 15 VOYAGE RMS RADIAL POSITION ERRORS

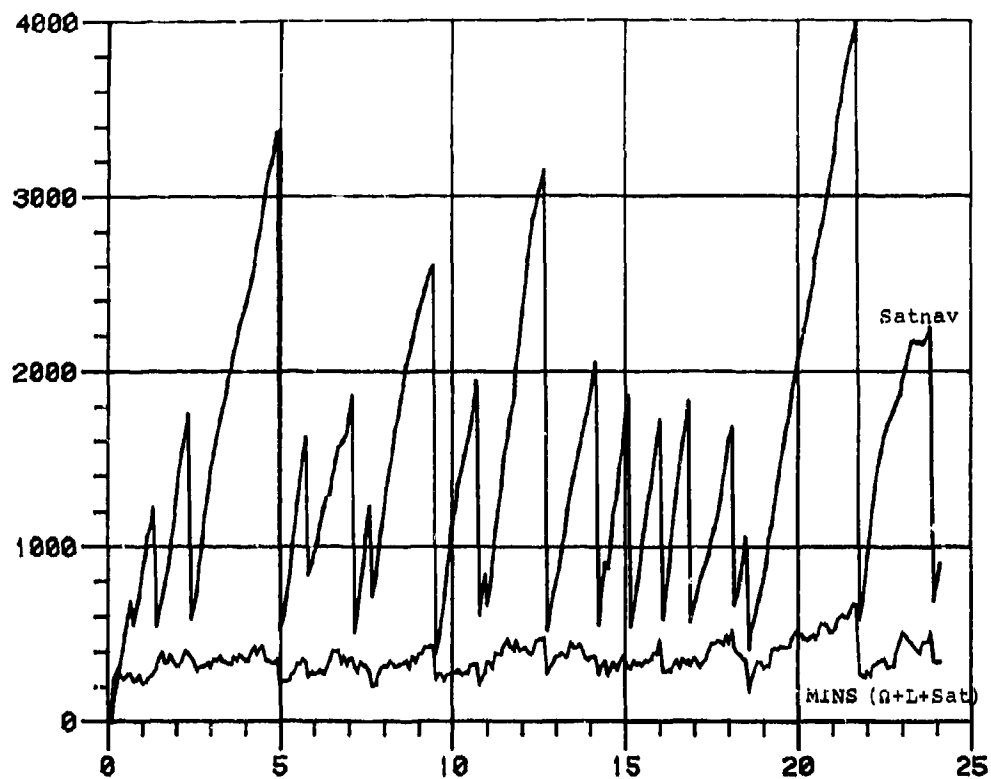


FIGURE 9. 15 VOYAGE RMS RADIAL POSITION ERRORS

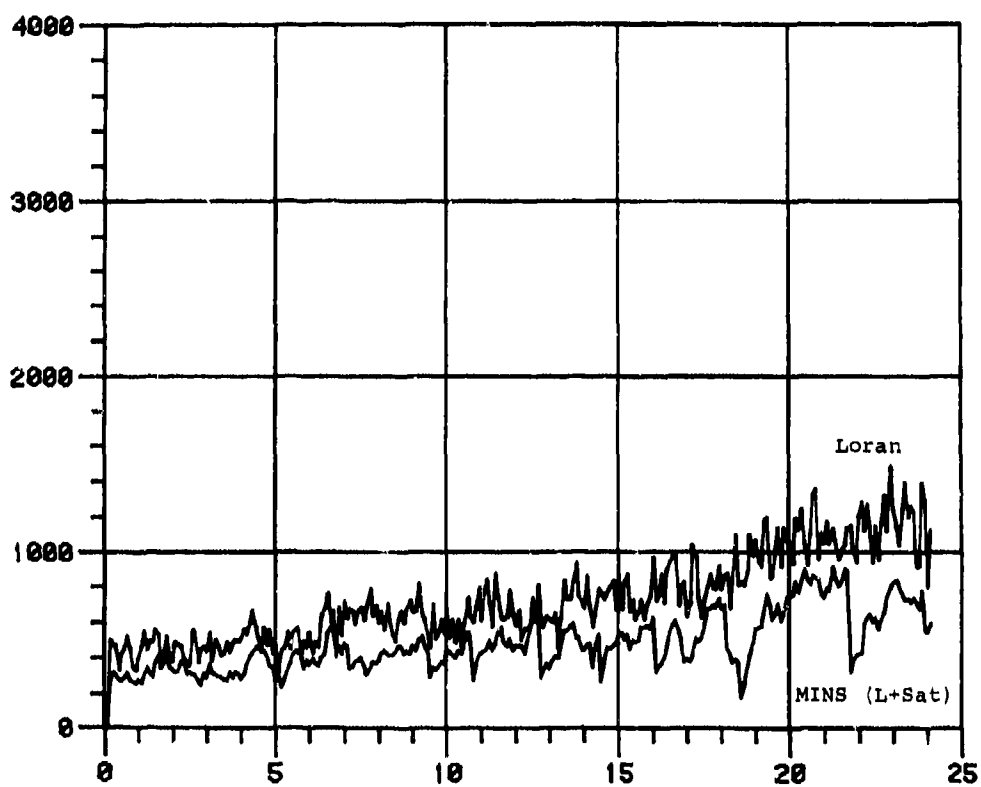


FIGURE 10. 15 VOYAGE RMS RADIAL POSITION ERRORS

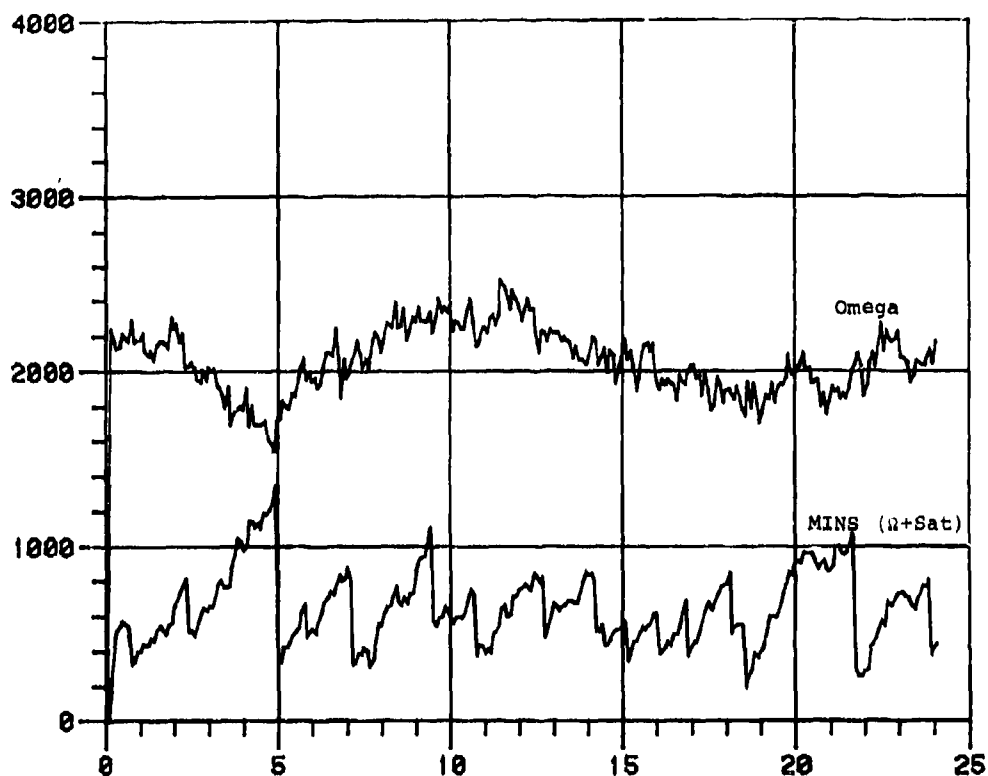


FIGURE 11. 15 VOYAGE RMS RADIAL POSITION ERRORS

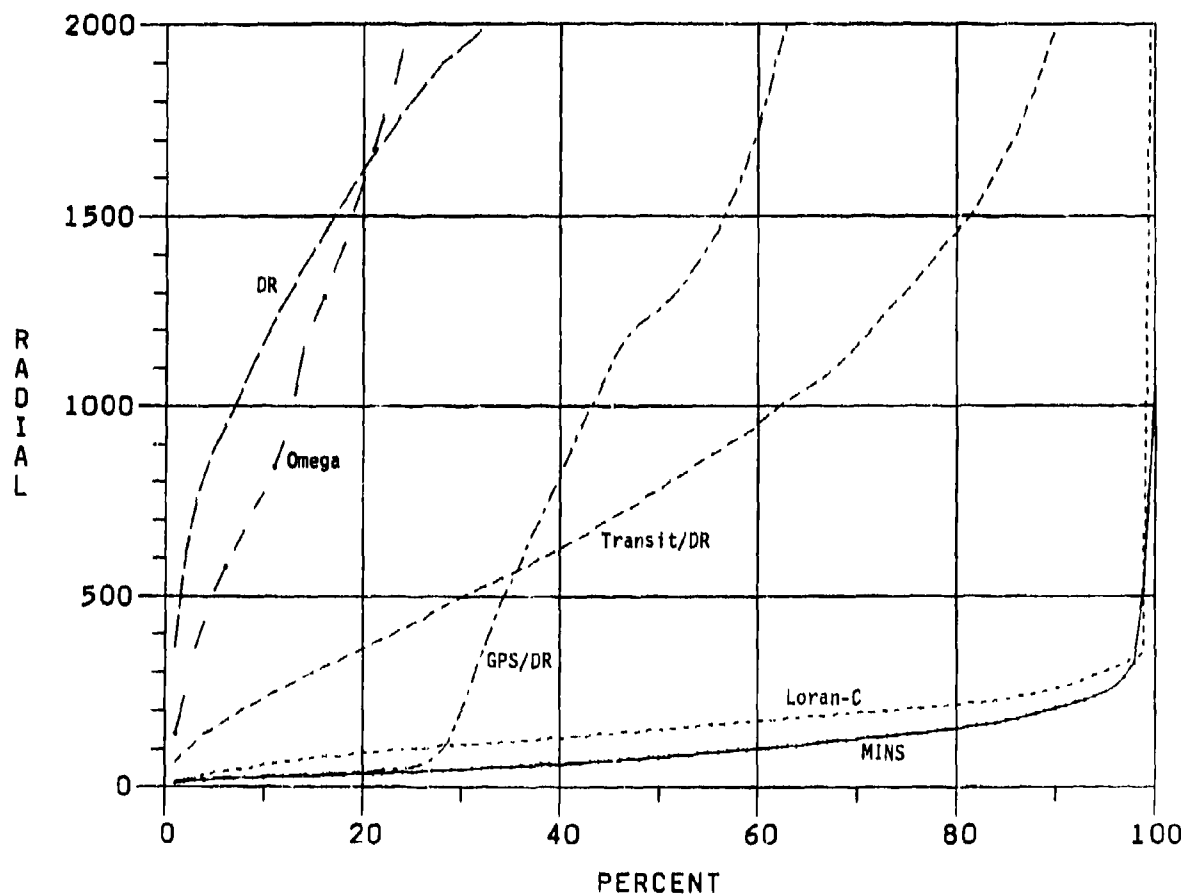


FIGURE 12. SEA TRIAL RADIAL POSITION ERRORS

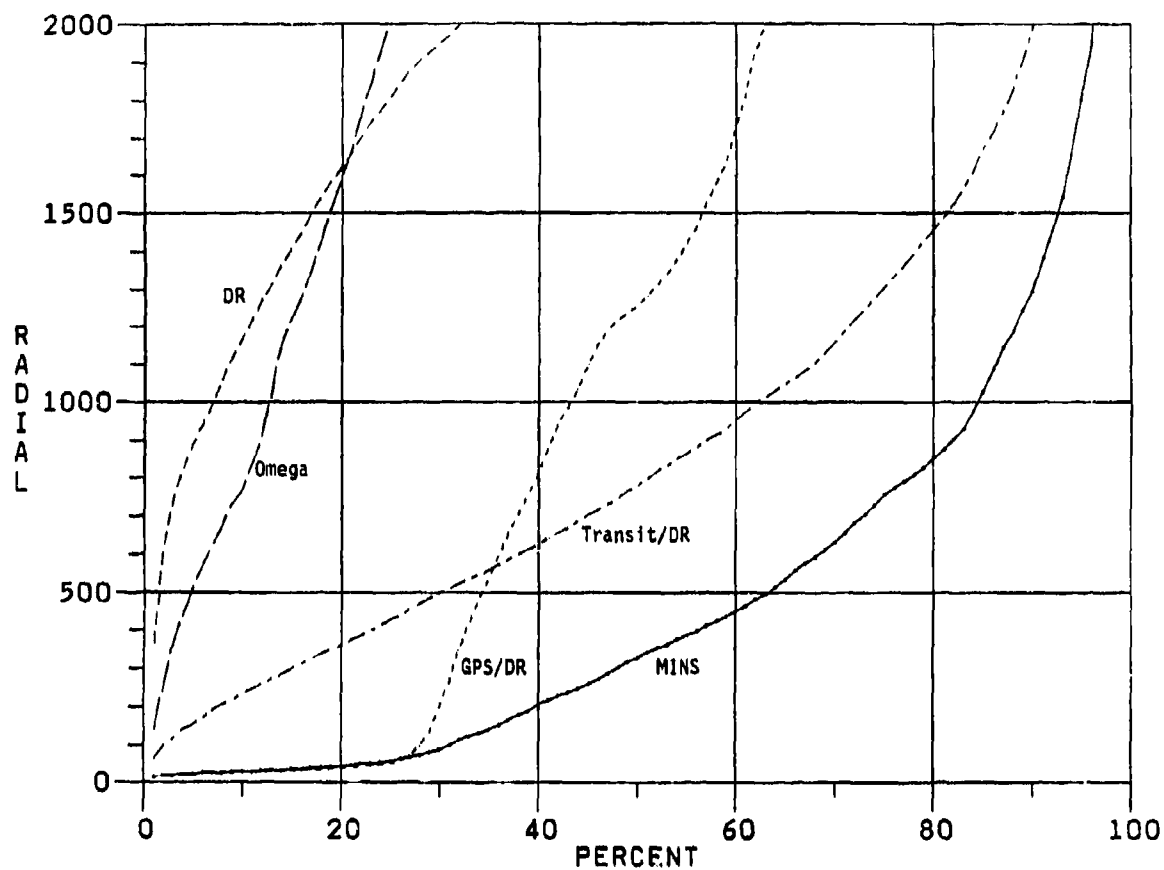


FIGURE 13. SEA TRIAL RADIAL POSITION ERRORS WITHOUT LORAN

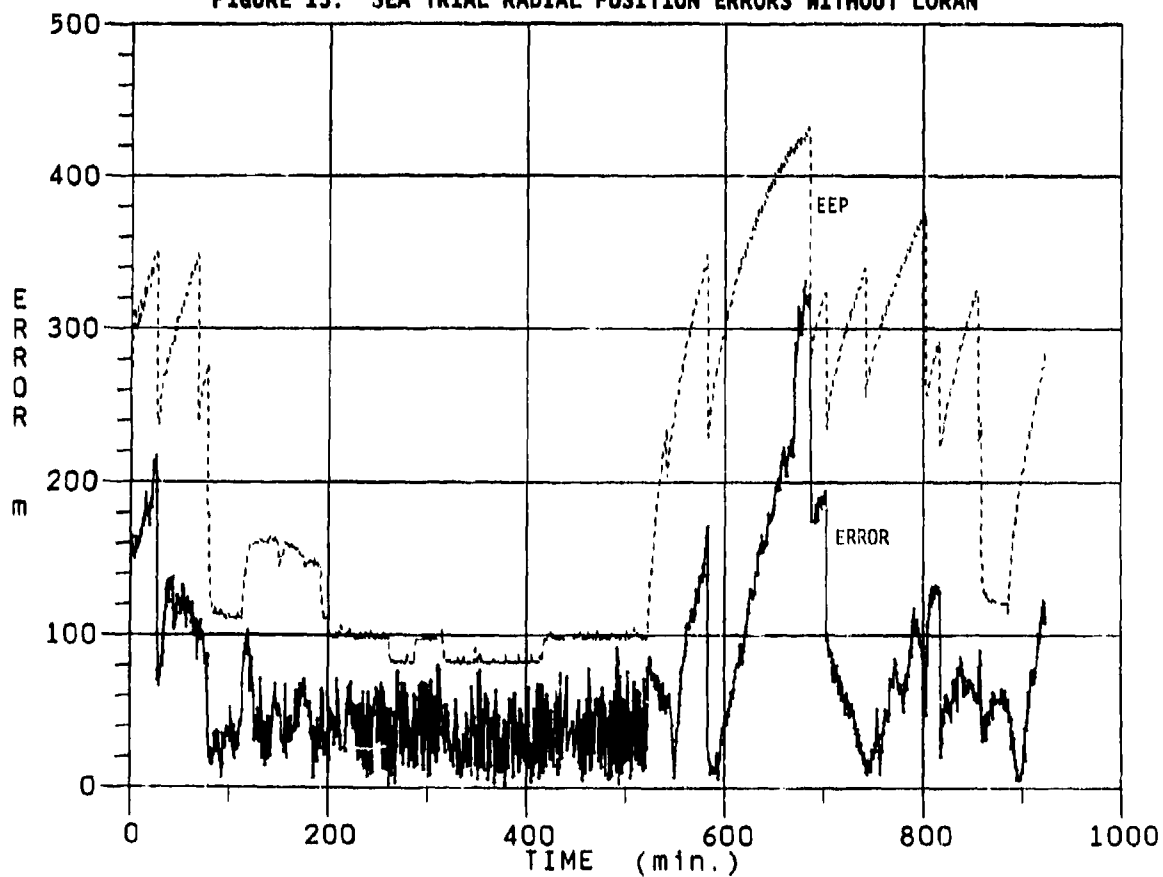


FIGURE 14. MINS ERRORS AND EEP ESTIMATES

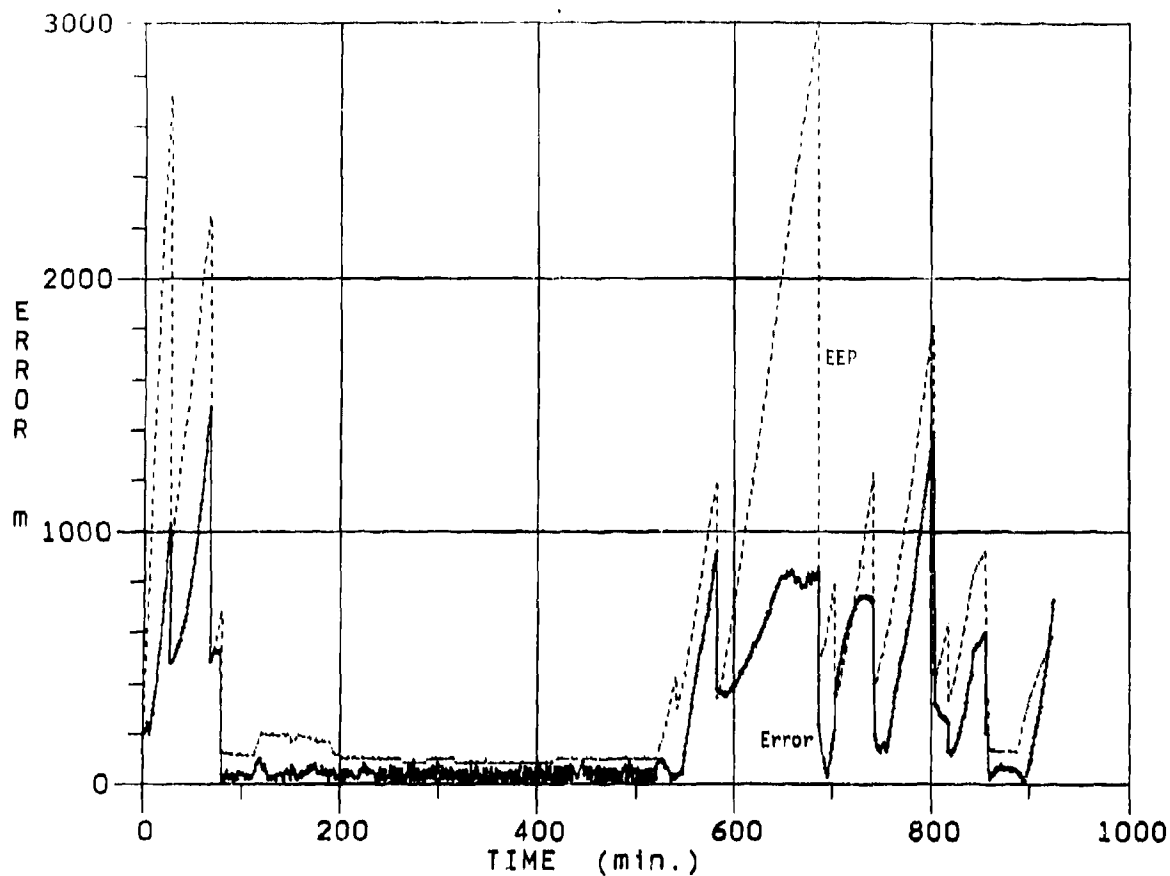


FIGURE 15. MINS ERRORS AND EEP ESTIMATES WITHOUT LORAN

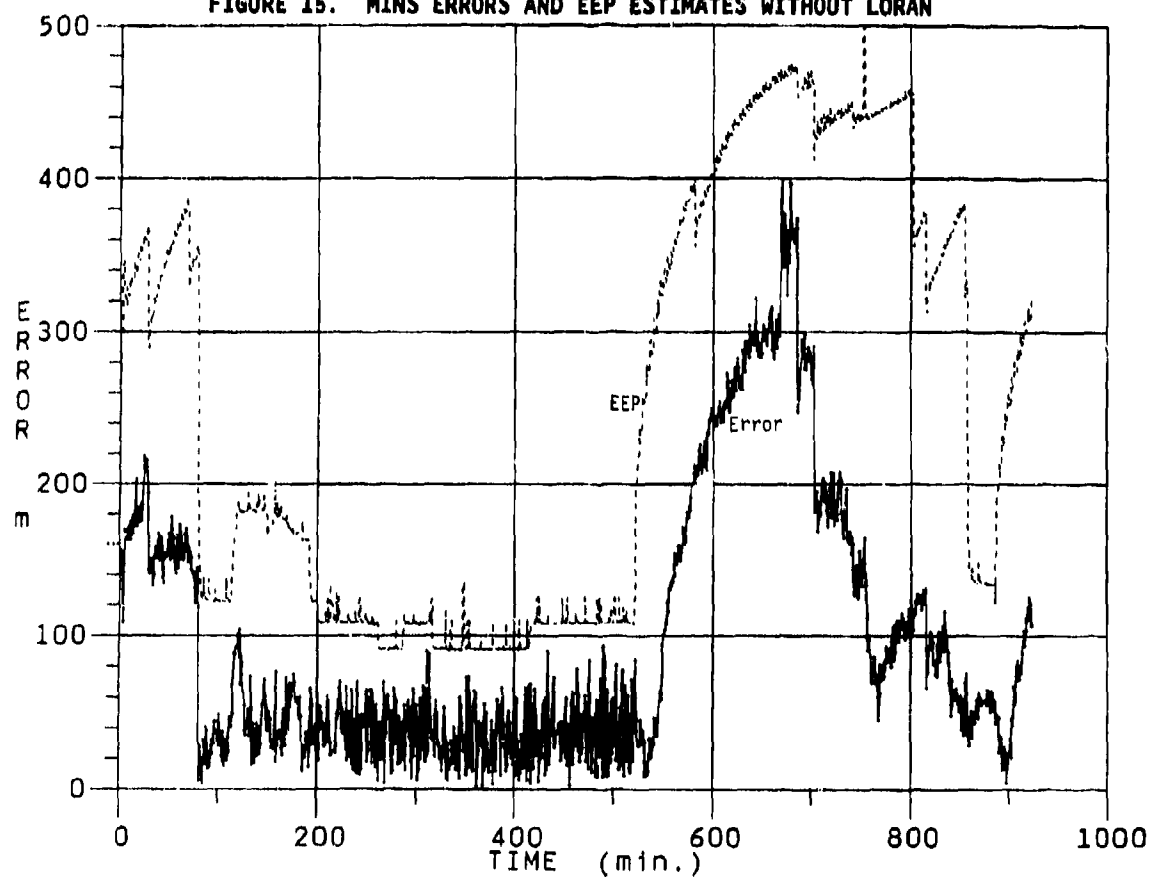


FIGURE 16. MINS ERROR AND EEP ESTIMATES WITHOUT SPEEDLOG

①

COMPONENT PART NOTICE

THIS PAPER IS A COMPONENT PART OF THE FOLLOWING COMPILATION REPORT:

TITLE: Kalman Filter Integration of Modern Guidance and Navigation Systems.

TO ORDER THE COMPLETE COMPILATION REPORT, USE AD-A214 284

THE COMPONENT PART IS PROVIDED HERE TO ALLOW USERS ACCESS TO INDIVIDUALLY AUTHORED SECTIONS OF PROCEEDING, ANNALS, SYMPOSIA, ETC. HOWEVER, THE COMPONENT SHOULD BE CONSIDERED WITHIN THE CONTEXT OF THE OVERALL COMPILATION REPORT AND NOT AS A STAND-ALONE TECHNICAL REPORT.

THE FOLLOWING COMPONENT PART NUMBERS COMPRISE THE COMPILATION REPORT:

AD#: P005 817 thru AD#: P005 822

AD#: _____ AD#: _____

AD#: _____ AD#: _____

Accession For	
NTIS GRA&I	<input checked="" type="checkbox"/>
DTIC TAB	<input type="checkbox"/>
Unannounced	<input type="checkbox"/>
Justification	
By _____	
Distribution/	
Availability Codes	
Dist	Avail and/or Special
A-1	

DTIC
ELECTE
NOV 16 1989
S E D

This document has been approved
for public release and sale; its
distribution is unlimited.

AD-7005 822

ADAPTIVE TRACKING OF MANEUVERING TARGETS BASED ON IR IMAGE DATA

Peter S. Maybeck

Department of Electrical and Computer Engineering
Air Force Institute of Technology / ENG
Wright-Patterson AFB, Ohio, USA 45433

Abstract

The capability of tracking dynamic targets from forward looking infrared (FLIR) measurements has been improved substantially by replacing standard correlation trackers with adaptive extended Kalman filters or enhanced correlator/Kalman filter combinations. This research investigates a tracker able to handle "multiple hot-spot" targets, in which digital and/or optical signal processing is employed on the FLIR data to identify the underlying target shape. Furthermore, multiple model adaptive filtering is investigated as a means of changing the field-of-view as well as the tracker bandwidth when target acceleration can vary over a wide range. Enhancements are developed and analyzed: (1) allowing some of the elemental filters within the adaptive algorithm to have rectangular fields-of-view and to be tuned for target dynamics that are harsher in one direction than others, (2) considering both Gauss-Markov acceleration models and constant turn-rate models for target dynamics, and (3) devising an initial target acquisition algorithm to remove important biases in the estimated target template to be used within the tracker. The performance potential of such a tracking algorithm is shown to be substantial.

1. Introduction

This paper addresses the problem of accurately tracking the azimuth and elevation of a highly maneuverable airborne target, using outputs from a forward-looking infrared (FLIR) sensor as measurements. The shape of the target intensity pattern on the FLIR image focal plane is not assumed to be well known a priori, and it may involve multiple "hot spots" and may also change significantly with time. Consequently, the target shape function must be identified adaptively in real time. Moreover, the target vehicle can exhibit many different dynamic behaviors, from benign straight-line trajectories to very harsh, high-g turning and jinking maneuvers. It is desired to maintain very precise tracking during the benign phases while also preventing loss-of-lock during maneuver initiation and sustained acceleration. Thus, a capacity to change filter gains and field-of-view rapidly and effectively must be incorporated.

In earlier research, a simple four-state extended Kalman filter [1,2] was developed to track a point source (distant) target with benign dynamics, based on FLIR measurements assumed to be corrupted by temporally and spatially uncorrelated noises [3,4]. This algorithm consistently exhibited an order of magnitude improvement in rms tracking errors over currently used correlation trackers, under nominally assumed conditions; between 0.2 and 0.8 pixel (picture element, 20 μ rad on a side) rms errors were attained in various scenarios. This enhanced accuracy was achieved by allowing the filter to exploit knowledge unused by the usual correlation trackers: size, shape and motion characteristics of the target, and spectral properties of atmospheric jitter.

Robustness studies [5,6] revealed a degradation in performance when the actual parameters in the tracking problem differed from those assumed by the filter. Variations in the spread, shape and height of the target intensity pattern in the FLIR image plane and differing target motion characteristics were significant, while changes in rms value or the temporal or spatial correlation of the background noise were of lesser importance for the signal-to-noise ratios under consideration. Design modifications and on-line adaptation were then incorporated to enable this type of filter to track maneuvering targets with spatially distributed and changing image intensity profiles, against background clutter [5-8]. Alternative target dynamics models were also explored to enhance tracking capabilities [9-11]. Although adaptive gain changing in the filter allowed for maintaining track during gradual target acceleration, it was not sufficient for the case of harsh maneuver initiation. Residual monitoring provided a means of

detecting harsh maneuver onset and responding appropriately. This included changing the gain immediately, reprocessing the most recent measurement, and altering the state estimate in an ad hoc fashion during a period of time following the maneuver detection [6-8]. As experienced by others [12-17], the appropriate adaptation to a changing set of target dynamics was a challenging issue; despite successful tracking in some demanding scenarios, it was still desired to explore alternative adaptation mechanisms.

Up to this point, however, all filter designs were based on the assumption that the target intensity profile in the FLIR image plane would be unimodal and well described by a bivariate Gaussian function, allowing elliptical constant-intensity contours to account for target shape effects. Research was then conducted on ways to handle multiple hot-spot targets, where neither the functional form of the hot spots' intensity nor their quantity or relative spacing could be provided a priori [18-19]. For this situation, online digital or optical signal processing techniques [20-23] would be used to derive a target shape function from the available FLIR sensor information. In one tracker formulation, this shape function is used in the measurement update portion of an extended Kalman filter that is otherwise identical to the previous designs. In an alternative tracker, the shape function is used as a template for an enhanced correlator, which then provides offset "measurements" to a linear Kalman filter rather than using an extended Kalman filter to process raw FLIR data directly. This latter design is considerably less demanding computationally, and so it is preferable if its performance is adequate. Initial research efforts [18-19] concentrated on demonstrating the feasibility of the adaptive shape function construction and considered only benign target dynamics. Ensuing research [24-25] evaluated performance potential of the two tracker formulations in more highly dynamic close-range scenarios, establishing comparable rms tracking errors; the extended Kalman filter exhibited larger biases but smaller standard deviations than the enhanced correlator/linear Kalman filter algorithm. However, this research also revealed a need for an effective and quickly responding adaptation to large-scale changes in the target dynamics.

Further research [26, 27] has investigated the use of multiple model adaptive estimation [2, 10, 14, 28-36] to provide adaptive expansion and contraction of the effective tracker field-of-view, as well as adaptive selection of an assumed target dynamics model, in order to increase the dynamic range of precision tracking. For the initial feasibility study, two independent filters have been used to generate state estimates from the shared sensor. One is tuned for best performance in the case of benign dynamics and uses a narrow field-of-view; the other is tuned for high-g target maneuvering and uses a wider field-of-view (reduced resolution is accepted in order to provide considerably lower probability of losing lock). Adaptive expansion and contraction of the tracker field-of-view is attained by generating the probabilistically weighted average of the two filter state estimates, or by selecting the one elemental filter with the highest computed probability of validity [37], with comparable results. Addition of a third elemental filter to the MMAF bank, based on intermediate levels of target dynamics, can yield significant improvement in tracker performance [37, 38].

However, rather large bias errors have persisted when the target executes harsh 20-g turn maneuvers, and an analysis of these error characteristics has suggested the potential of adding elemental filters to the bank with rectangular (rather than only square) fields of view, to expand that field only in the critical direction, while maintaining maximum resolution in the other. Also, since the currently used zero-mean Gauss-Markov target acceleration model does not accurately describe true dynamics during such maneuvers, particularly at close range, it has been suggested that a nonlinear constant turn-rate dynamics model might be embedded in at least some of the elemental filters in the multiple model bank. The most recent research [39, 40] has pursued these avenues to improved tracking.

II. Individual Filter Designs

The FLIR measurement model developed in [3] and [7], the target dynamics models of [7] and [9], and the adaptive target shape identification algorithm of [18] can form the basis for a tracker in the form of either an extended Kalman filter or a cascade of an enhanced correlator with a Kalman filter based on a linear measurement model. This section presents these models and the resulting filter designs. In the next section, a number of such elemental filters will be combined within a multiple model adaptive estimator.

We desire to track the centroid of a spatially distributed dynamic target based on FLIR measurements, in order to provide appropriate inputs to a pointing controller so that the target remains in the center of the field-of-view. This involves determining the pointing errors in two orthogonal directions of the FLIR image plane (and other states as well), given measurements of average intensity levels over each of 64 pixels in an 8-by-8 array ("tracking window") provided as a subset of a larger array by the FLIR at a 30 Hz rate. Letting $x_{\text{peak}}(t)$ and $y_{\text{peak}}(t)$ locate the centroid of the apparent target intensity function relative to the center of the 8-by-8 array, we can describe that intensity at any point (x, y) by the function

$$I_{\text{target}}([x - x_{\text{peak}}(t)], [y - y_{\text{peak}}(t)], t)$$

as depicted in Fig. 1. In earlier research [3-10], this function was assumed to be well modeled as bivariate Gaussian, possibly with some uncertain parameters to be identified. Here the entire I_{target} function is computed adaptively, as discussed later. The apparent centroid location is actually the sum of contributions due to true target dynamics and atmospheric jitter (ignoring vibration effects for a ground-based tracker):

$$x_{\text{peak}}(t) = x_d(t) + x_a(t) \quad (1)$$

and similarly for $y_{\text{peak}}(t)$. The objective of the tracker is to estimate x_d and y_d accurately so that they can be regulated by closed-loop control.

Even for benign dynamics, it is appropriate to estimate velocity (and perhaps acceleration) as well as position of a close-range target. Letting $x_d(t)$ and $y_d(t)$ be arrayed in a position vector $p(t)$, we can write (as an approximation, ignoring the effects of a rotating tracker coordinate frame):

$$\dot{p}(t) = v(t) \quad ; \quad \dot{v}(t) = a(t) \quad (2)$$

Whereas acceleration $a(t)$ can be modeled as a low-strength white noise for very benign conditions (straight-line flight trajectories, with white noise used for filter tuning), experience in this particular application [6-11, 24, 25] has indicated the performance desirability of two alternatives. First, one can treat acceleration as a first-order Gauss-Markov process,

$$\dot{a}(t) = -[1/T] a(t) + w(t) \quad (3)$$

where the correlation time T and strength of the white Gaussian noise $w(t)$ are treated as design tuning parameters to match an assumed level of target dynamics. Secondly, one can invoke a "constant turn-rate" model, very descriptive of many airborne target scenarios:

$$\dot{a}(t) = -\omega^2 v(t) + w(t) \quad ; \quad \omega = \frac{|v(t) \times a(t)|}{|v(t)|^2} \quad (4)$$

where ω is the turn rate. Unlike Eq. (3), this is a nonlinear dynamics model, so a tradeoff of performance versus computational loading must be conducted before its use is warranted for online implementation.

Atmospheric disturbances cause wavefront phase distortions, resulting in translational shifts in the FLIR image plane called "jitter". On the basis of spectral properties, atmospheric jitter processes x_a and y_a (see Eq. (1)) were each modeled as outputs of a third order shaping filter [1], described by a transfer function of $K\omega_1\omega_2^2(s+\omega_1)^{-1}(s+\omega_2)^{-2}$, driven by white Gaussian noise [41,42]. Since $\omega_1 \ll \omega_2$ ($\omega_1 = 14$ rad/sec, $\omega_2 = 660$ rad/sec) and the lower frequencies are more important, this was well approximated in the filter by the reduced-order model $K\omega_1(s+\omega_1)^{-1}$.

Combining these two states with the six target dynamics states that arise from augmenting Eq. (2) with either (3) or (4), forms the basis of an eight-state extended Kalman filter [2] propagation algorithm of the form:

$$\dot{\hat{x}}(t) = f[\hat{x}(t), u(t)] \quad (5)$$

$$\dot{P}(t) = F(t)P(t) + P(t)F^T(t) + Q(t) \quad (6)$$

where $P(t)$ is the state error covariance matrix and $Q(t)$ is the white noise strength matrix. If (3) is used, then $f[\hat{x}(t), u(t)] = F\hat{x}(t) + Bu(t)$, i.e., the propagation model is linear and time invariant, and thus is particularly easy to implement. If Eq. (4) is used, (5) is nonlinear and $F(t)$ in (6) is the partial of f with respect to the state x , evaluated at the current best state estimate.

At each sample time t_i , measurements of the average intensity over each pixel in the 8-by-8 tracking window become available. Let $z_{jk}(t_i)$ denote the scalar measurement corresponding to the j -th row and k -th column of that array, to write:

$$z_{jk}(t_i) = \frac{1}{A_p} \iint_{\text{REGION OF JK-TH PIXEL}} I_{\text{target}}([x - x_{\text{peak}}(t)], [y - y_{\text{peak}}(t)], t) dx dy + b_{jk}(t_i) + n_{jk}(t_i) \quad (7)$$

where A_p is the area of one pixel, I_{target} was described previously, $b_{jk}(t_i)$ models the background noise effects on the jk -th pixel and $n_{jk}(t_i)$ the internal FLIR noise effects on that pixel. The 64 scalar measurements of this form at sample time t_i are arrayed in a vector:

$$z(t_i) = h[x(t_i), t_i] + b(t_i) + n(t_i) \quad (8)$$

which can be used as the measurement model upon which to base an extended Kalman filter. Online identification of $h[x(t_i), t_i]$ will be discussed subsequently. The background and FLIR noises are assumed independent (so that their variances add for a given pixel) and temporally uncorrelated; FLIR noise is assumed spatially uncorrelated and the background noise has a correlation distance of about two pixels (the corresponding noise covariance matrix, $E\{v(t_i)v^T(t_i)\} = R(t_i)$, is thus sparse but not diagonal).

An 8-state, 64-measurement extended Kalman filter [2] was designed. To avoid online computation of a 64-by-64 matrix inversion, the usual update algorithm was replaced by the algebraically equivalent:

$$P^{-1}(t_i^+) = P^{-1}(t_i^-) + H^T(t_i)R^{-1}(t_i)H(t_i) \quad (9)$$

$$P(t_i^+) = [P^{-1}(t_i^+)]^{-1} \quad (10)$$

$$K(t_i) = P(t_i^+)H^T(t_i)R^{-1}(t_i) \quad (11)$$

$$\hat{x}(t_i^+) = \hat{x}(t_i^-) + K(t_i) \{z(t_i) - h[\hat{x}(t_i^-), t_i]\} \quad (12)$$

where $\hat{x}(t_i^+)$ and $P(t_i^+)$ are the state estimate and error covariance after updating the values $\hat{x}(t_i^-)$ and $P(t_i^-)$ with the measurement vector $z(t_i)$. Here $H(t_i)$ is the partial $\partial h/\partial x$ evaluated at $\hat{x}(t_i^-)$, and it is to be identified online along with $h[\hat{x}(t_i^-), t_i]$. This form only requires two 8-by-8 matrix inversions; $R^{-1}(t_i)$ is assumed to be generated once offline.

Up to this point, the lower (digital and/or optical) signal processing path of Fig. 2 has been described. Based on the FLIR intensity data $z(t_i)$ and the identified h and H functions, the extended Kalman filter produces state estimates $\hat{x}(t_i^+)$ and one-step-ahead predictions $\hat{x}(t_{i+1}^-)$. The latter can be used by a control algorithm to point the center of the field-of-view to where the target is predicted to be located, so that $\hat{x}_d(t_{i+1}^-)$ and $\hat{y}_d(t_{i+1}^-)$ are zeroed. The upper path [18] in Fig. 2 identifies h and its partial derivative H . It is based on the fact that the actual target image will change rather slowly relative to the sample period of 1/30 sec., while the background noises will typically change more rapidly, especially if a background is being swept behind a moving target. Thus, temporal averaging or filtering of sequential data frames should be exploited in target shape reconstruction; spatial or spatial frequency filtering may also be useful to discriminate between target and background IR intensity patterns [18].

Consequently, interframe smoothing is used to accentuate the target and attenuate the noise. First an FFT is performed on the FLIR data frame (for efficient processing and possible spatial frequency filtering, perhaps optically), and then a negating phase shift in accordance with the shift properties of discrete Fourier transforms [18-20] is applied to reconstruct the transform of the target image as though it were centered in the field-of-view in the original untransformed coordinates. The appropriate phase shift

for the frame at t_i is based on $\hat{x}_{\text{peak}}(t_i^+)$ and $\hat{y}_{\text{peak}}(t_i^+)$ derived from Eq. (1) and $\hat{x}(t_i^+)$ as produced by the filter.

Conceptually, this result can be averaged with the most recent M such centered and transformed data frames, to accentuate the target and attenuate noise. To implement this without requiring explicit storage of these M data sets, finite-memory averaging is approximated by exponential smoothing:

$$\hat{I}(t_i) = \alpha I(t_i) + [1-\alpha] \hat{I}(t_{i-1}) \quad (13)$$

where $\hat{I}(t_i)$ and $\hat{I}(t_{i-1})$ are the current and previous templates, respectively, and where $I(t_i)$ is the current data frame set of intensity values. Valid α 's lie in the range $[0,1]$, with smaller α 's corresponding to longer memory; sensitivity studies [18,19] yielded $\alpha = 0.1$. The output of the "Exponential Smoothing of Centered Data" block in Fig. 2 is a representation of the FFT of a template h associated with a centered target image.

Again through appropriate phase shifting, $h[\hat{x}(t_{i+1}^-), t_{i+1}]$ can be evaluated, assuming that the controller successfully zeroed out the estimated target dynamics position states in the sample period between t_i and t_{i+1} . The spatial derivative $H[\hat{x}(t_{i+1}^-), t_{i+1}]$ is readily produced by simple multiplication, using the derivative property of Fourier transforms: if f_x and f_y are spatial frequencies and \mathcal{F} denotes Fourier transform,

$$\mathcal{F}[\partial h(x,y)/\partial x] = j2\pi f_x \cdot \mathcal{F}[h(x,y)] \quad (14)$$

$$\mathcal{F}[\partial h(x,y)/\partial y] = j2\pi f_y \cdot \mathcal{F}[h(x,y)]$$

Finally, the inverse FFT of both results yields $h[\hat{x}(t_{i+1}^-), t_{i+1}]$ and $H[\hat{x}(t_{i+1}^-), t_{i+1}]$ for use in the Kalman filter at the next sample time, i.e., at t_{i+1} .

An alternative tracker was also described in [18]. The upper path of Fig. 2 is left intact except that H no longer requires evaluation. However, $h[\hat{x}(t_i^-), t_{i+1}]$ is now used as a template by an enhanced correlator that operates on the raw FLIR data to generate estimated offsets between the apparent target and field-of-view center. These are provided as two scalar measurements to a linear Kalman filter (assuming Eq. (3) is used rather than (4) for the basis of time propagation of estimates). Because the measurement dimension is now two, Eqs. (9) - (11) are replaced with the more conventional form of update equations [1]:

$$K(t_i) = P(t_i^-) H^T(t_i) [H(t_i) P(t_i^-) H^T(t_i) + R(t_i)]^{-1} \quad (15)$$

$$P(t_i^+) = P(t_i^-) - K(t_i) H(t_i) P(t_i^-) \quad (16)$$

The 2-by-2 measurement noise covariance matrix R for this filter is determined by statistical analysis of errors produced by the proposed correlator under controlled conditions. This correlator is enhanced over a conventional correlator in a number of ways. First, the current FLIR data frame is correlated with an estimated target template rather than merely a previous frame of data. Secondly, thresholding of the correlation function to suppress low noise-induced peaks and computing centroid summations are used to approximate correlation function peak detection with lower computational loading and lower sensitivity to multiple peak problems than other peak detection methods; a threshold of 30% of the maximum correlation value has been adopted based on empirical performance evaluations [38,39]. Finally, the FLIR/laser pointing commands are derived from the filter's propagated state estimate as shown in Fig. 2, and not just from the correlator offset outputs.

Thus, four possible configurations have been described. Two involve an extended Kalman filter that processes the raw FLIR data directly (64-dimensional measurements, nonlinearly modeled); one has a linear propagation cycle based on Eqs. (2) and (3), and the other has a nonlinear propagation based on (2) and (4). In contrast are the two "alternative" trackers based on an enhanced correlator feeding two-dimensional offset "measurements" (modeled linearly) to a Kalman filter; the filter is totally linear if the propagation cycle is based on Eqs. (2) and (3), and it is an extended Kalman filter if based on the nonlinear dynamics of (2) and (4).

Any of these configurations could be "tuned" [1,2] for best performance under benign target conditions by appropriate choice of noise strength Q in Eq. (6) (and correlation time T in Eq. (3) if it is the basis of the filter propagation cycle). If it is desired to tune for best performance under heavy target maneuvering, not only would Q and T be changed, but it would also be appropriate to adopt a larger field-of-view (this is also true for target acquisition).

III. Multiple Model Adaptive Filtering

One means of allowing rapid and effective changing of both the bandwidth and field-of-view of the tracker is multiple model adaptive filtering [2, 14, 26-40]. In this approach, a number of independent filters are processed in parallel, each based upon a particular model of target dynamics intensity and a corresponding field-of-view. By optimally combining the estimates of these filters at each sample time, an adaptive estimator is produced that will yield desirable high resolution for benign target trajectories while also maintaining lock on very dynamic targets.

Let a denote the vector of uncertain parameters in a given model; here it is composed of the strength of the white noise driving the target acceleration model (3) or (4), and the field-of-view size. In order to make identification of a tractable, its continuous range of values is discretized into K representative values. If we define the hypothesis conditional probability $p_k(t_1)$ as the probability that a assumes the value a_k (for $k = 1, 2, \dots, K$), conditioned on the observed measurement history $Z(t_1) = [z^T(t_0), z^T(t_1), \dots, z^T(t_1)]^T$, i.e.,

$$p_k(t_1) = \text{prob}(a=a_k | Z(t_1)=Z_1) \quad (17)$$

then it can be shown [2] that $p_k(t_1)$ can be evaluated recursively for all k in terms of conditional densities via:

$$p_k(t_1) = \frac{f_{z(t_1)|a, Z(t_{1-1})}(z_1|a_k, Z_{1-1}) \cdot p_k(t_{1-1})}{\sum_{j=1}^K f_{z(t_1)|a, Z(t_{1-1})}(z_1|a_j, Z_{1-1}) \cdot p_j(t_{1-1})} \quad (18)$$

and that the Bayesian estimate of the state is the probabilistically weighted average:

$$\hat{x}(t_1^+) = E(x(t_1)|Z(t_1)=Z_1) = \sum_{k=1}^K \hat{x}_k(t_1^+) \cdot p_k(t_1) \quad (19)$$

where $\hat{x}_k(t_1^+)$ is the state estimate generated by a Kalman filter based on the assumption that the parameter vector equals a_k . Thus, the multiple model filtering algorithm is composed of a bank of K separate Kalman filters, each based on a particular value a_1, \dots, a_K of the parameter vector, as depicted in Fig. 3. When the measurement z_1 becomes available at time t_1 , the residuals $r_1(t_1), \dots, r_K(t_1)$ are generated in the K filters and used to compute $p_1(t_1), \dots, p_K(t_1)$ via Eq. (18). Each numerator density in (18) is Gaussian if linear models are used and approximated as Gaussian if nonlinear models are employed, i.e.,

$$f_{z(t_1)|a, Z(t_{1-1})}(z_1|a_k, Z_{1-1}) = \frac{1}{(2\pi)^{m/2} |A_k(t_1)|^{1/2}} \exp(\cdot) \quad (20)$$

$$(\cdot) = (-1/2 r_k^T(t_1) A_k^{-1}(t_1) r_k(t_1))$$

where m is the measurement dimension and $A_k(t_1)$ is calculated in the k -th Kalman filter as:

$$A_k(t_1) = H_k(t_1) P_k(t_1^-) H_k^T(t_1) + R_k(t_1) \quad (21)$$

The denominator in Eq. (18) is simply the sum of all the computed numerator terms and thus is the scale factor required to ensure that the $p_k(t_1)$'s sum to one.

One expects that the residuals of the Kalman filter based upon the "best" model will have mean squared values most in consonance with its own computed $A_k(t_1)$, while "mismatched" filters will have larger residuals than anticipated through this matrix. Therefore, Eqs. (18)-(21) will most heavily weight the filter based upon the most

Table 1 - Description of Elemental Filters in the
Multiple Model Adaptive Estimator

Filter #	FOV (pixels)	Assumed x-Dynamics (Azimuth)	Assumed y-Dynamics (Elevation)
1	8-by-8	benign	benign
2	24-by-24	20 g	20 g
3	8-by-8	10 g	10 g
4	24-by-8	20 g	benign
5	8-by-24	benign	20 g

correct assumed parameter value. However, the performance of the algorithm depends on there being significant differences in the characteristics of residuals in the "correct" and "mismatched" filters. Therefore, each filter should be tuned for best performance when the true values of the uncertain parameters are identical to its assumed values of these parameters. One should specifically avoid the often-used "conservative" philosophy of adding considerable dynamics pseudonoise to open the filter bandwidth, since this tends to mask the difference between good and bad models. In this study, K has been chosen as 2, 3, or 5, and the elemental filters are the first 2, first 3, or all 5 of the filters as described in Table 1. The first filter in the bank has a narrow field-of-view and has been tuned for best performance for constant-velocity trajectories in inertial space, and the wider field-of-view second filter has been tuned for best performance on a 20-g pull-up maneuver. The third filter is tuned for intermediate dynamics and uses a small field-of-view. The last two filters assume different levels of severity of target dynamics in the two FLIR plane directions, and they use rectangular fields-of-view with the longer dimension along the direction of higher assumed severity. The tuning parameters (Q and possibly T) for these various assumed levels of maneuvering harshness for both the first-order Gauss-Markov acceleration model of Eq. (3) and the constant turn-rate model of Eq. (4) were determined empirically [27, 38-40]; filter #1 was always based upon a Gauss-Markov model.

To allow the algorithm to adapt to a changing parameter value, computed p_k 's were artificially bounded below by a small value, 0.01 [2,25-28,37-40]. (Other means are also available, as in [2,14,32].) Without such bounding, the p_k for a "mismatched" filter could converge to (essentially) zero, precluding appropriate response of the recursion in Eq. (18) to subsequent parameter changes. After lower bounding, the resultant probabilities are rescaled so that their sum remains equal to one.

For very severe target maneuvers, the estimates of one or more of the smaller field-of-view filters may diverge; due to the lower bounding on the p_k 's, this can eventually cause the entire algorithm to diverge. To preclude this, any time the target image centering shift magnitude for a filter exceeds 3 pixels, the states of that divergent filter are set equal to the weighted average of the nondiverging filters' estimates, and its error covariance is reset correspondingly.

IV. Performance Analysis

Monte Carlo analyses involving ten runs each have been used to test the previously described trackers against realistic scenarios. Sample means ± 1 standard deviation are plotted versus time to demonstrate transient characteristics, or temporally averaged over an interval of interest to allow compact comparisons. A three-hot-spot target of dimensions appropriate for a single-plane, two-engine aircraft was simulated in 3-space and then projected onto the FLIR image plane, using as trajectories:

- (1) straight-and-level flight at 1 km/sec for 5 sec, starting at about 20.5 km range and reaching minimum range of 20 km (with the trajectory in the plane orthogonal to the line of sight) at 5 sec;
- (2) same as (1) for 2 sec, then conducting a pull-up maneuver (at 2g, 10g, or 20g

levels), using an unrealistically harsh step change in pitch rate to tax the algorithm severely;

- (3) same as (2) for 3.5 sec of simulation time, but then returning to straight-line flight, again using a step change in pitch rate;
- (4) same as (3) except that, at 3.5 sec, the target turns in toward the tracker, causing more dramatic changes in the target shape in the FLIR image plane.

The ratio of target spot maximum intensity to background and FLIR noise rms value is 20, and the hot spots have squared glint dispersions (spreads) of 2.0 pixel². Atmospheric jitter is modeled with mean squared value of 0.2 pixel² and correlation time of 0.07 sec.

Initial performance results are presented for the algorithm based upon only the first two filters of Table 1 being used in the bank. Table 2 presents the sample mean \pm one standard deviation of the errors committed in estimating the target dynamics elevation position state y_d , averaged over 1.5 seconds of time after initial transients have died out. These are presented for the correlator/linear Kalman filter, the extended Kalman filter based on a Gauss-Markov acceleration model, and the extended Kalman filter based on a constant turn-rate dynamics model. Errors in $\hat{y}_d(t_1^-)$ are tabulated, followed by errors in $\hat{y}_d(t_1^+)$; the former indicates the accuracy of the command sent to the pointing controller and the latter portrays the best precision in state estimation, so these are the most pertinent statistics. The azimuth position statistics are not included because they provide no additional insight into performance and because the maneuvers being performed are predominantly in the y direction.

First consider the table entries for the straight-and-level trajectory 1; the corresponding time histories of statistics for the three forms of multiple model adaptive filter can be viewed in the first 2 seconds of results in Figs. 4-6. (As indicated by the initial transient in the plots, the filters were started with artificial knowledge of the true states; initial acquisition was investigated separately and did not cause difficulties.) From the table, it can be seen that the multiple model

Table 2 - Performance Analysis: Mean \pm Standard Deviation of Errors in $\hat{y}_d(t_1^-)$ and $\hat{y}_d(t_1^+)$

TEST CASE	CORRELATOR/ LINEAR KF	EXTENDED KF GAUSS-MARKOV ACC	EXTENDED KF CONST TURN-RATE
<u>STRAIGHT TRAJECTORY 1</u>			
MULTIPLE MODEL	-.001 \pm .063	-.241 \pm .114	-.208 \pm .121
	-.005 \pm .157	-.246 \pm .102	-.210 \pm .109
NARROW FOV	-.015 \pm .170	-.266 \pm .118	-.209 \pm .123
	-.020 \pm .152	-.270 \pm .106	-.210 \pm .112
WIDE FOV	-.017 \pm .289	.015 \pm .162	.013 \pm .166
	-.020 \pm .246	.013 \pm .128	.012 \pm .129
<u>PULL-UP TRAJECTORY 2</u>			
2g	-.157 \pm .225	-.802 \pm .129	-.435 \pm .145
	.118 \pm .209	-.737 \pm .119	-.432 \pm .134
10g	-.089 \pm .747	-.232 \pm .171	-.203 \pm .167
	.084 \pm .740	-.107 \pm .138	-.221 \pm .139
20g	-.243 \pm .450	-.923 \pm .181	-.285 \pm .160
	-.026 \pm .436	-.710 \pm .155	-.300 \pm .129
20g WITH WIDE FOV	-.264 \pm .250	-.884 \pm .204	-.117 \pm .194
	.036 \pm .214	-.674 \pm .181	-.123 \pm .162

filters have performance very similar to the narrow field-of-view single filters that are specifically tuned for this benign trajectory, indicating that the adaptation is appropriately weighting the narrow field-of-view filter very heavily. In the first column, as anticipated, the larger field-of-view filter has poorer performance on the benign trajectory. For the extended Kalman filters, the standard deviations are worse but the biases are reduced for the wide field-of-view case. This is due to tuning of the narrow field-of-view filters; larger assumed dynamics noise strength would reduce these biases, but this was not incorporated in order to retain very distinguishing characteristics in the residuals of the different filters of the multiple model tracker.

The bottom of Table 2 pertains to performance achieved by the multiple model filter against pull-up maneuvers at 2g, 10g, and 20g levels; the 2g case time histories are plotted in Figs. 4-6, while 10g case characteristics are exhibited in the first 3.5 sec of Figs. 7 and 8. The correlator/linear filter generally has smaller biases but larger standard deviations than the extended Kalman filters. Its rms errors are smaller for low-g maneuvers (again due to tuning of the narrow field-of-view extended filters), but the superiority of the extended Kalman filter based on constant turn-rate dynamics is clearly evident for harsher maneuvers. There the extended Kalman filters have much smaller rms errors and shorter transients, and the bias is considerably smaller when the filter is based on constant turn-rate dynamics rather than a Gauss-Markov acceleration model. At low g's, the adaptive filter performance resembles that of the narrow field-of-view filter, but quickly converges to that of the wide field-of-view filter after maneuver initiation. Note that the performance of the correlator/filter is actually worse at 10 g's than at 20 g's; there is no filter in the adaptive filter's bank that is expressly tuned for best performance at these conditions. As seen in the last two rows of Table 2, the performance of the adaptive filter is somewhat worse than that of the large field-of-view filter, due to the lower bounding of the conditional probabilities as discussed previously. The bound of 0.01 is the result of a tradeoff; higher values allow quicker reaction to maneuver initiation, but at the expense of an inappropriately heavy weight on a "wrong" model in the steady-state pull-up. No entry is made in the table for the narrow field-of-view filter, since it was unable to maintain lock on 10g or 20g targets.

As displayed in Figs. 7 and 8, the response to the straightening maneuver of trajectory 3 at 3.5 sec. is similar to that of the pull-up initiation at $t = 2$ sec. (Fig. 8 pertains to the Gauss-Markov acceleration model, but the constant turn-rate model yields very similar results.) Returning desirably heavy weight to the narrow field-of-view is not as rapid or effective as the response to maneuver onset, and this characteristic will be discussed more fully later.

Trajectory 4 evaluations were very similar to those of trajectory 2, demonstrating the ability to maintain good estimates of a shape function undergoing large changes in time, and thereby to maintain desirable tracking performance. Robustness to signal-to-noise ratio was tested by leaving the filter-assumed SNR at 20 while the real world was simulated with SNR of 10, resulting in about 35% larger rms errors for a 2g pull-up, equivalent rms errors at 10g, and 5% smaller rms errors at 20g; reduction of real world SNR to unity caused divergence in all cases, as noted previously [5-7]. Finally, as a performance bound, the adaptive filter was artificially told when the pull-up maneuver occurred and appropriate weightings were applied immediately. There was no change in steady state behavior and an imperceptible change in the time for the transients to die out; the only substantial difference was the peak value of the mean error excursion, which was reduced between 10 and 45 percent for the different filters and test trajectories.

Having evaluated the algorithm that uses only the first two elemental filters listed in Table 1, consider the tracker based on all five table entries and using the correlator/linear-measurement-model-filter structure. The original motivation for the addition of elemental filters with rectangular fields-of-view to the multiple model adaptive estimation (MMAE) algorithm came from biases observed in the operation of the earlier algorithm that incorporated three elemental filters, each with a square field-of-view (i.e., the first three filters listed in Table 1, all based on a Gauss-Markov model for acceleration). Fig. 9 illustrates a representative performance result of that previous algorithm: the mean \pm one standard deviation tracking error associated with the $\hat{x}(t_1^+)$ estimate in the FLIR azimuth direction when a 20-g maneuver is being performed by the target at a range of about 20 km., predominantly in the FLIR elevation direction [38]. The apparent ramping in the plot is, in fact, an error transient that begins at a

point 2 sec. into the simulation (at which time the high-g simulated maneuver was initiated); it continues for about 5 sec., after which an error bias persists in the estimation of the target position. This bias is induced by the maneuver, as is clear from the time of onset of the error transient and also from the fact that no such bias occurs in simulations that do not include such a high-g target maneuver. The mechanism largely responsible for this effect is the MMAE adaptation being based upon only elemental filters with square fields-of-view. When the maneuver begins at $t = 2$ sec., the large changes in the FLIR elevation channel cause the MMAE to place high weighting on the wide field-of-view elemental filter. This is appropriate to maintain lock on the maneuvering target. However, during this time, the variations in true target azimuth characteristics are rather benign, and so the MMAE is extremely mistuned for the azimuth channel state estimation. The validity of this interpretation was demonstrated by simulating a target with the same horizontal inertial-coordinate dynamics, but with vertical dynamics corresponding to a straight-and-level path. Under these conditions, azimuth error magnitudes were reduced by more than 50%. Since the MMAE was relieved of the task of tracking a highly dynamic elevation channel, weighting emphasis was appropriately placed on the small field-of-view filter.

Fig. 10 displays the elevation tracking performance of the MMAE based on the five elemental filters of Table 1, each assuming a Gauss-Markov model for acceleration, when the actual target undergoes a 10-g vertical pullup maneuver starting at 2 sec. into the simulation [39,40]. Table 3 divides the 5 second, 150-sample-period simulation into five intervals, indicating the elemental filters that are dominant during each of these intervals. About 6 sample periods after the (artificially harsh) step change in vertical acceleration is simulated, the probability weights shift to emphasize the filters appropriate to such a maneuver. At frames 74 and 75, all filters but filter # 2 are declared to have lost lock, and so the estimates in the other four filters are reset to match its state estimate and covariance, as explained at the end of Section III. Thereafter until frame 120, the filter tuned to harsh maneuvers in the FLIR x-direction (azimuth) receives substantial weight, even though the actual target maneuver takes place mostly in the y direction. To understand this, consider the acceleration profiles of the actual target maneuver, as shown in Fig. 11. Over time interval A, there is no acceleration in either direction, since the trajectory is straight-and-level. Time interval B provides a step change in the y-acceleration, from which a cosine function commences. Over time interval C, during which filter # 4 becomes a dominant filter, there is very little change in the y-acceleration, while the x-acceleration begins to increase as a sine function. When the resetting of the four divergent filters occurs at frames 74 and 75, a good estimate of target y-direction dynamics is transferred to these filters. Since most of the changes in the target's acceleration now occur in the x-direction, it is not surprising that filter # 4 receives a significant portion of the hypothesis conditional probability.

To assess how well this adaptive filter performs, it was compared to an artificial benchmark composed of a single filter that was tuned for benign conditions for the first

Table 3 - Profile of the Dominant Elemental Filters;
Simulation as in Fig. 10

<u>Interval (Frames)</u>	<u>Dominant Filter(s)</u>	<u>Comments</u>
1 - 65	#1	Adequate tracking of benign trajectory; target maneuver begins at frame 60
66 - 73	#2, #5	Y-directional target maneuver is recognized
74 - 75	#2	Filters #1, #3, #4, #5 "lose lock"
76 - 120	#2, #4	Wide FOV tracking
121 - 150	#3	10-g maneuver recognized

55 sample periods of simulation time, and then tuned specifically as the single elemental filter # 3 for a 10-g maneuver. Thus, the benchmark filter was artificially informed of the target maneuver five sample periods before the actual maneuver occurred, so that the bandwidth of the filter would be appropriately widened by the time the pullup was actually initiated. Tables 4 and 5 show a comparison of the MMAE and this benchmark filter, based on peak value of the mean error in target y-position (elevation) estimates at times t_1^- and t_1^+ , recovery time (time to recover from a maneuver; time to reach post-maneuver steady state error characteristics), and error mean and standard deviation temporally averaged over steady state periods before and after maneuver initiation for x- and y- target position and centroid estimates (see Eq. (1)). The MMAE can outperform the benchmark because the MMAE has in its bank filters which are tuned for maneuvers harsher than 10 g's, and thus are better able to handle the initial onset of the step change in simulated target acceleration. The adaptive mechanism within the MMAE is thus seen to be exceptionally fast and effective in its ability to adapt to even unrealistically harsh changes in target behavior.

Repeated performance evaluations for 20-g pullups and both 10-g and 20-g pullups

Table 4 - Error Statistics for MMAE When Target Initiates a 10-g Vertical Pullup at $t = 2$ Sec.

$\hat{\phi}$ peak-mean error (t_1^-) = -1.6 pixels $\hat{\phi}$ peak-mean error (t_1^+) = -0.7 pixels Recovery time = 0.40 seconds		
Temporally Averaged Error Parameter (mean / 1 sigma)	Time Interval	
	[0.5 , 2.0]	[3.5 , 5.0]
$\hat{\phi}_{err}(t_1^-)$	-0.0456 / 0.4262	0.2348 / 0.5335
$\hat{\phi}_{err}(t_1^-)$	-0.0105 / 0.3577	-0.0174 / 0.6655
$\hat{\phi}_{err}(t_1^+)$	-0.0354 / 0.3707	0.1908 / 0.4265
$\hat{\phi}_{err}(t_1^+)$	-0.0137 / 0.3173	0.1203 / 0.5814
x-cent. error (t_1^+)	-0.0006 / 0.0948	0.0874 / 0.1405
y-cent. error (t_1^+)	-0.0015 / 0.0536	0.3260 / 0.3139

Table 5 - Error Statistics for Single Filter Bound of Performance; 10-g Pullup at $t = 2$ Sec.; "Q" Increased at Frame 55

$\hat{\phi}$ peak-mean error (t_1^-) = -2.0 pixels $\hat{\phi}$ peak-mean error (t_1^+) = -1.3 pixels Recovery time = 0.80 seconds		
Temporally Averaged Error Parameter (mean / 1 sigma)	Time Interval	
	[0.5 , 2.0]	[3.5 , 5.0]
$\hat{\phi}_{err}(t_1^-)$	-0.0408 / 0.4095	0.1933 / 0.4943
$\hat{\phi}_{err}(t_1^-)$	-0.0099 / 0.3547	-0.2608 / 0.4425
$\hat{\phi}_{err}(t_1^+)$	-0.0310 / 0.3658	0.1333 / 0.4100
$\hat{\phi}_{err}(t_1^+)$	-0.0127 / 0.3138	-0.1035 / 0.3743
x-cent. error (t_1^+)	0.0082 / 0.0900	-0.0006 / 0.1022
y-cent. error (t_1^+)	0.0015 / 0.0614	0.0769 / 0.0804

followed by a resumption of straight inertial trajectories provided consistent results. The MMAE no longer outperformed the benchmark for the 20-g maneuvers, since the actual target acceleration matched the tuning of the widest bandwidth elemental filter. However, it still did nearly equal the performance of that benchmark. Also, the MMAE was somewhat more hesitant to reduce the bandwidth to an appropriate benign level when the target comes out of a turn, compared to the speed with which it opens the bandwidth at the onset of a pullup. This trait has been observed before in MMAE algorithms [26,27,30], and can be understood by considering Eqs. (18) and (20). Basically, small probabilities are assigned to filters with large ratios of [actual squared residual] to [filter-computed residual variance]. At pullup initiation, the actual squared residuals become much larger than anticipated through the filter-computed variance in the filters based on benign dynamics models. This ratio is not as large in the filters based on harsh assumed dynamics when the actual target trajectory straightens out.

The MMAE algorithm with all elemental filters based upon a Gauss-Markov model for acceleration clearly outperformed the MMAE with all but the most benign elemental filter based upon a nonlinear constant turn-rate model. Peak position estimate errors were greater in the latter by as much as a factor of four, while recovery times were greater by a factor of two. This was at least partially due to the tuning strategy that was necessary for the elemental filters in this MMAE. Unlike the case of the individual filters based on a Gauss-Markov acceleration model, the constant turn-rate filters had to be tuned such that the filter-computed rms position errors were consistently larger than the actual rms position errors by a considerable amount. Otherwise, the resulting MMAE would lose lock on harshly jinking targets. These elemental filters were then not particularly well suited for multiple model adaptation, which requires each elemental filter to be well tuned for its assumed parameter conditions. Distinguishing between "good" and "bad" models became more difficult in this case. This was evident from probability weightings that were very inconsistent from one sample time to the next, as well as from the degradation in performance as compared to the MMAE based totally on Gauss-Markov acceleration models.

Unfortunately, the tracking algorithm described to this point exhibits a consistent bias in state estimates if there are any initial pointing errors (i.e., in all realistic scenarios). Because of the manner in which the template generation algorithm of Fig. 2 operates, any original biases cause a corresponding bias in the reconstructed template. Therefore, once an adequate template shape has been constructed (ten frames of data were used for this "adequate" construction, in consonance with the use of α equal to 0.1 in Eq. (13)), the centroid of that template is calculated. Then a shift in the transformed domain is performed to correspond to placing that centroid at the center of the template array. The algorithm is repeatedly performed until the required centering shift is less than a criterion distance (chosen to be 0.5 pixels here), at which time the target is deemed "acquired" and normal tracking is resumed. In actual implementation, testing for the need to "reacquire" could be repeated at some frequency much lower than the sampling rate, but in the simulated tests, the routine was not executed after the target was first declared to be acquired.

Figs. 12 and 13 display the error mean \pm one standard deviation associated with $\hat{y}_d(t_1^+)$ and $\hat{y}_{peak}(t_1^+)$, respectively, for the case of initial biases of 3 pixels in the x direction and 4 pixels in the y direction. The acquisition routine was performed only twice, at the tenth and eleventh sample instants, since the second "shift" was less than 0.5 pixels. This procedure results in a substantial offset between the template and the following frame of FLIR measurement data. Due to the relative strengths of the dynamics vs. atmospheric jitter driving noises, the majority of this offset is interpreted (correctly) by the filter as being a result of target dynamics, and the target is acquired in the center of the field-of-view during the subsequent filter cycle. The final position bias in Fig. 13 is typically 0.1 pixel in the cases studied; the precision with which the location of the target's center of intensity is calculated and centered is an order of magnitude beyond the sensor resolution power. The errors associated with $\hat{y}_d(t_1^+)$ are about five times the $\hat{y}_{peak}(t_1^+)$ errors, since the centroid errors reflect direct measurements while the filter has the additional task of separating the measured quantities into the components due to target dynamics, atmospheric jitter, and noise. These trends are borne out more completely in Table 6, which presents the results of temporally averaging such statistics over the interval from 3.5 sec. to 5.0 sec. into the simulation. Moreover, the x- and y- filter induced errors are identical to three significant figures for other cases studied, using different amounts of initial acquisition biases.

Table 6 - Performance of Acquisition Algorithm: Steady State Characteristics for Straight Target Trajectory
Initial Biases = 3 Pixels (Az.), 4 Pixels (El.)

Error Mean \pm 1 Std. Deviation	
$\hat{x}_d(t_1^+) : 0.123 \pm 0.338$	$\hat{x}_{peak}(t_1^+) : 0.112 \pm 0.074$
$\hat{y}_d(t_1^+) : 0.023 \pm 0.324$	$\hat{y}_{peak}(t_1^+) : 0.112 \pm 0.069$

V. Summary

Algorithms have been developed for tracking dynamic targets in infrared image data, where the target pattern is uncertain a priori and may be composed of multiple hot spots. Digital and/or optical signal processing is used to identify this target shape adaptively in real time. Multiple model filtering has been shown to provide an effective means of changing the field-of-view and bandwidth of the tracker against a wide dynamic range of targets. In the initial version of this multiple model algorithm, one elemental filter is tuned to benign dynamics and uses a narrow field-of-view and another is tuned to harsher maneuvering and correspondingly uses a wider field-of-view. There are significant computational loading advantages to using a correlator / linear Kalman filter combination for each of these filters, but extended Kalman filters processing the raw FLIR data and based upon a constant turn-rate dynamics model may provide superior tracking capability, particularly for highly dynamic close-range targets.

Effective enhancements to such a multiple model adaptive estimator have been proposed and evaluated. Basing some of the elemental filters in the algorithm upon models for target dynamics that are harsher in one direction than in others, and allowing for rectangular fields-of-view with the longer dimension along that harsher direction, is shown to provide significant performance advantages. This feasibility study provided for the "harsh dynamics" direction to be aligned predominantly in the azimuth or elevation directions, but it would also be reasonable to align it with the estimated target acceleration direction. The online adaptation in this study was so effective that the adaptive algorithm outperformed what had been thought to be a severe benchmark: a single filter that is artificially told of a target maneuver enough before it occurs, that the filter bandwidth can be appropriately increased by the time the target actually maneuvers. Gauss-Markov acceleration models proved to yield better performance than constant turn-rate target dynamics models, in part due to necessary differences in filter tuning strategies. An initial acquisition algorithm was devised to remove the persistent tracking biases that had plagued earlier versions of this adaptive estimator.

Future research areas include investigation of a multiple model adaptive estimator with one elemental filter based on a rotatable rectangular field of view, and an enhanced acquisition algorithm able to handle target maneuvers during the initialization phase. Research is also continuing, to enhance performance in a number of ways: (1) evaluation of performance as a function of sample period, filter tuning / probability lower bounding combinations, and other pertinent parameters; (2) investigation of robustness to variation in target shape function, dynamic trajectories, atmospheric jitter, and background noise at low SNR; and (3) establishing performance sensitivity to combinations of sensor resolution and noise attributes, controller/ actuator dynamics, vibration effects, and other tracking environment characteristics.

References

1. Maybeck, P.S., Stochastic Models, Estimation and Control, Vol. 1, Academic Press, New York, 1979.
2. Maybeck, P.S., Stochastic Models, Estimation and Control, Vol. 2, Academic Press, New York, 1982.
3. Maybeck, P.S., and D.E. Mercier, "A Target Tracker Using Spatially Distributed

- Infrared Measurements," IEEE Trans. AC, Vol. AC-25, No. 2, pp. 222-225, April 1980.
4. Mercier, D.E., "An Extended Kalman Filter for Use in a Shared Aperture Medium Range Tracker," M.S. thesis, A.F. Inst. of Tech., Wright-Patterson AFB, Ohio, Dec. 1978.
 5. Maybeck, P.S., D.A. Harnly and R.L. Jensen, "Robustness of a New Infrared Target Tracker," Proc. IEEE Nat. Aerospace & Elec. Conf., Dayton, Ohio, pp. 639-644, May 1980.
 6. Harnly, D.A., and R.L. Jensen, "An Adaptive Distributed-Measurement Extended Kalman Filter for a Short Range Tracker," M.S. thesis, A.F. Inst. of Tech., Wright-Patterson AFB, Ohio, Dec. 1979.
 7. Maybeck, P.S., R.L. Jensen and D.A. Harnly, "An Adaptive Extended Kalman Filter for Target Image Tracking," IEEE Trans. AES, Vol. AES-17, pp. 173-180, Mar. 1981.
 8. Maybeck, P.S., "Advanced Applications of Kalman Filters and Nonlinear Estimators in Aerospace Systems," Control and Dynamic Systems (C.T. Leondes, ed.), Vol. 20, Academic Press, New York, pp. 67-154, 1983.
 9. Maybeck, P.S., W.H. Worsley and P.M. Flynn, "Investigation of Constant Turn-Rate Dynamics Models in Filters for Airborne Vehicle Tracking," Proc. IEEE Nat. Aerospace & Elec. Conf., Dayton, Ohio, pp. 896-903, May 1982.
 10. Flynn, P.M., "Alternative Dynamics Models and Multiple Model Filtering for a Short Range Tracker," M.S. thesis, A.F. Inst. of Tech., Wright-Patterson AFB, Ohio, Dec. 1981.
 11. "Firefly III IFFC Fire Control System," Tech. Rept. 19008 ACS 12004, General Electric Co., Aircraft Equip. Div., Binghamton, N.Y., Dec. 1979 (revised, Jan. 1981).
 12. Bakir, E., "Adaptive Kalman Filter for Tracking Maneuvering Targets," AIAA Jour. Guid. Cont. & Dyn., Vol. 6, No. 6, pp. 414-416, Sept. 1983.
 13. Berg, R.F., "Estimation and Prediction for Maneuvering Target Trajectories," IEEE Trans. AC, Vol. AC-28, No. 3, pp. 294-304, Mar. 1983.
 14. Chang, C.B., and J.A. Tabaczynski, "Application of State Estimation to Target Tracking," IEEE Trans. AC, Vol. AC-29, No. 2, pp. 98-109, Feb. 1984.
 15. Demetry, J.S., and H.A. Titus, "Adaptive Tracking of Maneuvering Targets," Tech. Rept. NPS-52DE8041A, Nav. Postgrad. Sch., Monterey, Cal., Apr. 1968.
 16. McAuley, R.J., and E. Denlinger, "A Decision-Directed Adaptive Tracker," IEEE Trans. AES, Vol. AES-9, No. 2, pp. 229-236, Mar. 1973.
 17. Nahi, N.E., and B.M. Schaefer, "Decision-Directed Adaptive Recursive Estimators: Divergence Prevention," IEEE Trans. AC, Vol. AC-17, No. 1, pp. 61-67, Jan. 1972.
 18. Maybeck, P.S., and S.K. Rogers, "Adaptive Tracking of Multiple Hot-Spot Target IR Images," IEEE Trans. AC, Vol. AC-28, No. 10, pp. 937-943, Oct. 1983.
 19. Rogers, S.K., "Enhanced Tracking of Airborne Targets Using Forward Looking Infrared Measurements," M.S. thesis, A.F. Inst. of Tech., Wright-Patterson AFB, Ohio, Dec. 1981.
 20. Oppenheim, A.V., and R.W. Schaffer, Digital Signal Processing, Prentice-Hall, Englewood Cliffs, N.J., 1975.
 21. Casasent, D.P., "Pattern Recognition: A Review," IEEE Spectrum, pp. 28-33, Mar. 1981.
 22. Casasent, D.P., J. Jackson and C. Neuman, "Frequency-Multiplexed and Pipelined Iterative Optical Systolic Array Processors," Applied Optics, Vol. 22, pp. 115-124, Jan. 1983.
 23. Roemer, W.A., and P.S. Maybeck, "An Optically Implemented Multiple-Stage Kalman Filter Algorithm," Proc. SPIE: Real Time Signal Processing VI, San Diego, Cal., pp. 221-228, Aug. 1983.
 24. Kozemchak, M.R., "Enhanced Image Tracking: Analysis of Two Acceleration Models in Tracking Multiple Hot-Spot Images," M.S. thesis, A.F. Inst. of Tech., Wright-Patterson AFB, Ohio, Dec. 1982.
 25. Millner, P.P., "Enhanced Tracking of Airborne Targets Using a Correlator / Kalman Filter," M.S. thesis, A.F. Inst. of Tech., Wright-Patterson AFB, Ohio, Dec. 1982.

26. Suizu, R.I., "Enhanced Tracking of Airborne Targets Using Multiple Model Filtering Techniques for Adaptive Field of View Expansion," M.S. thesis, A.F. Inst. of Tech., Wright-Patterson AFB, Ohio, Dec. 1983.
27. Maybeck, P.S., and R.I. Suizu, "Adaptive Tracker Field-of-View Variation Via Multiple Model Filtering," IEEE Trans. AES, Vol. AES-21, No. 4, pp. 529-539, July 1985.
28. Athans, M., and C.B. Chang, "Adaptive Estimation and Parameter Identification Using Multiple Model Estimation Algorithm," Technical Note 1976-28, ESD-TR-76-184, Lincoln Laboratory, Lexington, Mass., June 1976.
29. Brown, R.G., "A New Look at the Magill Adaptive Estimator as a Practical Means of Multiple Hypothesis Testing," IEEE Trans. Circuits & Sys., Vol. CAS-30, No. 10, pp. 765-768, Oct. 1983.
30. Korn, J., and L. Beean, "Application of Multiple Model Adaptive Estimation Algorithms to Maneuver Detection and Estimation," Tech. Rept. TR-152, Alphatech, Inc., Burlington, Mass., June 1983.
31. Magill, D.T., "Optimal Adaptive Estimation of Sampled Stochastic Processes," IEEE Trans. AC, Vol. AC-20, No. 3, pp. 359-362, June 1975.
32. Moose, R.L., "An Adaptive State Estimation Solution to the Maneuvering Target Problem," IEEE Trans. AC, Vol. AC-20, No. 3, pp. 359-362, June 1975.
33. Moose, R.L., H.F. Van Landingham and D.H. McCabe, "Modeling and Estimation for Tracking Maneuvering Targets," IEEE Trans. AES, Vol. AES-15, No. 3, pp. 448-456, May 1979.
34. Moose, R.L., and P.P. Wang, "An Adaptive Estimator with Learning for a Plant Containing Semi-Markov Switching Parameters," IEEE Trans. Sys., Man, Cyber., pp. 277-281, May 1973.
35. Tenney, R.R., R.S. Hebbert and N.R. Sandell, Jr., "A Tracking Filter for Maneuvering Sources," IEEE Trans. AC, Vol. AC-22, No. 2, pp. 246-261, Mar. 1977.
36. Thorp, J.S., "Optimal Tracking of Maneuvering Targets," IEEE Trans. AES, Vol. AES-9, No. 4, pp. 512-519, July 1973.
37. Loving, P.A., "Bayesian vs. MAP Multiple Model Adaptive Estimation for Field of View Expansion in Tracking Airborne Targets," M.S. thesis, A.F. Inst. of Tech., Wright-Patterson AFB, Ohio, Mar. 1985.
38. Netzer, A.S., "Characteristics of Bayesian Multiple Model Adaptive Estimation for Tracking Airborne Targets," M.S. thesis, A.F. Inst. of Tech., Wright-Patterson AFB, Ohio, Dec. 1985.
39. Tobin, D.M., "A Multiple Model Adaptive Tracking Algorithm for a High Energy Laser Weapon System," M.S. thesis, A.F. Inst. of Tech., Wright-Patterson AFB, Ohio, Dec. 1986.
40. Tobin, D.M., and P.S. Maybeck, "Substantial Enhancements to a Multiple Model Adaptive Estimator for Target Image Tracking," Proc. IEEE Conf. on Decision and Control, Los Angeles, Cal., pp. 2002-2011, Dec. 1987.
41. Hogge, C.B., and R.R. Butts, "Frequency Spectra for the Geometric Representation of Wavefront Distortions Due to Atmospheric Turbulence," IEEE Trans. Antennas and Prop., Vol. AP-24, No. 2, pp. 144-154, Mar. 1976.
42. "Advanced Adaptive Optics Control Techniques," Tech. Rept. TR-966-1, The Analytic Sciences Corp., Reading, Mass. (prepared for A.F. Weapons Laboratory, Kirtland AFB, New Mexico), Jan. 1978.

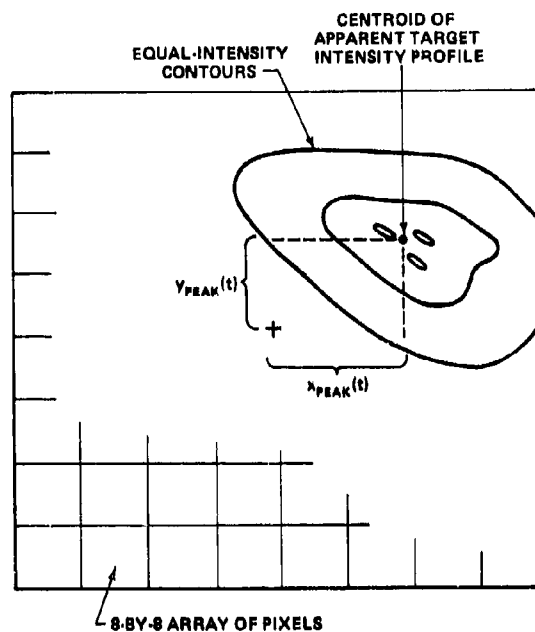


Fig. 1. Apparent Target Intensity Pattern on Image Plane

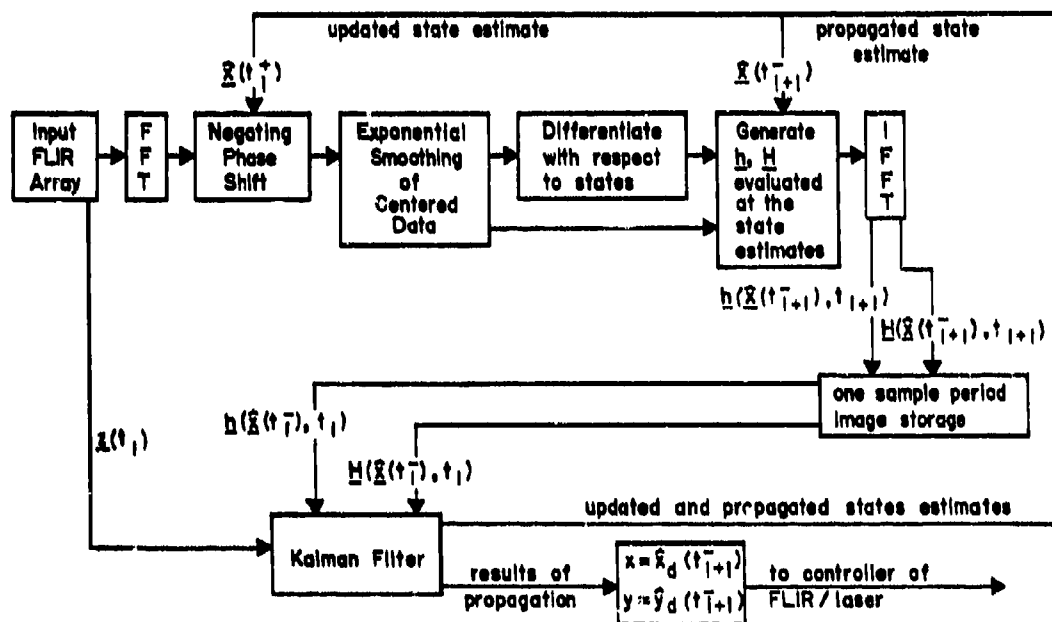


Fig. 2. Data Processing Algorithm (Underlined Symbols Correspond to Boldface Symbols in the Text)

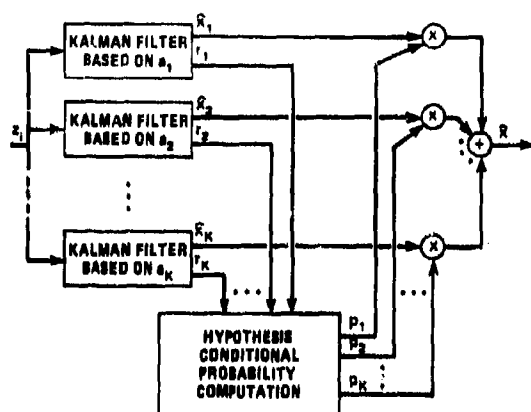


Fig. 3. Multiple Model Adaptive Estimation Algorithm

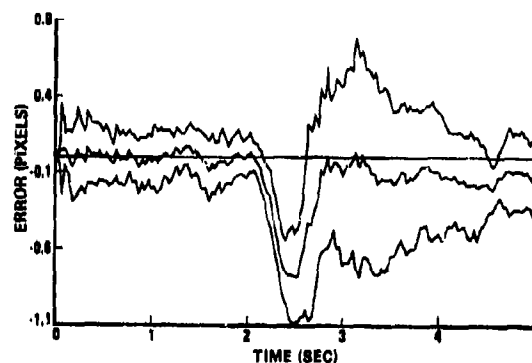
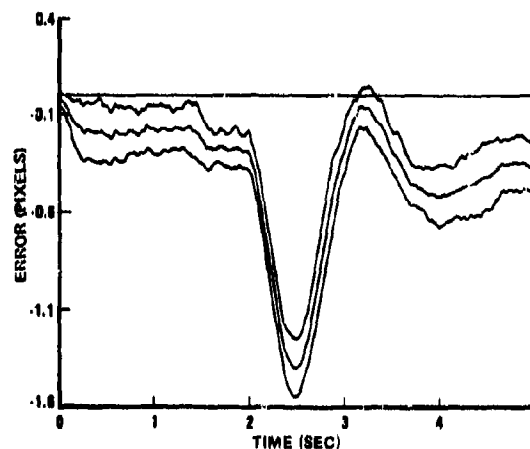
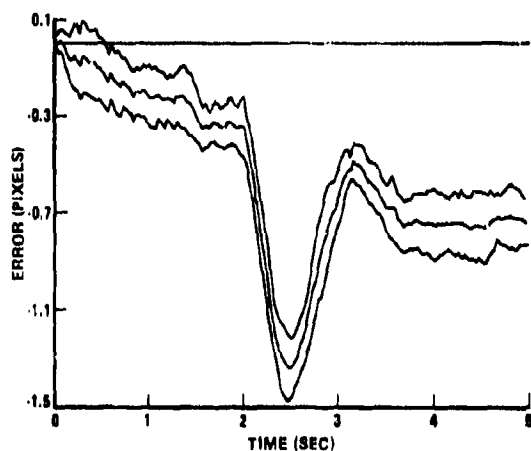
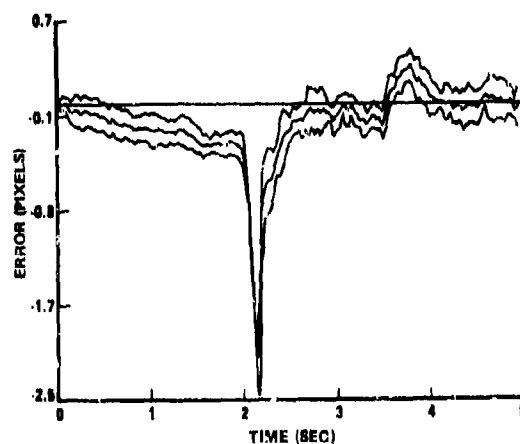
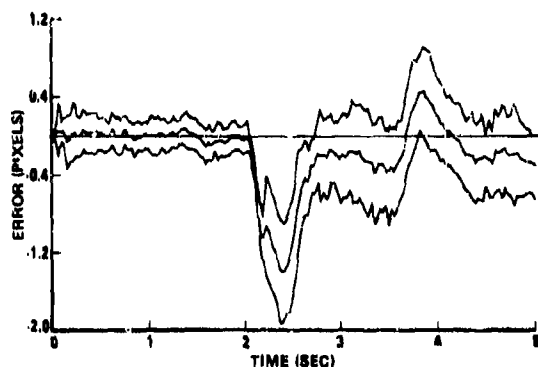


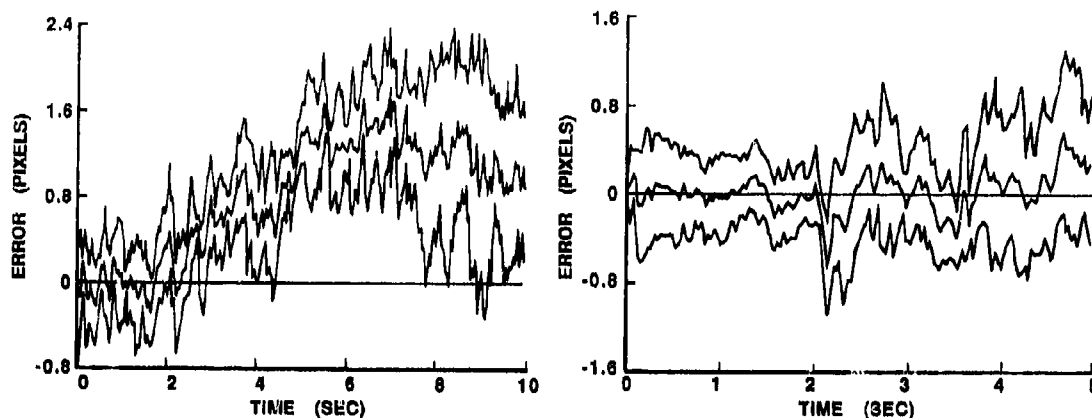
Fig. 4. $\hat{y}(t_1^+)$ Error Mean \pm One Std. Dev. for Correlator/KF on 2g Pull-up



Figs. 5 and 6. $\hat{y}(t_1^+)$ Error Mean \pm One Std. Dev. for EKF on 2g Pull-up (5: Based on Gauss-Markov Acc. Model; 6: Based on Const. Turn-Rate Model)



Figs. 7 and 8. $\hat{y}(t_1^+)$ Error Mean \pm One Std. Dev. on 10g Trajectory 3 (7: Correlator/KF; 8: Extended KF)



Figs. 9 and 10. $\hat{x}(t_1^+)$ Mean \pm 1 Std. Deviation Tracking Errors; Vertical Pullup by Target at $t = 2$ Sec. (9; Azimuth, 20-g Pullup; 10; Elevation, 10-g)

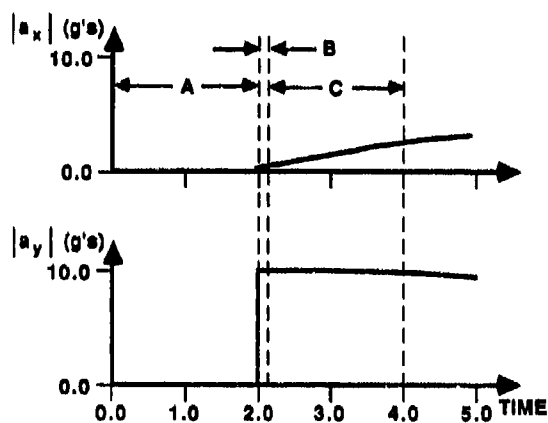
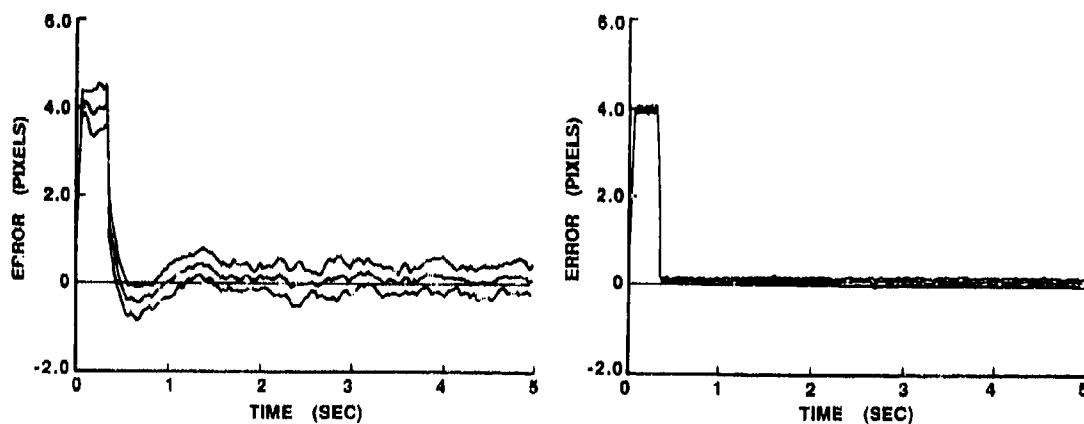


Fig. 11. Actual Target Acceleration Profile



Figs. 12 and 13. Initial Acquisition Algorithm: Error Mean \pm 1 Std. Deviation; Initial Error = 4 Pixels (12; $\hat{y}_d(t_1^+)$ Error; 13; $\hat{y}_{peak}(t_1^+)$ Error)

TRAJECTOGRAPHIE PASSIVE PAR AZIMUT : AMÉLIORATION DE LA QUALITÉ D'ESTIMATION

Pierre VACHER - Michel GAUVRI
C.E.R.T. D.S.R.A.
2, avenue E. Belin - B.P. 4025 - 31055 TOULOUSE Cedex - FRANCE.

Guy MAYNARD DE LAVALLETTE - Philippe MENECIER
GESTA-CAPCA
Las Coubinières - 83320 LE PRADET - FRANCE.

RÉSUMÉ

Outre les difficultés usuelles des problèmes de poursuite de cibles (non-linéarité, modélisation de l'évolution), la trajectographie passive par azimuth se caractérise par la grande pauvreté en information des mesures. En effet, dans certaines situations, la poursuite est mathématiquement inobservable.

Afin d'améliorer la qualité de l'estimation, deux possibilités ont été envisagées :

- La recherche d'une technique d'estimation appropriée
La nature non-linéaire de ce problème nous a conduit à étudier plusieurs systèmes de coordonnées (coordonnées curvilignes et polaires modifiées) ainsi que plusieurs méthodes d'estimation récursives et globales. De plus, la faible observabilité induit aussi une grande sensibilité numérique des résultats.
- L'augmentation du niveau d'observabilité par l'optimisation de la trajectoire de l'observateur.
Il s'agit, tout d'abord, de définir un indice scalaire d'observabilité qui constituera le critère d'optimisation. L'analyse des matrices d'information de ce problème fournit certains principes généraux concernant les évolutions favorables. Ces résultats théoriques ont permis d'optimisation de la trajectoire du lanceur tout en tenant compte des contraintes physiques de la poursuite.

La trajectographie passive par azimuth (TPA) consiste à estimer les éléments cinématiques d'une cible ou source sonore (S) à partir des seules mesures d'azimut bruitées effectuées depuis une plateforme mobile d'observation (L) dénommée observateur, porteur ou lanceur. L'étude présentée concerne le cas d'une poursuite bi-dimensionnelle en milieu sous-marin. Cependant, les résultats obtenus sont, dans une certaine mesure, généralisables à d'autres problèmes de poursuite et notamment les poursuites tri-dimensionnelles par mesures angulaires [13, 23, 24].

La principale caractéristique de la TPA est la grande pauvreté en information des mesures. En effet, certains scénarios sont inobservables c'est-à-dire les éléments cinématiques de S ne peuvent être déterminés à partir des seules mesures d'azimut. Cette particularité couplée à la non-linéarité des équations va être déterminante sur les performances des algorithmes classiques d'estimation. D'autre part, dans le cadre d'une poursuite réelle, la qualité des mesures obtenues de façon passive en environnement perturbé est souvent mauvaise. Ces deux aspects expliquent la nécessité d'algorithmes appropriés et robustes.

Après la présentation du problème, notre exposé se subdivise en deux parties. La première concerne l'analyse et la comparaison de différentes méthodes d'estimation. La seconde est dédiée à l'étude de l'observabilité de la poursuite et notamment à la génération de trajectoires lanceur favorables à la qualité de l'estimation.

Cette étude fut menée de 1984 à 1988 au CERT dans le cadre d'une convention DCAN/CAPCA [10, 11, 25, 26, 28, 29].

PRÉSENTATION DU PROBLÈME

Un observateur mobile L dont les éléments cinématiques sont supposés connus effectue la trajectographie d'un navire S à partir de mesures d'azimuts $z(t)$ (Figure 1). Le modèle d'évolution adopté pour la cible est un modèle à vecteur-vitesse constant. Dans la suite, ce modèle sera toujours supposé parfaitement respecté. Les résultats présentés sont donc issus de données simulées. Toutefois la plupart des techniques développées ont aussi été testées sur mesures réelles.

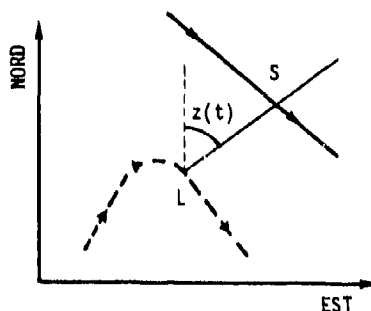


FIGURE 1 - Description du problème

Les propriétés d'observabilité spécifiques à ce problème vont guider le choix du système de coordonnées ainsi que celui de l'algorithme d'estimation. Ces propriétés seront abordées de façon intuitive. Nous introduirons ensuite les coordonnées et les algorithmes qui seront analysés au cours de cette conférence.

• Propriétés d'observabilité de la TPA

L'observabilité des poursuites par mesures angulaires n'a été établie de façon rigoureuse que récemment [9]. Nous en donnons ici une interprétation géométrique dans le cas de l'évolution à vitesse constante.

Lorsque les deux antagonistes sont animés d'une vitesse constante, la trajectoire relative de S dans le repère lié à L est aussi à vitesse constante. Pour ce cas, les mesures d'azimuts ne permettent pas de discerner la véritable trajectoire relative de S de l'ensemble des trajectoires de même cap relatif (figure 2). La distance D peut être choisie comme paramètre inobservable car sa connaissance permet le calcul des autres éléments cinématiques de S. Dans le cas extrême où les mesures d'azimut sont constantes, la vitesse radiale relative de S, \dot{D} est aussi inobservable. Une telle situation sera dénommée *doublément inobservable*.

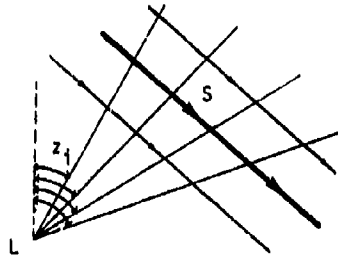


FIGURE 2 - Illustration de l'inobservabilité de la poursuite

Une manœuvre du lanceur est donc nécessaire pour rendre le système observable. Toutefois certaines manœuvres sont inappropriées. En effet pour des évolutions telles que les mesures d'azimut aux instants d'échantillonnage sont identiques à celles qui auraient été obtenues si le lanceur avait suivi une trajectoire à vitesse constante, la poursuite reste inobservable. Cette trajectoire fictive à vitesse constante peut être celle obtenue à partir des éléments cinématiques initiaux de L (figure 3a) ou une trajectoire rectiligne quelconque (figure 3b).

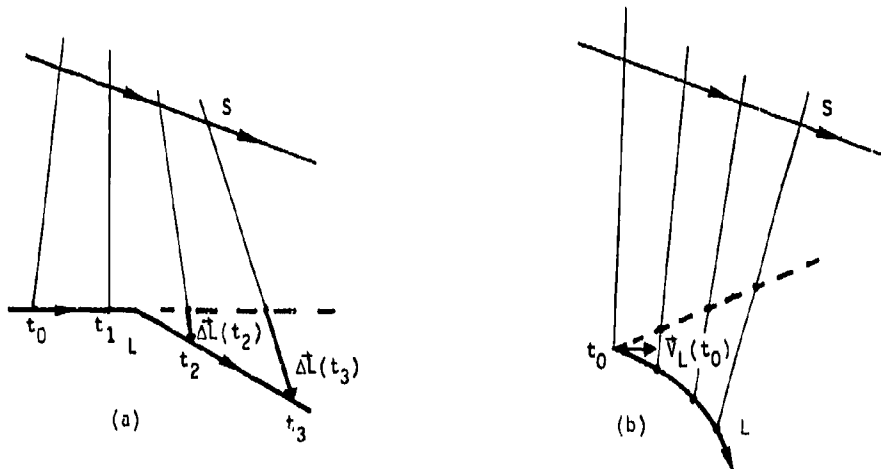


FIGURE 3 - Manœuvres du lanceur non favorables à l'observabilité

Comme le lanceur procède en pratique par segments rectilignes parcourus à vitesse constante, le premier cas est le seul rencontré. Si $\Delta L(t)$ est le vecteur des déviations de L par rapport à la trajectoire nominale (figure 3a), la poursuite sera alors observable s'il existe un instant de mesure t tel que $\Delta L(t)$ et la direction $z(t)$ ne sont pas colinéaires ou du façon équivalente si la projection de $\Delta L(t)$ sur l'orthogonale à $z(t)$ est non nulle.

Ces résultats obtenus dans un cadre théorique (mesures non bruitées, trajectoires parfaitement rectilignes) vont se traduire en pratique par la faible qualité de l'estimation de certains paramètres. Notons aussi que toute poursuite comporte une phase initiale inobservable où de plus la variation d'azimut z est généralement faible à cause de distances initiales importantes.

• Systèmes de coordonnées

Parmi les nombreuses manières de formuler ce problème de poursuite, nous nous limiterons aux deux systèmes les plus courants :

- Les coordonnées cartésiennes absolues dont les avantages sont l'interprétation physique immédiate des composantes et la simplicité des équations.
- Les coordonnées polaires modifiées qui sont bien adaptées à la TPA.

Pour les coordonnées cartésiennes, la position et la vitesse de la cible sont exprimées dans un repère fixe dont l'axe Y est orienté vers le Nord. Le vecteur d'état est alors donné par

$$X(t) = (x_s(t), y_s(t), v_{sx}, v_{sy})^T \quad (1)$$

L'évolution de $X(t)$ avec le temps est linéaire. Par contre, l'équation de mesure est non linéaire et égale à :

$$z(t) = \text{Arctg} \left[\frac{x_s(t) - x_L(t)}{y_s(t) - y_L(t)} \right] + v(t) \quad (2)$$

où le bruit $v(t)$ sera supposé blanc gaussien et centré de variance σ_z^2 .

Pour les coordonnées polaires modifiées, le vecteur d'état est constitué de l'azimut $z(t)$, de sa dérivée $\dot{z}(t)$, du rapport $\dot{\rho}(t) = \dot{D}(t)/D(t)$ et de l'inverse de la distance $s(t) = 1/D(t)$. Ainsi à l'instant t ,

$$X(t) = (z, \dot{z}, \dot{\rho}, s)^T \quad (3)$$

Le premier avantage de ce système est de faire apparaître les grandeurs éventuellement inobservables ($\dot{\rho}$ et s) en tant que composantes de l'état. L'emploi de $s(t)$ sera justifié au paragraphe 1.2.

Avant toute évolution du lanceur, l'azimut $z(t)$ peut donc se calculer avec les trois seules variables $z, \dot{z}, \dot{\rho}$ exprimées à l'instant t_0 (figure 4a) :

$$z(t) = z(t_0) + \text{arctg} \frac{L_C}{L_D} \quad (4)$$

où

$$L_C = \dot{z}(t-t_0) \quad (5)$$

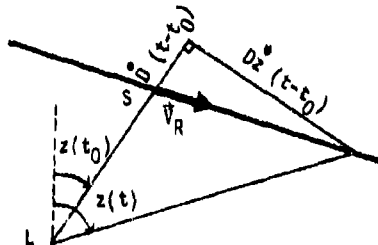
$$L_D = 1 + \dot{\rho}(t-t_0)$$

Lorsque le lanceur effectue une manœuvre, la séquence des azimuts est dépendante des déviations $\Delta L(t)$. Dans le repère lié à L , celles-ci se traduisent par des déviations relatives $-\Delta L(t)$ de la cible. Le déplacement relatif total de S entre t_0 et t est donc égal à $V_R(t-t_0) - \Delta L(t)$ (Figure 4b). Si W_C et W_D représentent les projections orthogonale (Cross-range) et radiale (Down-range) de $-\Delta L(t)$, $z(t)$ s'exprime alors par :

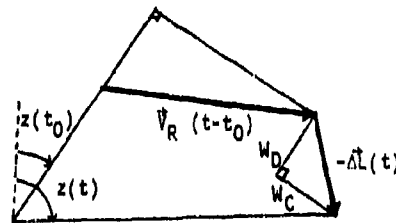
$$z(t) = z(t_0) + \text{Arctg} \frac{S_C}{S_D} \quad (6)$$

avec

$$\begin{aligned} S_C &= L_C + s W_C \\ S_D &= L_D + s W_D \end{aligned} \quad (7)$$



(a)



(b)

FIGURE 4 - Coordonnées polaires modifiées

Ainsi, les grandeurs W_C et W_D , par la modification qu'elles apportent sur l'évolution de $z(t)$ rendent la variable s observable. Elles devront cependant vérifier la condition $L_C W_D = L_D W_C$ afin de ne pas obtenir une situation inobservable similaire à la figure 3a. L'action de W_C et W_D sera d'autant plus grande que la distance d'observation sera faible. De plus, pour de petites variations angulaires, l'action de W_C sur $z(t)$ est directe alors que W_D n'intervient qu'au second ordre puisqu'elle entraîne surtout une modification de la distance. Ces remarques seront utiles pour la recherche d'une trajectoire lanceur favorable à l'estimation.

Le calcul des équations d'évolution de ce système peut s'obtenir de façon géométrique par projection dans le repère lié à $z(t)$ et elles sont données dans la référence [2].

• Algorithmes d'estimation

L'hypothèse d'une trajectoire parfaitement rectiligne de la cible autorise l'utilisation de plusieurs algorithmes pour les systèmes de coordonnées précédents.

Le filtre de Kalman étendu est d'une utilisation courante en trajectographie et, en l'absence de bruit d'évolution, il peut fournir soit l'estimation $\hat{X}_{k/k}$ de l'état courant à l'instant t_k de la mesure, soit l'estimation $\hat{X}_{0/k}$ de l'état initial en t_0 . Si, pour un système linéaire, ces deux options donnent des résultats équivalents, des différences apparaissent avec des équations non linéaires du fait de processus de linéarisation distincts.

Comme l'évolution des coordonnées cartésiennes est linéaire, l'instant d'estimation de l'état importe peu. Les algorithmes présentés réaliseront l'estimation de l'état courant X_k . Pour les coordonnées polaires modifiées évolutives, les deux options ont été testées. L'estimation de l'état présent X_k sera dénommée *polaires modifiées évolutives* et celle de l'état initial sera appelée *polaires modifiées fixes*.

La faible observabilité de la poursuite peut néanmoins entraîner, pour les deux systèmes de coordonnées, des erreurs de linéarisation affectant la qualité des résultats. Ceci nous conduit à l'utilisation d'une méthode d'estimation globale telle le maximum de vraisemblance qui, sous les hypothèses formulées, est la valeur de X_k qui minimise :

$$J(X_k) = \sum_{i=1}^k [z_i - H(X_k, t_i)]^2 \quad (8)$$

Notons qu'une interprétation statistique du filtre de Kalman consiste à minimiser le critère $J(X_k)$ additionné d'un terme portant sur l'état initial [14]. La technique de base que nous utiliserons, est l'algorithme de Gauss-Newton où le minimum est obtenu itérativement par

$$X_k^{i+1} = X_k^i - \Delta X \quad \text{avec} \quad \Delta X = W^{-1} G \quad (9)$$

où G est le gradient de J en X_k^i et W l'approximation du hessien

$$W = \sigma_z^{-2} \sum_{i=1}^k \frac{\partial H}{\partial X}(X_k^i) \frac{\partial H}{\partial X}(X_k^i)^T \quad (10)$$

L'avantage de cette procédure réside dans la linéarisation des équations de mesure qui est effectuée à chaque itération.

* Plan de la conférence

Pour l'amélioration de la qualité de l'estimation, deux objectifs ont été envisagés :

- La mise au point d'une technique d'estimation performante tout en assurant une charge de calcul raisonnable
- L'augmentation du niveau intrinsèque de l'observabilité par l'optimisation de la trajectoire du lanceur.

Dans la première partie, les problèmes de linéarisation du filtre de Kalman seront étudiés pour les deux systèmes de coordonnées retenues. Le faible niveau d'observabilité induit aussi des problèmes de stabilité numérique qui seront analysés dans le second paragraphe. Ensuite nous montrerons comment une méthode globale peut être appliquée à ce problème de poursuite. Celle-ci offre en outre la possibilité de prendre en compte une connaissance a priori sur le module de la vitesse de la cible.

Dans la deuxième partie, nous établirons comment, dans le cadre général des systèmes dynamiques, peut être défini un indice scalaire d'observabilité qui constituera le critère d'optimisation de la trajectoire du lanceur. L'analyse des matrices d'information de la TPA mettra ensuite en évidence certains principes généraux concernant les évolutions du lanceur favorables. Enfin l'objectif principal de cette partie réside dans l'optimisation de la trajectoire de L qui doit tenir compte des contraintes physiques du problème.

1ère PARTIE - ANALYSE DES ALGORITHMES D'ESTIMATION

1 - PROBLEMES DE LINEARISATION

Une technique fréquemment utilisée pour les problèmes d'estimation non linéaires consiste à utiliser un filtre linéaire traitant des pseudo-mesures. Concernant la TPA, on peut transformer l'équation 2 pour utiliser cette méthode. Cependant les résultats fournis sont très biaisés ce qui proscriit l'utilisation de cette technique dans la plupart des scénarios rencontrés [1].

Nous sommes donc contraints d'utiliser des procédures d'estimation adaptées à la nature non linéaire des équations. Cependant du fait de la faible observabilité, les algorithmes récursifs (Filtre de Kalman) se révèlent parfois insuffisants. L'étude de cas simplifiés montrera comment une procédure globale améliore la précision des résultats et quelle est l'influence du système de coordonnées. Dans le cadre de la TPA, les performances des coordonnées cartésiennes et polaires modifiées seront ensuite analysées.

1.1 - Influence de la méthode d'estimation

Considérons l'estimation d'un vecteur d'état constant (coordonnées polaires modifiées fixes par exemple). A chaque instant, le filtre de Kalman ne comporte qu'une étape d'estimation qui peut s'écrire sous la forme :

$$\hat{X}_k = \hat{X}_{k-1} + \frac{P_k H_k^T}{\sigma_z} [z_k - H(\hat{X}_{k-1})] \quad (11)$$

$$P_k^{-1} = P_{k-1}^{-1} + \frac{H_k^T H_k}{\sigma_z} = P_0^{-1} + \sum_{i=1}^k \frac{H_i^T H_i}{\sigma_z} \quad (12)$$

avec

$$H_i = \frac{\partial H}{\partial X} |_{X=\hat{X}_{i-1}} \quad (13)$$

Ainsi, par comparaison avec les équations 9 et 10, on en déduit que le filtre de Kalman étendu constitue la première itération d'un algorithme de Gauss-Newton initialisé par \hat{X}_{k-1} et opérant sur le critère

$$J_K(X) = (X - \hat{X}_{k-1})^T P_{k-1}^{-1} (X - \hat{X}_{k-1}) + \sigma_z^{-2} [z_k - H(X)]^2 \quad (14)$$

Le filtre de Kalman qui, comme signalé en introduction, peut être envisagé comme la minimisation du critère 8 sur les mesures additionné de la connaissance a priori sur l'état initial, est en fait une procédure de minimisation comportant trois restrictions :

- Il n'est procédé à chaque instant qu'à une seule itération.
- L'information des mesures passées est condensée sous la forme linéaire quadratique (\hat{X}_{k-1}, P_{k-1})
- Chaque mesure est linéarisée une seule fois autour de l'état prédit \hat{X}_{k-1} .

Pour de fortes non linéarités ou une estimation X_{k-1} erronée à cause de la faible observabilité, les linéarisations H_k sont imprécises. Ceci va entraîner, par l'équation 12, l'accumulation d'une information inexacte durant la phase inobservable qui va affecter la convergence du filtre pour les phases ultérieures plus observables.

L'algorithme de Gauss-Newton qui procède à la relinéarisation des mesures passées, permet de limiter les effets de ces erreurs. Afin de conserver une efficacité suffisante pour le traitement en temps réel tout en palliant ces problèmes de linéarisation, une version simplifiée et récursive de cet algorithme est utilisée. Son adaptation aux phases initiales peu observables de la poursuite sera exposée dans la section 3. A l'image du filtre de Kalman, une seule itération initialisée par X_{k-1} est effectuée à chaque instant pour minimiser le critère 8 sur les mesures. A l'instant t_k , nous avons le traitement suivant :

$$\hat{X}_k = \hat{X}_{k-1} - \Delta X \quad \text{avec} \quad \Delta X = W^{-1} G \quad (15)$$

et

$$W = \sigma_z^{-2} \sum_{i=1}^k H_i^T H_i \quad \text{où} \quad H_i = \frac{\partial H}{\partial X} \Big|_{X=\hat{X}_{k-1}} \quad (16)$$

Ainsi dans l'équation 16, les mesures sont toutes linéarisées autour de la dernière prédiction \hat{X}_{k-1} . Les erreurs de linéarisation diminueront donc au fur et à mesure de l'amélioration des résultats.

Ces conclusions s'étendent aisément aux systèmes comportant une évolution déterministe, des problèmes supplémentaires apparaissant alors au niveau de la linéarisation des équations d'évolution. Cette méthode globale simplifiée exige cependant des temps de calcul beaucoup plus grands que le filtre de Kalman.

1.2 - Influence du système de coordonnées

Le choix du système de coordonnées peut aussi altérer la nature des non-linéarités et donc l'importance des erreurs de linéarisation. Afin d'illustrer ce phénomène, nous allons considérer le cas de la détermination de la position d'un point immobile par mesures d'azimut. Le vecteur d'état est de dimension deux et, par analogie avec la TPA, plusieurs systèmes de coordonnées sont envisageables :

- Les coordonnées cartésiennes : $X = (x_s, y_s)^T$
- Les coordonnées polaires : $X = (z_r, D_r)^T$
- Les coordonnées polaires modifiées : $X = (z_r, s_r)^T$

Pour les deux systèmes polaires, un point de référence P_r doit être choisi pour calculer la position relative de S . z_r , D_r , s_r représentent alors respectivement l'azimut, la distance et son inverse par rapport à P_r .

D'après les équations de l'algorithme de Gauss-Newton (9, 10), nous constatons que, pour un point d'initialisation X_0 , le critère sur les mesures est approximé par la forme quadratique

$$J_g(X) = J(\hat{X}) + (X - \hat{X})^T W^{-1} (X - \hat{X}) \quad (17)$$

où

$$\hat{X} = X_0 - W^{-1} G \quad (18)$$

et W est linéarisé en X_0 .

Afin d'étudier les trois systèmes de coordonnées précédents, nous avons réalisé, pour le scénario de la figure 5, le tracé de certains isocritères de $J(X)$ et $J_g(X)$. Ces derniers sont donc des ellipses dans le repère correspondant. A des fins de comparaisons, ces isocritères ont été ramenés dans le plan cartésien.

Pour la figure 5, le point X_0 coïncide avec le minimum de $J(X)$. Pour les coordonnées cartésiennes et polaires, les isocritères linéarisés diffèrent notablement de ceux de $J(X)$ alors que l'approximation est quasiment parfaite pour les polaires modifiées. Dans le cadre d'une formulation probabiliste, les isocritères de $J(X)$ limitent des domaines de confiance et ceux obtenus par linéarisation autour de la valeur vraie de X sont les ellipsoïdes d'incertitude issues de la borne de Cramer-Rao. Pour ce problème où le conditionnement n'est pourtant pas important, la borne de Cramer-Rao des deux premiers systèmes ne sera donc pas très représentative des véritables erreurs d'estimation.

Si le point de départ X_0 est erroné en distance (variable la moins observable), le minimum calculé par la première itération de Gauss-Newton pour les systèmes cartésiens et polaires est très distant du vrai minimum. Pour les polaires modifiées, il est presque confondu. Ainsi, pour une erreur d'initialisation en distance, la convergence de l'algorithme de minimisation sera beaucoup rapide avec ce dernier système. D'autre part, lors de l'utilisation du filtre de Kalman, l'état et la variance reflèteront plus fidèlement l'information contenue dans les mesures, même pour une estimation imprécise de la distance.

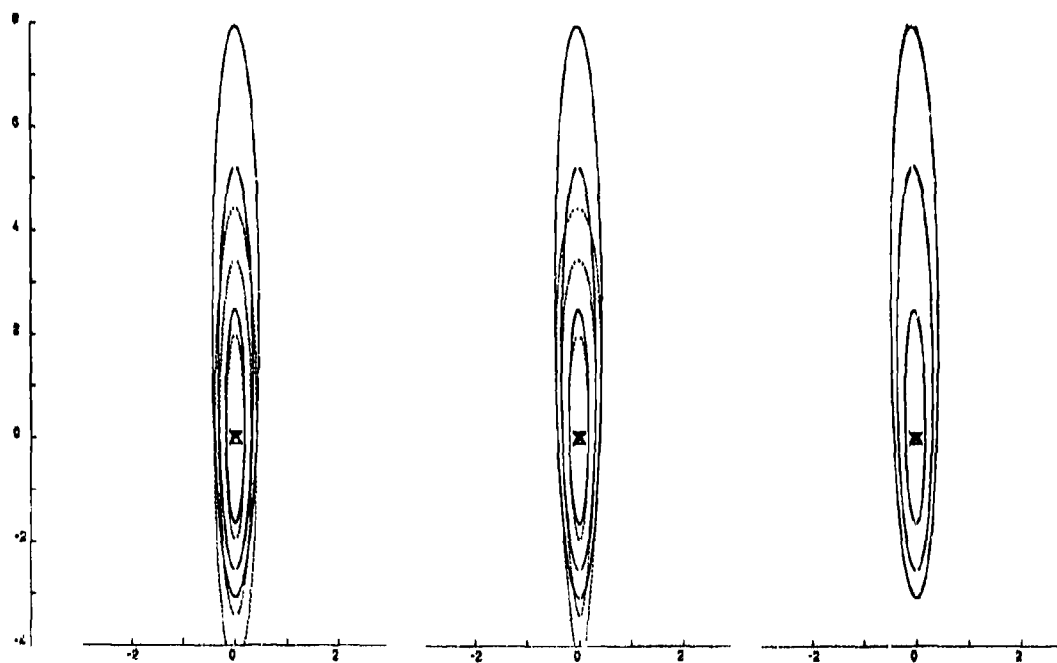
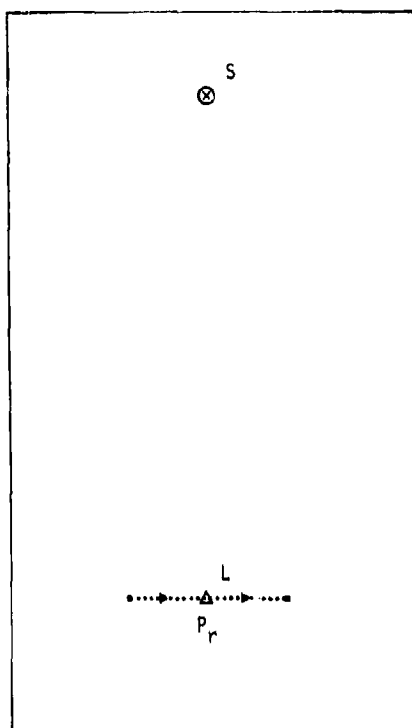
L'analyse de l'équation de mesure de ce dernier système de coordonnées révèle que, sous les deux conditions (différence angulaire faible entre $z(t)$ et z_r et déplacements faibles du lanceur par rapport à P_r suivant l'axe z_r), elle peut être approximée par :

$$z(t) = z_r + w_g(z_r) s_r \quad (19)$$

où w_g est la composante orthogonale de l'opposé du déplacement de L par rapport à P_r . Ainsi l'équation de mesure est presque linéaire par rapport à la variable la moins observable s_r . On montre alors que, dans une région relativement large autour du minimum, les isocritères de $J_g(X)$ sont très proches de ceux de $J(X)$ pourvu que la linéarisation soit effectuée autour d'un point X_0 d'azimut exact.

L'approximation 19 va cependant dépendre du point de référence P_r et, pour le scénario de la figure 5, le point retenu constitue un choix idéal. Ce point de référence peut être, en outre, considéré comme un facteur de réglage afin d'améliorer la linéarisation. Dans l'exemple traité, le barycentre des points de mesure de L semble être en général bien adapté.

Dans un cadre plus général, la condition que doivent vérifier les systèmes de coordonnées pour assurer de bonnes propriétés de linéarisation, est une faible dépendance du gradient des équations de mesure par rapport aux variables peu observables. Pour le filtre de Kalman, des erreurs de linéarisation interviennent aussi au niveau de l'étape de prédiction si l'évolution du système est non linéaire. On peut aussi montrer de façon intuitive qu'il faut éviter la propagation de variables mal déterminées par des fonctions non linéaires.



Coordonnées cartésiennes

Coordonnées polaires

Coordonnées polaires modifiées

FIGURE 5 - Influence du système de coordonnées

Ces notions quoique qualitatives et intuitives permettent néanmoins d'expliquer les causes des erreurs de linéarisation et de comparer plusieurs systèmes de coordonnées. Pour certaines situations, cependant une analyse expérimentale est aussi nécessaire.

1.3 - Analyse des systèmes de coordonnées de la TPA

• Coordonnées cartésiennes

L'évolution étant linéaire, les effets de la linéarisation interviennent donc dans le traitement des mesures. Le gradient de l'équation de mesure est égal à

$$H_k = \frac{1}{\hat{D}_{k/k-1}} \begin{bmatrix} \cos \hat{z}_{k/k-1} & -\sin \hat{z}_{k/k-1} & 0 & 0 \end{bmatrix} \quad (20)$$

qui fait apparaître la dépendance par rapport à la distance prédite $\hat{D}_{k/k-1}$ peu observable durant la phase initiale de la poursuite. Ceci explique les performances moyennes du filtre en coordonnées cartésiennes ainsi que sa sensibilité à l'initialisation de la distance. Il est donc préférable de ne pas utiliser de méthodes récursives pour ces coordonnées. Quant aux résultats d'une méthode globale, ils ne seront exploitables que si la distance est suffisamment observable.

• Coordonnées polaires modifiées fixes

Sous des hypothèses similaires à l'obtention de l'approximation 19, l'équation 6 peut être approchée par

$$z(t) = z(t_0) + \dot{z}(t_0)(t-t_0) + s(t_0) W_C \quad (21)$$

Cette expression révèle la dépendance favorable de $z(t)$ par rapport aux trois composantes z , \dot{z} et s . Cependant \dot{p} est alors peu observable et l'approximation 21 dépend de la valeur estimée de cette grandeur. De plus, la dépendance de $z(t)$ par rapport à cette seule variable \dot{p} ne paraît pas aussi favorable.

Au niveau du gradient de la mesure, ce système présente une propriété remarquable. En effet, avant la première manoeuvre de L ($W_C = W_D = 0$), il se réduit à :

$$H_k = \begin{bmatrix} 1 & \frac{(t_k - t_0) L_D}{L_C^2 + L_D^2} & -\frac{(t_k - t_0) L_C}{L_C^2 + L_D^2} & 0 \end{bmatrix} \quad (22)$$

Ainsi durant cette première phase où s est inobservable, H_k est complètement indépendant de cette grandeur et les erreurs de linéarisation par rapport à s sont inexistantes. Cependant des problèmes peuvent théoriquement survenir lorsque la poursuite n'est encore que faiblement observable. Expérimentalement, ces coordonnées se révèlent beaucoup plus robustes à l'initialisation de D même si cette grandeur est mal déterminée pendant une longue phase de la poursuite.

Lorsque \dot{p} est aussi inobservable, la linéarisation va, dans ce cas, dépendre de l'estimation de \dot{z} . Pour une estimation parfaite $\dot{z} = 0$, H_k s'écrit

$$H_k = \begin{bmatrix} 1 & \frac{t_k - t_0}{1 + p(t_k - t_0)} & 0 & 0 \end{bmatrix} \quad (23)$$

qui fait apparaître la variable \dot{p} et qui suggère une sensibilité potentielle. Cependant, ces effets restent également faibles en pratique.

• Coordonnées polaires modifiées évolutives

Pour ce type de coordonnées, la linéarisation est effectuée à l'étape de prédiction du filtre de Kalman. Avant toute évolution du lanceur, la linéarisation $\phi_{k,k-1}$ des équations d'évolution est de la forme :

$$\phi_{k,k-1} = \begin{bmatrix} 1 \times \times 0 \\ 0 \times \times 0 \\ 0 \times \times 0 \\ 0 \otimes \otimes \times \end{bmatrix} \quad (24)$$

où \times sont des termes non nuls et \otimes des termes dépendants de s . Cette dépendance est proportionnelle à s et ces termes seront d'autant plus faibles que la distance estimée sera grande. Cependant des effets d'accumulation peuvent se produire car ces calculs sont réalisés à chaque instant d'échantillonnage. Par rapport, au cas précédent où l'indépendance par rapport à s était parfaite, on peut a priori prévoir une dégradation des résultats.

Si \dot{p} est inobservable et si nous supposons $\dot{z} = 0$, la linéarisation $\phi_{k,k-1}$ dépend des estimations des deux variables s et \dot{p} . Dans cette situation, la jacobienne des équations d'évolution paraît moins performante que la linéarisation des polaires modifiées fixes.

En pratique, l'effet de ces problèmes de linéarisation apparaît limité et des résultats supérieurs au filtre cartésien sont obtenus. Une étude statistique plus approfondie serait nécessaire pour confirmer les remarques formulées sur les deux options des coordonnées polaires modifiées.

1.4 - Conclusion

Cette étude nous a permis d'évaluer l'aptitude des différentes coordonnées pour les algorithmes d'estimation récursifs.

• Coordonnées polaires modifiées fixes.

Elles apparaissent les plus robustes du fait de l'indépendance de la mesure par rapport à s avant la première évolution du lanceur. De plus, des études expérimentales [12] confirment cette insensibilité. L'emploi d'une méthode globale ne se justifie que pour des scénarios très peu observables.

- Coordonnées polaires modifiées évolutives

Les équations semblent a priori plus sensibles aux problèmes de linéarisation bien que les tests réalisés n'aient pas, à première vue, révélé cet état de fait. La référence [15] signale que l'estimation de \hat{p} et s est biaisée. Ces biais nous ont paru cependant faibles.

- Coordonnées cartésiennes

Elles se sont avérées les plus fragiles car le gradient dépend de la distance prédite. Les résultats obtenus sont toutefois très exploitables si la poursuite devient suffisamment observable.

2 - SENSIBILITE NUMERIQUE DU FILTRE DE KALMAN

La littérature expose divers cas d'instabilité numérique du filtre de Kalman. Des erreurs de calcul peuvent, en effet, apparaître lorsque l'information des mesures est très hétérogène suivant les différentes directions de l'espace d'état. La TPA constitue donc un exemple privilégié pour ce type d'étude.

Ces problèmes peuvent être contournés par l'utilisation d'une précision de calcul plus grande. Cependant, pour l'analyse de l'efficacité d'un algorithme au niveau du temps d'exécution, il convient d'examiner en détail les diverses implantations possibles.

Nous analyserons tout d'abord le filtre de Kalman en coordonnées cartésiennes qui est très démonstratif des problèmes numériques. Dans un second paragraphe, la sensibilité des coordonnées polaires modifiées sera ensuite étudiée.

2.1 - Filtre en coordonnées cartésiennes

Dans un premier temps, nous allons examiner comment se manifestent et apparaissent ces erreurs de calcul. Puis nous déterminerons quelle est l'influence de l'implantation sur l'émergence des problèmes numériques et sur leur propagation. Enfin des procédures visant à diminuer la sensibilité du filtre seront analysées.

2.1.1 - Apparition des erreurs numériques

Il est souvent admis que les problèmes de calcul sont liés au conditionnement de la variance du filtre. En fait, cette grandeur reflète très imparfaitement les possibilités d'apparition d'erreurs numériques.

Un filtre de Kalman en simple précision (6 chiffres significatifs) a, à cet effet, été comparé au même programme en double précision (15 chiffres significatifs). Sur la figure 6a, on constate des différences appréciables entre les deux versions et les erreurs numériques affectent aussi les résultats en phase observable puisqu'il subsiste un léger biais final de la version en simple précision. La valeur du conditionnement de ce scénario ne dépasse pas $2.0 \cdot 10^{10}$. Pour la figure 6b, aucune différence n'apparaît entre les deux versions du filtre alors que le scénario est doublement inobservable durant la longue phase initiale et le conditionnement supérieur à 10^{14} .

Pour illustrer ce phénomène, considérons une matrice de variance P de dimension 2 qui a pour valeurs propres λ_1 et λ_2 . Soit ϵ la valeur relative des erreurs provenant de l'arrondi et du calcul en représentation flottante de chaque coefficient de P . Dans le repère où cette matrice est diagonale, les erreurs relatives seront donc égales, au maximum, à ϵ . Dans le repère où les vecteurs propres sont à 45° , P a pour expression :

$$P = \frac{1}{2} \begin{pmatrix} \lambda_1 + \lambda_2 & \lambda_1 - \lambda_2 \\ \lambda_1 - \lambda_2 & \lambda_1 + \lambda_2 \end{pmatrix} \quad (25)$$

Pour un rapport λ_2/λ_1 du même ordre de grandeur que ϵ , les erreurs sur les coefficients de P seront de la taille de λ_2 expliquant la modification éventuellement importante de cette valeur propre qui peut, à la limite, devenir négative.

Les termes de couplage (extra-diagonaux) de la matrice de covariance sont donc responsables de la sensibilité numérique.

Pour la figure 6b, les mesures d'azimut sont sensiblement alignées avec l'axe Nord-Sud assurant un découplage partiel entre les axes de coordonnées et expliquant l'insensibilité des résultats à la précision de calcul. Ceci n'est apparemment pas le cas de la figure 6a. Une simulation similaire dont l'azimut moyen est parallèle à un axe de coordonnées (figure 6c) se révèle insensible à la précision de calcul. A l'inverse, le filtre de Kalman en simple précision diverge pour le scénario de la figure 6d où l'azimut moyen est à 45° des axes. Cette dernière situation très sévère sera utilisée pour tester la robustesse des algorithmes et sera dénommée *simulation TEST*.

Afin de pouvoir analyser la robustesse de différents systèmes de coordonnées ou implantations, il importe de définir une mesure de la sensibilité de la variance P .

L'erreur au 1er ordre sur la valeur propre $\lambda(k)$ de la variance, du fait d'erreurs Δp_{ij} sur les coefficients de P est égale à

$$\Delta \lambda(k) = \sum_{i,j} \left| \frac{\partial \lambda(k)}{\partial p_{i,j}} \right| \Delta p_{i,j} \quad (26)$$

Si des erreurs relatives ϵ sont commises sur les coefficients, l'erreur relative au 1er ordre sur $\lambda(k)$ est donnée par :

$$\frac{\Delta \lambda(k)}{\lambda(k)} = \left\{ \underbrace{\sum_{i,j=1}^n \left| \frac{\partial \lambda(k)}{\partial p_{i,j}} \right| p_{i,j}}_{= s(\lambda(k))} \right\} \frac{1}{\lambda(k)} \epsilon \quad (27)$$

Cette formule est une majoration de l'erreur possible sur $\lambda(k)$ car elle suppose des erreurs maximales sur tous les coefficients et de signe tel que leurs actions se cumulent. Cependant elle tient compte de la structure de P . Notamment si P est diagonale, les erreurs relatives sont toutes égales à ϵ . L'équation 27 fait apparaître un facteur d'amplification des erreurs $s(\lambda(k))$ que nous

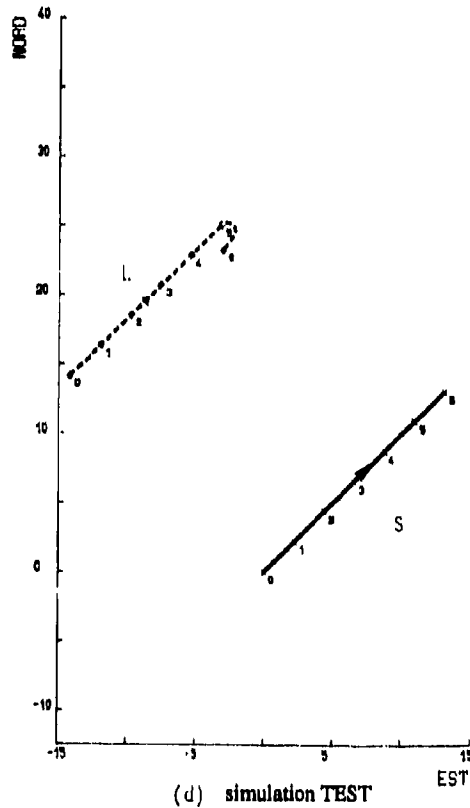
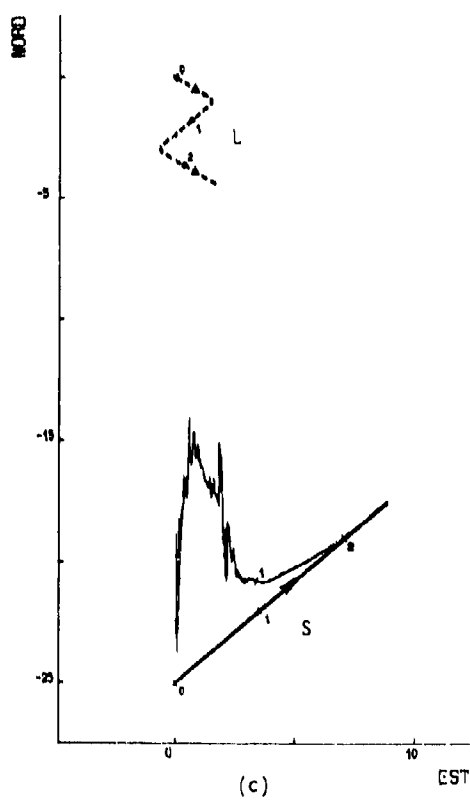
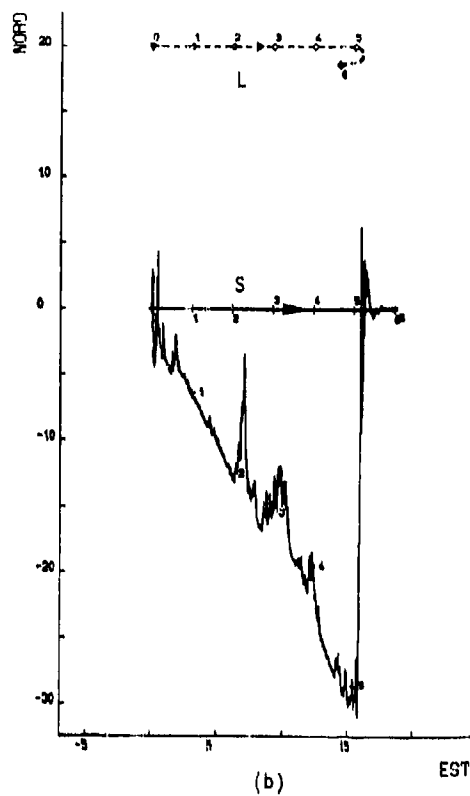
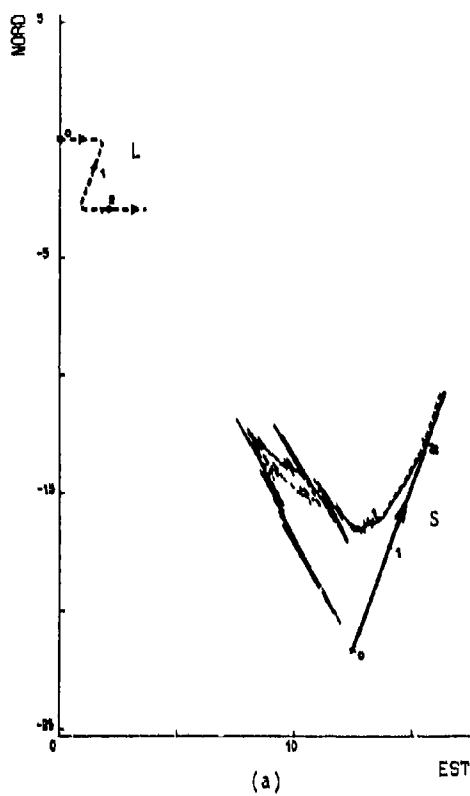


FIGURE 6 - Sensibilité numérique : Influence des termes de couplage
 Double précision
 Simple précision

appelons *sensibilité de la valeur propre* $\lambda(k)$. La *sensibilité globale* $S(P)$ de P peut être définie comme la plus grande des valeurs $s(\lambda(k))$.

Pour l'exemple de dimension 2, nous trouvons :

$$s(\lambda_{\max}) = 1 \quad \text{et} \quad s(\lambda_{\min}) = C \sin^2 2\theta + \cos^2 2\theta \quad (28)$$

Alors que λ_{\max} est insensible aux erreurs de calcul, λ_{\min} le sera d'autant plus que le conditionnement C sera grand et que l'angle de couplage θ se rapprochera de $\pi/4$.

Une autre mesure de la sensibilité de P est l'erreur relative maximale sur toutes les directions de l'espace et l'ensemble des représentations flottantes "admissibles" de la variance [6] :

$$\Lambda(P) = \epsilon^{-1} \max_{\Delta P, u} \frac{u^T \Delta P u}{u^T P u} \quad \text{avec} \quad |\Delta p_{i,j}| \leq \epsilon |p_{i,j}| \quad (29)$$

Cette grandeur peut être encadrée par les inégalités :

$$\frac{1}{\lambda_{\min}(\tilde{P})} \leq \Lambda(P) \leq \frac{n}{\lambda_{\min}(\tilde{P})} \quad \text{où} \quad \tilde{P}_{ij} = \frac{P_{ij}}{\sqrt{P_{ii} P_{jj}}} \quad (30)$$

Par rapport à $S(P)$, cette sensibilité $\Lambda(P)$ prend aussi en compte les variations éventuelles des vecteurs propres de P puisque, dans l'équation 29, le maximum est calculé sur toutes les directions u de l'espace et non sur les seules directions propres. Nous verrons cependant que la différence entre ces deux mesures est minime en pratique. Les inégalités 30 impliquent aussi une conséquence très importante pour l'implantation des algorithmes. Il apparaît en effet que *des changements d'unités du vecteur d'état ou la normalisation de la matrice P n'ont aucune influence sur les éventuels problèmes de sensibilité numérique.*

Les figures 7a et b représentent respectivement les diverses sensibilités des scénarios des figures 6b et 6d. Similairement au cas de dimension 2, la sensibilité de λ_{\max} est sensiblement égale à 1 et λ_{\min} est souvent peu robuste. Pour les sensibilités globales, le conditionnement donne toujours des valeurs très pessimistes par rapport à $S(P)$ et $\Lambda(P)$. Enfin $S(P)$ est toujours comprise dans l'encadrement de $\Lambda(P)$ prouvant que les perturbations sur les seules directions propres reflètent bien la sensibilité de la variance. Ces valeurs confirment de plus les résultats obtenus pour l'estimation.

Pour la simulation TEST, la figure 8 illustre la dégradation des valeurs propres du filtre en simple précision. Les plus affectées (aspect chahuté des courbes) sont la première et la troisième qui sont effectivement, d'après la figure 7b, les plus sensibles ; λ_{\min} devient d'ailleurs négative. La dégradation de la plus grande valeur propre qui n'intervient que dans un second temps provient sans doute, vu l'aspect régulier de la courbe, d'erreurs de linéarisation qui résultent de la dégradation de l'estimation engendrée par l'altération de λ_1 et λ_3 .

Ces modifications sur les valeurs propres vont entraîner des erreurs sur l'état estimé qui provient du calcul défectueux du gain K du filtre de Kalman. Pour analyser plus facilement la liaison entre la dégradation des valeurs propres et celle de l'état, considérons la relation entre la mesure corrigée $\hat{z}_+ = H \hat{x}_+$ et la mesure prédite $\hat{z}_- = H \hat{x}_-$.

$$\hat{z}_+ = \hat{z}_- + H K (z - \hat{z}_-) \quad (31)$$

Le coefficient HK de correction est compris entre 0 et 1 et est égal à :

$$HK = \frac{H P H^T}{H P H^T + \sigma_z^2} \quad (32)$$

Les dégradations de la matrice P vont affecter la valeur de l'expression HPH^T et donc celle de HK . Les erreurs sur ce coefficient vont donc dégrader la correction 31. Si HK reste compris entre 0 et 1, le filtre garde son aptitude à générer des résultats cohérents. Néanmoins ses performances sont dégradées par rapport au cas optimal sans erreur de calcul. Si ce coefficient est négatif, le sens de la correction HK est erroné. Une valeur HK négative pendant plusieurs itérations ou importante en valeur absolue peut entraîner la divergence de l'algorithme comme le montre la figure 9 dans la simulation TEST. Ces résultats obtenus au niveau des mesures estimées et prédites vont, bien sûr, se refléter sur le sous-espace correspondant par H de l'espace d'état.

On peut donc résumer les conditions d'apparition et les effets des erreurs numériques dans le filtre de Kalman :

- Une valeur importante du conditionnement de la matrice de covariance est une condition *nécessaire mais non suffisante* pour l'apparition de problèmes numériques. Les termes de couplage entre les différentes composantes du vecteur d'état sont en effet responsables de la sensibilité de cette matrice.
- Les erreurs numériques se manifestent parfois par des *dégradations non divergentes* des résultats même lorsque la variance du filtre de Kalman n'est plus positive. Il convient donc d'être vigilant lors de l'emploi d'une précision de calcul limitée même si les grandeurs estimées paraissent cohérentes.
- La normalisation de la variance ou les changements d'unités du vecteur d'état n'ont pas d'influence sur les éventuels problèmes numériques.

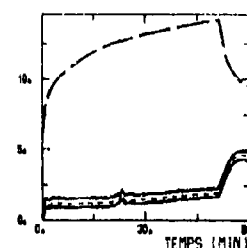
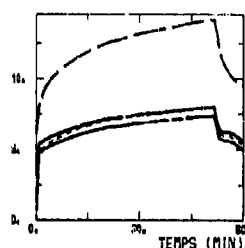
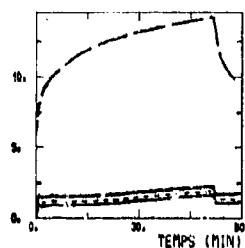
2.1.2 - Influence de l'implantation

L'altération des valeurs propres de la variance va fortement dépendre de la façon dont vont être conduits les calculs. En effet on constate déjà des différences suivant la version optimisée ou non de la compilation d'une même programme. On conçoit donc que l'implantation est décisive sur la qualité des résultats.

Pour l'algorithme de Kalman, il existe deux procédures classiques pour la mise à jour de la variance :

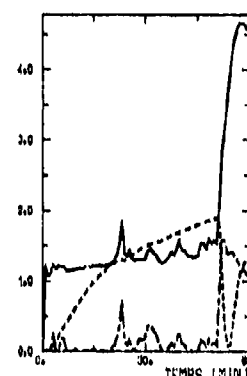
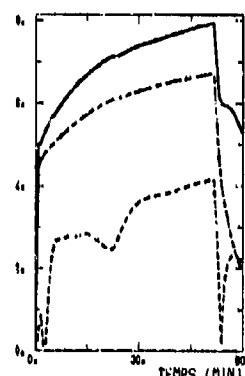
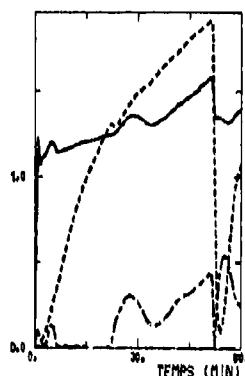
Sensibilités globales

- conditionnement
 — $\lambda(P)$ (eq. 30)
 - - - $S(P)$ (eq. 27)



Sensibilités des valeurs propres

- $\lambda_1 = \lambda_{\min}$
 - - - λ_2
 - - - λ_3
 - - - $\lambda_4 = \lambda_{\max}$



(a) simulation 6b

(b) simulation TEST

(c) filtre hybride

FIGURE 7 - Sensibilité de la variance du filtre cartésien (Logarithme décimal)

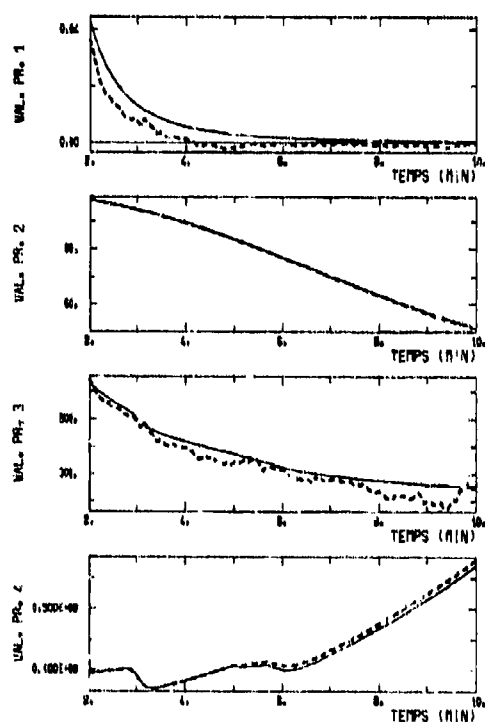


FIGURE 8 - Dégradation des valeurs propres
 du filtre cartésien
 — Double précision
 - - - Simple précision

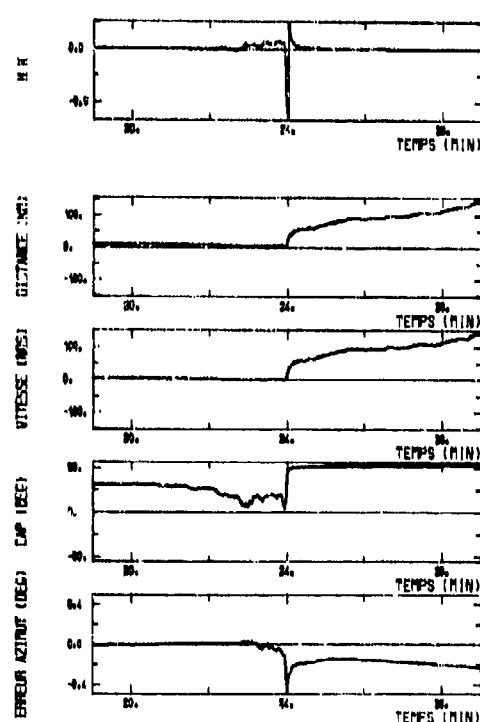


FIGURE 9 - Divergence du filtre de Kalman
 cartésien en simple précision

La forme conventionnelle de Kalman

$$P_+ = (I - KH) P_- \quad (33)$$

• La forme stabilisée de Joseph, réputée plus stable

$$P_+ = (I - KH) P_- (I - KH)^T + K R K^T \quad (34)$$

Pour la forme conventionnelle, la référence [31] révèle qu'il est primordial de préserver la symétrie de la variance si l'évolution du système est instable. Un modèle d'évolution à vitesse constante étant à la limite de stabilité, il convient donc de garder le caractère symétrique de P en ne calculant, par exemple que sa moitié supérieure.

Pour la forme de Joseph, la mise en jour est exacte pour toute valeur de K alors que la forme conventionnelle n'est valable qu'avec la valeur optimale du gain. D'autre part [7], les erreurs sur la variance ne dépendent qu'au deuxième ordre des erreurs sur K . Pour programmer l'équation 34, plusieurs solutions sont possibles. La plus immédiate est d'utiliser des produits matriciels symétriques du type $C = A B A^T$ où C et B sont symétriques. Cependant cette méthode demande beaucoup de calculs. D'autre part, elle s'est révélée, en pratique, la plus sensible sur tous les cas traités. Il existe d'autres implantations de la forme de Joseph qui sont à la fois plus rapides et plus stables [4,27]. Elles se sont révélées d'égale robustesse, les résultats dépendant des simulations traitées, et nettement moins sensibles que la solution avec les produits symétriques. Cependant, elles n'apportent, en général, aucune amélioration aux résultats de la forme conventionnelle qui sont quelquefois plus exacts.

De toute façon les deux formes 33 et 34 ne sont pas suffisamment insensibles pour des cas mal conditionnés comme la simulation TEST pour lesquels on obtient des variances non positives voire même des termes diagonaux négatifs.

Les résultats expérimentaux obtenus pour la TPA confirment ceux de la référence [5] en ce qui concerne l'instabilité numérique de la forme de Joseph. Si le problème traité ne présente pas de difficultés numériques particulières, l'algorithme conventionnel de Kalman où est assurée la symétrie de la variance, sera donc préférable car plus rapide. Dans le cas contraire, il conviendra d'utiliser une procédure adaptée que nous allons présenter dans le paragraphe suivant.

2.1.3 - Implantations numériquement stables

La sensibilité de la représentation naturelle de la variance est responsable des problèmes numériques intervenant dans le filtre de Kalman. Il s'agit donc de trouver une représentation équivalente d'un point de vue mathématique mais moins sensible aux problèmes numériques tout en présentant des temps de calcul acceptables.

Nous avons analysé deux types de méthodes : un filtre hybride [6], et les procédures factorisées notamment celle de Bierman et Thornton [4,5,16,27].

• Filtre hybride

Dans le cas des coordonnées cartésiennes, la sensibilité de la variance est fortement dépendante de l'orientation du repère choisi. L'idée de base du filtre hybride consiste à représenter la variance dans le repère lié à la mesure prédite afin de diminuer au moins partiellement les termes de couplage.

L'algorithme comporte donc à chaque étape une rotation de la variance pour réaligner la représentation de P avec la nouvelle prédiction de la mesure ainsi qu'une rotation pour le calcul du gain dans le repère d'origine. Bien que quelques précautions soient à prendre au niveau de la programmation des rotations, cet algorithme en simple précision supporte parfaitement des situations comme la simulation TEST.

La figure 7c révèle en effet des sensibilités très faibles durant la phase inobservable et comparable à celles de la figure 7a. Cependant, lors de la manœuvre du lanceur, l'augmentation des sensibilités montre que le repère lié à la mesure prédite n'est pas le plus adapté. En effet, durant la longue phase initiale de ce scénario (figure 6d), les directions propres de P vont s'orienter suivant l'axe de la mesure constante et son orthogonal. La première évolution du lanceur entraîne une évolution de la mesure prédite. Toutefois, l'information recueillie par les premières mesures de cette seconde phase est insuffisante pour modifier les directions propres de P . Ceci explique l'apparition de termes de couplage dans la représentation de P liée à la mesure prédite et aussi la faible sensibilité de la poursuite de la figure 6b.

• Filtre factorisé

Ces techniques ont fondées sur la racine de Cholesky de P . En effet, toute matrice symétrique positive peut se décomposer sous la forme :

$$P = R^T R \quad (35)$$

où R est une matrice triangulaire supérieure ou inférieure. L'avantage de cette factorisation est double car elle assure d'une part la positivité de P . D'autre part, le conditionnement de R est égal à la racine carrée de celui de P révélant ainsi une sensibilité a priori plus faible de cette représentation. Une autre factorisation possible est la suivante :

$$P = U^T D U \quad (36)$$

où D est une matrice diagonale et U une matrice triangulaire supérieure ou inférieure comportant des 1 sur sa diagonale. Cette forme est obtenue de façon identique à la décomposition 35 mais les pivots sont rassemblés dans la matrice D . L'utilisation de cette factorisation évite ainsi le calcul de racines carrées qui sont généralement coûteuses en charge de calcul.

Les procédures de Kalman factorisées consistent alors à mettre à jour directement les décompositions 35 ou 36 de la variance. Il est possible, de façon similaire à l'équation 27, de définir la sensibilité au 1er ordre des valeurs propres de P pour les deux représentations précédentes.

Pour un exemple de dimension 2, l'expression de ces sensibilités révèle notamment qu'elles sont bornées par rapport au conditionnement par les valeurs respectives 6 et 3. En outre, les décompositions seront moins sensibles si elles sont effectuées par ordre décroissant des pivots.

Concernant la TPA, les décompositions avec R ou U *triangulaires supérieures* qui correspondent approximativement à factoriser P par ordre décroissant des pivots, donnent des sensibilités nettement plus faibles que les décompositions avec R ou U *inférieures* (figure 10). Contrairement, au cas de dimension 2 cependant, les sensibilités ne semblent pas bornées par rapport au conditionnement. Toutefois les valeurs obtenues sont, dans tous les cas, beaucoup plus petites que celles de la représentation conventionnelle de la variance et suffisantes pour la précision généralement utilisée sur les calculateurs actuels. D'autres considérations telles que la rapidité des calculs seront alors prises en compte pour le choix d'une décomposition.

Notons aussi que, à la différence de la représentation naturelle de P, la normalisation ou le choix des unités de l'état influent sur la sensibilité des factorisations (des termes de même ordre de grandeur n'étant pas forcément le gage d'une plus grande robustesse).

Un filtre factorisé a été testé pour la forme UD (équation 36) avec U triangulaire *inférieure* (situation "la moins favorable") car elle se révèle plus rapide pour le calcul de la prédiction de la variance avec un modèle à vitesse constante. La forme triangulaire supérieure serait plus adaptée à l'étape de mise à jour du filtre. Pour toutes les simulations traitées, cette implantation s'est avérée complètement insensible aux problèmes numériques. D'autre part, ce filtre de Kalman factorisé s'est révélé plus rapide que l'algorithme conventionnel de même précision.

Bien que le filtre hybride permette une diminution de la sensibilité, son utilisation et sa structure sont très liées au problème traité. Les implantations factorisées sont donc préférables car elles offrent une stabilité numérique beaucoup plus grande en toutes circonstances sans pour autant dégrader les temps de calcul.

2.2 - Sensibilité numérique des coordonnées polaires modifiées

Le choix de ces coordonnées permet de s'abstraire de l'orientation des mesures dans le repère de base. En outre, le fait que leurs composantes représentent les grandeurs inobservables va engendrer des propriétés de découplage bénéfiques qui vont dépendre de la configuration retenue pour le filtre.

• Coordonnées polaires modifiées fixes

Il est possible d'assurer un découplage parfait de la variable s inobservable avant toute manœuvre du lanceur [2]. En effet, si la variance du filtre de Kalman a été initialisée avec une matrice de la forme :

$$P_{0/0} = \begin{pmatrix} \Gamma_0 & 0 \\ 0 & \sigma_0(s)^2 \end{pmatrix} \quad (37)$$

la matrice de variance conservera cette forme durant toute la phase précédant la première évolution du lanceur car la dérivée de la mesure par rapport à s est alors nulle (équation 22). Si la poursuite est doublement inobservable, la dérivée de l'équation de mesure par rapport à β ne sera nulle que si \dot{z} est nul. Dans ce cas, la qualité du découplage va dépendre de la qualité de l'estimation de \dot{z} .

Sur la figure 11 qui concerne la simulation TEST initialement doublement inobservable, on constate d'abord que ces coordonnées impliquent des valeurs du conditionnement beaucoup plus faibles que les cartésiennes. Durant la phase initiale, la sensibilité associée à s (2ème valeur propre) est égale à 1 du fait du découplage parfait de cette grandeur. Celle associée à β (3ème valeur propre) est aussi faible et se rapproche de 1 au fur et à mesure que la détermination de \dot{z} s'améliore. Lors de la première manœuvre de L, les termes de couplage qui apparaissent produisent une augmentation des sensibilités qui reste toutefois très limitée.

Expérimentalement, on constate une grande insensibilité de ce filtre aux erreurs numériques même en présence d'une implantation peu favorable. Il est cependant important de remarquer que cette insensibilité provient du fait que la plupart des scénarios comportent une *phase inobservable relativement longue* suivie par une évolution du lanceur permettant de lever assez rapidement l'inobservabilité. Cependant, pour une poursuite qui est l'inverse temporel de la simulation TEST, c'est-à-dire qui comporte une phase initiale très courte puis une faible manœuvre du lanceur suivie d'une longue phase rectiligne, la sensibilité aux erreurs numériques est importante.

• Coordonnées polaires modifiées évolutives

Pour ce type de coordonnées, le découplage n'est pas aussi net. En effet, même si la variance du filtre a été initialisée suivant la formule 37, l'expression de la jacobienne de l'équation d'évolution en l'absence de manœuvre du lanceur (équation 24) montre que des termes de couplage vont apparaître entre s et les autres variables.

Pour la simulation TEST (figure 12), ces couplages se traduisent par une évolution plus prononcée que le cas précédent des valeurs propres associées à s et β durant la phase inobservable. Ceci engendre des sensibilités différentes de 1 mais cependant très faibles. Comme les coordonnées polaires évolutives sont orientées suivant l'azimut prédit à un instant donné, il se produit, lors de la première manœuvre de L, un phénomène similaire à celui rencontré avec le filtre hybride (figure 7c). La rotation des coordonnées résultant de l'évolution du lanceur fait apparaître des valeurs momentanément importantes des sensibilités. Sur cette simulation, nous n'avons néanmoins pas observé des dégradations numériques visibles.

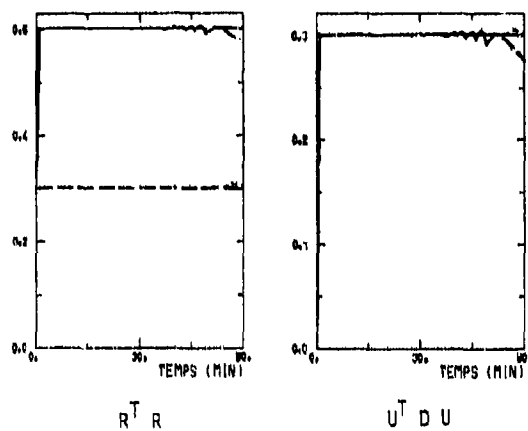
2.3 - Conclusion

Les erreurs numériques qui proviennent de la sensibilité de la représentation de la variance du filtre de Kalman peuvent être éliminées par l'utilisation de procédures factorisées.

Les différents systèmes de coordonnées de la TPA ont été analysés. La sensibilité de la variance des *coordonnées cartésiennes* rend indispensable l'emploi d'implantations stables numériquement. Les *coordonnées polaires modifiées fixes* sont au contraire très robustes pour la plupart des scénarios. Quant aux *coordonnées polaires modifiées évolutives*, elles constituent un intermédiaire entre les deux systèmes précédents.

Ainsi, tant du point de vue des erreurs de linéarisation que de la stabilité numérique, les coordonnées polaires modifiées fixes apparaissent les plus adaptées. Cependant le choix d'un système de coordonnées pour une poursuite réelle devra aussi prendre en compte d'autres considérations comme la sensibilité par rapport à des incertitudes non modélisées : nature du bruit de mesure, incertitudes sur les paramètres lanceur, perturbations sur l'évolution de la cible.

Matrices triangulaires supérieures



Matrices triangulaires inférieures

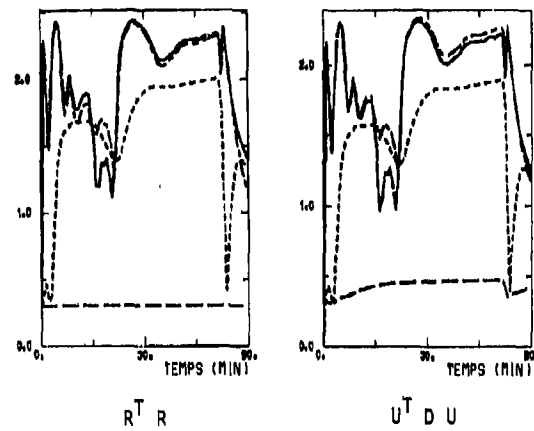


FIGURE 10 - Sensibilité des filtres cartésiens factorisés (Logarithme décimal)
Simulation TEST

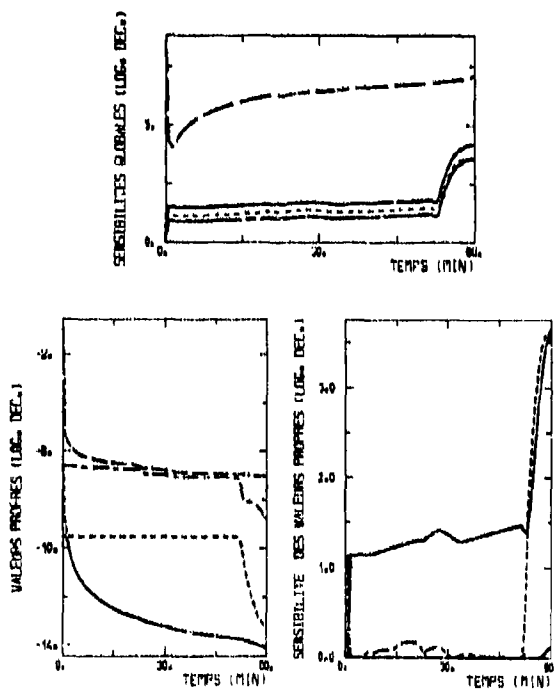


FIGURE 11 - Sensibilité des coordonnées polaires
modifiées fixes
Simulation TEST

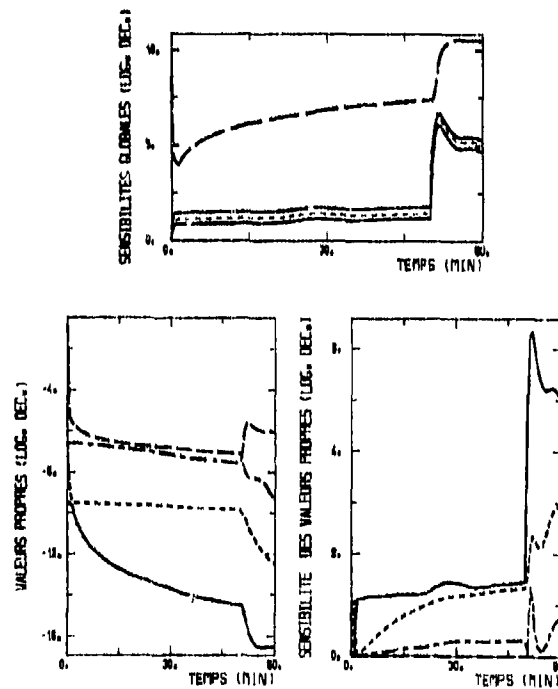


FIGURE 12 - Sensibilité des coordonnées polaires
modifiées évolutives.
Simulation TEST

3 - ESTIMATION PAR METHODE GLOBALE

L'utilisation d'une méthode globale se justifie tout d'abord par ses meilleures propriétés de linéarisation, notamment lors des phases très peu observables. En outre, elle autorise la prise en compte de la connaissance a priori du module de la vitesse de S qui permet parfois de lever l'inobservabilité avant la première manœuvre du lanceur.

L'algorithme utilisé dans ce paragraphe est la version récursive de l'algorithme de Gauss-Newton (Equations 15 et 16). Les résultats précédents inclinent à l'emploi des coordonnées polaires modifiées car elles sont plus appropriées aux aspects de non-linéarité et de faible observabilité de ce problème. L'option évolutive a été utilisée puisque le problème de l'évolution non linéaire de la variance ne se pose pas avec une méthode globale d'estimation.

Nous développerons deux points concernant le traitement des phases peu observables :

- L'adaptation de la méthode globale.

Du fait de la faible observabilité et des bruits de mesure, le minimum du critère quadratique 8 est souvent aberrant. Il s'agit donc d'éviter la convergence vers des états erronés sans pour autant bloquer l'estimation dès que réapparaît l'observabilité.

- La prise en compte de la connaissance de la vitesse de la cible.

Si l'information apportée améliore la qualité des résultats, elle entraîne souvent l'apparition de faux minimums qui perturbent la convergence même lors des phases observables.

3.1 - Adaptation aux phases peu observables

En décomposant le hessien approché (équation 10) en ses éléments propres, la correction ΔX (Equation 9) s'écrit :

$$\Delta X = \sum_{i=1}^n \left[\frac{v(i)^T G}{\lambda(i)} \right] v(i) \quad (38)$$

Suivant les directions peu observables ($\lambda(i)$ faible), la correction ΔX sera donc importante. Du fait de la non-linéarité du critère traité, on peut aboutir en un point où la valeur de J est supérieure à celle du point de départ. En outre, de part l'effet combiné de la faible observabilité et des bruits de mesure, l'état réalisant le minimum de J(X) peut n'avoir aucune signification physique.

Pour maîtriser la convergence de l'algorithme durant ces phases peu observables, on peut agir soit sur le gradient G, soit sur le hessien approché W. Pour le filtre de Kalman, la divergence durant ces phases est évitée par la connaissance a priori sur l'état et la variance ($X_0/y_0, P_0/y_0$). Ceci est équivalent à modifier à la fois G et W dans la méthode globale. Toutefois les variations sur les paramètres estimés par cette méthode sont plus rapides à cause de la relinéarisation de l'ensemble des mesures. Cette connaissance initiale sur X et P devrait être alors plus serrée et pourrait altérer la convergence lors des phases observables. En outre, l'action sur G qui, par analogie, peut être pensée comme une "force de rappel" à un état initial fixé pose des problèmes de convergence si cet état est inexact, notamment lorsqu'on tient compte de la connaissance sur la vitesse de S. L'action sur W que nous avons utilisée limite la taille des corrections ΔX .

L'idée de base de la méthode développée est d'ajouter une information complémentaire fictive sur les composantes mal déterminées de l'état afin de limiter les variations de l'estimation. Pour que cette information n'altère pas la précision des résultats si la poursuite devient observable, elle est adaptée à chaque instant en fonction de l'information contenue dans les mesures.

L'algorithme se présente donc de la façon suivante. A partir du hessien W, on détermine l'information réduite¹ w_i sur chaque composante x_i de X et le complément d'information α_i est fixé par :

$$\alpha_i = \begin{cases} e_i - w_i & \text{si } w_i < e_i \\ 0 & \text{sinon} \end{cases} \quad (39)$$

où e_i est un seuil d'information minimale sur la composante x_i . On utilise l'algorithme de Gauss-Newton avec le hessien complété $W_c = W + C$ où $C = \text{diag}(\alpha_i)$. Le calcul des informations w_i est rapide si on utilise une décomposition de Cholesky de W. De plus, pour la TPA, il suffit de considérer les deux variables les moins observables s et p.

Cette méthode agit comme une relaxation adaptée durant les phases peu observables. Si, par contre l'information sur les mesures est suffisante, la convergence n'est pas affectée puisque $C = 0$.

3.2 - Utilisation de la connaissance de la vitesse de la cible

Pour tenir compte de cette connaissance, on minimise le critère

$$J_v(X) = J(X) + \frac{[V_s - V(X)]^2}{2\sigma_{V_s}} \quad (40)$$

Les faux minimums que l'on rencontre parfois (figure 13) proviennent de l'association des mesures de la phase initiale avec cette connaissance de V_s pour laquelle deux solutions sont possibles, c'est-à-dire deux minimums de même valeur pour $J_v(X)$. Ce phénomène peut se poursuivre en phase observable car les mesures postérieures à la première manœuvre de L sont alors inefficaces à effacer la fausse solution. Il existe deux situations où se manifestent ces problèmes de convergence :

- Phase initiale doublement inobservable ($\dot{z} = 0$)

La composition des vitesses $\vec{V}_R = \vec{V}_S - \vec{V}_L$ (figure 14), montre que, dans ce cas où \vec{V}_R est colinéaire à z, il existe deux solutions de module identique pour le vecteur \vec{V}_S . Les deux cas possibles sont alors symétriques par rapport à l'orthogonal de l'azimut. Pour cette situation V_s n'apporte alors aucune information sur la distance.

¹ L'information réduite sera présentée dans le paragraphe 4.2 et est égale à l'inverse de la variance de la composante x_i si le hessien W n'est pas singulier.

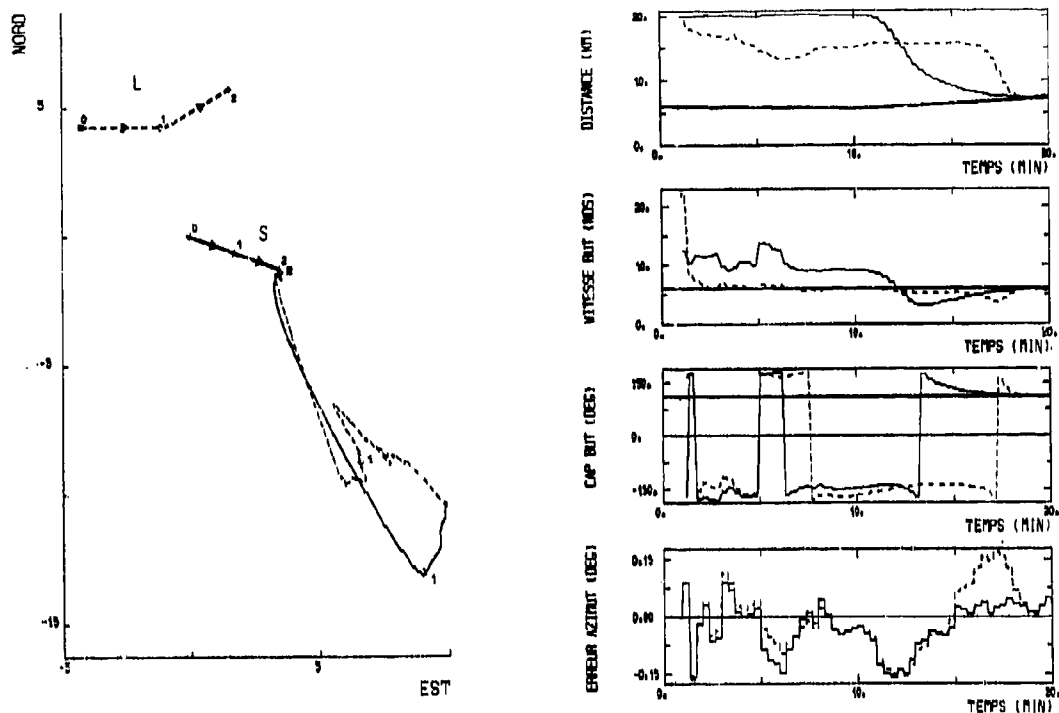


FIGURE 13 - Illustration de l'apparition de faux minimums

— Sans connaissance a priori de V_S
 - - - Avec connaissance a priori de V_S

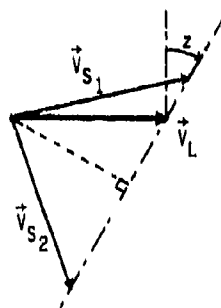


FIGURE 14 - Composition des vitesses ($\dot{z} = 0$)

• Vitesse lanceur supérieure à vitesse cible ($\dot{z} \neq 0$ et $V_L > V_S$)

Dans ce cas (figure 15a) deux couples de valeurs sont possibles pour la distance et le cap. Pour ce dernier, les deux solutions sont symétriques par rapport à l'orthogonal du cap relatif (C_r). La simulation de la figure 13 correspond à une telle situation. Si $V_L < V_S$, les deux solutions pour le cap et la distance existent aussi mais l'une d'elle comporte une distance négative (figure 15b).

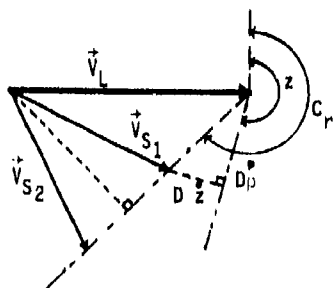


FIGURE 15a - Composition des vitesses ($\dot{z} = 0$ et $V_L > V_B$)

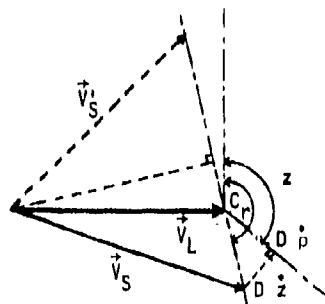


FIGURE 15b - Composition des vitesses ($\dot{z} = 0$ et $V_L < V_B$)

Outre le fait de garantir la cohérence des résultats en phase peu observable, la méthode d'estimation présentée dans le paragraphe précédent fournit les niveaux d'observabilité des variables p et s qui sont utilisés pour détecter l'apparition de ces deux situations.

Ces faux minimums impliquent aussi l'existence de courbures négatives pour J_V qui rendent la minimisation plus difficile et justifient l'emploi d'une méthode globale dans le but, par exemple, de relinéariser les équations après la convergence vers une solution erronée.

Une fois les précautions prises pour se prémunir de ces minimums multiples, la connaissance a priori sur V_S permet, dans tous les cas, d'améliorer la précision et la robustesse des résultats et parfois de lever l'inobservabilité avant la première manœuvre du lanceur.

3.3 - Conclusion

Dans cette première partie, ont été présentés et analysés divers algorithmes d'estimation.

Ainsi les coordonnées polaires modifiées semblent très adaptées à ce problème de poursuite tant au niveau des problèmes de linéarisation que de la sensibilité numérique. Pour la procédure d'estimation, une méthode globale ne se justifie que pour des situations très peu observables ou pour tenir compte d'une information a priori sur la vitesse de la cible.

Cependant certaines hypothèses simplificatrices ont été formulées de façon à cerner les difficultés propres à ce problème et à évaluer les possibilités des algorithmes d'estimation. En particulier, nous avons supposé la trajectoire de la cible parfaitement rectiligne ce qui n'est jamais le cas en réalité. Il est donc nécessaire de tenir compte de perturbations sur l'évolution de S . L'introduction d'un bruit d'évolution dans le filtre de Kalman permet aussi de rendre l'algorithme moins sensible aux problèmes de linéarisation et d'erreurs numériques. Toutefois, il conviendra de sélectionner attentivement la nature de ce bruit afin de ne pas perdre la partie utile de l'information contenue dans les mesures.

La prise en compte de perturbations sur l'évolution de S est, à première vue, plus difficile pour certains algorithmes tel le filtre de Kalman en polaires modifiées fixes ou les méthodes globales. Le filtre de Kalman en coordonnées cartésiennes semble, par contre le plus adapté à l'introduction d'un bruit d'évolution. En fait l'alternance des diverses méthodes est souhaitable. L'algorithme de poursuite peut donc comporter plusieurs étapes comme, par exemple, un filtre de Kalman en polaires modifiées fixes ou une méthode globale avec prise en compte de V_S pour les phases peu observables qui commute sur un filtre cartésien avec bruit d'évolution lorsque le niveau d'observabilité est suffisant.

Les caractéristiques de ce bruit, sa variance en particulier, sont inconnues. Ils peuvent être estimés, par exemple, par une technique bayésienne qui consiste à quantifier l'ensemble des valeurs possibles et à mettre à jour, pour chaque hypothèse, une probabilité a posteriori. Une idée originale développée dans [25,26] consiste à utiliser un indice d'observabilité au lieu des probabilités a posteriori pour pondérer les différentes hypothèses. Cette méthode appliquée à la TPA donne de meilleurs résultats.

L'évolution de la cible comporte aussi des manœuvres franches et l'algorithme devra donc comporter une procédure de détection et de traitement de ces évolutions.

Au cours de la phase peu observable, certains paramètres peuvent être déterminés, z , \dot{z} et souvent p . A partir de ces trois grandeurs, on peut, moyennant une paramétrisation de la distance, calculer la valeur du cap et de la vitesse de la cible. Cette technique développée au CAPCA [8] permet d'exploiter l'information sur la cible avant que la poursuite ne soit observable. La superposition des résultats associés à deux segments rectilignes de la trajectoire du lanceur permet aussi la détermination des éléments de S .

L'optimisation de la trajectoire du lanceur permet, outre l'amélioration apportée à la qualité de l'estimation, de rendre l'algorithme plus robuste aux particularités difficilement modélisables de la poursuite réelle.

2ème PARTIE - OPTIMISATION DE LA TRAJECTOIRE DU LANCEUR

4 - CALCUL D'UN INDICE SCALAIRE D'OBSERVABILITE

La détermination d'un indice d'observabilité représentatif de la précision de l'estimation est une étape indispensable pour l'optimisation de la trajectoire du lanceur. Cependant tels qu'ils furent initialement introduits dans la théorie des systèmes dynamiques, les concepts d'observabilité et de gouvernabilité ne fournissent qu'une réponse binaire, à savoir le système est ou n'est pas observable.

Pour le calcul de cet indice, nous nous placerons dans le cadre général des systèmes linéaires variants discrets. Pour les systèmes non linéaires, on supposera que les critères calculés par linéarisation autour d'une bonne trajectoire (trajectoire estimée) fournissent des mesures acceptables du niveau d'observabilité.

Un indice d'observabilité qualifie intuitivement la façon dont peut être reconstitué l'état à partir de l'observation des mesures $Z_N = \{z_1, \dots, z_N\}$. Le gramien d'observabilité est souvent utilisé comme grandeur de départ pour le calcul de cet indice. Son expression est donnée par

$$W(t_r, N) = \sum_{i=1}^N \Phi(t_i, t_r) H_i^T R_i^{-1} H_i \Phi(t_i, t_r) \quad (41)$$

où Φ est la matrice de transition du système et t_r un temps de référence.

Si l'on envisage l'estimation de l'état $X(t_r)$ à l'instant t_r par la minimisation du critère $J(X)$ sur les mesures (équation 8), on montre alors que, pour un système linéaire,

$$J(X) = J(\hat{X}) + (X - \hat{X})^T W(t_r, N) (X - \hat{X}) \quad (42)$$

Ainsi la matrice W reflète la forme du critère J autour du minimum \hat{X} . Si W est "grande" dans toutes les directions de l'espace, $J(X)$ sera alors très creusé et la détermination de X sera moins sensible à d'éventuelles perturbations. Si, par contre, il existe une direction où W est faible, l'état sera mal déterminé suivant cet axe.

Dans le cadre d'une interprétation stochastique, la variance P_N d'un filtre de Kalman sans bruit d'évolution est donnée par

$$P_N^{-1} = \left[\phi(t_N, t_0) P_0 \phi^T(t_N, t_0) \right]^{-1} + W(t_N, N) \quad (43)$$

Pour le cas général où le système comporte un bruit d'évolution, la variance de ce filtre vérifie les inégalités ([14])

$$(W + V^{-1})^{-1} \leq P_N \leq W + V \quad (44)$$

où V est le gramien de gouvernabilité associé au bruit d'évolution. Enfin l'inverse de W calculé par linéarisation d'un système non linéaire à évolution déterministe (équation 10), est la borne de Cramer-Rao. W est égal, dans ce cas, à la matrice d'information de Fisher.

Plusieurs étapes interviennent dans le calcul d'un indice d'observabilité sur W .

4.1 - Choix du temps de référence

La valeur de t_r n'a pas d'importance pour l'étude "binaire" de l'observabilité. En effet, nous avons la correspondance:

$$W(t_r, N) = \phi^T(t_r, t_2) W(t_r, N) \phi(t_r, t_2) \quad (45)$$

Puisque ϕ est toujours inversible, les propriétés de singularité du gramien sont indépendantes du temps de référence. Par contre, pour la définition d'un indice de qualité, il importe de choisir une valeur adaptée. Le choix naturel pour t_r est l'instant de calcul de l'état qui est en général égal, pour les problèmes d'estimation, à l'instant de la dernière mesure prise en compte.

4.2 - Calcul d'une information réduite

Pour certains problèmes, toutes les composantes de l'état ne présentent pas le même intérêt. En effet, des termes peuvent avoir été introduits pour tenir compte de phénomènes physiques (la coloration des bruits par exemple). Dans les problèmes de poursuite, on utilise des modèles d'évolution du 1er ou du 2ème ordre, mais en définitive, seule la position de la cible à l'instant t_r importe peut-être à l'utilisateur.

Si $X = \begin{bmatrix} X_1 \\ X_2 \end{bmatrix}$ représente une partition de l'état où X_1 sont les composantes d'intérêt, le gramien W peut se décomposer sous la forme correspondante de matrices bloc :

$$W = \begin{bmatrix} W_{11} & W_{12} \\ W_{12}^T & W_{22} \end{bmatrix} \quad (46)$$

Pour représenter la qualité de l'estimation de X_1 , on pourrait considérer la matrice W_{11} appelée *sensibilité en X_1* [17,18]. D'un point de vue probabiliste W_{11}^{-1} représente la variance de l'erreur sur X_1 conditionnée par l'événement $X_2 = \hat{X}_2$. Pour un exemple de dimension 2 (figure 16), la grandeur $I_1 = 1/\sqrt{W_{11}}$ représente la variation possible de X_1 dans l'ellipsoïde à 1 sigma en supposant $X_2 = \hat{X}_2$.

Pour obtenir une bonne estimation, il est donc désirable d'avoir une sensibilité importante. Cependant cette matrice ne tient pas compte des corrélations entre X_1 et X_2 . A la limite, comme nous le verrons pour la TPA, les sensibilités en X_1 et X_2 peuvent être non singulières alors que W est singulière et l'état X inobservable. En d'autres termes, *une grande sensibilité est une condition nécessaire mais non suffisante pour obtenir une estimation précise.*

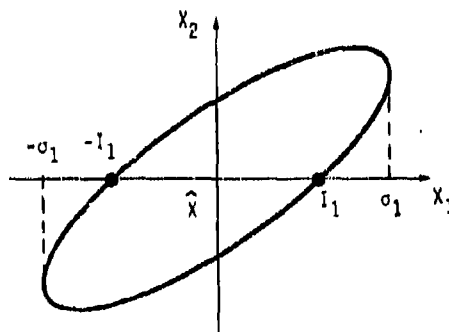


FIGURE 16 - Illustration de la sensibilité et de l'information réduite

Afin de tenir compte du couplage entre X_1 et X_2 , il faut considérer l'information réduite en X_1 :

$$\tilde{W}_{11} = W_{11} - W_{12} W_{22}^{\#} W_{12}^T \quad (47)$$

où $W_{22}^{\#}$ est la pseudo-inverse de W_{22} .

En l'absence de singularité, W_{11} est l'inverse de la variance non conditionnée sur X_1 . Pour l'exemple de dimension 2 (figure 16), la grandeur $S_1 = 1/\sqrt{W_{11}}$ représente l'erreur à 1 sigma sur X_1 en autorisant l'ensemble des composantes de X à parcourir l'ellipsoïde d'incertitude.

Au niveau des singularités de W , la matrice W_{11} ne reflète pas celles qui sont propres à W_{22} , c'est-à-dire les vecteurs du noyau de W de la forme $\begin{pmatrix} 0 \\ v \end{pmatrix}$. Par contre, les autres singularités notamment celles provenant du couplage entre X_1 et X_2 seront transmises à W_{11} . Si $\begin{pmatrix} u \\ v \end{pmatrix}$ est la partition d'un vecteur du noyau de W avec $u \neq 0$, ce vecteur u est alors élément du noyau de W_{11} .

Ainsi, par rapport à la sensibilité W_{11} , les couplages entre X_1 et X_2 apportent toujours une dégradation et peuvent être responsables de la singularité de l'information réduite W_{11} .

Lorsque les grandeurs d'intérêt T sont une fonction vectorielle linéaire $T = G X$ de l'état, on peut calculer, par une procédure de même type, une information réduite W_T sur le vecteur T . Si la relation entre T et X est non linéaire, l'information W_T peut être calculée par linéarisation. Dans le cas où la matrice W n'est pas singulière, ces diverses grandeurs sont obtenues facilement à partir de l'inverse $P = W^{-1}$.

4.3 - Normalisation du gramien

La matrice d'information W concerne souvent des grandeurs de nature et donc d'unité différentes. Si nous choisissons un critère scalaire $\rho(W)$, celui-ci sera dépendant des unités utilisées pour chaque composante de l'état. Pour la plupart des indices, un changement d'unité va engendrer des pondérations différentes sur chaque terme de W et va conduire à des résultats d'optimisation différents.

Il importe donc de normaliser cette matrice de façon à la rendre adimensionnelle et à obtenir un critère $\rho(W)$ intrinsèque au problème traité. A cette fin, on pré et post-multiplie W par une matrice diagonale positive :

$$W_N = U W U \quad (48)$$

Dans [30], les auteurs proposent de considérer les *erreurs maximales* (e_i) que l'on veut tolérer sur chaque composante de l'état lors de l'estimation ($U = \text{diag}(e_i)$). Ainsi plus on désirera obtenir une erreur faible sur un paramètre, plus l'information associée devra être importante et vice-versa. Par ce principe, on se définit une *échelle d'équivalence* des erreurs d'estimation entre les différentes grandeurs. Par exemple si le vecteur d'état comporte des composantes de position et de vitesse, on peut choisir les pondérations traduisant le fait qu'une erreur de 1 km en position est équivalente à une erreur de 1 n/s.

On peut par exemple choisir U de façon à traduire des erreurs relatives identiques sur les composantes ($U = \text{diag} |X_i|$) ou à analyser leurs corrélations ($U = \text{diag} (1/\sqrt{W_{ii}})$).

4.4 - Indice scalaire sur le gramien normalisé

Dans la littérature [19,20] on trouve de nombreux candidats :

- $\lambda_{\min}(W)$ qui représente la quantité d'information dans la direction la moins observable
- $1/\text{tr}(W^{-1})$ qui est égal à l'inverse de la variance de l'erreur
- $\sqrt{\det(W)}$ qui est inversement proportionnel au volume de l'ellipsoïde d'incertitude
- $\text{tr}(W)$ qui traduit la sensibilité des sorties par rapport à l'état
- $c(W) = \lambda_{\max}/\lambda_{\min}$ le conditionnement qui reflète la disparité de l'information.

On rencontre aussi d'autres indices plus spécifiques d'un problème traité [25,30].

Si ρ est un indice d'observabilité sur l'ensemble des matrices symétriques positives, les propriétés souhaitables pour cet indice sont :

- (a) $\forall W, \rho(W) \geq 0$ et $\rho(W) = 0$ si et seulement si W est inobservable ($\det W = 0$)
- (b) $\rho(I) = 1$ (I : identité) et $\forall \lambda \in \mathbb{R}^+, \rho(\lambda W) = \lambda \rho(W)$
- (c) $\forall W_1$ et $W_2, \rho(W_1 + W_2) \geq \rho(W_1) + \rho(W_2)$
- (d) ρ est indépendant du repère orthonormé choisi sur \mathbb{R}^n .

La propriété (a) est indispensable pour que ρ constitue le prolongement de la notion binaire d'observabilité.

La propriété (b) définit une normalisation des indices ρ et elle permet ainsi la comparaison de plusieurs critères. Au niveau des unités, ρ est alors homogène à l'inverse d'une variance.

(c) est l'inverse de l'inégalité triangulaire que l'on rencontre habituellement dans la définition mathématique d'une mesure. La TPA fournit une illustration typique de cette propriété. En effet, si W_1, W_2 représente les matrices d'information associées à deux phases rectilignes de la trajectoire du lanceur, la poursuite étant inobservable pour chaque phase, nous avons $\rho(W_1) = \rho(W_2) = 0$. Par contre, l'information totale $W = W_1 + W_2$ ne sera pas singulière ($\rho(W) \neq 0$) si une manœuvre judicieuse est intervenue entre ces deux phases. Cette propriété peut aussi se justifier par une partition du vecteur de mesure si sa dimension est supérieure à 1.

La propriété (d) traduit le fait que la mesure d'observabilité est intrinsèque au système considéré du fait de la normalisation du paragraphe précédent.

Par les propriétés 49, l'indice ρ se distingue d'une norme matricielle. En fait, une norme mesure la *taille* d'une matrice alors qu'un indice d'observabilité est une mesure de sa *petitesse*. Dans [20], les auteurs montrent que des indices peuvent être calculés par la formulation :

$$\rho_s(W) = \left[\frac{\sum_{i=1}^n \lambda_i^s}{n} \right]^{1/s} = \left[\frac{\text{tr}(W^s)}{n} \right]^{1/s} \quad (50)$$

Pour différentes valeurs s , on trouve les critères suivants ([18], [37]) :

$s \rightarrow -\infty$	$\lambda_{\min}(W)$
$s = -1$	$n/\text{tr}(W^{-1})$
$s = 0$	$\sqrt[n]{\det(W)}$
$s = 1$	$\text{tr}(W)/n$
$s \rightarrow +\infty$	$\lambda_{\max}(W)$

Cependant [3], seuls les indices calculés pour $s \leq 0$ vérifient les propriétés 49 et sont donc acceptables comme indice d'observabilité. Leur évolution toujours croissante en fonction de s est illustrée par la figure 17.

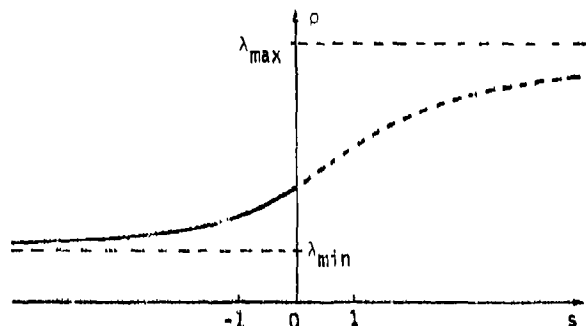


FIGURE 17 - Evolution de $\rho_s(W)$ en fonction de s

Pour les deux indices extrêmes :

- $\rho_{-\infty}(W) = \lambda_{\min}(W)$ est une *marge d'observabilité*
- $\rho_0(W) = \sqrt[n]{\det W}$ reflète la *quantité totale d'information* contenue dans les mesures

Les autres valeurs de s constituent donc des intermédiaires et le conditionnement traduit la disparité de la répartition de l'information et donc des valeurs de ces indices. Notons aussi que la maximisation de λ_{\min} favorise à la fois la décroissance du conditionnement et l'augmentation de la quantité d'information alors que l'optimisation du déterminant n'assure pas l'amélioration du conditionnement.

4.5 - Conclusion

La nature du problème traité guidera la sélection d'un indice adapté. Cependant, pour l'optimisation de l'observabilité, les contraintes du problème peuvent limiter les actions possibles et la solution obtenue être ainsi peu sensible à l'indice retenu.

En ce qui concerne la TPA, l'analyse des matrices d'information du prochain paragraphe permettra de justifier en partie l'indice choisi pour l'optimisation de la trajectoire du lanceur.

5 - ANALYSE DES MATRICES D'INFORMATION DE LA TPA

Nous allons étudier, dans cette section, le comportement de l'information totale et de l'information réduite en position de la TPA pour le cas d'une formulation en coordonnées cartésiennes.

Dans le paragraphe 1, ces coordonnées étaient apparues moins adaptées aux non linéarités de ce problème. Cependant, la matrice d'information calculée par relinéarisation de l'ensemble des mesures se révèle moins sensible au choix du système de coordonnées lorsque le niveau d'observabilité augmente. D'autre part, l'étude des équations en coordonnées cartésiennes permet une analyse théorique plus facile des trajectoires favorables.

La matrice d'information totale $W(t_r, N)$ peut se décomposer sous la forme :

$$W(t_r, N) = \begin{bmatrix} A(N) & B(t_r, N) \\ B^T(t_r, N) & C(t_r, N) \end{bmatrix} \quad (51)$$

où les matrices A et C sont les sensibilités en position et en vitesse et la matrice B , qui est ici symétrique, traduit le couplage position-vitesse. Comme les termes de ces matrices ne dépendent que des séquences t_i, z_i, D_i , l'observabilité de la poursuite sera entièrement déterminée par la trajectoire relative du lanceur dans le repère lié à la cible.

La matrice d'information réduite en position a donc pour expression :

$$W_p(t_r, N) = A - B C^{-1} B^T \quad (52)$$

Puisque nous sommes concernés par l'observabilité de l'état à l'instant t_N de la dernière mesure, le temps de référence évolue en même temps que N ($t_r = t_N$). Il est donc intéressant d'examiner la dépendance des matrices W et W_p par rapport à ces deux

paramètres. Cette trajectographie est, d'autre part, caractérisée par une faible observabilité même parfois pour des configurations où la variation de l'azimut est grande. L'analyse de cette particularité nous permettra de dégager des principes pour des manoeuvres du lanceur favorables à la qualité de l'estimation.

5.1 - Evolution temporelle de l'information

A chaque nouvelle mesure, l'évolution des matrices W et W_p est dépendante de l'apport d'information de cette mesure mais aussi du changement du temps de référence passant de t_{N-1} à t_N .

A t_r fixé, l'évolution de W se réalise suivant l'équation :

$$W(t_r, N) = W(t_r, N-1) + H^T H \quad (53)$$

où H est la linéarisation en t_r de l'équation de mesure. Ainsi $W(t_r, N)$ est croissante avec N , c'est-à-dire la différence $W(t_r, N) - W(t_r, N-1)$ est une matrice positive. Pour $W_p(t_r, N)$, on montre aussi que, à t_r fixé, le traitement d'une nouvelle mesure se traduit par la croissance de cette matrice.

Si nous supposons N fixé, l'évolution de l'information par rapport à t_r est régie par l'équation 45. Pour un modèle d'évolution à vitesse constante, certaines caractéristiques de W se révèlent indépendantes de t_r :

- la sensibilité en position A
- le déterminant de W
- l'information réduite en vitesse W_v .

Par contre, l'information réduite en position W_p et la sensibilité en vitesse C sont dépendantes de t_r . Dans le cas particulier analysé dans le paragraphe 5.3 où $B(t_r, N) = 0$, nous avons les inégalités :

$$W_p(t_{r2}, N) \leq W_p(t_{r1}, N) \quad \text{et} \quad C(t_{r2}, N) \geq C(t_{r1}, N) \quad (54)$$

L'illustration de ce dernier cas par un exemple de dimension 1 (figure 18) montre que l'ellipsoïde d'incertitude dont le volume reste constant s'étire suivant l'axe position lorsque t_{r2} s'éloigne de t_{r1} . Le changement du temps de référence entraîne donc une redistribution de la même quantité d'information suivant des directions différentes et se traduit, pour cette situation, par une diminution de l'information W_p en position.

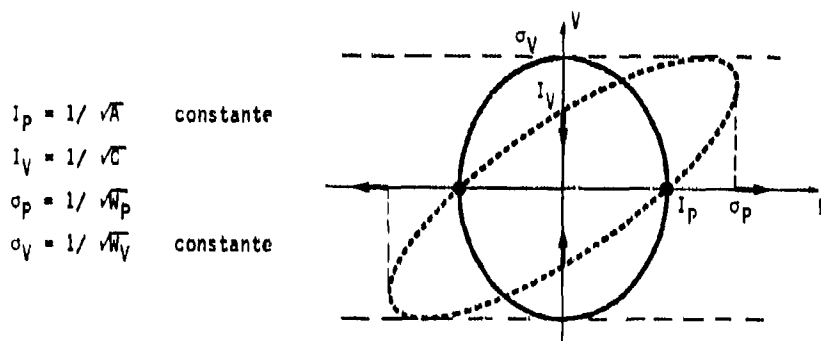


FIGURE 18 - Evolution des informations et des sensibilités en fonction de t_r

Pour la TPA, les résultats sont plus complexes car la matrice W_p peut croître suivant une direction et décroître suivant la direction orthogonale. Cependant, cette réflexion montre intuitivement la façon dont évoluent les diverses grandeurs et expliquent pourquoi la qualité de l'estimation de la position se détériore parfois au cours de la poursuite. Dans ce cas, en effet, l'information apportée par les mesures est insuffisante à compenser la dégradation résultant de l'évolution du temps de référence. Cette analyse peut aussi se généraliser à tout système à évolution à vitesse constante ou accélération constante.

5.2 - Analyse de la matrice d'information totale

Dans ce paragraphe, la sensibilité en position A et la matrice de couplage B vont être brièvement étudiées. Nous examinerons aussi comment se manifeste l'observabilité de la poursuite au niveau de la matrice W .

* Etude de composantes de la matrice d'information

La matrice de sensibilité en position A constitue une sorte "d'idéal" pour la matrice W_p puisque, d'après le paragraphe 4.2, elle représenterait l'information en position si la vitesse de la cible était parfaitement connue. Cette matrice est singulière si et seulement si les azimuts sont constants. Ses éléments propres se calculent facilement. D'après la dépendance en $1/D_i^2$ des valeurs propres, de faibles distances d'observation sont favorables à l'amélioration de A . Cependant la répartition des valeurs propres, notamment le conditionnement de A dépendra de la séquence des mesures. Pour étudier ce lien, deux scénarios théoriques qui comportent une distance d'observation et une période d'échantillonnage constantes, ont été analysés.

Pour le premier exemple, nous supposons une variation uniforme des azimuts $z_i = \omega t_i + z_0$. La figure 19a illustre un exemple de trajectoire. Les valeurs propres de A sont alors égales à

$$\lambda = \frac{N}{2D^2} \left(1 \pm \frac{\sin \Delta z}{\Delta z} \right) \quad (55)$$

où Δz est l'écart total en azimut soit $\Delta z = z_N - z_0$. Dans cette équation, le second terme traduit la répartition des valeurs propres. Son évolution en fonction de Δz est tracé sur la figure 20a.

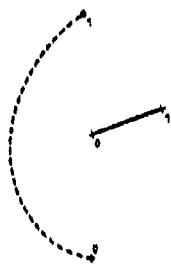
Lorsque N et D sont fixés, il existe une séquence théorique des mesures qui donne de plus faibles valeurs du conditionnement pour $\Delta z \leq 90^\circ$. Elle consiste à répartir les azimuts en deux groupes autour d'une valeur moyenne z soit :

$$\begin{aligned} \text{Pour } i \leq \frac{N}{2} \quad z_i &= \bar{z} - \frac{\Delta z}{2} \\ \text{Pour } i > \frac{N}{2} \quad z_i &= \bar{z} + \frac{\Delta z}{2} \end{aligned} \quad (56)$$

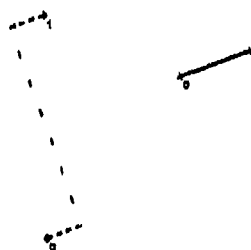
Pour cette séquence qui constitue notre deuxième exemple, illustré par la figure 19b, la répartition des valeurs propres est donnée par

$$1 \pm \cos \Delta z \quad (57)$$

Celle-ci permet un gain d'un facteur 3 à 4,5 sur le conditionnement (figure 20b). Si ce scénario est irréaliste, il montre que, pour améliorer le conditionnement de A lorsque $\Delta z \leq 90^\circ$, les mesures doivent être réparties aux points extrêmes de la trajectoire.



(a) Exemple 1



(b) Exemple 2

FIGURE 19 - Illustration des scénarios théoriques

Concernant le couplage $B(t_r, N)$, il s'agit, afin d'augmenter l'information réduite en position ou en vitesse, de diminuer voire d'annuler la valeur de B . L'examen des termes de cette matrice révèle que trois égalités doivent être vérifiées pour avoir $B = 0$, notamment :

$$\left[\sum_{i=0}^N \frac{1}{D_i^2} \right] t_r = \sum_{i=0}^N \frac{t_i}{D_i^2} \quad (58)$$

On en déduit $t_0 \leq t_r \leq t_N$. Si la période d'échantillonnage et la distance sont constantes, cette égalité implique que $t_r = (t_0 + t_N)/2$. Ainsi un couplage strictement nul ne pourra être obtenu pour $t_r = t_N$.

Lorsque les mesures ne sont pas constantes, les sensibilités A et C ne sont pas singulières. Cependant, lorsque les deux navires suivent une trajectoire rectiligne, il est théoriquement possible d'obtenir une variation d'azimut $\Delta z = 180^\circ$ sans faire apparaître l'observabilité. Dans ce cas, la singularité ne peut provenir que du couplage B .

* Etude de la singularité de la matrice d'information

On peut caractériser la direction inobservable de W par ses projections $u = \begin{bmatrix} \sin \alpha \\ \cos \alpha \end{bmatrix}$ et $v = \begin{bmatrix} \sin \beta \\ \cos \beta \end{bmatrix}$ sur les plans position et vitesse. En recherchant à quelle condition la restriction de W au plan (u, v) est singulière, on montre que W sera inobservable si

$$\exists \gamma \quad \forall i \quad \sin(z_i - \alpha) = \gamma(t_i - t_r) \sin(z_i - \beta) \quad (59)$$

Si le lanceur et la cible suivent des trajectoires rectilignes, cette expression nous permet de retrouver les directions inobservables en position et en vitesse établies en introduction (figure 2) à savoir

$$\alpha = z(t_r) \quad \beta = z(t_r) + \text{Arctg} \left[\frac{\dot{z}(t_r)}{\rho(t_r)} \right] \quad (60)$$

Ainsi les termes de couplage qui dégradent toujours l'information réduite par rapport à la sensibilité, sont, pour cette situation, responsables de la singularité de W .

5.3 - Etude de la matrice d'information réduite en position

L'étude de la trace de cette matrice montrera l'existence d'une valeur optimale pour W_p . Des trajectoires du lanceur qui permettent la diminution des effets du couplage et de tendre vers la valeur optimale de W_p seront ensuite étudiées.

* Valeur optimale de W_p

Contrairement aux matrices A , B et C , la trace de W_p est liée à la séquence des mesures z_i . Cependant, en supposant C inversible, on montre l'inégalité :

$$\text{tr}(W_p) \leq T_{r_{\max}} = \text{tr}(A) \cdot \frac{[\text{tr}(B)]^2}{\text{tr}(C)} \quad (61)$$

L'égalité a lieu si et seulement si $B = 0$, ou B et C sont diagonalisables dans une même base et possèdent le même conditionnement. La borne supérieure $T_{r_{\max}}$ est, bien entendu, indépendante des azimuts.

Une inégalité similaire peut être établie pour l'information réduite en vitesse W_v . Ces deux inégalités sont révélatrices de la dégradation causée par les couplages. Une situation idéale serait une séquence de mesures assurant la valeur maximale pour les traces de W_p et W_v . Dans ce cas on montre l'équivalence.

$$[\text{tr}(W_p) \text{ et } \text{tr}(W_v) \text{ maximales}] \Leftrightarrow [W_p = \rho A \text{ avec } \rho = \frac{T_{r_{\max}}}{\text{tr}(A)}] \quad (62)$$

La matrice ρA est donc la valeur optimale de W_p . La répartition optimale des valeurs propres de W_p est celle de la sensibilité en position. Le coefficient ρ vérifie $0 \leq \rho \leq 1$ et ne dépend que de N , t_r et $(D_i)_{i \in [1, N]}$. Il traduit une *dégradation inévitable due aux corrélations position-vitesse* qui, dans le cas optimal, est uniforme sur toutes les directions de l'espace.

Pour $t_r = t_N$, et D et Δt constantes, nous obtenons la valeur $\rho = 1/4$. Pour cette situation qui correspond aux deux exemples du paragraphe 5.2, la valeur optimale de W_p est $A/4$. Si la distance évolue de façon linéaire avec le temps, la figure 21 qui représente la valeur de ρ en fonction du rapport $D(t_N)/D(t_0)$, montre qu'une distance décroissante est favorable car elle entraîne l'augmentation de ρ mais aussi de la trace de A .

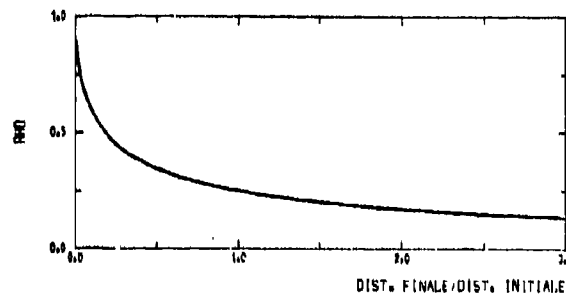


FIGURE 21

* Trajectoires favorables au découplage

Les figures 20c et 20d représentent, pour les deux exemples du paragraphe 5.2, la répartition en fonction de Δz des valeurs propres de $W_p(t_N, N)$ normalisées afin que la valeur maximale de leur demi-trace soit égale à 1. Dans ces deux cas, on constate une dégradation importante de la trace et du conditionnement par rapport à la matrice de la sensibilité. Notamment, sur le premier exemple, la plus petite valeur propre de W_p reste très faible pour des valeurs Δz importantes.

Puisque l'équation 58 interdit l'annulation des couplages qui sont à l'origine de ces dégradations, nous allons étudier les trajectoires annulant B au temps intermédiaire $\theta = (t_0 + t_N)/2$. Dans le cas général une solution consiste à rejouer à l'envers le même scénario (dans le repère lié à S) à partir de l'instant θ . Ceci se traduit par les équations

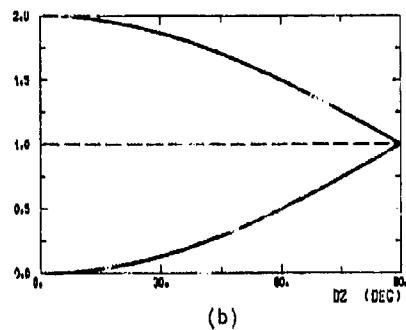
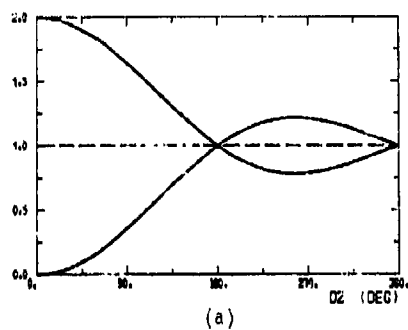
$$\forall i \in [1, N/2] \quad \begin{cases} t_{N-i} - \theta = \theta - t_i \\ z_{N-i} = z_i \\ D_{N-i} = D_i \end{cases} \quad (63)$$

La figure 22 illustre de telles trajectoires construites à partir des deux exemples étudiés. La répartition des valeurs propres de $W_p(t_N, N)$ correspondantes (figures 20c et f) confirme la nette amélioration apportée par cette stratégie au niveau de la trace et du conditionnement de W_p . Pour le premier exemple, le conditionnement passe en effet de 10^4 à 39 pour $\Delta z = 45^\circ$. Pour le deuxième exemple, l'amélioration porte surtout sur la trace de W_p .

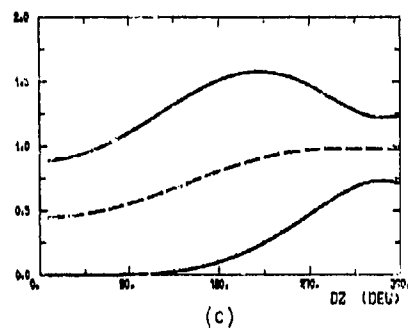


FIGURE 22 - Trajectoires favorables au découplage position vitesse

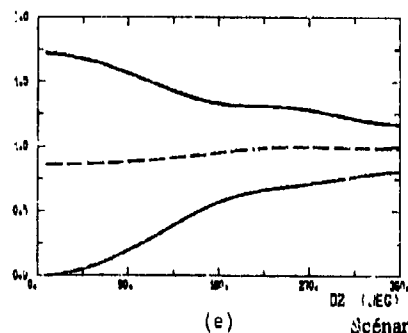
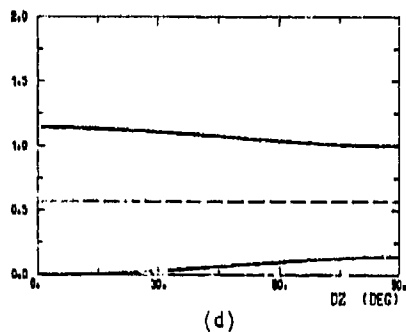
SENSIBILITE EN POSITION



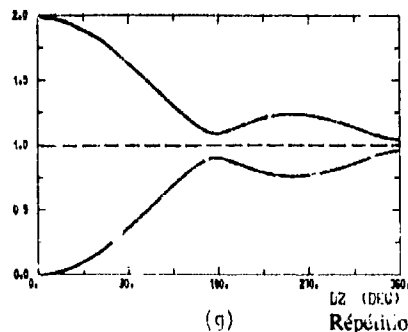
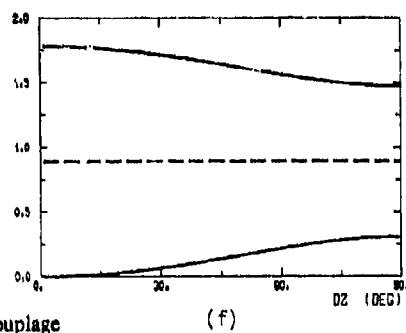
INFORMATION REDUITE EN POSITION



Scénarios de base



Scénarios favorables au découplage



Répétition de scénarios favorables (m=2)

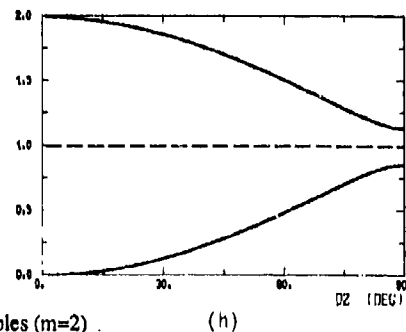


FIGURE 20 - Valeurs propres normalisées de la sensibilité et l'information réduite en position

* Trajectoires théoriques optimales

Pour une trajectoire favorable au découplage qui vérifie les équations 63, les positions relatives de L par rapport à S aux instants t_0 et t_N sont donc identiques. Il est alors possible de rejouer le même scénario (figure 23 pour les deux exemples traités).



FIGURE 23 - Répétition de scénarios favorables au découplage ($m=2$)

Soit m le nombre d'exécution du scénario de base vérifiant 63. D'après l'expression des matrices d'information, on montre que, lorsque m croît, le coefficient p de couplage minimum (équation 62) référencé au temps final total t_f tend $1/4$. De la même façon, l'information réduite en position $W_p(t_f, N)$ tend vers $A/4$.

Ainsi la répétition d'un scénario vérifiant les équations 63 permet d'atteindre l'optimum théorique de W_p soit $A/4$.

De plus, cette convergence est rapide comme le prouvent les figures 20g et 20h correspondant à $m = 2$ pour les deux exemples étudiés.

5.4 - Conclusion

L'analyse théorique réalisée dans ce paragraphe permet de formuler certains principes concernant les trajectoires du lanceur favorables à l'estimation lorsque l'écart-type des mesures est constant :

- distance d'observation faible ou décroissante
- écart total en azimut Δz important
- couplage position-vitesse faible.

(64)

Les résultats sont améliorés par une répartition adaptée des azimuts et la répétition d'un scénario assurant le découplage au temps intermédiaire de la poursuite.

L'optimisation de la trajectoire de L doit donc réaliser un compromis de ces principes tout en respectant les contraintes physiques du problème. La comparaison des exemples traités montre aussi qu'une optimisation globale de la trajectoire sur plusieurs manœuvres du lanceur est préférable à une optimisation locale c'est-à-dire à chaque instant de manœuvre.

6 - DETERMINATION DE TRAJECTOIRES OPTIMALES REALISTES

Pour la détermination d'une trajectoire favorable du lanceur, il importe tout d'abord de définir un indice scalaire d'observabilité. D'autre part, les contraintes du problème notamment la limitation de la vitesse du lanceur vont restreindre les trajectoires possibles. Nous présenterons ensuite une optimisation globale de la trajectoire où les éléments cinématiques de la cible seront supposés connus. Cette optimisation ne sera, en pratique, réalisable que si une estimation suffisamment précise est disponible. L'optimisation de la première manœuvre du lanceur sera, par contre, fondée sur une connaissance partielle du vecteur d'état.

6.1 - Choix d'un indice d'observabilité

Divers indices issus de la formule 50 ont été analysés avec la matrice W_p d'information réduite en position et avec la matrice W_N qui est égale à l'information totale normalisée (équivalence position-vitesse $1 \text{ km} \Leftrightarrow 1 \text{ m/s}$).

Une première comparaison a été effectuée par l'examen de leur comportement obtenu sur des simulations où la précision de l'estimation était connue. Une optimisation locale (à chaque instant d'échantillonnage) du cap de L a été aussi réalisée. En effet, l'optimisation constituant la motivation principale de la définition d'un indice, ce dernier test est bien adapté à l'analyse des performances des diverses solutions étudiées.

Il est ainsi apparu que la grandeur qui semble la plus apte à l'optimisation des trajectoires est la plus petite valeur propre de l'information réduite en position : $\lambda_{\min}[W_p(t_N, N)]$.

En effet, la matrice $W_p(t_N, N)$ reflète bien tous les phénomènes de singularité et d'évolution temporelle de l'information qui sont spécifiques de la TPA. De plus, le calcul d'un critère d'observabilité sur W_p évite le choix d'une normalisation arbitraire sur les composantes de l'état.

La plus petite valeur propre de cette matrice vérifie les propriétés 49 souhaitables à un indice d'observabilité. Son évolution reflète fidèlement la qualité de l'estimation de façon plus sensible que les autres valeurs de s (équation 50). Les résultats de l'optimisation locale du cap sont aussi cohérents avec les principes 64 du paragraphe précédent. Cet indice a aussi une interprétation physique puisqu'il permet le calcul de l'écart-type maximum de l'erreur d'estimation en position. Enfin, la maximisation de cette plus petite valeur propre améliore à la fois le conditionnement et le volume de l'information en position.

6.2 - Contraintes imposées par la vitesse maximale du lanceur

Si la vitesse V_L du lanceur est supérieure à la vitesse V_S de la cible, on peut théoriquement respecter les trois principes (64) pour améliorer l'observabilité. Les contraintes, dans ce cas, proviennent de la rapidité des variations de D et z qui est limitée et de la durée de la poursuite.

Si $V_L < V_S$, les évolutions du lanceur dans le repère lié à la cible sont restreintes. Concernant l'évolution de la distance, on peut déterminer trois zones dans ce repère (figure 24a).

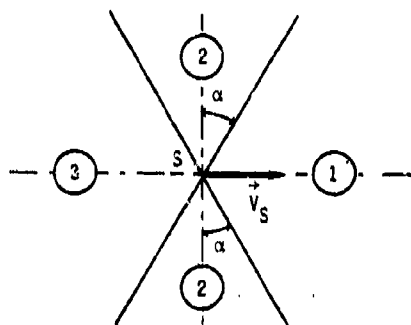


FIGURE 24a

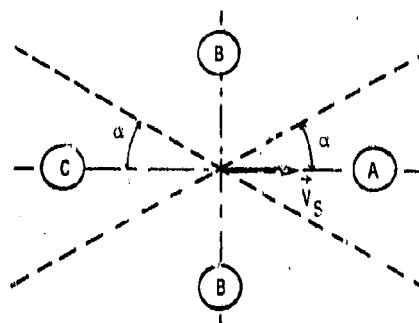


FIGURE 24b

- (1) La distance sera décroissante quel que soit le cap du lanceur
- (2) La distance peut être croissante ou décroissante suivant C_L
- (3) La distance est toujours croissante.

Similairement à l'évolution de la distance, on peut définir trois zones pour l'évolution de l'azimut (figure 24b).

- (A) Des variations d'azimut de signe quelconque sont possibles dans cette zone et ceci permet des manoeuvres favorables au découplage. Cependant, si l'on quitte cette région, le retour dans cette zone est impossible.
- (B) Le sens de variation de l'azimut est unique (le lanceur se fait dépasser par la cible) ce qui explique le retour impossible en zone A. Ainsi les manoeuvres favorables au découplage ne seront pas réalisables.
- (C) Des variations de signes quelconques sont possibles mais la variation totale Δz est limitée à 2α .

D'autre part, pour de faibles distances d'observation, les variations d'azimut peuvent être plus rapides. Ceci ajoute donc un argument supplémentaire en faveur de l'obtention d'une distance faible.

En combinant ces deux résultats, on détermine suivant la position de L par rapport à S, quelles sont les limitations sur l'évolution de la distance et de l'azimut. Si dans certaines zones, notamment celle en avant de la cible, il est possible d'obtenir des évolutions de D et z favorables, elles sont, dans les autres cas, limitées.

Cette étude permet par l'analyse purement graphique de la trajectoire et compte tenu des résultats du paragraphe 5, de déterminer une initialisation cohérente pour l'optimisation de la trajectoire lanceur.

6.3 - Optimisation globale de la trajectoire du lanceur

En supposant connus les éléments cinématiques de S, on peut, pour une trajectoire du lanceur donnée, calculer la matrice d'information et donc l'indice d'observabilité associée. Il est ainsi possible de déterminer, à un instant donné, la trajectoire de L qui sera favorable à l'estimation. En pratique, une telle procédure peut être utilisée lorsqu'une estimation assez précise de la cible est disponible.

Pour cette optimisation, nous ferons l'hypothèse pour le lanceur d'une trajectoire rectiligne par morceaux de durée fixée. Il s'agit alors de déterminer une séquence de M valeurs de son cap C_L et sa vitesse V_L . Si la limitation de la vitesse du lanceur réduit parfois fortement les évolutions possibles, d'autres contraintes interviennent aussi :

- La manoeuvrabilité qui limite les variations du cap et de la vitesse
- L'écart-type des mesures σ_z qui est en fait fonction de la distance, de la vitesse de L et du gisement α de la cible
- La distance d'observation qui doit être bornée inférieurement.

A partir d'une position initiale de L par rapport à S fixée, il est possible, pour un jeu quelconque de valeurs de C_L et V_L , de calculer par intégration une trajectoire du lanceur qui tient compte des manoeuvrabilités en cap et en vitesse. Le critère d'observabilité qui doit refléter la dépendance de σ_z par rapport à D , V_L et α et la distance minimale sur la trajectoire s'en déduisent aisément.

L'optimisation est réalisée par une procédure de programmation linéaire avec contraintes et consiste donc à rechercher le vecteur $Y = [C_{L1}, V_{L1}, \dots, C_{LM}, V_{LM}]^T$ qui maximise $\lambda_{\min}(W_p(t_N, N))$ sous les contraintes $D \geq D_{\min}$ et $0 \leq V_{L1} \leq V_{L_{\max}}$.

Il existe parfois plusieurs solutions de qualité très différentes à ce problème surtout lorsque la contrainte sur la distance est active c'est-à-dire lorsque la distance atteint la limite inférieure D_{\min} . Cependant les résultats du paragraphe précédent permettent généralement de déterminer une initialisation valable qui évite la convergence vers des trajectoires inappropriées. Nous avons ainsi vérifié que des trajectoires réalistes fondées sur les exemples théoriques du paragraphe 5 constituaient un optimum pour l'algorithme.

La figure 25 où la vitesse maximale du lanceur est inférieure à V_S et l'écart de l'azimut constant, révèle les résultats de l'optimisation pour trois positions initiales différentes du lanceur. Sur la figure 25c, on constate d'ailleurs que le passage du lanceur d'une zone latérale à une zone arrière se traduit par un changement de stratégie.

Lorsque la contrainte sur la distance minimale n'est pas active et l'écart-type σ_z constant, la vitesse optimale est égale à la vitesse maximale ce qui se justifie facilement de façon intuitive. Cependant, si la manoeuvrabilité du lanceur est plus faible et l'écart-type de la mesure dépendant du gisement, des manoeuvres en vitesse se révèlent parfois favorables.

6.4 - Optimisation de la 1ère manoeuvre du lanceur

L'étude précédente n'est applicable à la détermination de la première évolution que si la connaissance a priori de V_S (paragraphe 3.2) apporte une information suffisante. Dans la plupart des cas cependant, il faut se contenter, à l'instant final t_1 de la première phase de la trajectoire de L , que de renseignements partiels accumulés pendant la durée $[t_0, t_1]$ de cette phase. Celle-ci peut être simplement inobservable et $z, \dot{z}, \dot{\phi}$ sont connus ou doublement inobservable et seuls z, \dot{z} sont déterminés. Il s'agit donc de calculer la manoeuvre du lanceur de telle sorte qu'avec les mesures du prochain segment $[t_1, t_2]$ de la trajectoire, la précision de l'estimation à l'instant t_2 soit la meilleure possible.

Pour le calcul de cette manoeuvre, l'espace des grandeurs inobservables (D et éventuellement \dot{D}) est alors paramétré et les valeurs du cap C_{L_2} et de la vitesse V_{L_2} de la deuxième phase sont déterminées de façon analogue au paragraphe précédent. Cette optimisation est effectuée à partir des coordonnées polaires modifiées qui sont adaptées aux phases inobservables. Le critère d'optimisation utilisé est l'information réduite en distance au temps t_2 qui, sauf pour des situations très observables, est pratiquement égale à $\lambda_{\text{min}}(W_p)$. Les mêmes contraintes physiques que précédemment ont été adoptées. En outre, la limitation de la vitesse de S permet de restreindre les plages de variations de D et éventuellement \dot{D} .

Pour des contraintes physiques identiques à la figure 25, la figure 26 fait apparaître les résultats d'optimisation à partir d'un scénario doublement inobservable.

Comme précédemment, si la contrainte sur D n'est pas active, la vitesse optimale de la seconde phase est la vitesse maximale. Pour d'autres configurations cependant, une manoeuvre en vitesse peut être favorable. En outre, lorsque D croît, le cap C_{L_2} tend vers une limite qui, pour les cas doublement inobservables, est commune aux différentes hypothèses sur \dot{D} . Cette limite peut être mise en évidence de façon théorique en faisant tendre D vers l'infini et en formulant des hypothèses simplificatrices (manoeuvrabilité infinie du lanceur, écart-type de la mesure constant). Dans ce cas, la manoeuvre théorique optimale du lanceur est celle qui maximise en valeur absolue, la composante V_C transversale à l'azimut à l'instant t_1 de la variation $\dot{V}_{L_1} \cdot \dot{V}_{L_2}$ de la vitesse de L , on obtient donc :

$$\begin{aligned} V_{L_2} &\sim V_{L_{\max}} \\ \hat{C}_{L_2} &= \begin{cases} z(t_1) + \pi/2 & \text{si} \quad \sin[C_{L_1} - z(t_1)] < 0 \\ z(t_1) - \pi/2 & \text{si} \quad \sin[C_{L_1} - z(t_1)] > 0 \end{cases} \end{aligned} \quad (65)$$

Ce résultat corrobore les notions intuitives mises en évidence en introduction générale. En effet, la composante W_C du vecteur $-\dot{\Delta L}$ (équation 7) de la seconde phase est égale, sous ces hypothèses simplificatrices à :

$$W_C(t) = (t - t_1) V_C \quad (66)$$

Maximiser V_C revient donc à maximiser l'ensemble des valeurs W_C de la seconde phase. Pour des distances d'observations importantes, cette grandeur est la façon la plus directe et la plus efficace d'intervenir sur l'évolution de l'azimut (figure 4b). Par rapport aux résultats du paragraphe 5, cette action permet une diminution des couplages d'autant plus favorable à l'amélioration de l'observabilité que Δz est faible.

Dans le cas de la figure 25, le cap théorique 65 est égal à 86° qui est proche de la valeur obtenue dans l'hypothèse $D = 30 \text{ km}$ ($C_{L_2} = 95^\circ$).

6.5 - Conclusion

L'étude à la fois théorique et expérimentale menée dans cette partie fait apparaître des concepts simples pour l'élaboration de trajectoires favorables pour le lanceur :

- *Obtention d'une distance finale la plus faible possible.*
En effet, une distance faible engendre une augmentation de la matrice de sensibilité en position et permet des variations plus rapides et plus importantes de l'azimut. D'autre part, une distance décroissante dans le temps se traduit par une diminution de la dégradation minimale provenant des couplages position-vitesse. Dans les cas où cette décroissance n'est pas possible, il faut s'opposer à son augmentation.
- *Ecart angulaire total Δz important.*
Cette grandeur est favorable à la sensibilité en position et à la répartition des valeurs propres. Cependant l'obtention d'une valeur importante de Δz est souvent contradictoire avec une évolution favorable de la distance.
- *Évolutions de signes opposés ou contrastés de l'azimut.*
Celles-ci permettent la diminution des effets dégradants des couplages position-vitesse au moins suivant la direction de la plus petite valeur propre de l'information réduite en position. Cette action est très importante car elle permet, même en présence de valeurs Δz faibles, d'augmenter considérablement la qualité des résultats.

Ce dernier point qui s'attaque directement à la cause même de l'inobservabilité de la poursuite (les couplages position-vitesse) justifie notamment la première manoeuvre du lanceur (équation 65). Ces règles permettent d'ébaucher graphiquement et facilement des trajectoires favorables pour le lanceur. Ces résultats peuvent être ensuite affinés par un programme d'optimisation tenant compte des contraintes physiques de la poursuite.

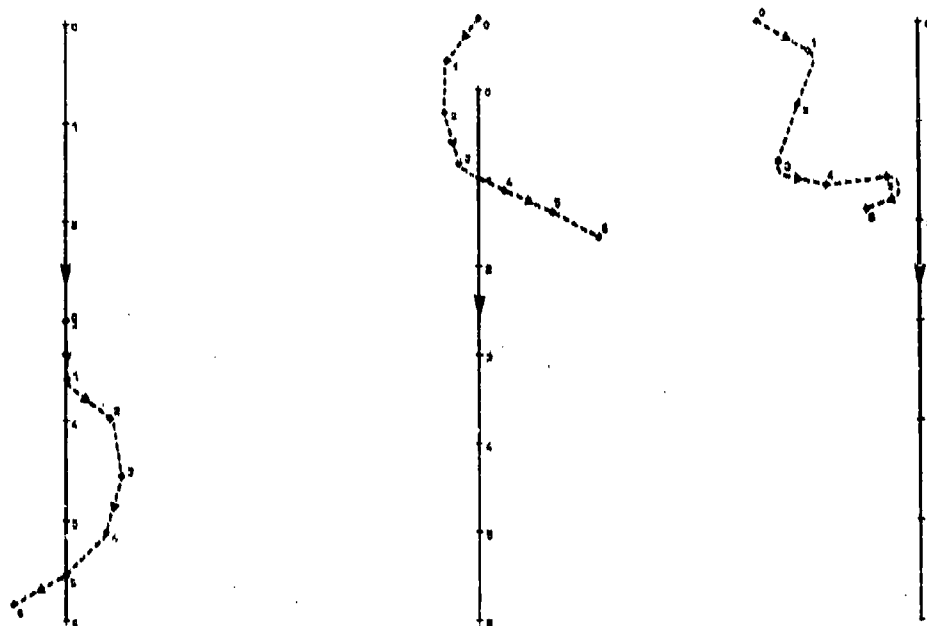
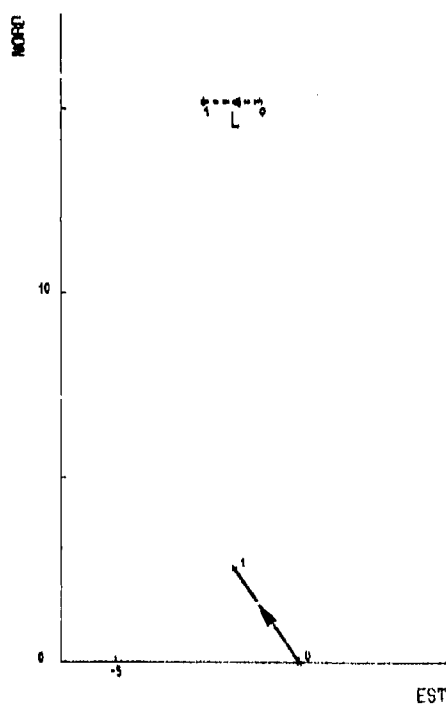
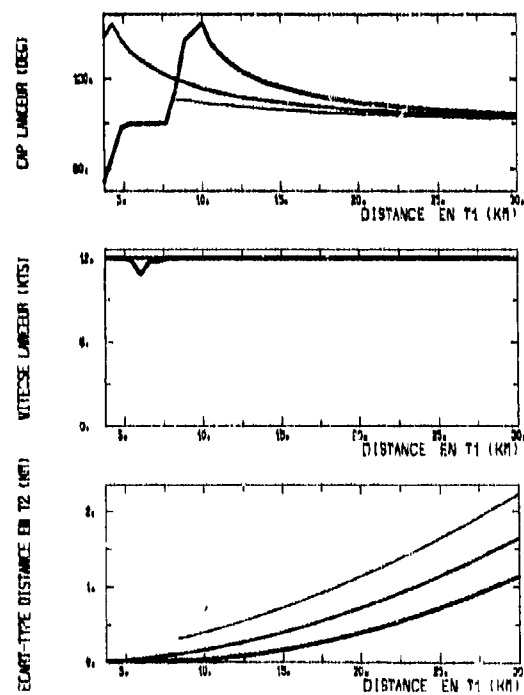


FIGURE 25 - Optimisation globale de la trajectoire du lanceur



(a) Scénario de base
 $\dot{D}_{\text{réel}} \approx -8 \text{ kts}$
 $D(t_f)_{\text{réel}} \approx 12.7 \text{ km}$



(b) Résultats de l'optimisation
 $\dot{D} = 19 \text{ kt}$
 $\dot{D} = 0 \text{ kt}$
 $\dot{D} = -19 \text{ kt}$

FIGURE 26 - Optimisation de la 1ère manœuvre du lanceur

CONCLUSION GENERALE

Parmi les différents aspects abordés lors de cette conférence, deux présentent certaines similarités : la sensibilité numérique et l'observabilité car elles sont liées aux termes de couplage des matrices de covariance ou d'information. Afin de clarifier la différence entre ces deux concepts, on peut schématiquement diviser un problème général d'estimation en deux niveaux :

- Le niveau utilisateur où les différentes grandeurs en jeu ont une signification physique
- Le niveau calculateur où les grandeurs sont considérées comme des nombres sur lesquels sont appliquées des opérations mathématiques.

Au niveau utilisateur sont définies des grandeurs *intrinsèques au problème traité* comme l'observabilité qui correspond à certains critères (erreur de l'estimation inférieure à un seuil donné). Ceux-ci sont donc indépendants de la méthode et de l'implantation utilisée pour réaliser l'estimation.

Au niveau calculateur les grandeurs ont perdu leur signification physique. Ce qui importe alors c'est la façon dont sont effectués les calculs (rapidité, précision, stabilité). Ainsi les sensibilités des matrices (équations 27 et 29) seront comparées à la précision du calculateur et vont justifier le choix d'une implantation.

Cette classification sommaire doit aussi se refléter au niveau de la programmation. Des langages de programmation fortement typés comme ADA permettent pour le niveau utilisateur de traduire la signification physique des grandeurs et donc de veiller à la cohérence des résultats. Les anomalies telle la divergence d'un algorithme sont ainsi détectées.

Lors de la conception d'une procédure d'estimation, il s'agit de traduire les souhaits parfois flous de l'utilisateur sous une forme mathématiquement exploitable (définition d'un indice d'observabilité par exemple). Le problème principal cependant concerne la modélisation des conditions de la poursuite de façon à extraire l'information utile contenue dans les mesures. Parmi toutes les représentations équivalentes, certaines sont parfois plus adaptées (coordonnées polaires modifiées pour la TPA). Ce dernier point reste actuellement un domaine de recherche particulièrement ouvert.

BIBLIOGRAPHIE

- [1] AIDALA V.J., NARDONE C.N.
Biased estimation properties of the pseudo-linear tracking filter.
IEEE Transactions on Aerospace and Electronic Systems - Vol.AES-18, n°4 - Juillet 1982 -
- [2] Vincent J. AIDALA, Sherry E. HAMMEL
Utilization of modified polar coordinates for bearings-only tracking.
IEEE Transactions on Automatic Control, AC-28 (3) : 283-294 - March 1983 -
- [3] BECKENBACH E.F., BELLMAN R.
Inequalities.
Springer-Verlag - 1983 -
- [4] Gerald J. BIERMAN
Factorization Methods for Discrete Sequential Estimation
Volume 128 of Mathematics in Science and Engineering. Academic Press - 1977 -
- [5] Gerald J. BIERMAN, Catherine L. THORNTON
Numerical comparison of Kalman filter algorithms : Orbit determination case study.
Automatica, 13 : 23-35 - 1977 -
- [6] K.R. BROWN, A.O. COHEN, E.F. HARROLD, G.W. JOHNSON
Covariance coordinates : A key to efficient radar tracking.
In EASCON-77, Arlington, V.A., September 1977. Electronics and Aerospace Systems Convention.
- [7] BUCY R.S. JOSEPH P.D.
Filtering for stochastic processes with application to guidance.
Interscience publishers, John Wiley and Sons - 1968 -
- [8] B. DELLERY, Ph. MENNECIER, J.P. ROUSSELOT
Characterization and Identification of Trajectories Using a leg by leg Approach of Bearings - Only Target Motion Analysis.
IEEE - IECEJ - ASJ International Conference on Acoustics, Speech and Signal - Processing TOKYO - 1986 -
- [9] Eli FOGEL, Moni GAVISH
Nth - Order Dynamics Target Observability from Angle Measurements.
IEEE Transactions on Aerospace and electronic systems - AES 24, n°3 - May 1988 -
- [10] M. GAUVRIT, P.VACHER
Etude des performances d'une méthode globale pour la poursuite azimétrique.
Rapport Final CAPCA/DERA n°1/7402 - Centre d'Etudes et de Recherches de TOULOUSE - Septembre 1985 -
- [11] Michel GAUVRIT, Sergio G. TABOADA, Pierre VACHER
Synthèse de filtres pour la poursuite azimétrique.
Rapport Final DERA n°7/7458, Centre d'Etudes et de Recherches de Toulouse - Décembre 1986 -

- [12] *Sherry E. HAMMEL, Vincent J. AIDALA, Kai F. GONG, Allen G. LINDGREN*
Recursive versus batch processing algorithms for bearings-only tracking.
In *Oceans 83*, pages 50-61. Marine Technol. Society, Oceanic Engin. Society, IEEE - August 1983 -
- [13] *HULL D.G., SPEYER J.L., TSENG C.Y.*
Maximum-Information guidance for homing missiles
J. Guidance vol.8 n°4 - July-August 1985 -
- [14] *Andrew H. JAZWINSKI*
Stochastic Processes and Filtering Theory.
Volume 64 of Mathematics in Science and Engineering. Academic Press, London - 1970 -
- [15] *G.W. JOHNSON, A.O. COHEN, E.J. MODUGNO, SHIER C.W.*
Optimal passive localization from a single sensor using multiple linear hypotheses.
In *Proceedings of the IEEE International Conference on Acoustics, Speech and Signal Processing*, San Diego, C.A. - March 1984 -
- [16] *Paul G. KAMINSKI, Arthur E. BRYSON, Jr, Stanley F. SCHMIDT*
Discrete square root filtering : A survey of current techniques.
IEEE Transactions on Automatic Control, AC-16 (6) : 727-735 - December 1971 -
- [17] *MAINE R.E., ILIFF K.W.*
Estimation of the accuracy of dynamic flight determined coefficients.
AIAA 18th Aerospace Sciences meeting - January 1980 -
- [18] *MAINE R.E., ILIFF K.W.*
Identification of Dynamics systems. Theory and formulation.
NASA publication n°1138 - Chapter 11 - February 1985 -
- [19] *MEHRA R.K.*
Optimal Input Signals for Parameter Estimation in Dynamic Systems. Survey and new results.
IEEE Trans. on Automatic Control, Vol; AC-19, n°6 - December 1974 -
- [20] *MULLER P.C., WEBER H.J.*
Analysis and optimization of certain qualities of controllability and observability for linear dynamical systems.
Automatica, Vol.8 - 1972 -
- [21] *NARDONE S.C., AIDALA V.J.*
Observability Criteria for Bearings-only target motion analysis.
IEEE Trans. on Aerospace and Electronic Systems - Vol. AES-17 n°2 - March 1981 -
- [22] *NARDONE S.C., LINDGREN A.G., GONG K.F.*
Fundamental properties and performances of conventional bearings only target motion analysis.
IEEE Transactions on Automatic Control - Vol; AC-29 n°9 - Septembre 1984 -
- [23] *SPEYER J.L., HULL D.G., TSENG C.Y., LARSON S.W.*
Estimation enhancement by trajectory modulation for homing missiles.
J. Guidance, Vol. 7 n°2 - March-April 1984 -
- [24] *SPEYER J.L., HULL D.G., BERNARD W.P.*
Performance of the modified-gain extended Kalman filter along an enhanced information path for a homing missile.
AIAA Paper n°86-2261 - 1986 -
- [25] *TABOADA S.G.*
Synthèse de filtres non linéaires appliqués à la poursuite 3D et à l'azimétrie.
Thèse de Docteur-Ingénieur, Ecole Nationale Supérieure de l'Aéronautique et de l'Espace - Septembre 1986 -
- [26] *S.G. TABOADA, M. GAUVRIT*
Observabilité et entrée sensibilisante en poursuite azimétrique.
Traitement du Signal. Volume 4 n°3 - 1987 -
- [27] *Catherine L. THORNTON, Gerald J. BIERMAN*
Filtering and error analysis via the UDU^T covariance factorization.
IEEE Transactions on Automatic Control, AC-23 (5) : 901-907 - October 1978 -
- [28] *Pierre VACHER*
Etude de l'observabilité de la poursuite azimétrique et détermination des trajectoires du lanceur optimales.
Rapport Final DERA n° 2/7520, Centre d'Etudes et de Recherches de Toulouse - Décembre 1987 -
- [29] *Pierre VACHER*
Etude des phases faiblement observables de la poursuite azimétrique.
Rapport Final DERA n° 2/7549, Centre d'Etudes et de Recherches de Toulouse - Décembre 1988 -
- [30] *VANDERVELDE W.E., CARIGNAN C.R.*
A dynamic measure of controllability and observability for the placement of actuators and sensors on large space structures.
Rapport NASA-CR-168520 - January 1982 -
- [31] *Michel VERHAEGEN, Paul Van DOOREN*
Numerical aspects of different Kalman filter implementations.
IEEE Transactions on Automatic Control, AC-31 (10) : 907-917 - October 1986 -

SELECTIVE BIBLIOGRAPHY

This bibliography with abstracts has been prepared to support AGARD Lecture Series No. 166 by the Scientific and Technical Information Division of the U.S. National Aeronautics and Space Administration, Washington, D.C., in consultation with the Lecture Series Director, Dr. George T. Schmidt, The Charles Stark Draper Laboratory, Inc., Cambridge, Massachusetts.

UTTL: Fault tolerant inertial navigation system
AUTH: A/VANDERWERF, KEVIN; B/NEFELD, NUT PAA: B/(Honeywell, Inc., Minneapolis, MN) IN: AIAA/IEEE Digital Avionics Systems Conference, 8th, San Jose, CA, Dec. 17-20, 1988, Technical Papers, Part 2 (A89-18051 05-06). Washington, DC, American Institute of Aeronautics and Astronautics, 1988, p. 821-829.

ABS: This paper describes the sensor redundancy management concept employed in a fault-tolerant inertial reference system. The concept uses a sensor hexad and employs separate fault detection and isolation (FDI) algorithms for navigation computations and outputs to the FCS. The FDI algorithm implementation is based on the generalized likelihood ratio test (GLRT). Enhancements to the failure isolation logic virtually eliminate the probabilities of false detection and wrong isolation inherent with the basic GLRT concept, thus making the GLRT scheme practical in the real world of high reliability requirements
RPT# AIAA PAPER 88-4024 88/00/00 89A18175

UTTL: New insights into minimum-variance reduced-order filters

AUTH: A/SETTERLUND, ROY H. PAA: A/(Charles Stark Draper Laboratory, Inc., Cambridge, MA) Journal of Guidance, Control, and Dynamics (ISSN 0731-5090), vol. 11, Nov.-Dec. 1988, p. 495-499.

ABS: The minimum-variance reduced-order (MVRO) filter is an algorithm that has become popular in the guidance and navigation community as a tool for designing and evaluating the performance of candidate reduced-order filters. Its utility rests on the assumption that the MVRO algorithm yields the optimum (in a minimum-variance sense) performance possible with a given reduced-order filter. The analysis and examples in this paper show that this is not the case and that the MVRO algorithm merely yields an optimal estimate immediately after the first measurement update. It is shown how a new MVRO gain matrix may be derived that will yield optimum results at some specified time in the future. The main point of the analysis is to prove that, in general, it is not possible to specify a discrete reduced-order filter that is always minimum-variance. The minimum-variance condition can only be achieved at a specific time - before and after that time, other filter gain histories could provide better performance. 88/12/00 89A16153

UTTL: Multiple beam combination with pupil geometry maintenance

AUTH: A/HENTZ, KARL P. PAA: A/(USAF, Weapons Laboratory, Kirtland AFB, NM) Optical Engineering (ISSN 0091-3286), vol. 27, Sept. 1988, p. 740-748.

ABS: This paper presents the issues pertinent to a multivariable control system for a phased telescope array imaging system. A description of the envisioned system,

the discrete time state space model of the system, the measurement techniques, estimation/control algorithms, and Monte Carlo simulation results are presented. Initially, an extended Kalman filter is used as the estimator and its simulation performance is compared with that of a linearized Kalman filter with no difference in performance found. Additionally, successful test results from a laboratory two-beam prototype control system tested are presented. 88/09/00 88A55007

UTTL: Optimal feedback control of a bioreactor with a

remote sensor
AUTH: A/AIRANJAN, S. C.; B/SAM, K. Y. PAA: B/(Rice University, Houston, TX) CMAP: Rice Univ., Houston, TX, IN: 1988 American Control Conference, 7th, Atlanta, GA, June 15-17, 1988, Proceedings, Volume 2 (A88-54401 24-63). New York, Institute of Electrical and Electronics Engineers, 1988, p. 1106-1111.

ABS: Sensors used to monitor bioreactor conditions directly often perform poorly in the face of adverse morphological conditions. One way to circumvent this is to use a remote sensor block. However, such a configuration usually causes a significant time lag between measurements and the actual state values. Here, the problem of implementing feedback control strategies for such systems, described by nonlinear equations, is addressed. The problem is posed as an optimal control problem with a linear quadratic performance index. The linear control law so obtained is used to implement feedback. A global linearization technique as well as an expansion using Taylor series is used to linearize the nonlinear system, and the feedback is subsequently implemented. 88/00/00 88A54538

UTTL: Filtering and implementation for air-to-air target tracking

AUTH: A/VORREEST, ERIK I.; B/HADDAD, ABRAHAM H. PAA: B/(Georgia Institute of Technology, Atlanta) IN: 1988 American Control Conference, 7th, Atlanta, GA, June 15-17, 1988, Proceedings, Volume 1 (A88-54401 24-63). New York, Institute of Electrical and Electronics Engineers, 1988, p. 143-148.

ABS: A discussion is presented of some aspects of the design problem involved in the choice of a realization or approximation of a desired system behavior (as for instance dictated by the analytical solutions to a filtering problem) by parameters that can only be approximately adjusted, e.g., due to quantization, component tolerances (analog case), and finite word-length (discrete case). The authors first address the mathematical characterization of this robustness problem, and its solutions under various criteria of optimality. Earlier results are extended to multimode systems which can arise in nonlinear approximation problems. The

feasibility of this approach in multimode filtering is shown and is illustrated by an air-to-air tracking example. 88/00/00 88A54415

UTTL: An assessment of air-to-air missile guidance and control technology

AUTH: A/CLOUTIER, J. R.; B/EYERS, J. H.; C/FEELEY, J. J.
PAA: B/(USAF, Armament Laboratory, Eglin AFB, FL);
C/(Idaho, University, Moscow) IN: 1988 American Control Conference, 7th, Atlanta, GA, June 15-17, 1988.
Proceedings. Volume 1 (ABA-54401 24-63). New York, Institute of Electrical and Electronics Engineers, 1988, p. 133-142.

ABS: An assessment is provided of current air-to-air missile guidance and control technology. Areas explored include target state estimators, advanced guidance laws, and bank-to-turn autopilots. The assumptions, benefits, and limitations of recent applications of nonlinear filtering, adaptive filtering, modern control, adaptive control, dual control, differential game theory, and modern control design techniques to the air-to-air missile problem are discussed. 88/00/00 88A54414

UTTL: Kalman filter design for integration of Phase III GPS with an Inertial Navigation System

AUTH: A/BLETZACKER, F. R.; B/ELLER, D. H.; C/FORGETTE, T. M.; D/SEIBERT, G. L.; E/VAVRUS, J. L. PAA: E/(Computing Applications Software Technology, Los Alamitos, CA) IN: Institute of Navigation, National Technical Meeting, Santa Barbara, CA, Jan. 26-29, 1988, Proceedings (AB8-51701 22-04). Washington, DC, Institute of Navigation, 1988, p. 113-129.

ABS: CAST is involved in the development of navigation software to integrate the Rockwell-Collins aided Phase III GPS receiver with an Inertial Navigation System. The software receives inputs from the aided five-channel Phase III receiver and two Singer-Kearfott SNU-84-3 Inertial Navigation Systems. This paper discusses the features of the design that are of general interest and that will be most useful in similar applications. In addition, those aspects of the aided five-channel Phase III GPS receiver's operation that are most limiting to the overall performance of an integrated system are described. Several simple modifications to the Phase III receiver processing are recommended that would greatly enhance the ability to achieve improved performance through further processing of the Phase III receiver data. 88/00/00 88A51711

UTTL: The GPS users integration guide

AUTH: A/GREENSPAN, RICHARD L.; B/DONNA, JAMES I.; C/SOLTZ, J. ARNOLD PAA: C/(Charles Stark Draper Laboratory, Inc., Cambridge, MA) IN: Institute of Navigation, National Technical Meeting, Santa Barbara, CA, Jan. 26-29, 1988,

Proceedings (AB8-51701 22-04). Washington, DC, Institute of Navigation, 1988, p. 104-112.

ABS: The major themes of the GPS Users Integration Guide are synthesized. The management of GPS integration is addressed, including the responsibilities of the system manager and of the system integrator. Architectural and performance issues are examined. Flight test issues are considered, stressing the lack of satisfactory velocity laboratory testing and the lack of a satisfactory velocity reference system for flight testing. 88/00/00 88A51710

UTTL: Common Kalman Filter - Fault-tolerant navigation for next generation aircraft

AUTH: A/LODHIS, PETER V. W.; B/CARLSON, NEAL; C/BERARDUCCI, MICHAEL P. PAA: A/(TAU Corp., Los Gatos, CA); B/(Integrity Systems, Inc., Winchester, MA); C/(USAF, Avionics Laboratory, Wright-Patterson AFB, OH) IN: Institute of Navigation, National Technical Meeting, Santa Barbara, CA, Jan. 26-29, 1988, Proceedings (AB8-51701 22-04). Washington, DC, Institute of Navigation, 1988, p. 38-45.

ABS: The Common Kalman Filter (CKF), an ongoing USAF Avionics Laboratory program to develop, simulate, and evaluate computational techniques and software architectures that will enhance the robustness and reliability of integrated navigation systems for the next generation of military aircraft, is addressed. The CKF design, which is nearing maturity and is currently entering a computer simulation test cycle, is described. Approaches to sensor information requirements definition, local sensor integration/filtering, master filter modeling, automatic fault detection/isolation, and system reconfiguration are discussed. Failure modes which will be the basis for the evaluation of CKF failure response in subsequent simulations are described. 88/00/00 88A51705

UTTL: Global Positioning System (GPS) autonomous user system

AUTH: A/AMANDA, M. P.; B/BERNSTEIN, H.; C/FEES, W. A.; D/PAUGESTAT, T. C. PAA: C/(Aerospace Corp., Los Angeles, CA); D/(USAF, Space Div., Los Angeles, CA) Navigation (ISSN 0028-1522), vol. 35, Summer 1988, p. 197-216.

ABS: The GPS autonomous user system (AUS) which has been designed to provide interim full-system accuracy if the GPS operational control segment (OCS) fails is examined. The parameters and algorithm of the AUS are discussed and tests of the system are presented. It is shown that the AUS performance over a 180-day period without an OCS is comparable to the GPS performance with a fully operational OCS. The sensitivity to the prediction time of the reference trajectory extended navigation messages seem minimal. It is suggested that as long as this predicted trajectory is within the linear range, roughly equivalent accuracies can be obtained. 88/00/00 88A51381

Electronics Conference, Dayton, OH, May 23-27, 1988. Volume 4 (A88-50526 22-01). New York, Institute of Electrical and Electronics Engineers, 1988, p. 1214-1220. The authors describe the architecture and design of the EXNAV intelligent system that is under development for integrating various navigation sensors with different performance characteristics for an optimal navigation solution. EXNAV, which mixes reasoning with conventional processing for problem solving, consists of an executive and a set of cooperating mini-experts, each responsible for a particular sensor. Using classical Kalman filter algorithm, EXNAV combines all sensor information based on the best sensor configuration. In addition, it provides facilities for sensor-level diagnosis, reconfiguration, and monitoring. Each mini-expert has specialized knowledge about the diagnostics and procedures associated with a particular sensor. The knowledge engineering approach involved in the EXNAV design is discussed. 88/00/00 88A51030

ABS:

UTTL: Terrain-aided navigation test results in the AFTI/F-16 aircraft
AUTH: A/BOUZER, DRAYTON D.; B/FELLERHOFF, J. RICHARD PAA: B/(Sandia National Laboratories, Albuquerque, NM) Navigation (ISSN 0028-1522), vol. 35, Summer 1988, p. 161-175.
ABS: A low-level attack terrain-aided navigation algorithm which uses extended Kalman filter theory to provide essentially continuous terrain-aided navigation has been integrated into the Advanced Fighter Technology Integration (AFTI)/F-16 aircraft. The required performance is less than 100 m median horizontal radial error over 200 nmi trajectories that are flown over gently rolling terrain. The aircraft was tested between September 1986 and February 1987. It is concluded that the system determines aircraft position within an initial 0.5 nmi, tracks aircraft horizontal position with an accuracy of 75 m median radial error using digital terrain elevation data, and estimates altitude with less than 17 m rms error. 88/00/00 88A51378

UTTL: Kalman filter design for control surface failure detection and isolation

AUTH: A/LEE, HOWARD P.; B/DUDGINSKI, ROBERT J. PAA: B/(Lockheed Aeronautical Systems Co., Burbank, CA) IN: NAECOM 88: Proceedings of the IEEE National Aerospace and Electronics Conference, Dayton, OH, May 23-27, 1988. Volume 4 (A88-50526 22-01). New York, Institute of Electrical and Electronics Engineers, 1988, p. 1495-1503. The use of Kalman filters for residual generation for control surface failure detection and isolation (FDI) is studied. The FDI algorithm investigated consists of two main components: a Kalman filter for residual generation, and a set of pairwise log-likelihood-ratio (LLR) tests for decision processing. The performance of several Kalman filter designs under a severe gust level of 20-fps RMS is evaluated. The performance of the FDI algorithm is measured in terms of the probabilities of detection and false alarm which are closely related to the signal-to-noise ratios (SNRs) of the decision LLRs. The filter design process is aided by evaluating the SNRs of the different Kalman filter configurations. It was found that including the gust-shaping filters in the Kalman filter equations improved the FDI performance under severe wind turbulence. However, all the filter configurations evaluated were sensitive to parameter variations. 88/00/00 88A51044

UTTL: EXNAV: An intelligent sensor integrator
AUTH: A/HUI, PATRICK J.; B/NAVAK, ABIYA R. PAA: B/(Canadian Marconi Co., Avionics Div., Kanata, Canada) IN: NAECOM 88: Proceedings of the IEEE National Aerospace and

UTTL: Analytical redundancy using band-limiting filters
A/JONES, J. G.; B/CORBIN, M. J. PAA: B/(Royal Aircraft Establishment, Farnborough, England) IEEE Proceedings, Part D - Control Theory and Applications (ISSN 0143-7054), vol. 135, pt. D, no. 4, July 1988, p. 257-267.

ABS: The paper presents a method in which control system faults may be detected on the basis of the generation and cross-comparison of bandlimited signals from dissimilar sources. While signals measured at different points in the system may differ widely when viewed over a wide bandwidth, it is shown that, over limited pass bands, there are simple relationships that can be verified by means of appropriate filtering and comparison logic. In effect, the band-limiting filters are used to monitor the propagation of information originating in the structure of external inputs through the system. 88/07/00 88A47931

UTTL: Analytic redundancy management for systems with appreciable structural dynamics
A/EDMUNDSON, RAYMOND C. PAA: A/(NASA, Langley Research Center, Hampton, VA) COMP: National Aeronautics and Space Administration, Langley Research Center, Hampton, VA. International Association for Mathematics and Computers in Simulation, World Congress on Scientific Computation, 12th, Paris, France, July 18-22, 1988, Paper. 4 p.

ABS: This paper deals with analytic redundancy management of systems that have appreciable structural dynamics and require active control. The class of systems considered is large, lightweight spacecraft that have large numbers of distributed sensors and actuators. Both preliminary design and on-line operations are studied. For the preliminary design we deal with the placement of the sensor and actuator components on a highly flexible spacecraft. For

on-line operation an analytic redundancy management system based on examination of the residuals of a Kalman filter is considered. A large, flexible grid made of overlapping aluminum bars is used to experimentally evaluate this analytic redundancy management system. Results of the experimental evaluation are included in the paper.
88/07/00 88A0773

UTTL: GPS integrity monitoring for commercial applications using an IRS as a reference

AUTH: A/BRENNER, MATS A. PAA: A/(Honeywell Inc., Air Transport Systems Div., Saint Louis Park, MN) IN: Institute of Navigation, Technical Meeting, 1st, Colorado Springs, CO, Sept. 21-25, 1987, Proceedings (A88-37376 15-04).

ABS: An integrated GPS/inertial reference system (IRS) approach for integrity monitoring in commercial applications is presented, with special attention being given to the soft-type failure (failures that cause the error in pseudorange to grow slowly). Simulation results provide values for the smallest detectable drift in pseudorange. Crucial factors which effect the performance are shown to be the time between update of the satellite health status and the selective availability noise. If soft failure occurs in a satellite for which no redundant satellite information is available, the GPS/IRS Kalman filter will detect the failure using statistical data describing the error in measured pseudorange or delta-range values.
87/00/00 88A37412

UTTL: Integration of differential GPS with INS for precise position, attitude and azimuth determination

AUTH: A/AGGARWAL, A. K. PAA: A/(Magnavox Advanced Products and Systems Co., Torrance, CA) IN: Institute of Navigation, Technical Meeting, 1st, Colorado Springs, CO, Sept. 21-25, 1987, Proceedings (A88-37376 15-04).

ABS: The NAVSTAR Global Positioning System (GPS), currently being developed for the Department of Defense, is a space-based navigation system that will provide the user with precise position, velocity and time information on a 24-hour basis and in all-weather conditions at any point on the globe. Differential operation, wherein a high quality, surveyed-in receiver installation determines satellite pseudorange errors and communicates them to nearby users, offers a promising technique for further improving the GPS position accuracy on a local scale. A GPS receiver, under differential operation and when integrated with an Inertial Measurement Unit (IMU) provides a very high quality navigation system for a variety of applications. The resulting navigation system overcomes many of the weaknesses of a stand-alone GPS or IMU by providing: (1) high rate/accuracy position and

velocity estimates during dynamics, (2) the reduced position and velocity error growth during GPS signal outage, (3) improved jamming resistance through code loop aiding, and (4) the availability of very precise attitude and azimuth of the vehicle. This makes the differential GPS/INS suitable for truth navigation systems, for calibration, and instrumentation. 87/00/00 88A37405

UTTL: GPS integration with low-cost inertial navigation unit

AUTH: A/KUEHRT, DONALD T. PAA: A/(Magnavox Advanced Products and Systems Co., Torrance, CA) IN: Institute of Navigation, Technical Meeting, 1st, Colorado Springs, CO, Sept. 21-25, 1987, Proceedings (A88-37376 15-04).

ABS: A successful integration is described that involves a one-channel GPS receiver tightly coupled with a low-cost inertial navigation unit (IMU). The combination is intended for low cost military applications. A 17-state Kalman navigation filter was used that performs in-flight calibration and alignment of the IMU using GPS receiver measurements of pseudorange and delta range. By including IMU gyro and accelerometer error states in the Kalman filter, the low-cost IMU performs as well as units costing much more. Conversely, IMU velocity data is used to extend the GPS receiver tracking threshold against jammers, and to improve reacquisition of signals after a loss. Sensor error models, Kalman filter design and system-level performance predictions are briefly described. Field test methodology is described, and field test results obtained to date are presented. 87/00/00 88A37402

UTTL: An integrated GPS/strapdown inertial navigator

AUTH: A/DU HART, J. H., III; B/SEHLER, J. R. PAA: 8/(Interstate Electronics Corp., Anaheim, CA) IN: Institute of Navigation, Technical Meeting, 1st, Colorado Springs, CO, Sept. 21-25, 1987, Proceedings (A88-37376 15-04).

ABS: A postmission data processor has been developed to provide high-fidelity postmission platform trajectories for use in the evaluation of Trident II (D-5) weapon system performance. The postmission processor synergizes accelerometer and gyro data from an inertial measurement unit using pseudorange and carrier-phase data from the p-code correlator and carrier-phase tracking loops of a GPS receiver. The inertial data is inputted to the strapdown navigator, and the navigator's position, velocity, and attitude are employed as Kalman filter predictions for processing the GPS data. Error estimates of an extended Kalman filter are used to correct the state estimate predictions. 87/00/00 88A37401

Springs, CO, Sept. 21-25, 1987, Proceedings (A88-37376 15-04). Washington, DC, Institute of Navigation, 1987, p. 119-129.

ABSTRACT: The PA9050 series of stat receivers perform a digital correlation at baseband using five parallel tracking channels. There are three correlators in each tracking channel and automatic mode is provided to maximize dynamic performance under the prevailing signal-to-noise environment. Pseudorange measurements are used at 10 Hz, with pseudorange updates at 1 Hz, to generate the navigation solution using a Kalman filter which has up to 11 state elements, depending on application. Kalman filter modeling occurs during periods of bad geometry, and an uncoupled height bias estimator filter is also provided. Open-loop correction of the incoming IN data is performed within the PA9050 receiver using the GPS position and velocity solution as the reference data. Demonstrator receivers have been extensively and successfully tested in rotary and fixed-wing aircraft as well as on surface vessels and land vehicles; stand-alone and IN-aided trials have been carried out. 87/00/00 88A37392

ABSTRACT: UTTL: Reference trajectories from GPS measurements A/ROBBINS, JAMES E. PAA: A/(General Dynamics Services Co., Yuma, AZ) IN: Institute of Navigation, Technical Meeting, 1st, Colorado Springs, CO, Sept. 21-25, 1987, Proceedings (A88-37376 15-04). Washington, DC, Institute of Navigation, 1987, p. 72-80. USAF-sponsored research. Reference trajectories for vehicles for which GPS measurements are available are determined which can be used as a reference for the evaluation of GPS user-equipment and integrated host vehicle navigation. Three GPS solutions have been used in obtaining the reference trajectories: (1) a closed-form solution of the GPS pseudorange equations; (2) an unaided Kalman filter; and (3) an inertially-aided Kalman filter. It is noted that all of the solutions operate with or without differential GPS. Observed differences between the present system and the Yuma proving ground laser tracking system demonstrate that the system and the lasers both have at least a 5-m rms accuracy. 87/00/00 88A37386

ABSTRACT: UTTL: Performance and operation of selected aspects of GPS/Host Vehicle integration schemes A/BARCKLEY, K.; B/DEDDER, D.; C/SINHA, P. PAA: C/(Intermetrics, Inc., Huntington Beach, CA) IN: Institute of Navigation, Technical Meeting, 1st, Colorado Springs, CO, Sept. 21-25, 1987, Proceedings (A88-37376 15-04). Washington, DC, Institute of Navigation, 1987, p. 36-43.

ABSTRACT: During the Phase III Program, Global Positioning System (GPS) User Equipment (UE) will be produced and integrated into various Host Vehicle (HV) platforms to enhance navigation performance. In particular, the synergistic

UTTL: A fully integrated GPS/Doppler/inertial navigation system

AUTH: A/ROUNDS, STEPHEN F.; B/CASEY, JEAN M. PAA: B/(Singer Co., Electronic Systems Div., Wayne, NJ) IN: Institute of Navigation, Technical Meeting, 1st, Colorado Springs, CO, Sept. 21-25, 1987, Proceedings (A88-37376 15-04). Washington, DC, Institute of Navigation, 1987, p. 184-187. The ability of a Doppler system integrated with a GPS/inertial system to maintain system accuracy during periods of GPS outage has been demonstrated. Doppler system modeling is considered, in addition to the use of GPS/inertial data to calibrate the elements of the model using a Kalman filter. Trade-off studies on the use of a Doppler system vs the use of a higher accuracy INS indicate that the addition of the Doppler may be approximately equivalent to an INS improvement of 60 percent. 87/00/00 88A37400

UTTL: Integration of GPS receivers into existing inertial navigation systems

AUTH: A/TAZARTES, D. A.; B/MARK, J. E. PAA: B/(Litton Industries, Guidance and Control Systems Div., Woodland Hills, CA) IN: Institute of Navigation, Technical Meeting, 1st, Colorado Springs, CO, Sept. 21-25, 1987, Proceedings (A88-37376 15-04). Washington, DC, Institute of Navigation, 1987, p. 176-183.

ABSTRACT: Many inertial navigation systems of both platform and ring laser strapdown types are currently in service. This paper discusses the possibility and desirability of incorporating a small GPS receiver in these systems. Advances in technology such as microprocessors, gate arrays and surface mount devices allow the existing INS electronics to be replaced in a reduced volume. The remaining space in many cases is sufficient to permit the insertion of a small GPS Receiver. Locating the GPS receiver in an inertial navigation system (INS) solves many of the usual system integration problems. Tight coupling between the GPS and INS can be achieved since data latency is minimized and well controlled. In such a configuration, rate aiding of the GPS is easily achieved. This approach also leads to greater flexibility and enhanced overall performance since all GPS and INS data are simultaneously available. While not providing the ultimate in redundancy, the integrated INS/GPS approach does offer greater simplicity with enhanced performance. This makes it a very attractive solution. 87/00/00 88A37399

UTTL: Architecture and field test results of a digital GPS receiver

AUTH: A/MOYLE, CHRIS; B/THOMAS, JAMES; C/LEASURE, STEVEN PAA: C/(Plessey Avionics, Ltd., Havant, England) IN: Institute of Navigation, Technical Meeting, 1st, Colorado

benefits of integrating GPS with other sensors, e.g., inertial navigation systems (INS) will be exploited to achieve precise navigation and to provide augmented capabilities for each system viz., in-flight alignment for the INS, and improved anti-jam margin and rapid signal acquisition for GPS. This paper outlines several possible schemes for integrating GPS with other on-board systems under the constraints of the available Phase III User Equipment interfaces and examines selected aspects of the integrations. These include: Operation of dual Kalman filter configurations; effects of GPS position and (or) velocity data incorporation rates on HV navigation performance including INS ground and air alignments; use of covariance versus Expected Position Error (EPE) and Expected Vertical Error (EVE) to characterize GPS measurements; and effects of INS resets on GPS. 87/00/00 88A37381

UTTL: Institute of Navigation, Technical Meeting, 1st, Colorado Springs, CO, Sept. 21-25, 1987. Proceedings Meeting sponsored by the Institute of Navigation. Washington, DC, Institute of Navigation, 1987, 320 p. For individual items see A98-37377 to A88-37413.

ABS: Papers are presented on GPS phase III multichannel user equipment. GPS accuracy performance tests, and software architecture of the family of DOD standard GPS receivers. Also considered are a GPS hover position sensing system, GPS applications to carrier-based naval aircraft, and a potential GPS user architecture for the NASA Space Station based on Landsat 4/5 experience. Other topics include GPS integration with a low-cost inertial navigation unit, an integrated GPS/IRS design approach, and differential GPS with a sequencing receiver. Papers are also presented on a Kalman filter approach to self-contained GPS failure detection, receiver autonomous integrity monitoring using a 24-satellite GPS constellation, and GPS integrity monitoring for commercial applications using an IRS as a reference. 87/00/00 88A37376

UTTL: On fast filter design and synthesis
AUTH: A/PACUT, A.; B/KOLODZIEJ, W. J.; C/MOHLER, R. R. PAA: C/(Oregon State University, Corvallis) IN: IEEE Conference on Decision and Control, 26th, Los Angeles, CA, Dec. 9-11, 1987. Proceedings. Volume 3 (A88-34702 13-63). New York, Institute of Electrical and Electronics Engineers, Inc., 1987, p. 1850, 1851.

ABS: Research to develop various Kalman-filter fast implementations is reported. The aim is to design dedicated computer architectures. Preliminary results of continuing research and a systematic overview are presented. 87/00/00 88A34858

UTTL: On the design of an adaptive Kalman filter for

on-line processing of sensor signals
AUTH: A/MDJCIK, PIOTR J. PAA: A/(Alberta Research Council, Calgary, Canada) IN: IEEE Conference on Decision and Control, 26th, Los Angeles, CA, Dec. 9-11, 1987. Proceedings. Volume 2 (A88-34702 13-63). New York, Institute of Electrical and Electronics Engineers, Inc., 1987, p. 1605-1611.

ABS: Algorithms are presented for online estimation of the optimal parameters of the Kalman filter applied to sensor signals when the structure of the signal model is known exactly, but all the parameters of the signal and noise are unknown. A first-order spectrum of a pure signal and white Gaussian measurement noise have been assumed. The proposed adaptive algorithms have been examined for various spectra of the pure signal and for various signal to noise ratios. The effect of the length of an adaptation step and a sampling frequency on the mean-square errors of the pure signal estimation has also been tested. The results may be helpful for synthesizing optimal linear digital filters for sensor signals in the case of unknown parameters of the signal and noise. Although that particular algorithm has been applied to stationary signals, its modifications can also be used successfully for time-varying sensor signals when the signal and noise parameters vary slowly in comparison to the length of the adaptation step. A method for the best choice of the adaptation step and the sampling frequency for filtering nonstationary signals is proposed. 87/00/00 88A34828

UTTL: Covariance analysis of gravity models for land navigation

AUTH: A/ZAVATTEKO, PAUL PAA: A/(Northrop Corp., Electronics Div., Hawthorne, CA) AIAA, Guidance, Navigation and Control Conference, Monterey, CA, Aug. 17-19, 1987. 17 p. An algorithm for propagating system error covariances when gravity errors are assumed to be a zero-mean spatially correlated random process is presented. The dual-state mechanization approach is used to study a navigation problem in which external updates are incorporated by an on-board filter. The on-board filter suboptimally models gravity errors and instrument errors while applying control to navigation-indicated quantities. 87/00/00 88A29767

UTTL: Low cost Doppler aided strapdown inertial navigation systems
AUTH: A/YUAN, XIN; B/YU, ZAIXIN PAA: B/(Nanjing Aeronautical Institute, People's Republic of China) (Acta Aeronautica et Astronautica Sinica, vol. 7, Oct. 1986, p. 471-481) Chinese Journal of Aeronautics (ISSN 1000-9361), vol. 1, Jan. 1988, p. 49-57. Translation. Previously cited in issue 09, p. 1196. Accession no. A87-24719. 88/01/00 88A29363

88A27771

UTTL: A research of non-linear observers for lateral motion of aircrafts

AUTH: A/WANG, ZONGXUE PAA: A/(Beijing Institute of Aeronautics and Astronautics, People's Republic of China) Acta Aeronautica et Astronautica Sinica (ISSN 1000-6893), vol. 3, Nov. 1987, p. A 507-A 596. In Chinese, with abstract in English.

ABS: The paper introduces several nonlinear observers which are used to estimate the lateral motion state parameters of an aircraft. The results of ground simulation and experiment are given which show that these observers have several advantages. They are simple and easy to implement with good performance and the algorithms possess certain adaptive and antisturbance abilities. Simplified estimation equations of nonlinear observers, a principle block diagram, and the results of experiment are also given in this paper. 87/11/00 88A29244

UTTL: Autonomous navigation of a geostationary satellite according to measurements with low information content

AUTH: A/KAMYSHANOV, A. P.; B/KARLOV, V. I.; C/KRASIL'SHIKOV, M. N. Kosmicheskii Issledovanie (ISSN 0023-4206), vol. 26, Jan.-Feb. 1988, p. 154-157. In Russian.

ABS: A fast algorithm is developed which provides for high accuracy of autonomous navigation for a geostationary satellite. The algorithm is based on the use of analytical formulas for quasi-circular motion, a quasi-linear Kalman filter, and an optimal strategy for the measurement of the navigation parameters. RMS errors of the estimation of satellite orbit period are determined in the framework of the proposed approach. 88/02/00 88A28345

UTTL: Points of view on linear and nonlinear filtering in aeronautics

AUTH: A/LEVINE, J. PAA: A/(Paris, Ecole des Mines, Fontainebleau, France) IN: Automatic systems in aeronautics; National Colloquium, Paris, France, Mar. 17-19, 1986, Proceedings (A88-27751 63-10). Toulouse, Cepadues-Editions, 1986, p. 541-551. In French.

ABS: The advantages and disadvantages of the Kalman filter for linear systems, the extended Kalman filter for nonlinear systems, and other filtering methods for nonlinear systems are considered. Reference is given to aeronautical applications such as navigation and missile guidance. Difficulties encountered in the linear case include the regulation of noise levels, the compensation for biases due to modeling errors, and the selection of suboptimal filters. Two categories of linear filtering methods which are exact or approximate are discussed: (1) methods using the conditional law to obtain approximations of moments or the existence properties of finite-dimension filters; and (2) methods using an appropriate choice of coordinates to describe the system in a more agreeable form. 86/00/00

UTTL: Failure detection and flight control reconfiguration

AUTH: A/BASSEVILLE, MICHELE PAA: A/(CHRS, Institut de Recherches en Informatique et Systemes Aeronautiques, Hermes, France) IN: Automatic systems in aeronautics; National Colloquium, Paris, France, Mar. 17-19, 1986, Proceedings (A88-27751 63-10). Toulouse, Cepadues-Editions, 1986, p. 431-453. In French.

ABS: Problems related to failure detection in sensors and actuators are discussed in addition to methods for determining the cause of failure and the reconfiguration of the system following detection. Failure detection via the generation of indicator signals which are null in the absence of failure involves the use of redundancy or filtering techniques for the compression of information in the signal. Methods of material and analytic redundancy are considered, and techniques for arriving at redundancy relations of minimal complexity and optimal robustness (with respect to modeling error and uncertainty) are explored. Statistical tools for developing sequential decision rules are considered which are based on likelihood methods. 86/00/00 88A27767

UTTL: Modern control methods applied to a line-of-sight stabilization and tracking system

AUTH: A/HACSSIG, DAVID, JR.; B/DEGOTIIS, JAMES PAA: B/(Singer Co., Kearfoot Div., Little Falls, NJ) IN: 1987 American Control Conference, 5th, Minneapolis, MN, June 10-12, 1987, Proceedings, Volume 2 (A88-27301 10-63). New York, Institute of Electrical and Electronics Engineers, 1987, p. 1491-1498. Research supported by the Singer Co. and Texas Instruments, Inc.

ABS: Modern control methods are used to develop compensators for a precise optical positioning system designed to track a commanded line-of-sight (LOS) position while rejecting the vibrational environment of an F-16 fighter aircraft, the vehicle upon which the device will be mounted. The physical system being controlled consists of two gimbals that effect large changes in the LOS position, and a mirror assembly that is used, because of its fast dynamic response (but limited range of motion), to reduce LOS jitter (i.e. angular disturbances above 5 Hz that cause blurring). Compensators are designed that include models of the motion to reject and of the motion to track. These models become part of each compensator and enable them to distinguish aircraft vibration from aircraft maneuvers, rejecting the former and tracking the latter. The vibrational disturbance that must be rejected has a magnitude of 560 microrads rms, which is magnified by the optical system to 1400 microrads of LOS motion. Simulation of closed-loop performance with a nonlinear dynamic model of the system demonstrated that LOS jitter is reduced to about 130 microrads rms. A tradeoff between stabilization

and tracking is demonstrated. Compensator robustness to unmodelled disturbances is increased using the Loop-Transfer-Recovery technique. 87/00/00 88A27399

UTTL: Extensions of modern control and estimation methods to a military drive system

AUTH: A/KROK, MICHAEL J.; B/MUELLER, FREDERICK A. PAA: 8/(General Electric Co., Ordnance Systems Div., Pittsfield, MA) IN: 1987 American Control Conference, 6th, Minneapolis, MN, June 10-12, 1987, Proceedings, Volume 1 (A88-27301 10-63). New York, Institute of Electrical and Electronics Engineers, 1987, p. 737-744.

ABS: This paper investigates the application of Linear Quadratic Gaussian control to a nonlinear, military drive system. The major objective of this design is to eliminate the need of an expensive sensor used for disturbance measurement and, if possible, improve the system performance. Special attention is paid towards selecting efficient, accurate, control and estimator plant models. The resulting controller consists of a four state Linear Quadratic Regulator coupled with a eight state extended Kalman Filter, in addition to a nonlinear compensator to reduce multiplicative perturbations. The combined system was designed and evaluated via a detailed simulation. Baseline and sensitivity results indicate that the 'modern' controller performs as well as the classically designed system, but without the need for an expensive sensor used for disturbance measurement. 87/00/00 88A27394

UTTL: Order reduction in linear state estimation under performance constraints

AUTH: A/BARAM, YORAM; B/KALIT, GEDALIA PAA: A/(NASA, Ames Research Center, Moffett Field, CA); B/(Rafael Armament Development Authority, Haifa, Israel) CORP: National Aeronautics and Space Administration. Ames Research Center, Moffett Field, CA.; Rafael Armament Development Authority, Haifa (Israel). IEEE Transactions on Automatic Control (ISSN 0018-9286), vol. AC-32, Nov. 1987, p. 983-989.

ABS: The design and analysis of minimal-order state estimators for possibly time-varying linear systems, under constraints on the maximal allowable mean-square error, are considered. A global lower bound on the optimal error is derived, along with a lower bound on the minimal estimator order, needed for meeting the performance constraint. The ideal reduced-order estimator which satisfies the lower bound is derived, along with conditions for its realizability. When the ideal estimator is not realizable, its structure forms a suboptimal estimator, which maintains, in some sense, a local optimality property and is called the pseudooptimal estimator. The mean-square error of the pseudooptimal estimator defines upper bounds on the optimal error and on

the estimator order needed for meeting the performance constraint. The lower and the upper bounds on the order define a reduced search set for the design problem. When the distance between the ideal and the pseudooptimal estimators is sufficiently small in a certain numerical sense, the pseudooptimal estimator may be considered optimal for practical purposes. 87/11/00 88A18569

UTTL: New integration scheme of GPS-INS hybrid navigation system for maneuvering spacecraft

AUTH: A/TANABE, T.; B/HARIGAE, M.; C/KOYAMA, H. PAA: C/(Tokyo, University, Japan) IN: Automatic control in space 1985 (A88-16276 04-18). Oxford and New York, Pergamon Press, 1986, p. 211-217.

ABS: Integration schemes of the GPS with INS are considered. In the conventional navigation scheme, information from INS is usually used in the form of velocity-aiding signal to the receiver-tracking loops. In this paper, a new integration scheme is proposed which performs more effective information exchange so that it is more tolerant to RF interferences and unmodeled INS errors than the conventional scheme. These results are obtained from theoretical analyses and confirmed by computer simulations including GPS receiver dynamics. 86/00/00 88A16302

UTTL: On the hierarchical control of the Space Station common module thermal system

AUTH: A/LEWIS, F.; B/CHENG, J.; C/DAVEY, K.; D/VACHTSEVANDS, G.; E/PURVES, B. PAA: D/(Georgia Institute of Technology, Atlanta); E/(Boeing Aerospace Co., Huntsville, AL) IN: IEEE Conference on Decision and Control, 25th, Athens, Greece, Dec. 10-12, 1986, Proceedings, Volume 2 (A88-14926 04-63). New York, Institute of Electrical and Electronics Engineers, Inc., 1986, p. 868-872. Research supported by the Boeing Aerospace Co.

ABS: Bode plots of singular values vs. frequency were used to design several types of controllers for the Space Station common module Thermal Control System. Several controllers were designed, including a classical lead control loop with a multivariable disturbance input, and a multivariable output feedback controller. Singular value information was used to impose a hierarchical structure on the controller even though this structure was not natural to the plant; this permitted the design of local controllers with specified compensator structures; no undesirable additional dynamics in the form of observers or Kalman filters was needed. In addition, a method using singular values based on plant parameter variations was used to avoid gain scheduling. 86/00/00 88A14980

UTTL: Modeling of parameter variations and asymptotic LOG synthesis

AUTH: A/TAMK, MINJEA; B/SPEYER, JASON L. PAA: A/(Integrated Systems, Inc., Santa Clara, CA); B/(Texas, University, Austin) IEEE Transactions on Automatic Control: (ISSN 0018-9286), vol. AC-32, Sept. 1987, p. 793-801. Research supported by the General Dynamics Corp.

ABS: Conventional approaches in modern robustness and sensitivity theory are not adequate for the problems associated with parameter variation since the structure of parameter variations cannot be modeled properly or included in the synthesis procedure. A new modeling technique is proposed to handle a class of structured plant uncertainties in a direct way. The key is to treat deterministic parameter variations as an internal feedback loop so that the structure of parameter variations is embedded in its model. An asymptotic LQG design synthesis based on this modeling method is also presented. An important relationship between the structure of plant uncertainties and the LQG weighting matrices is obtained. This relationship clearly specifies the kind of parameter variations allowable for the LQG/LTR method. 87/09/00 87A52717

UTTL: Integral LQG controller design for a fighter aircraft.

AUTH: A/THOMPSON, CLAY M.; B/COLEMAN, EDWARD E.; C/BLIGHT, JAMES D. PAA: C/(Boeing Military Airplane Co., Seattle, WA) IN: AIAA Guidance, Navigation and Control Conference, Monterey, CA, Aug. 17-19, 1987, Technical Papers, Volume 2 (A87-50401 22-08). New York, American Institute of Aeronautics and Astronautics, 1987, p. 866-895.

ABS: An integral LQG design technique is presented using a manual lateral command and stability augmentation control law as an example. Rudder and ailerons are used to control sideslip and roll rate. An integral linear quadratic model-following regulator is used to obtain steady-state command following and robustness to aircraft parameter variations. An integral Kalman estimator provides steady-state sensor estimate tracking and robustness. The design technique addresses performance and flying qualities through the specification of explicit models and obtains robustness via the integral structure of both the regulator and estimator. The example control law shows excellent performance and robustness characteristics at the nominal design point and over a wide flight envelope using minimal gain scheduling.

RPT#: AIAA PAPER 87-2452 87/00/00 87A50498

UTTL: An application of modern decision and estimation theory to multimode guidance and data fusion

AUTH: A/TSO, GILBERT T.; B/FOX, JACKIE S. PAA: B/(Boeing Aerospace Co., Seattle, WA) IN: AIAA Guidance, Navigation and Control Conference, Monterey, CA, Aug. 17-19, 1987, Technical Papers, Volume 1 (A87-50401 22-08).

New York, American Institute of Aeronautics and Astronautics, 1987, p. 587-594.

ABS: Projected threat capabilities indicate increasingly more demanding requirements be met by the tracking and guidance system of advanced tactical missiles. In this paper, an approach to the problem of tracking a maneuvering target in a degraded environment is presented. The terminal guidance system studied is based upon a dual-mode, or multimode architecture where more than one complementary sensor is available for target acquisition and tracking. An approach for fusing measurements from multiple sensors via data compression and an invariant hypothesis testing technique derived from maximum a posteriori, Entropy Minimax rules operating on a set of sufficient statistics is discussed. This rule-based data fusion algorithm is combined with an adaptive Extended Kalman filter to provide the capability of maintaining an accurate track of a maneuvering target under non-ideal conditions. The performance of this approach is assessed against a typical air-to-air encounter in the presence of false targets and decoys.

RPT#: AIAA PAPER 87-2385 87/00/00 87A50470

UTTL: Estimation using a multirate filter

AUTH: A/ANDRISZHI, DOMINICK, II; B/CAU, CHIENG-FU PAA: B/(Purdue University, West Lafayette, IN) IEEE Transactions on Automatic Control (ISSN 0018-9286), vol. AC-32, July 1987, p. 653-656.

ABS: This note presents both optimal and suboptimal filtering algorithms for estimating state variables based on measurements sampled at two different data rates. The optimal algorithm consists of two parallel Kalman filters; one processes the fast rate measurement and is of reduced-order, and the other processes the residuals from the first filter along with the slow-rate measurement. This algorithm is used to design a suboptimal algorithm that has decreased computational requirements with only a small performance penalty. 87/07/00 87A46305

UTTL: Standard Integration Filter (SIF) - Design tradeoffs for strapdown INS

AUTH: A/CREMER, PAUL M.; B/GEYER, E. MICHAEL; C/GRAHAM, WILLIAM R. PAA: C/(Analytic Sciences Corp., Reading, MA) IN: PLANS '86 - Position Location and Navigation Symposium, Las Vegas, NV, Nov. 4-7, 1986, Record (A87-41351 18-17). New York, Institute of Electrical and Electronics Engineers, 1986, p. 468-475.

ABS: A 27-state three-axis Standard Integration Filter (SIF) which integrates the USAF Standard INS with external navigation aids has been formulated. This paper summarizes two key tradeoff investigations which were conducted in conjunction with the design of that portion of the filter which interfaces with the ring-laser gyro strapdown Standard INS. First, the state vector used to correct

AB5-43827. 87/06/00 87A40862

UTTL: Complementing INS with air data - An improved navigation system
 AUTH: A/ZHENG, E.; B/QIN, YONGYUAN PAA: B/(Northwestern Polytechnical University, Xian, People's Republic of China) Acta Aeronautica et Astronautica Sinica, Vol. 8, March 1987, p. A211-A215. In Chinese, with abstract in English.

ABS: In this paper, the characteristics of the hybrid navigation system which is composed of an air data computer and an inertial navigation system and is integrated by a Kalman filter are analyzed. The result of the computer simulation shows that it is possible to obtain a medium accurate hybrid system with use of a low accurate inertial system. The hybrid system can detect and compensate drifts of gyros and perform platform realignment during flying. 87/03/00 87A39411

UTTL: Suboptimal recursive estimation algorithms in navigation systems
 AUTH: A/ALEKSEEV, V. I. Radioelektronika (ISSN 0021-3470), vol. 30, March 1987, p. 34-39. In Russian.

ABS: Suboptimal recursive-search and nonresearch estimation algorithms are developed which are based on nonparametric averaging-operators. The properties of the algorithms are indicated, and computer-simulation results are presented on a linearized version of the recursive-search algorithm. 87/03/00 87A36040

UTTL: GR0 attitude control and determination
 AUTH: A/JERKOVSKY, M.; B/KERANEN, L.; C/KOEHLER, F.; D/TUNG, F.; E/WARD, B. PAA: D/(TRW, Inc., TRW Space and Technology Group, Redondo Beach, CA); E/(NASA, Goddard Space Flight Center, Greenbelt, MD); CORP: TRW, Inc., Redondo Beach, CA.; National Aeronautics and Space Administration. Goddard Space Flight Center, Greenbelt, MD. IN: Guidance and Control 1986; Proceedings of the Annual Rocky Mountain Guidance and Control Conference, Keystone, CO, Feb. 1-5, 1986 (AB7-32726 :3-18). San Diego, CA, Univelt, Inc., 1986, p. 177-198.

ABS: Design features of the attitude control and determination (ACAD) system for the Gamma Ray Observatory (GRO) that will eventually be launched on the Shuttle are described. A tabulation of the ACAD system components is provided and the various standby and normal pointing operational modes of the system are summarized. The system software and sensors will maintain a quaternion model of the GRO attitude on the bases of kinematic equations and inertial data. The software is standardized and has previously been used on the Solar Maximum Mission and Landsat-D. Details of the processing components, redundant electronics for sensor processing, data handling and actuator control are

level-axes INS errors is described and associated navigation error projections are presented. Then, the computational and accuracy tradeoffs involved in selecting the propagation algorithm for numerically integrating the filter differential equations are described. 86/00/00 87A41400

UTTL: Relativity correction in GPS user equipment
 AUTH: A/JORGENSEN, PAUL S. PAA: A/(Aerospace Corp., El Segundo, CA) IN: PLANS '86 - Position Location and Navigation Symposium, Las Vegas, NV, Nov. 4-7, 1986, Record (AB7-41351 18-17). New York, Institute of Electrical and Electronics Engineers, 1986, p. 177-183.
 ABS: The composite relativistic effects encountered in GPS satellite operations and requiring compensation in the user's associated equipment are due both to special relativity, as a consequence of the satellite's velocity, and general relativity, in virtue of gravitational potential differences. The dominant element in the composite effect is bias, which is compensated for by an offset of the satellite atomic frequency standards; the smaller element of the composite effect, on which emphasis is presently placed, involves corrective computations by means of an algorithm. 86/00/00 87A41374

UTTL: SITAN implementation in the SAINT system
 AUTH: A/FELLERHOFF, J. R. PAA: A/(Sandia National Laboratories, Albuquerque, NM) IN: PLANS '86 - Position Location and Navigation Symposium, Las Vegas, NV, Nov. 4-7, 1986, Record (AB7-41351 18-17). New York, Institute of Electrical and Electronics Engineers, 1986, p. 89-95.
 ABS: USAF-supported research.

The AFTI/F-16 Sandia Inertial Terrain-Aided Navigation (SITAN) system, which is a flight computer algorithm that yields accurate position corrections to an inertial navigation system, has been adapted for integration into the Sandia Aided-Inertial Navigation Testbed (SAINT) system and subsequently flight-tested. Attention is presently given to the AFTI/SITAN algorithm in the SAINT system, as well as to the flight test results obtained, which demonstrated reliable, accurate, and continuous estimation of aircraft position in the presence of large initial horizontal position errors. 86/00/00 87A41365

UTTL: On-line aircraft state and stability derivative estimation using the modified-gain extended Kalman filter
 AUTH: A/SPEYER, JASON L.; B/CRUES, EDWIN Z. PAA: B/(Texas, University, Austin) (Atmospheric Flight Mechanics Conference, 12th, Snowmass, CO, Aug. 19-21, 1985, Technical Papers, p. 1-9) Journal of Guidance, Control, and Dynamics (ISSN 0731-5090), vol. 10, May-June 1987, p. 262-268. Research sponsored by General Dynamics Corp. previously cited in issue 21, p. 3051, Accession no.

outlined and illustrated with block diagrams. Tests applied to validate the ACAD design are outlined, as are ground support which will be implemented once the GRD is launched.

RPT#: AAS PAPER 86-032 86/00/00 87A32737

UTTL: Extrapolation methods of design and control
AUTH: A/RASTRIGIN, LEONID ANDREEVICH; B/PONDOMAREV, IURII PETROVICH Moscow, Izdatel'stvo Mashinostroenie, 1986, 120 p. In Russian.

ABS: The present work considers the use of the multidimensional linear extrapolation (MLE) method to predict the parameters of complex systems with reference to their design and control. Numerous examples illustrate the performance of specific MLE algorithms; the accuracy of the MLE method is assessed; and ways to improve MLE methods are described. 86/00/00 87A32724

UTTL: A simulation tool for the study of satellite based navigation systems

AUTH: A/DE PAGTER, P. J.; B/DEKKER, G. J.; C/JOOSTEN, L. J. M. PAA: C/(Nationaal Lucht- en Ruimtevaartlaboratorium, Amsterdam, Netherlands) IN: International Symposium on Space Technology and Science, 15th, Tokyo, Japan, May 19-23, 1986, Proceedings, Volume 2 (A87-32276 13-12). Tokyo, AGNE Publishing, Inc., 1986, p. 1177-1185.

ABS: The development of the simulator, referred to as PROMISE, to study the system performance of various design alternatives for the Navsat system is examined. The simulation system consists of a library with independent models that simulate a specific part of the Navsat system and a simulator building tool that composes specific simulations from models selected from the library. The simulation models utilized to design the Navsat system are described. Consideration is given to orbit prediction error modeling, ionosphere modeling, and the user position estimation algorithm. 86/00/00 87A32433

UTTL: Filter controllers for bank-to-turn CLOS guidance
AUTH: A/FLEMING, R. J.; B/IRWIN, G. W. PAA: A/(Short Brothers, PLC, Belfast, Northern Ireland); B/(Belfast, Queen's University, Northern Ireland) IEE Proceedings, Part D - Control Theory and Applications (ISSN 0143-7054), vol. 134, pt. D, no. 1, Jan. 1987, p. 17-25.

ABS: Linear quadratic optimal filtering theory is used to extend a deterministic system for bank-to-turn control under CLOS guidance, for use in stochastic conditions. Both stationary and moving targets are treated, and the modifications to the deterministic designs are established. Simulation results demonstrate the potential of the new filter controllers for BTT control in terms of improved terminal accuracy and reduced susceptibility to noise-induced roll motion. 87/01/00 87A30391

UTTL: The LOG/LTR procedure for multivariable feedback control design
AUTH: A/STEIN, GUNTER; B/ATHENS, MICHAEL PAA: A/(Honeywell Systems and Research Center, Minneapolis, MN; MIT, Cambridge, MA); B/(MIT, Cambridge, MA) CORP: Honeywell Systems and Research Center, Minneapolis, MN.; Massachusetts Inst. of Tech., Cambridge, IEEE Transactions on Automatic Control (ISSN 0018-9236), vol. AC-32, Feb. 1987, p. 105-114. Research supported by the Honeywell Internal Research and Development Funds.

ABS: This paper provides a tutorial overview of the linear quadratic Gaussian with loop-transfer recovery (LOG/LTR) design procedure for linear multivariable feedback systems. LOG/LTR is interpreted as the solution of a specific weighted H-squared tradeoff between transfer functions in the frequency domain. Properties of this solution are examined for both minimum-phase and nonminimum-phase systems. This leads to a formal weight augmentation procedure for the minimum-phase case which permits essentially arbitrary specification of system sensitivity functions in terms of the weights. While such arbitrary specifications are not possible for nonminimum-phase problems, a direct relationship between weights and sensitivities is developed for nonminimum-phase SISO and certain nonminimum-phase MIMO cases which guides the weight selection process. 87/02/00 87A30091

UTTL: Linear-quadratic-Gaussian with loop-transfer recovery methodology for an unmanned aircraft
AUTH: A/REIDGELY, D. BRETT; B/BANDA, SIVA S.; C/MCQUADE, TIMOTHY E.; D/LYNCH, P. J. PAA: D/(USAF, Flight Dynamics Laboratory, Wright-Patterson AFB, OH) (AIAA, Guidance, Navigation, and Control Conference, Snowmass, CO, Aug. 19-21, 1985) Journal of Guidance, Control, and Dynamics (ISSN 0731-5090), vol. 10, Jan.-Feb. 1987, p. 82-89.

ABS: The linear-quadratic-Gaussian with loop-transfer-recovery methodology is considered for flight control design. Several advantages of this method, as well as some precautions that practicing designers should consider during application, have been highlighted. A roll attitude control system is designed for an unmanned aircraft using this methodology. It is demonstrated that this methodology is transparent in addressing such issues as uncertainty descriptions, stability robustness, trade-offs between robustness and available actuator power, bandwidth limitations, and prefilter design.

RPT#: AIAA PAPER 85-1927 87/02/00 87A28912

UTTL: Low cost Doppler aided strapdown inertial navigation system

AUTH: A/YUAN, XIN; B/YU, ZAIXIN PAA: B/(Nanjing Aeronautical Institute, People's Republic of China) Acta Aeronautica et Astronautica Sinica, vol. 7, Oct. 1986, p. 471-481. In Chinese, with abstract in English.

ABS: This paper presents a Doppler-aided strapdown inertial navigation system which adopts low accuracy inertial sensors. The configuration and dynamic equations of the integrated system are discussed and derived. One optimum Kalman filter and four suboptimum Kalman filters are designed and evaluated. A covariance analysis of the integrated system performance is completed. The results of the covariance analysis indicate that the integrated system which adopts the gyros with a random drift of 0.1 deg/h and the accelerometers with a bias of 10 to the -4th g can achieve the navigation accuracy of 1 nm/h by means of the Kalman filter. 86/10/00 87A24719

UTTL: Two-satellite navigation using LORAN and GPS
AUTH: A/KRUCZYNSKI, L.; B/ESCHENBACH, R. PAA: B/(Triable Navigation, Sunnyvale, CA) IN: Institute of Navigation, Annual Meeting, 42nd, Seattle, WA, June 24-26, 1986, Proceedings (A87-19351 06-04). Washington, DC, Institute of Navigation, 1986, p. 22-25.

ABS: A technique in which two satellites and one time difference (TD) are combined to generate a position fix is presented. The need for two satellite navigation is discussed. The basics of the algorithm are described, and interim test results are provided. Using this technique, up to 17 hours of position fixing is possible in locations where only one TD is available. This allows for position fixes when neither GPS nor LORAN are capable of position fixes on their own. 86/00/00 87A19354

UTTL: A modular flight control and navigation system for the next generation of Army aviation
AUTH: A/BYE, C. T.; B/BAKKEN, J. T.; C/SNYDER, S. I. PAA: C/(Honeywell, Inc., Minneapolis, MN) IN: American Helicopter Society, Annual Forum, 42nd, Washington, DC, June 2-4, 1986, Proceedings, Volume 2 (A87-19201 06-01). Alexandria, VA, American Helicopter Society, 1986, p. 1079-1089.

ABS: Unprecedented demands will be placed on the flight control and navigation equipment of the next-generation of Army helicopters to enable single crewmember operability in tactical environments. These demands require a degree of automation, and assurance of a level of pilot confidence not yet achieved on conventional present-generation vehicles. Trade studies have been performed concerning the significant issues involved in developing an optimum system architecture. The resulting architecture maximizes the sharing of sensor and computational resources in a flight-critical environment, and employs modular equipment packaging, dual fault-tolerant tetrad ring laser gyro inertial measurement units, and triplex self-checking

processor pair-based flight critical processing channels. 86/00/00 87A19282

UTTL: LQG/LTR design of a flight controller for a short take-off and landing aircraft
AUTH: A/GROSS, G. L.; B/HUSTON, R. A.; C/MAYBECK, P. S. PAA: C/(USAF, Institute of Technology, Wright-Patterson AFB, OH) IN: MAECON 1986; Proceedings of the National Aerospace and Electronics Conference, Dayton, OH, May 19-23, 1986, Volume 2 (A87-16726 05-01). New York, Institute of Electrical and Electronics Engineers, 1986, p. 415-420.

ABS: Two robust controllers for a STOL vehicle are developed via LQG/LTR methods. One of these controllers is developed for maneuvers at altitude and the other is for the approach and landing phase. Reduced-order full-state feedback controllers are synthesized using CGI/PI synthesis, specifically using implicit model following to provide good robustness characteristics in the full-state feedback case. The robustness is fully assessed using realistic simulations with meaningful deviations from design conditions. Once a Kalman filter is embedded in the loop to estimate states (rather than assuming artificial access to all states), LTR methodology is used to preserve as much robustness as possible. A full assessment of performance and robustness of these final implementable designs is provided. 86/00/00 87A16769

UTTL: GPS/INS integration using decoupled residual data
AUTH: A/EDSH, M. K.; B/YAKOS, M. D. PAA: B/(Rockwell International Corp., Collins Government Avionics Div., Cedar Rapids, IA) IN: ION, National Technical Meeting, Long Beach, CA, January 21-23, 1986, Proceedings (A87-19352 02-04). Washington, DC, Institute of Navigation, 1986, p. 117-119.

ABS: This paper describes a technique to efficiently integrate GPS with an INS. The proposed method uses GPS pseudorange and delta range residual data for incorporation into a central navigation Kalman filter. A data decoupling algorithm is described which allows use of the same residual data in two Kalman filters: one in the GPS set and the other in the central navigator. Data decoupling avoids the instability and correlation problems associated with operating two Kalman filters in a closed loop system. Performance data from field tests, using a single channel GPS receiver integrated with a strapdown INS, concludes this paper. 86/00/00 87A13546

UTTL: A tutorial on the LQG/LTR method
AUTH: A/ATHANS, M. PAA: A/(MIT, Cambridge, MA) CURP: Massachusetts Inst. of Tech., Cambridge, MA IN: 1986 American Control Conference, 5th, Seattle, WA, June 18-20, 1986, Proceedings, Volume 2 (A87-13301 03-63). New York,

Institute of Electrical and Electronics Engineers, 1986, p. 1289-1296.

ABS:

In this paper the so-called Linear-Quadratic-Gaussian method with Loop-Transfer-Recovery is surveyed. The objective is to provide a pragmatic exposition, with special emphasis on the step-by-step characteristics for designing multivariable feedback control systems.

86/00/00 87A13417

UTTL: Modern control theory for design of autopilots for bank-to-turn missiles

AUTH:

A/WILLIAMS, D. E.; B/FRIEDLAND, B. PAA: B/(Singer Co., Kearfoot Div., Little Falls, NJ) IN: 1986 American Control Conference, 5th, Seattle, WA, June 18-20, 1986, Proceedings, Volume 2 (A87-13301 03-63). New York, Institute of Electrical and Electronics Engineers, 1986, p. 1130-1136.

ABS:

The state-space techniques of modern control theory are used to develop a methodology for the design of autopilots for bank-to-turn missiles. The methodology accommodates the gyroscopic and coriolis cross-coupling between the pitch and the yaw axes that result due to the high roll rates that can be present. The design uses the assumption that the roll rate is constant, but not zero, and results in an autopilot structure in which there are cross-couplings between the pitch and yaw channels that are dependent on the roll rate. The autopilot gains are also scheduled as functions of the dynamic pressure. A reduced-order extended Kalman filter, with fixed gains, is used to estimate the actuator states and the commanded acceleration. The performance of an autopilot designed by this methodology was evaluated in a six-degree of freedom simulation using the dynamics of a typical high-performance tactical missile. Excellent performance was obtained in terms of low miss distance and small side-slip.

86/00/00 87A13405

UTTL: Residual gravity error modelling for high accuracy land navigation

AUTH:

A/HUBBS, R. A.; B/PINSON, D. C.; C/SMITH, J. M. PAA: C/(Rockwell International Corp., Autonetics Strategic Systems Div., Anaheim, CA) AIAA, Guidance, Navigation and Control Conference, Williamsburg, VA, Aug. 18-20, 1986, 15 p.

ABS:

Starting with a radially symmetric, covariant description of the earth's anomalous gravity field, techniques for finding the residual errors after local modelling are developed. The effects of using different measurement quantities (e.g. anomalies only or deflections only) are explored. For instance, it is shown for regularly gridded data, that specifying measurements of average anomaly is better than specifying samples of anomaly at the grid points. The implications of a limited rather than an infinite grid of measurements are discussed. Gauss-Markov

approximating models can be obtained for all cases using the Yule-Walker equations, spectral factorization, and some numerical curve fitting techniques. It is shown that models with as few as eight total states provide excellent approximations while retaining the important anomaly-track deflection correlation. Error analysis of a hypothetical, high accuracy, guidance system operating in a land navigation mode demonstrates a substantial performance advantage resulting from using residual gravity models which retain this physically motivated correlation. Some of the practical problems that would be encountered in an actual implementation of these techniques are discussed.

RPT#: AIAA PAPER 86-2099 86/08/00 86A47514

UTTL: Design considerations for flight test of a fault inferring nonlinear detection system algorithm for avionics sensors

AUTH:

A/CAGLAYAN, A. K.; B/CODINALA, P. M.; C/MORRELL, F. R. PAA: B/(Charles River Analytics, Inc., Cambridge, MA); C/(NASA, Langley Research Center, Hampton, VA) CORP: Charles River Analytics, Inc., Cambridge, MA.; National Aeronautics and Space Administration, Langley Research Center, Hampton, VA. AIAA, Guidance, Navigation and Control Conference, Williamsburg, VA, Aug. 18-20, 1986, 10 p.

ABS:

This paper summarizes the modifications made to the design of a fault inferring nonlinear detection system (FINDS) algorithm to accommodate flight computer constraints and the resulting impact on the algorithm performance. An overview of the flight data-driven FINDS algorithm is presented. This is followed by a brief analysis of the effects of modifications to the algorithm on program size and execution speed. Significant improvements in estimation performance for the aircraft states and normal operating sensor biases, which have resulted from improved noise design parameters and a new steady-state wind model, are documented. The aircraft state and sensor bias estimation performances of the algorithm's extended Kalman filter are presented as a function of update frequency of the piecewise constant filter gains. The results of a new detection system strategy and failure detection performance, as a function of an update frequency, are also presented.

RPT#: AIAA PAPER 86-2030 86/08/00 86A47511

UTTL: Frequency and time domain designs of a strapdown vertical determination system

AUTH:

A/BAR-ITZHACK, I. Y.; B/ZIV, I. PAA: A/(Technion - Israel Institute of Technology, Haifa, Israel) IN: Guidance, Navigation and Control Conference, Williamsburg, VA, August 18-20, 1986, Technical Papers (A86-47401 23-63). New York, American Institute of Aeronautics and Astronautics, 1986, p. 505-515. Research sponsored by Condor Pacific, Ltd.

ABS: An attractive alternative to the gyro for determining the direction of the vertical is introduced. The bulky inertial sensors are replaced by a couple of small strapdown lighter and smaller than the gyro, consumes less power, has larger MTBF, and its maintenance cost is lower. The system is described, and the computation involved in the determination of the vertical is shown. The filter design problem is described and addressed using the frequency domain approach. The time domain design of the system using the extended Kalman filter is described.

RPT#: AIAA PAPER 86-2148 56/00/00 86A47457

UTTL: A theory for fault-tolerant flight control combining expert system and analytical redundancy concepts

AUTH: A/STENGEL, R. F.; B/HADJELMAN, D. A. PAA: A/(Princeton University, NJ) IN: Guidance, Navigation and Control Conference, Williamsburg, VA, August 18-20, 1986. Technical Papers (A86-47401 23-63). New York, American Institute of Aeronautics and Astronautics, 1986, p. 375-384.

ABS: This paper presents a theory for rule-based fault-tolerant flight control. The objective is to define methods for designing control systems capable of accommodating a wide range of aircraft failures, including sensor, control, and structural failures. A software architecture is described that integrates qualitative analytical redundancy techniques and heuristic expert system concepts for the purpose of in-flight, real-time fault tolerance. The resultant controller uses a rule-based expert system approach to transform the problem of failure accommodation task scheduling and selection into a problem of search. Control system performance under sensor and control failures is demonstrated using linear discrete-time deterministic simulations of a tandem-rotor helicopter's dynamics. It is found that the rule-based control theory can be used to enhance existing redundancy management systems. This approach to control system design also provides inherent parallelism for computational speed, smooth integration of algorithmic and heuristic computation, a search-based decision-making mechanism, straightforward system organization and debugging, and an incremental growth capability.

RPT#: AIAA PAPER 86-2032 86/00/00 86A47442

UTTL: New V-Lambda square root filter

AUTH: A/BAR-ITZHACK, I. Y.; B/USHMANI, Y. PAA: A/(Technion - Israel Institute of Technology, Haifa) IN: Conference on Decision and Control, 24th, Fort Lauderdale, FL, December 11-13, 1985, Proceedings. Volume 3 (A86-42851 20-63). New York, Institute of Electrical and Electronics Engineers, Inc., 1985, p. 1640-1645.

ABS: Two new square-root Kalman filtering algorithms are presented. Both algorithms are based on the spectral

factors V-Lambda of the covariance matrix, where V is the matrix whose columns are the eigenvectors of the covariance and Lambda is the diagonal matrix of its eigenvalues. The algorithms use the covariance mode in the time-propagation stage and the information mode in the measurement-update stage. This switch between modes, which is trivial in the V-Lambda representation, increases the efficiency of the algorithms. In the first algorithm, which is continuous/discrete, the V and square root Lambda matrices are propagated in time in a continuous manner, while the measurement update is a discrete-time procedure. In the second algorithm, which is discrete/discrete, the time propagation of the V-square root Lambda factors is also performed in discrete time. The square-root nature of the algorithm is demonstrated numerically through a typical example. While promising all the virtues of square-root routines, the V-Lambda filters are also characterized by their ability to exhibit singularities as they occur.

85/00/00 86A42987

UTTL: The optimal projection equations for reduced-order, discrete-time modelling, estimation and control

AUTH: A/BERNSTEIN, D. S.; B/DAVIS, L. D.; C/GREELEY, S. W.; D/HYLAND, D. C. PAA: D/(Harris Corp., Government Aerospace Systems Div., Melbourne, FL) IN: Conference on Decision and Control, 24th, Fort Lauderdale, FL, December 11-13, 1985, Proceedings. Volume 1 (A86-42851 20-63). New York, Institute of Electrical and Electronics Engineers, Inc., 1985, p. 573-578.

ABS: The optimal projection equations derived previously for reduced-order, continuous-time modelling, estimation and control are developed for the discrete-time case. The design equations are presented in a concise and unified manner to facilitate their accessibility for the development of numerical algorithms for practical applications. As in the continuous-time case, the standard Kalman filter and linear-quadratic-Gaussian results are immediately obtained as special cases of the estimation and control results. 85/00/00 86A42901

UTTL: Linear quadratic approach to optimal control and estimation in bank-to-turn CLOS guidance

A/RODDY, D. J.; B/IRWIN, G. W.; C/FLEMING, R. J. PAA: C/(Belfast, Queen's University, Northern Ireland) IN: Control 85; Proceedings of the International Conference, Cambridge, England, July 9-11, 1985, Volume 2 (A86-40751 19-63). London/New York, Institution of Electrical Engineers/IEE Inspec, 1985, p. 458-463.

ABS: A PD controller has been designed which optimizes the step response of the roll loop in the command-to-line-of-sight (CLOS) guidance of a bank-to-turn missile. Improved performance is achieved in terms of keeping the roll error small and in reducing the cross-coupling between roll and lateral dynamics. The introduction of rudder action, to

deal with cross-coupling directly, is discussed; and an LQ optimal control law for the rudder angle is derived; the success of this is demonstrated by computer simulation results. Finally, the single-plane controller design is augmented by the use of a Kalman filter for state estimation. 85/00/00 86A40770

UTTL: Factorized extended Kalman filter for optical processing

AUTH: A/FISHER, J. L.; B/CASASENT, D. P.; C/NEUMAN, C. P.

PAA: C/(Carnegie-Mellon University, Pittsburgh, PA)
Applied Optics (ISSN 0003-6935), vol. 25, May 15, 1986, p. 1615-1621. DDD-supported research.

ABS: Kalman filtering represents formidable linear algebra computational requirements for each new input measurement vector. An architecture-motivated implementation of a discrete-time Kalman filter algorithm is presented. This particular formulation takes advantage of the following features of the optical processor architecture: the ability to perform matrix-vector operations, floating-point capabilities, and specially designed matrix-vector LU decomposition operations. A factorized LDL(T) algorithm is used to propagate the covariance matrices between sample times. The air-to-air missile guidance problem is used as a case study wherein an extended Kalman filter is required due to the nonlinear nature of the measurement equations.

RPT#: AD-A179299 86/05/15 86A40640

UTTL: Evaluation of performance characteristics for a space antenna system subjected to stochastic disturbances

AUTH: A/ANANTHAKRISHNAN, S.; B/BAIUM, P. M.; C/REDDY, A. S.

S. R. PAA: C/(Howard University, Washington, DC) CORP: Howard Univ., Washington, DC. IN: Dynamics and control of large structures; Proceedings of the Fifth Symposium, Blacksburg, VA, June 12-14, 1985 (A86-39476 18-18). Blacksburg, VA, Virginia Polytechnic Institute and State University, 1985, p. 77-91. Research supported by Howard University.

ABS: Control system synthesis for a large space antenna system is investigated based on stochastic linear optimal control techniques and the minimization of a quadratic Gaussian performance index. Parametric studies indicate that suitable combinations of plant and sensor noise characteristics, and state weighting matrices, can be found to meet the mission RMS pointing requirements. Using a combination of the Kalman filter and linear feedback, an optimal control law for the finite element model of the Hoop/Column structural system without damping is obtained. Removing the hoop-mounted actuator resulted in an increase in the RMS errors, an increased control effort, and an increase in the least damped modal time constant. Removing the hoop-mounted sensor resulted in an RMS error increase and estimator performance degradation, with less system

RMS performance degradation than noted for removal of the hoop-mounted actuator. 85/00/00 86A39482

UTTL: Design and simulation of closed-loop ground alignment of inertial platforms with sway motion

AUTH: A/VATHSAL, S. PAA: A/(NASA, Goddard Space Flight Center, Greenbelt, MD) CORP: National Aeronautics and Space Administration, Goddard Space Flight Center, Greenbelt, MD. Journal of Guidance, Control, and Dynamics (ISSN 0731-5090), vol. 9, May-June 1986, p. 332-338. Research supported by the Alexander von Humboldt-Stiftung and U.S. National Research Council.

ABS: This paper is concerned with the application of optimal estimation and control concepts to the ground alignment of inertial platforms subjected to random sway motion. A seventh-order Kalman filter has been designed for estimating the platform misalignments and sway motion. Using the linear quadratic optimal regulator techniques, feedback controller gains have been designed to drive the initial misalignments to a small value. A reconfiguration of the filter controller scheme has been proposed and verified by Monte Carlo simulation for improving the speed of alignment without changing the alignment accuracy.

86/06/00 86A39040

UTTL: Adaptive flight control of unstable helicopters during transition

AUTH: D/GHITA, H.; B/YOKOKURA, S.; C/NIKIFORUK, P. N.; D/GUPTA, M. M. PAA: B/(Nagoya University, Japan); D/(Saskatchewan, University, Saskatoon, Canada) IN: A

bridge between control science and technology. Volume 2 (A86-33143 14-63). Oxford and New York, Pergamon Press, 1985, p. 1045-1050. Research supported by the Ministry of Education of Japan.

ABS: The design of an adaptive control system for a helicopter during transitional flight conditions is discussed. A mathematical model of the controlled plant and a model reference adaptive system (MRAS) is described. The identification speed and control performance of the system are examined. Simulation studies that reveal the problems associated with the identification and control techniques are presented. An adaptive algorithm based on MRAS and developed using the discrete Kalman filter is proposed. Stability derivative data are employed to predict the time-varying characteristics of the parameters. Examples displaying the applicability of the adaptive flight control system are provided. 85/00/00 86A33178

UTTL: Dual control for identification and guidance

AUTH: A/BIRNIVAL, K.; B/BAR-SHALOM, Y. PAA: B/(Connecticut, University, Storrs) IN: A bridge between control science and technology. Volume 2 (A86-33143 14-63). Oxford and New York, Pergamon Press, 1985, p. 841-846.

ABS:

An adaptive dual control guidance algorithm is presented for intercepting a moving target in the presence of an interfering target (decoy) in a stochastic environment. Two sequences of measurements are obtained at discrete points in time; however, it is not certain, which sequence came from the target of interest and which from the decoy. Associated with each track, the interceptor also receives noisy, state dependent feature measurements. The optimum control for the interceptor which is given by the solution of the stochastic dynamic programming equation is not numerically feasible to obtain. An approximate solution of this equation is obtained by evaluating the value of the future information gathering. This is done through the use of preposterior analysis—approximate prior probability densities are obtained and used to describe the future learning and control. In this way, the interceptor control is used for information gathering in order to reduce the future target and decoy inertial measurement errors and enhance the observable target/decoy feature differences for subsequent discrimination between the true target and the decoy. 85/00/00 86A33163

UTTL: Design of radio signal filter systems

AUTH: A/KAZARINOV, I.U. M.; B/SOKOLOV, A. I.; C/IURCHENKO, I.U. S. Leningrad, Izdatel'stvo Leningradskogo Universiteta, 1985, 160 p. In Russian.

ABS: Methods for the design of filter systems for radio signals that are used in problems of secondary signal processing are examined, with particular attention given to the design of suboptimal filters. In contrast to the well-known optimal recurrent filtering algorithms of the Kalman filter type, suboptimal filters require less computational effort and therefore are widely used in radio systems employing minicomputers and microprocessors. Simple methods are presented for evaluating filtering efficiency in systems of automatic signal analysis and location of objects in space. 85/00/00 86A29845

UTTL: GPS aided inertial navigation

AUTH: A/NIELSON, J. T.; B/SWEARINGEN, G. W.; C/WITSMEER, A. J. PAA: C/(Boeing Aerospace Co., Seattle, WA) IEEE Aerospace and Electronic Systems Magazine (ISSN 0885-8985), vol. 1, March 1986, p. 20-26.

ABS: The Global Positioning System is an extremely accurate satellite-based navigation system which, after its completion in 1989, will provide users worldwide, 24 hour, all weather coverage. A joint research project among Boeing, Rockwell-Collins, and Northrop has been completed in which a GPS receiver was integrated with a low-cost strap-down inertial navigation system and a flight computer. A Kalman filter in the latter allows in-flight alignment and calibration of the INS. In addition, feedback from the INS to the GPS receiver improves the system's ability to reacquire satellite signals after

outages. The resulting system combines the accuracy of GPS with the jamming immunity and autonomy of inertial navigation. System tests were conducted in which a Boeing owned T-33 jet aircraft was flown through known test patterns to align and calibrate the INS. Earlier tests, including test against an airborne jammer, were conducted in a modified passenger bus. 86/03/00 86A29300

UTTL: Adaptive field of view expansion via multiple model filtering for tracking dynamic target images

AUTH: A/MAYBECK, P. S.; B/SUITZ, R. I. PAA: B/(USAF, Institute of Technology, Wright-Patterson AFB, OH) IN: NAEDCM 1985; Proceedings of the National Aerospace and Electronics Conference, Dayton, OH, May 20-24, 1985. Volume 1 (A86-28326 12-04). New York, Institute of Electrical and Electronics Engineers, 1985, p. 364-373.

ABS: Multiple model adaptive estimation is investigated as a means of changing the field-of-view as well as the bandwidth of an infrared image tracker against a wide dynamic range of targets. The multiple models are created by tuning the filters for best performance at differing conditions of exhibited target behavior and differing the physical size of their respective fields of view, and probabilistically weighted averaging provides the adaptation mechanism. Each filter involves online identification of the target shape function, so that this algorithm can be used against ill-defined and/or multiple-hot-spot targets. When each individual filter has the form of an enhanced correlator/linear Kalman filter, computational loading is very low, whereas an extended Kalman filter, processing the raw infrared data directly and assuming a nonlinear constant turn-rate target dynamics model provides superior tracking capability, especially for harsh maneuvers. 85/00/00 86A28371

UTTL: JTIDS RELNAV performance evaluation

AUTH: A/MURPHY, M. S.; B/LINDGREN, J. PAA: A/(VERAC, Inc., San Diego, CA); B/(USAF, Eglin AFB, FL) IN: NAEDCM 1985; Proceedings of the National Aerospace and Electronics Conference, Dayton, OH, May 20-24, 1985. Volume 1 (A86-28326 12-04). New York, Institute of Electrical and Electronics Engineers, 1985, p. 343-350.

ABS: The Joint Tactical Information Distribution System (JTIDS) Test Data Optimal Processor (JTIDS TDOP) has been developed, as a tool for the postflight assessment and error allocation of the JTIDS relative navigation (RELNAV) function, which is scheduled for testing during 1985/1986. The JTIDS TDOP utilizes advanced numerical techniques to implement an extended Kalman filter-based navigation smoothing algorithm, which integrates test data from JTIDS, INS, and test-range tracking instrument sources. The Optimal Processor will create accurate trajectory estimates, assess JTIDS RELNAV compliance to accuracy requirements, and analyze actual navigation errors into

the contributing causes, thus providing a tool for DT&E test planning. The performance expected from the JTIDS TDOP system was tested on a simulated three-aircraft scenario. 85/00/00 86A28369

UTTL: Decentralization filtering and redundancy management/failure detection for multisensor integrated navigation systems

AUTH: A/KERR, T. H. PAA: A/(Intermetrics, Inc., Cambridge, MA) IN: Institute of Navigation, National Technical Meeting, San Diego, CA, January 15-17, 1985, Proceedings (A86-26426 11-04). Washington, DC, Institute of Navigation, 1985, p. 191-208.

ABS: Current failure detection isolation and reconfiguration procedures applicable to navigation systems are reviewed. The design of a failure detection/redundancy management technique which incorporates voter monitoring methodology, decentralized Kalman filter mechanization, and a semiautonomous multisensor navigation system is described. The technique involves the use of Gaussian confidence regions to account for the inherent difference in accuracy between the various sensor subsystems and on-line estimates of covariances from the Kalman filter are utilized for this assessment. The technique evaluates the probability of detecting failed component subsystems and the probability of false alarms to be incurred. The development of a Kalman filter on a chip is analyzed. 85/00/00 86A26443

UTTL: Global positioning system operational control system accuracies

AUTH: A/BOWEN, R.; B/SWANSON, P. L.; C/MINN, F. B.; D/RHODUS, W. W.; E/FEES, W. A. PAA: A/(USAF, Space Div., El Segundo, CA); E/(Aerospace Corp., El Segundo, CA) IN: Institute of Navigation, National Technical Meeting, San Diego, CA, January 15-17, 1985, Proceedings (A86-26426 11-04). Washington, DC, Institute of Navigation, 1985, p. 60-66.

ABS: The present study examines the stability, consistency, and accuracy of the Global Positioning System's Initial Control System (ICS), and the Operational Control System (OCS) replacing it. OCS improvements include a global network of ground antennas to upload satellite navigation data, and a refined Kalman filter capable of continuously estimating the GPS satellite ephemerides, clock phases, and frequencies. Using real and simulated GPS pseudo range radiometric tracking data, a detailed error analysis reveals that the satellite clock noise contributes more than 90 percent of the total satellite-to-user pseudo range error. With the planned increase in OCS uploads to three a day, the accuracy of the navigation service is expected to improve by nearly a factor of three because the clock-noise contribution to the range error increases linearly with time. The analysis data presented also show

the consequence of satellite ephemeris uncertainties in the GPS navigation application. 85/00/00 86A26430

UTTL: The proper computation of the matrix pseudoinverse and its impact in MVRO filtering

AUTH: A/KERR, T. H. PAA: A/(Intermetrics, Inc., Cambridge, MA) IEEE Transactions on Aerospace and Electronic Systems (ISSN 0018-9251), vol. AES-21, Sept. 1985, p. 711-724.

ABS: Simple nonpathological counterexamples are used to demonstrate the problems inherent in conventional approaches to matrix pseudoinverse calculation for navigation applications. An alternative matrix pseudoinverse algorithm based on the singular-value decomposition (SVD) approach is described, and some sample calculations are carried out. Specific results are presented for a minimum variance reduced-order (MVRO) design methodology for selecting reduced-order filters for navigation applications. The nontrivial block calculations and condition-checking procedures in the MVRO are discussed, and a potential source of error in applying the MVRO to Kalman filter design is identified. 85/09/00 86A10199

UTTL: Finite wordlength design of digital Kalman filters for state estimation

AUTH: A/WILLIAMSON, D. PAA: A/(New South Wales, University, Kensington, Australia) IEEE Transactions on Automatic Control (ISSN 0018-9286), vol. AC-30, Oct. 1985, p. 930-939.

ABS: The optimal design of a Kalman filter is considered with respect to its finite wordlength (FWL) characteristics taking into account the roundoff noise due to state quantization. The issues are particularly relevant in the design of FWL Kalman filters for continuous-time systems operating under a fast sampling rate. In this respect, the results demonstrate one compromise between the selection of the sampling rate and the selection of the state wordlength. The optimum filter structure includes state residue feedback compensation which can result in the saving of many bits of additional state wordlength. 85/10/00 86A10180

UTTL: Linear statistical methods for the processing of measurements on an increasing sample in the presence of errors in the spacecraft-motion model

AUTH: A/NEVOLKO, M. P.; B/MIKHAILOV, A. V.; C/KULNEV, V. V. Kosmicheskie Issledovaniya (ISSN 0023-4206), vol. 23, July-Aug. 1985, p. 535-546. In Russian.

ABS: An algorithm for processing full-sample measurements in the state-vector estimation of a spacecraft with errors in the motion model is presented. A rigorous solution of the navigation problem requires the examination of a set of nonlinear two-point boundary value problems, which in the

linear case yield recursive Kalman-Bucy algorithms. A theorem is demonstrated concerning the equivalence of estimates obtained through the solution of linear two-point boundary value problems and estimates obtained through the processing of the full sample of measurements or an increasing sample with inclusion of the error vector in the motion model. Equations for an increasing sample with an expanded state vector due to errors in the motion model are compared with estimates obtained through the solution of the Wiener-Hopf matrix equation without an increase in the dimensionality of the state vector.

85/06/00 85A49754

UTTL: Control system reconfiguration

AUTH: A/VANDER VELDE, W. E. PAA: A/(MIT, Cambridge, MA)
CORP: Massachusetts Inst. of Tech., Cambridge. IN: 1984
American Control Conference, San Diego, CA, June 6-8,
1984, Proceedings. Volume 3 (A85-47676 23-63). New York,
IEEE, 1984, p. 1741-1745.

ABS: The problem of reconfiguring a control system to accommodate the failure of a sensor or actuator is discussed in the context of several different system configurations. First, some ground rules under which the reconfiguration algorithms are to function are established. A variety of control system configurations is then considered, and it is found that the approach to reconfiguration is obvious in some cases but not clear in others. Several possible strategies for reconfiguration, applicable to different situations, are examined.

84/00/00 85A47793

UTTL: The modified gain extended Kalman filter and parameter identification in linear systems

AUTH: A/SUNG, T. L.; B/SPEYER, J. L. PAA: B/(Texas, University, Austin) IN: 1984 American Control Conference, San Diego, CA, June 6-8, 1984, Proceedings. Volume 2 (A85-47676 23-63). New York, IEEE, 1984, p. 1077-1084.

ABS: For a special class of systems, a general formulation and stochastic stability analysis of a new nonlinear filter, called the modified gain extended Kalman filter (MGKEF), is presented. Used as an observer, it is globally exponentially convergent. In the stochastic environment a nominal nonrealizable filter algorithm is developed for which global stochastic stability is proven. With respect to this nominal filter algorithm, conditions are obtained such that the effective deviations of the realizable filter are not destabilizing. In an appropriate coordinate frame, the parameter identification problem of a linear system is shown to be a member of this special class. For the example problems, the MGKEF shows superior convergence characteristics without evidence of instability.

84/00/00 85A47751

UTTL: Star-sensor-based satellite attitude/rate estimator
AUTH: A/GAI, E.; B/DALY, K.; C/HARRISON, J.; D/LEMONS, L.
PAA: B/(Charles Stark Draper Laboratory, Inc., Cambridge, MA) JOURNAL OF Guidance, Control and Dynamics (ISSN 0731-5090), vol. 8, Sept.-Oct. 1985, p. 560-565.

ABS: Up to now, sensitivity and bandwidth limitations of available star sensors have prevented the use of such devices as a primary sensor for on-orbit attitude rate determination. Recent advances in star sensor technology make it possible to consider practical implementations of on-orbit attitude determination and control systems based solely on star sensor measurements. The present paper provides a description of the design and evaluation of a star-sensor-based attitude determination and control system for some special applications. Particular attention is given to the development of a practical filter implementation for estimating attitude and attitude rate based solely on star sensor measurements. 85/10/00 85A46328

UTTL: Distributed Kalman filter in an integrated SAHRS/GFS navigation system

AUTH: A/CHIN, H. H. PAA: A/(Grumman Corp., Bethpage, NY) IN: Guidance, Navigation and Control Conference, Snowmass, CO, August 19-21, 1985, Technical Papers (A85-45876 22-08). New York, AIAA, 1985, p. 209-222. Research supported by Grumman Corp.

ABS: A new system design of a distributed Kalman filter (DKF) for a navigation system with integrated sensors is discussed which will ease computer load and improve system reliability. The system is based on three major components, the Global Positioning System, the Strapdown Attitude Heading Reference System, and the DKF; the latter blends information from the other two. The algorithm for the DKF is presented, and a simulation analysis is given. The performance verification of the design is reported.

RPT#: AIAA PAPER 85-1878 85/00/00 85A45901

UTTL: Bandwidth requirements for sea skimming guidance

AUTH: A/DOWDLE, J. R.; B/KIM, P. PAA: B/(Martin Marietta Aerospace, Orlando, FL) IN: Guidance, Navigation and Control Conference, Snowmass, CO, August 19-21, 1985, Technical Papers (A85-45876 22-08). New York, AIAA, 1985, p. 170-175.

ABS: This paper addresses the problem of implementing a full-state attitude control law for a supersonic sea skimming missile using state estimates from a Kalman filter. Specifically, the performance of the attitude control system is evaluated as a function of the Kalman filter bandwidth for a given full-state feedback design, and the optimal bandwidth is selected. Simulation results are included to indicate expected system performance.

RPT#: AIAA PAPER 85-1867 85/00/00 85A45896

image processing, target recognition/acquisition, airborne radar and fire control, navigation, air data, weapon guidance and control, Kalman filtering, power generation and control, and flying qualities. Attention is given to integrated control, flight management, multivariable control, self-repairing flight control, all-electric aircraft, digital flight control architecture and reliability, advanced software tools, software acquisition and test issues, software management and quality assurance, expert systems, trends in artificial intelligence, and engineering management. Other areas considered include system performance and workload assessment, human/machine system analysis, advanced avionics display content, reliability, life cycle cost, and flight training and simulation. 84/00/00 85A44976

UTTL: Atmospheric Flight Mechanics Conference, 12th.

Snowmass, CO, August 19-21, 1985. Technical Papers Conference sponsored by AIAA. New York, AIAA, 1985, 553 p. For individual items see A85-43827 to A85-43877.

ABS: Among the topics discussed are the estimation of aircraft stability derivatives by means of the modified gain-extended Kalman filter, robust parameter identification for nonlinear systems using a principal-components regression algorithm, a Joukowski airfoil with circulation control, aircraft wake hazard alleviation associated with roll oscillations, predicting the nonlinear aerodynamic characteristics of maneuvering missiles, minimum time-turning, energy management in three-dimensional minimum time interception, cross-coupling in pilot/vehicle systems, and the aerodynamic effects of asymmetric vortex shedding from slender bodies. Also covered are the vortex flow effects of a fighter forebody with unconventional cross section, drag reduction by means of controlled separated flows, a historical review of canard configurations, supersonic flow prediction, Godunov's method for supersonic tactical missile computations, the application of inviscid multiple zones to supersonic missiles, an atmospheric guidance law for planar skip trajectories, measurements of canard-induced roll oscillations, and optical flight paths through microburst wind profiles. 85/00/00 85A43826

UTTL: Observability of relative navigation using range-only measurements

AUTH: A/SCHNEIDER, A. M. PAA: A/(California, University, La Jolla) IEEE Transactions on Aerospace and Electronic Systems (ISSN 0018-9251), vol. AES-21, July 1985, p. 569-581.

ABS: A stimulation tool is described which is capable of determining the observability of various fleet configurations and maneuvers in a relative navigation environment. The motion of the relative grid established by the navigation controller is explicitly modeled as a

UTTL: Robustness enhancement for LQG digital flight controller design

AUTH: A/MAYBECK, P. S.; B/MILLER, W. G.; C/HOMEY, J. M. PAA: C/(USAF, Institute of Technology, Wright-Patterson AFB, OH) IN: NAECON 1984: Proceedings of the National Aerospace and Electronics Conference, Dayton, OH, May 21-25, 1984. Volume 1 (A85-44976 21-01). New York, IEEE, 1984, p. 518-525.

ABS: Controllers designed by means of the LQG (Linear system Quadratic cost - Gaussian noise) methodology have the structure of a full-state feedback controller, but with states as estimated by a Kalman filter. Full-state feedback controllers vary in robustness, but all meet or exceed fundamental stability robustness guarantees, while insertion of the filter into the controller removes such guarantees. To enhance controller characteristics, implicit model-following is used to generate very robust full-state feedback laws, and then the filter is tuned in a particular manner to allow a symptotic recovery of these particularly good robustness properties. These two means of enhancement are applied to a specific digital flight controller design and their capabilities are assessed. 84/00/00 85A45048

UTTL: Interfacing Kalman filters with the standard INS

AUTH: A/GRIFFITHS, B. E.; B/GEYER, E. M.; C/BERNING, S. L. PAA: B/(Analytical Sciences Corp., Reading, MA); C/(USAF, Wright Aeronautical Laboratories, Wright-Patterson AFB, OH) IN: NAECON 1984: Proceedings of the National Aerospace and Electronics Conference, Dayton, OH, May 21-25, 1984. Volume 1 (A85-44976 21-01). New York, IEEE, 1984, p. 414-421.

ABS: This paper presents initial results of an ongoing assessment of integrated navigation system accuracy sensitivity to the mechanization and instrument characteristics of the Standard Medium Accuracy INS. Linear covariance analysis is employed to predict integrated system performance for two flight trajectories, gimbaled platform and ring laser gyro strapdown INSs, and two NAVJAD suites. Cases where the associated Kalman filter is matched and mismatched to the INS are considered. 84/00/00 85A45033

UTTL: NAECON 1984: Proceedings of the National Aerospace and Electronics Conference, Dayton, OH, May 21-25, 1984. Volumes 1 & 2 Conference sponsored by IEEE, New York, IEEE, 1984, Vol. 1, 736 p.; Vol. 2, 768 p. For individual items see A85-44977 to A85-45161.

ABS: Developments related to VLSI are discussed along with topics concerned with signal processing, cartographic data uses, data transmission, avionics system topics, multiapplication signal processing architectures, airborne

function of the errors in his dead-reckoning sensors. The simulation uses centralized, optimal processing of an extended Kalman filter. Results show observability on a good geometry, with some degradation in performance when dead-reckoning sensor errors change rapidly. 85/07/00 85A42399

UTTL: Algorithms for improved, heading assisted, maneuver tracking
AUTH: A/LEFAS, C. C. PAA: A/(Nuclear Research Centre, Athens, Greece) IEEE Transactions on Aerospace and Electronic Systems (ISSN 0018-9251), vol. AES-21, May 1985, p. 351-359. Research supported by EUROCONTROL.

ABS: The evolution of the SSR mode S system makes it possible to receive airborne measurements at the ground station. The possibility of using data-linked heading measurements to assist present trackers to track maneuvering aircraft is investigated. The quality to be expected from heading measurements is investigated from available on-board recordings. Maneuver detection and false measurement rejection schemes are developed, and finally suitable maneuver tracking filters are constructed and evaluated. 85/05/00 85A39458

UTTL: Integration of the B-52G Offensive Avionics System (OAS) with the Global Positioning System (GPS)
AUTH: A/FOOTE, A. L.; B/PLUMTZE, S. C. PAA: A/(Logicon, Inc., Dayton, OH); B/(USAF, Space Div., Los Angeles, CA) IN: Institute of Navigation, National Technical Meeting, San Diego, CA, January 17-19, 1984, Proceedings (A85-38526 17-04). Washington, DC, Institute of Navigation, 1984, p. 201-209.

ABS: Integration of the B-52G OAS with the GPS has been accomplished by modification of existing OAS software. GPS derived position and velocity data are used to enhance the quality of the OAS inertial and dead reckoning navigation systems. The engineering design and the software development process used to implement this design are presented. 84/00/00 85A38545

UTTL: JTIDS relative navigation with measurement sharing - Design and performance
AUTH: A/WIDNALL, W. S.; B/KELLEY, J. F. PAA: A/(MIT, Cambridge, MA); B/(Hughes Aircraft Co., Ground Systems Group, Fullerton, CA) IN: PLANS '84 - Position Location and Navigation Symposium, San Diego, CA, November 26-29, 1984, Record (A85-3780: 17-17). New York, Institute of Electrical and Electronics Engineers, Inc., 1984, p. 327-334.

ABS: Alternate approaches for conducting relative navigation (relnav) using the JTIDS communication network are presented. The design and performance of the current JTIDS relnav with estimate sharing of discussed, including its

shortcomings. We offer first a conceptually simpler alternate design that provides more accurate relnav between a pair of members, provided they have time to maneuver. A second alternate design includes the features of the first plus adds measurement sharing by designated primary members. It has even better performance including faster more accurate relnav fixes and relaxed maneuvering requirements. Simulation results are presented showing the superior performance of the new designs. The advantages and disadvantages of relnav with measurement sharing compared with relnav with estimate sharing are summarized. 84/00/00 85A37836

UTTL: The design, development, and flight testing of a modern-control-designed autoland system
AUTH: A/HJESCHEN, R. M. PAA: A/(NASA, Langley Research Center, Hampton, VA) CORP: National Aeronautics and Space Administration, Langley Research Center, Hampton, VA. Institute of Electrical and Electronics Engineers and American Automatic Control Council, American Control Conference, Boston, MA, June 19-21, 1985, Paper, 9 p. This paper discusses the design, development, and flight test results of a full-state feedback

modern-controls-designed autoland system - the Digital Integrated Automatic Landing System (DIALS). The lateral and longitudinal control laws were designed by formulating a linear quadratic regulator with disturbances problem. Although the designs were independent of each other, in implementation cross-coupling of the lateral and longitudinal variables does occur. A brief discussion of the control modes - localizer capture, localizer track, decrab, glideslope capture, glideslope track, and flare - and the modifications made to the basic design during the simulation phase to achieve desired performance is given. Some of the efforts required to implement the system in the flight computers and some problems encountered in the ground hardware simulation checkout are discussed. Finally, flight test data is presented for this system which performed 10 'hands off' automatic landings. The flight test data includes the performance of the aircraft in mild, gust, and wind shear conditions. 85/06/00 85A35581

UTTL: Global stability/local optimality trade-offs in a class of decentralized integrated communication-navigation filters
AUTH: A/CHIN, L.; B/FAM, A. PAA: A/(U.S. Naval Material Command, Naval Air Development Center, Warminster, PA); B/(New York, State University, Amherst, NY) IN: Conference on Decision and Control, 22nd, San Antonio, TX, December 14-16, 1983, Proceedings, Volume 1 (A85-33251 14-63). New York, Institute of Electrical and Electronics Engineers, Inc., 1983, p. 347-352.

ABS: Application of decentralized filters to improve the

performance of relative navigation functions of an integrated communication-navigation system is discussed. The general form of the Supplemental Partitioning Approach (SPA) decentralized algorithm is derived. Trade-off criteria between global stability and local optimality of the decentralized system is introduced. It is found that the Riccati equation perturbation method seems to be a promising approach to investigate the global stability problem associated with decentralized filters. 83/00/00 85A32274

UTTL: Development and evaluation of a generic active helicopter vibration controller

AUTH: A/DAVIS, M. W. PAA: A/(United Technologies Research Center, East Hartford, CT) CORP: United Technologies Research Center, East Hartford, CT. IN: American Helicopter Society, Annual Forum, 40th, Arlington, VA, May 16-18, 1984. Proceedings (A85-31951 14-01). Alexandria, VA, American Helicopter Society, 1984 p. 581-595.

ABS: A computerized generic active vibration controller is developed, which alleviates helicopter vibration by closed-loop implementation of higher harmonic control (HHC). In the system, the higher harmonic blade pitch is input through a standard helicopter washplate; for a four-blade helicopter rotor the 4/rev vibration in the rotorcraft is minimized by inducing cyclic pitch motions at 3, 4, and 5/rev in the rotating system. The controller employs the deterministic, cautious, and dual control approaches and two linear system models (local and global), as well as several methods of limiting control. Based on model testing, performed at moderate to high values of forward velocity and rotor thrust, reductions in the rotor test apparatus vibration from 75 to 95 percent are predicted, with HHC pitch amplitudes of less than one degree. Good performance is also noted for short-duration maneuvers. 84/00/00 85A32004

UTTL: Dual control guidance for simultaneous identification and interception

AUTH: A/BERNIMAN, K. PAA: B/(Connecticut, University, Storrs, CT) AUTOMATICA (ISSN 0005-1098), vol. 20, Nov. 1984, p. 737-749.

ABS: An adaptive dual-control guidance algorithm is presented for intercepting a moving target in the presence of an interfering target (decoy) in a stochastic environment. Two sequences of measurements are obtained at discrete points in time; however, it is not certain which sequence came from the target of interest and which from the decoy. Associated with each track, the interceptor also receives noisy, state-dependent feature measurements. The optimum control for the interceptor which is given by the solution of the stochastic dynamic programming equation is not numerically feasible to obtain. An approximate solution of this equation is obtained by evaluating the value of the

future information gathering. This is done through the use of preposterior analysis - approximate prior probability densities are obtained and used to describe the future learning and control. In this way, the interceptor control is used for information gathering in order to reduce the future target and decoy inertial measurement errors and enhance the observable target/decoy feature differences for subsequent discrimination between the true target and the decoy. Simulation studies have shown the effectiveness of the scheme.

RPT#: AD-A154607 AFOSR-TR-85-0439 84/11/00 85A27510

UTTL: Information approach to fixed-gain design

AUTH: A/BARAM, Y. PAA: A/(Technion - Israel Institute of Technology, Haifa, Israel); B/(Israel Ministry of Defence, Tel Aviv, Israel) IEEE Transactions on Aerospace and Electronic Systems (ISSN 0018-9251), vol. AES-21, Jan. 1985, p. 47-55.

ABS: A method for designing fixed-gain controllers and filters for systems with large parameter variation is presented. The approach is based on finding the minimax point of the Kullback information measure between the fixed-gain system and the optimal system at a given operating point. The effectiveness of the proposed approach is illustrated by designing a fixed-gain system for the short-period control of a high-performance aircraft and evaluating its performance over the flight envelope. 85/01/00 85A26608

UTTL: Suboptimal filtering for aided GPS navigation

AUTH: A/WEISSMAN, D. C.; B/BOCHEM, J. H.; C/CALDWELL, D. G.; D/HIGGINS, W. T., JR. PAA: C/(Sperry Corp., Sperry Flight Systems, Phoenix, AZ); D/(Arizona State University, Tempe, AZ) IN: Institute of Navigation, Annual Meeting, 40th, Cambridge, MA, June 25-28, 1984 (A85-14826 04-04). Washington, DC, Institute of Navigation, 1984, p. 73-81.

ABS: A navigational algorithm which includes features of both an empirical complementary filter and an optimal Kalman filter is defined for implementation in a GPS receiver. The Kalman filter formalism is modified to eliminate cross-coupling terms and a prefilter which assumes velocity gains is defined. The prefilter is superposed on the suboptimal filter and the system is expanded to solve for errors. The system performance was tested with a simulation of an aircraft on a round the world racetrack and by mounting receiver equipment in a mobile van. Satisfactory results were obtained in 1/30th of the computational time required by an optimized Kalman filter. 84/00/00 85A14832

UTTL: Hypervelocity orbital intercept guidance

AUTH: A/ALFANO, SALVATORE CORP: Air Force Inst. of Tech.,

Wright-Patterson AFB, OH.

ABS:

Terminal guidance of a hypervelocity exo-atmospheric orbital interceptor with free end-time is examined. The pursuer is constrained to lateral thrusting with the evader modeled as an ICBM in its final boost phase. Proportional navigation, optimal control using certainty equivalence, dual control, and control with optimum thrust spacing are all examined. Also, a new approach called certainty control is developed for this problem. This algorithm constrains the final state to a function of projected estimate error to reduce control energy expenditure. All methods model the trajectories using splines and employ eight state Extended Kalman Filters with line-of-sight and range updates. The relative effectiveness of these control strategies is illustrated by applying them to various intercept problems.

RPT#: AD-A197149 AFIT/CI/NR-88-165 88/04/14 89N13456

UTTL: Numerical methods for the guidance and control of air-to-air missiles

AUTH: A/SHIEH, ALIN CORP: California Univ., Los Angeles.

ABS: An indirect numerical solution method for the guidance and control problem of general air-to-air missiles is presented. The system model is formulated as a nonlinear two-person zero-sum differential game. The system equations of motion consist of eight relative kinematic variables to describe the dynamics of the pursuing missile and its evading target both maneuvering freely in a real three-dimensional space. Control functions are subjected to state dependent constraints. The information structure is nonlinear and allows different types of noise. The quadratic payoff functional is to be minimized by the missile and maximized by its target. The original problem is decomposed into three smaller solvable problems: the open-loop perfect information differential game problem; the real-time state estimation problem, and the near-closed-loop updating problem. Jacobson and Mayne's second order Differential Dynamic Programming method is extended to the differential games problems with state dependent control constraints. The real-time nonlinear state estimator algorithm is similar to the Extended Kalman Filter. It minimizes the variance of the error propagation matrix and uses the most recent measurement data only to compute the filter updates. Numerical simulations are performed for several types of target interception problems. Many optimal pursuit and evasion tactics are found. The solution method shows very promising future toward the realization of differential game methodology for missile guidance problems. 87/00/00 89N12561

UTTL: Kalman filter-based algorithms for estimating depth from image sequences

AUTH: A/MATTHIES, LARRY; B/SZELISKI, RICHARD; C/KANADE, TAKEO

CORP: Carnegie-Mellon Univ., Pittsburgh, PA. CSS: (Robotics Inst.)

ABS:

Sequences is important in robotics applications such as navigation and manipulation. For many applications, having an on-line, incremental estimate of depth is important. To permit the blending of new measurements with old estimates, it is essential that the representation include not only the current depth estimate, but also an estimate of the current uncertainty. Kalman filtering provides the needed framework to integrate new measurements and reduce the uncertainty over time. Previous applications of Kalman filtering to depth from motion have been limited to the estimation of depth at the location of a sparse set of features. In this paper, we introduce a new pixel-based (iconic) algorithm that estimates depth from an image sequence and incrementally refines its estimate over time. We also present a feature-based version of the algorithm which is used for comparison. We compare the performance of both approaches mathematically, with quantitative experiments using images of a flat scene, and with qualitative experiments using images of a realistic outdoor scene model. The results show that the method is an effective way to extract depth from lateral camera translations.

RPT#: AD-A195818 CMU-RI-TR-88-1 88/01/00 88N30380

UTTL: A positioning system based on NAVSAT
AUTH: A/DEREUS, N. M.; B/WOEK, G.; C/OLSDER, G. J. PAA:
C/(Technische Hogeschool, Delft, Netherlands) CORP: (National Aerospace Lab., Amsterdam (Netherlands)). CSS: (Informatics Div.) Submitted for publication

ABS: The user position estimator of the NAVSAT system is described. Motion of the users is modelled by splines. The estimation procedure is based on the extended Kalman filter approach. The estimator was included in a NAVSAT system simulator. Various designs with respect to number of satellites, accuracy of the clocks, magnitude of modelling errors, and order of the spline approximation used, can be evaluated using this simulator. Results of two runs with the filter are presented. Based on second order spline approximations of the user trajectory, absolute position accuracies of a few meters are obtained. Using third order splines does not give better results; this may depend on the particular user trajectories simulated and on the fact that noise on these trajectories only influences the acceleration directly (and not the velocity or third derivatives of the position). The estimation of Regional Center clock biases works reasonably well.

RPT#: NLR-WP-87018-U B8803893 ETN-88-92610 PB88-209143
AD-81f9166L 87/02/24 88N23358

UTTL: A design study of onboard navigation and guidance

during aerocapture at Mars
AUTH: A/FURRY, DOUGLAS PAUL CORP: Draper (Charles Stark) Lab.,
Inc., Cambridge, MA.

ABS: The navigation and guidance of a high lift-to-drag ratio sample return vehicle during aerocapture at Mars are investigated. Emphasis is placed on integrated systems design, with guidance algorithms synthesis and analysis based on vehicle state and atmospheric density uncertainty estimates provided by the navigation system. The latter utilizes a Kalman filter for state vector estimation, with useful update information obtained through radar altimeter measurements and density altitude measurements based on IMU-measured drag acceleration. A three-phase guidance algorithm, featuring constant bank numeric predictor/corrector atmospheric capture and exit phases and an extended constant altitude cruise phase, is developed to provide controlled capture and depletion of orbital energy, orbital plane control, and exit apopsis control. Integrated navigation and guidance systems performance are analyzed using a four degree-of-freedom computer simulation. The simulation environment includes an atmospheric density model with spatially correlated perturbations to provide realistic variations over the vehicle trajectory. Navigation filter initial conditions for the analysis are based on planetary approach optical navigation results. Results from a selection of test cases are presented to give insight into systems performance.
RPT#: NASA-CR-172053 NAS 1.26:172053 CSDL-T-986 88/05/00
88N24654

UTTL: New stable, vectorisable Kalman filter algorithms based on orthogonal transformations

AUTH: A/HOTOP, HANS-JUERGEN CORP: Deutsche Forschungs- und Versuchsanstalt fuer Luft- und Raumfahrt, Brunswick (Germany, F.R.). CSS: (Abteilung Traegheitsortung und Navigation.)

ABS: A stable Kalman filter algorithm based on a Givens transformation is developed theoretically together with three separate update formulations. The backward filter of Rauch-Tung-Striebel is reformulated. As an alternative orthogonal transformation the singular value decomposition is investigated. The advantage of the Kalman filter algorithm vs. conventional formulations is examined for the support of inertial navigation systems (simulation and flight data) on serial computers and a vector processor.
RPT#: DFVLR-FB-87-52 ISSN-0171-1342 ETN-88-92324 AD-B121336L
87/12/00 88N23494

UTTL: Advanced guidance algorithms for homing missiles with bearings-only measurements

AUTH: A/SPEYER, JASON L.; B/HILL, DAVID G CORP: Texas Univ., Austin. CSS: (Dept. of Aerospace Engineering and Engineering Mechanics.)
ABS: Homing missile guidance is formulated as an optimal

stochastic control problem where the special nonlinear structure of the missile-target engagement is exploited. Since this stochastic control problem assumes a nested information pattern, the filter structure can be developed independently of the guidance scheme. However, the guidance scheme is dependent on and affects filter performance. Significant progress is being made on both the estimation problem and the guidance problem. The investigation of the nonlinear estimators especially tailored to the homing missile problem has produced not only a good deal of insight but responsive and mechanizable schemes. Although these schemes are applicable to active sensors, our emphasis has been on the more difficult passive sensor case where only angles are available. Recently-developed schemes based on coordinate transformations and on a assumed probability density function perform well, but the modified-gain extended Kalman filter has been used as the basis of a stochastic adaptive flight control scheme. Two important current efforts in missile guidance with bearings-only information are in development of the guidance schemes that enhance an information measure by trajectory modulation and in target acceleration detection.

RPT#: AD-A190435 AFOSR-87-1962TR 87/11/00 88N22026

UTTL: Simultaneous estimation and detection of bias shifts for inertial navigation systems

AUTH: A/SPENCER, RICHARD V.; B/CLEMENTS, KEVIN PAA: B/(Worcester Polytechnic Inst., Mass.) CORP: General Electric Co., Pittsfield, MA. In Test Group (6585th), 13th Biennial Guidance Test Symposium, Volume 1 10 p (SEE N88-19427 12-04)

ABS: The problem of detecting and estimating the magnitude of shifts in otherwise constant parameters is considered. An algorithm is presented in which multiple shifts can be detected and estimated within the framework of a multiply partitioned estimation algorithm, thus alleviating the computational burden of a bank of Kalman filters. The performance of the algorithm is demonstrated by simulation of a rocket sled test of an inertial guidance system.
87/10/15 88N19429

UTTL: GPS vertical axis performance enhancement for helicopter precision landing approach

AUTH: A/DENARD, ROBERT P.; B/BESER, JACQUES CORP: Theory and Applications Unlimited Corp., Los Gatos, CA.

ABS: Several areas were investigated for improving vertical accuracy for a rotorcraft using the differential Global Positioning System (GPS) during a landing approach. Continuous deltaranging was studied and the potential improvement achieved by estimating acceleration was studied by comparing the performance on a constant acceleration turn and a rough landing profile of several filters: a position-velocity (PV) filter, a

position-velocity-constant acceleration (PVAC) filter, and a position-velocity-turning acceleration (PVAT) filter. In overall statistics, the PVAC filter was found to be most efficient with the more complex PVAT performing equally well. Vertical performance was not significantly different among the filters. Satellite selection algorithms based on vertical errors only (vertical dilution of precision or VDOP) and even-weighted cross-track and vertical errors (XVDOP) were tested. The inclusion of an altimeter was studied by modifying the PVAC filter to include a baro bias estimate. Improved vertical accuracy during degraded DOP conditions resulted. Flight test results for raw differential results excluding filter effects indicated that the differential performance significantly improved overall navigation accuracy. A landing glidepath steering algorithm was devised which exploits the flexibility of GPS in determining precise relative position. A method for propagating the steering command over the GPS update interval was implemented.

RPT# : NASA-CR-177443 NAS 1.26:177443 86/09/00 88N12477

UTTL: Configuration design of a helicopter integrated navigation system

AUTH: A/FINGEROTE, S. I.; B/REID, D. B.; C/LIANG, D. F.; D/VALLOT, L.; E/GREENE, C.; F/MAHESH, J. PAA:

F/Honeywell Systems and Research Center, Minneapolis, Minn.) CORP: Honeywell Advanced Technology Centre, North York (Ontario). In AGARD, Advances in Guidance and Control Systems and Technology 9 p (SEE N87-29474 24-04) Results are presented from the configuration performance study phase of the Helicopter Integrated Navigation System project. A configuration assessment is presented including processor selection, and a discussion of system architecture and configuration tradeoffs leading to a recommended configuration. Results of the system error analysis and the Kalman filter design are presented demonstrating integrated system performance. 87/07/00 87N29480

UTTL: Simulation of strapdown systems for error analysis, and modeling for navigation with other sensor systems

AUTH: A/STIELER, BERNHARD CORP: Deutsche Forschungs- und Versuchsanstalt fuer Luft- und Raumfahrt, Brunswick (Germany, F.R.). In its Modeling of Systems for Aircraft Guidance and Air Traffic Control for Research, Development, and Evaluation p 81-104 (SEE N87-28530 23-04)

ABS: The simulation of strapdown systems for the investigation of systems errors in conventional and novel systems concepts, and for the support of the integration of novel systems, was examined. The covariance and Monte Carlo simulation for the determination of the error behavior of strapdown systems are presented. It is shown that the required navigation accuracy in conventional systems can only be obtained with laser gyroscope strapdown systems.

Error modeling of a laser gyroscope strapdown system for application in a Kalman filter is explained. The navigation accuracy does not only depend on the sensor accuracy, but also on the system configuration. Strapdown system configurations which allow a better accuracy and a broader application domain are presented. 86/11/00 87N28535

UTTL: Modeling of the fault situation in navigation systems

AUTH: A/HURRASS, KARLHEINZ CORP: Deutsche Forschungs- und Versuchsanstalt fuer Luft- und Raumfahrt, Brunswick (Germany, F.R.). In its Modeling of Systems for Aircraft Guidance and Air Traffic Control for Research, Development, and Evaluation p 67-80 (SEE N87-28530 23-04) Functional models for the description of the fault behavior of navigation systems are treated. Radio navigation systems and airborne autonomous systems (Doppler navigation, air data navigation, and inertial navigation) are considered. Examples show that the description of the fault behavior in the form of functional models is required for integrated navigation systems, simulations, and routing design. 86/11/00 87N28534

AUTH: A/LLORET, P.; B/CAPIT, B. CORP: Societe d'Applications Generates d'Electricite et de Mecanique, Paris (France). In AGARD, Aeronautique. In AGARD Efficient Conduct of Individual Flights and Air Traffic or Optimum Utilization of Modern Technology for the Overall Benefit of Civil and Military Airspace Users 23 p (SEE N87-21881 15-04)

ABS: The coupling of inertial navigation methods with the Global Positioning System (GPS) is examined. The characteristics of various types of inertial systems are reviewed and past attempts at inertial/radiationavigation hybridizations including those with multi- and VDR-DME (VHF omnidirectional range - distance measuring equipment), Transit, OMEGA, ILS (instrument landing systems), and altitude correlation are discussed. The possible configurations for an inertial/GPS systems, given the type (classical platform and strap-down) and classes of inertial designs and the number of GPS channels utilized, are defined and performance characteristics are outlined for each. Simulation and in-flight studies of prototype systems are discussed. Signal properties and Kalman filtering are addressed. Finally, perspectives on the continuing development of inertial/GPS hybrid systems are offered. 86/12/00 87N21885

UTTL: Design document for differential GPS (Global Positioning System) ground reference station pseudorange correction generation algorithm CORP: Air Force Wright

ABS: Aeronautical Labs., Wright-Patterson AFB, OH.
The algorithms described in this report determine the differential corrections to be broadcast to users of the Global Positioning System (GPS) who require higher accuracy navigation or position information than the 30 to 100 meters that GPS normally provides. Properly equipped marine users receiving the broadcasted corrections are expected to achieve better than 10 meters accuracy with the Differential GPS system. The Differential GPS program involves the fabrication of a differential GPS testbed, consisting of an 8-channel GPS receiver for the reference station, data processing hardware and software to generate the corrections and perform channel management and integrity functions, user receiver, and data acquisition hardware and software. The system will be tested in 1987.
RPT#: AD-A177190 DOT-CG-N-03-86 DOT-TSC-CG-86-2 86/12/00 87N21880

UTTL: Study on NAVSAT system simulation
AUTH: A/DEPAGTER, P. J.; B/KLAASE, A. A. C. CORP: National Aerospace Lab., Amsterdam (Netherlands). CSS: (Informatics Div.)

ABS: A software package to perform digital simulations of the satellite-based navigation system NAVSAT was developed. The package can simulate not only NAVSAT concepts, but also totally different navigation system concepts. Software development control methods are summarized.

RPT#: NLR-MP-85051-J ETN-87-99289 AD-B104489L 85/03/08 87N19374

UTTL: Advanced guidance algorithms for homing missiles with bearing-only measurements

AUTH: A/SPEYER, J. L.; B/HULL, D. G. CORP: Texas Univ., Austin. CSS: (Dept. of Aerospace Engineering and Engrg. Mech.)

ABS: The research of this grant is directed toward the development of an advanced guidance system (navigation filter and guidance law) for a short-range air-to-air missile having a passive seeker (angle-only measurements). During this year, four subjects have been investigated. First, additional experience has been gained with the modified-gain extended Kalman filter; it is becoming apparent that it works the same as or better than the extended Kalman filter for the homing missile problem. Second, a new target-acceleration model has been developed to replace the first-order Gauss-Markov process normally used; this model allows target acceleration vector to rotate and keeps its magnitude within bounds. Third, because the homing missile problem with angle-only measurements is nonlinear, the guidance law affects the performance of the filter; a new guidance law based on maximizing a measure of the size of the information matrix has been developed and has been shown to improve filter performance. Fourth, a study of the use of new theory on

fault detection has been initiated; the intent is to use this theory to detect target maneuvers (the target maneuver appears as a fault) so that the filter can be restarted.

RPT#: AD-A170833 AFOSR-86-0595TR 86/05/20 87N12583

UTTL: Reliability issues in active control of large flexible space structures

AUTH: A/VANDERVELDE, W. E. CORP: Massachusetts Inst. of Tech., Cambridge. CSS: (Dept. of Aeronautics and Astronautics.)

ABS: Efforts in this reporting period were centered on four research tasks: design of failure detection filters for robust performance in the presence of modeling errors, design of generalized parity relations for robust performance in the presence of modeling errors, design of failure sensitive observers using the geometric system theory of Wonham, and computational techniques for evaluation of the performance of control systems with fault tolerance and redundancy management

RPT#: NASA-CR-179758 NAS 1.26:179758 86/02/04 86N32512

UTTL: Global Radio Navigation System (GRANAS) simulation
AUTH: A/EULER, H.; B/KOHLER, K.; C/PLUEGER, G.; D/TAENZER, K. CORP: Standard Elektrik Lorenz A.G., Stuttgart (Germany, F.R.). Sponsored by Bundesministerium fuer Forschung und Technologie

ABS: The accuracy of the satellite position, of the clock synchronization and of the user's position are calculated using statistical evaluation procedures to simulate GRANAS navigation principles and operation. The satellite position is determined by numerical tests and parameters derived from a Kalman filter. The satellite motion is simulated using physical boundary conditions. The quartz clock inaccuracy is assessed and included in the one-way remote measurement inaccuracy. A nonlinear Kalman filter is produced to determine the user's dynamic behavior. The simulation shows a position inaccuracy of Circular Error Probability (CEP) 14 m during a uniform motion and of CEP 30 m in the acceleration phase. The 3D errors amount to spherical error probability 17 m or 36 m. The method can be further optimized.

RPT#: BMFT-FB-W-85-028 ISSN-0170-1339 ETN-86-97470 85/12/00 86N32422

UTTL: Self-tuning control principles applied to bilinear systems

AUTH: A/BURNHAM, K. J.; B/JAMES, D. J. G.; C/SIELDS, D. N. CORP: Lanchester Polytechnic, Coventry (England). CSS: (Dept. of Systems and Control.)

ABS: A quasi-linear self-tuning control algorithm for a class of single input single output bilinear systems is derived. It involves an extended statespace pole-assignment approach which is applied to a linearized model of the

bilinear system, updated at each sample point. The extended approach uses an adaptive steady state Kalman filter for state estimation, and an adaptive least squares scheme, employing a variable forgetting factor, for parameter estimation.

RPT#: IR-SC-85-2 ETN-86-97261 85/00/00 86N32183

UTTL: Improvement of strapdown system performance by means of numerical methods

AUTH: A/SUITKAMP, H.; B/ENDERLEIN, K.; C/EVERETT, G.; D/KIRCHHOFF, U.; E/KLEINSCHMIDT, M.; F/OZDES, D.; G/STIER, P. CORP: Litton Technische Werke, Freiburg (Germany, F.R.). Sponsored by Bundesministerium fuer Forschung und Technologie

ABS: Software methods to improve the performance of strapdown systems, and the simulation tools used in the analysis of system mechanisms are presented. Models of the inertial and external sensors to compensate for systematic errors; correct timing of the data flow of the sensors; multiposition alignment to eliminate the day-to-day repeatability of gyro biases; design control loops with optimal/suboptimal filters for special tasks of a strapdown unit (e.g., helicopter mission, initial alignment) are described. Kalman filters are used to reduce the influence of stochastic errors and for cross calibration of the sensors.

RPT#: BWFT-FB-W-85-011 ISSN-0170-1339 LITEF-105-793 85/11/00 86N27275

UTTL: Two time scale output feedback regulation for ill-conditioned systems

AUTH: A/CALISE, A. J.; B/MOERDER, D. D. CORP: Drexel Univ., Philadelphia, PA. CSS: (Dept. of Mechanical Engineering and Mechanics.)

ABS: Issues pertaining to the well-posedness of a two time scale approach to the output feedback regulator design problem are examined. An approximate quadratic performance index which reflects a two time scale decomposition of the system dynamics is developed. It is shown that, under mild assumptions, minimization of this cost leads to feedback gains providing a second-order approximation of optimal full system performance. A simplified approach to two time scale feedback design is also developed, in which gains are separately calculated to stabilize the slow and fast subsystem models. By exploiting the notion of combined control and observation spillover suppression, conditions are derived assuring that these gains will stabilize the full-order system. A sequential numerical algorithm is described which obtains output feedback gains minimizing a broad class of performance indices, including the standard LQ case. It is shown that the algorithm converges to a local minimum under nonrestrictive assumptions. This procedure is adapted to and demonstrated for the two time scale design formulations.

RPT#: NASA-CR-3972 NAS 1.26:3972 86/05/00 86N26056

UTTL: Kalman filter design for the long range intercept function of the F-4E/G fire control system
A/HALBERT, R. C. CORP: Air Force Inst. of Tech., Wright-Patterson AFB, OH. CSS: (School of Engineering.)

ABS: This study examines reduced-order Kalman filters designed to improve performance of the F-4E/G long range air-to-air missile capability (LRI function). Operational requirements dictate a high degree of accuracy and constraints imposed by existing hardware mandate minimal complexity. Two linear dynamics models are proposed, one based on constant target velocity, and the other based on time-correlated target acceleration. Both are defined in inertial Cartesian coordinates aligned with north, east, and down. A nonlinear model is developed for measurements available in the existing F-4E/G hardware, including range, range rate, radar antenna gimbal angles, and radar antenna rates. The models are implemented in extended Kalman filter formulations employing linear propagation equations to avoid on-line numerical integration. Performance evaluations are performed on three test trajectories using Monte Carlo analysis. Filter tuning, error budgets, adaptive techniques, and observability issues are addressed during filter evaluation. Results of the evaluation indicate the filter designs can meet the requirements of the F-4E/G fire control system. Recommendations are made for continued testing and for operational implementation.

RPT#: AD-A164205 AFIT/GE/ENG/85D-20 85/12/00 86N24926

UTTL: Algorithms for the automatic four-dimensional guidance of aircraft, taking into account the current wind situation

AUTH: A/LECHNER, W. CORP: European Space Agency, Paris (France).

ABS: An automatic time-of-arrival control flight mode covering the terminal maneuvering area was developed for the digital flight-control system of the HFB 320 test aircraft and flight tested. The algorithms used for computing four dimensional flight paths taking into account the current wind situation are described. Methods for measuring, filtering, and predicting the wind vector are developed and discussed with reference to the results of the flight tests. Evaluation shows that time error limits of + or - 5 sec can be achieved under varied wind situations. The aircraft-oriented method of wind prediction by extrapolation, based on the Kalman filter method, proves to be particularly efficient.

RPT#: ESA-IT-908 DFVLR-FB-84-40 85/10/00 86N21531

UTTL: Recursive gradient estimation using splines for navigation of autonomous vehicles

AUTH: A/SHEN, C. N. CORP: Army Armament Research and Development Command, Watervliet, NY. CSS: (Large Caliber Weapon Systems Lab.)

ABS: Terrain gradient estimation is needed for navigation of an autonomous vehicle in climbing the hills. The in-path and cross-path terrain slopes are estimated from the set of corresponding range slopes. A two-dimensional recursive smoothing algorithm using polynomial splines in the third dimension is developed for this purpose. Approximations are introduced in the sub-optimal system so that the computation time increases only linearly with the size of the two-dimensional data.

RPT#: AD-A159883 AD-E440295 ARLCB-TR-85022 85/07/00 86N18768

UTTL: Adaptive filtering for large space structures: A closed-form solution

AUTH: A/RAUCH, H. E.; B/SCHAECHTER, D. B. CORP: Lockheed Missiles and Space Co., Palo Alto, CA. In JPL Proc. of the Workshop on Identification and Control of Flexible Space Struct., Vol. 3 p 161-173 (SEE N85-31195 20-18)

ABS: In a previous paper Schaechter proposes using an extended Kalman filter to estimate adaptively the (slowly varying) frequencies and damping ratios of a large space structure. The time varying gains for estimating the frequencies and damping ratios can be determined in closed form so it is not necessary to integrate the matrix Riccati equations. After certain approximations, the time varying adaptive gain can be written as the product of a constant matrix times a matrix derived from the components of the estimated state vector. This is an important savings of computer resources and allows the adaptive filter to be implemented with approximately the same effort as the nonadaptive filter. The success of this new approach for adaptive filtering was demonstrated using synthetic data from a two mode system. 85/04/01 85N31206

UTTL: The AFTI/F16 terrain-aided navigation system

AUTH: A/BOOZER, D. D.; B/LAU, M. K.; C/FELLERHOFF, J. R. CORP: Sandia National Labs., Albuquerque, NM.

ABS: A recursive, real time, terrain aided navigation algorithm, AFTI/SILAN, was designed for use on the Advanced Fighter Technology Integration (AFTI) F16 aircraft. The algorithm implemented in a Zilog Z8001 microprocessor, can reliably locate the aircraft's position within a 926-m (0.5 nm) CEP circle and accurately estimate its position continuously (3 Hz). The design and execution of the algorithm are described, and simulation results using actual flight test data are presented. A median accuracy of less than 100 m was achieved over gently rolling, forested terrain using cartographic-based digital terrain elevation data.

RPT#: DE85-008411 SAND-85-0223C CONF-8505116-1 85/00/00 85N28935

UTTL: Perturbations of Kalman filtering process

AUTH: A/CHEKMOV, A. A.; B/YASTREBOV, V. D. CORP: Joint Publications Research Service, Arlington, VA. In its USSR Rept.: Space (JPRS-USP-85-003) p 26 (SEE N85-25284 15-12)

ABS: Formulas are derived for calculating perturbations of the estimation of a state-vector estimate obtained on the basis of a Kalman discrete filtering algorithm. The following perturbation sources are considered: perturbations of the covariance matrix of measurement noise, the covariance matrix of filtering errors, the measurement matrix, and the transition matrix of the system; and perturbations of the state-vector estimate at the preceding step. The results obtained can be used to analyze the performance of spacecraft navigation systems. 85/03/04 85N25305

UTTL: Algorithms for automatic four-dimensional aircraft guidance, considering the momentary wind situation

AUTH: A/LECHNER, W. CORP: Deutsche Forschungs- und Versuchsanstalt fuer Luft- und Raumfahrt, Brunswick (Germany, F.R.). CSS: (Abteilung Steuerung und Regelung.)

ABS: An automatic four dimensional mode covering a terminal maneuvering area was developed and flight tested for the automatic digital flight control system of the HFB 320 test aircraft. Algorithms for the computation of the flight path take into account the current wind situation. Techniques for wind measurement, filtering and prediction were developed. The results of the flight trials are discussed. It is shown that temporal error limits of 5 sec are obtained under the most differing wind situations. The aircraft-oriented wind prediction extrapolation system based Kalman filtering techniques is very efficient.

RPT#: DFVLR-FB-84-40 ISSN-0171-1342 84/09/00 85N21146

UTTL: High accuracy Doppler navigation employing optimum integrated position fix information

AUTH: A/HUG, H. CORP: Standard Elektrik Lorenz A.G., Stuttgart (Germany, F.R.). In AGARD Helicopter Guidance and Control Systems for Battlefield Support 8 p (SEE N85-16797 08-01)

ABS: The basic accuracy limitations of today's Doppler navigation systems are mainly caused by sensor errors and calibration errors. The navigation error of a typical Doppler system equipped with a magnetic compass is therefore about 1% to 2% of the distance travelled. The presented approach for improved accuracy is based on the usually applied method of position fixing to reset the error at specific waypoints. The measured errors are used as an input to a Kalman Filter which estimates various error parameters and continuously compensates for the

actual navigation error. Details of the implemented Kalman Filter algorithm are given. Simulation results based on computer generated synthetic flight data and recorded real flight data are presented. 84/08/00 85N16803

UTTL: Application of modern guidance control theory to a bank-to-turn missile
AUTH: A/SHIN, B. CORP: Naval Postgraduate School, Monterey, CA.

ABS: Control laws of a bank-to-turn missile using an optimal estimator in terminal guidance were designed and the effect of increasing the number of measurement sensors in the missile to generate more information on the state was investigated. In design of the control law, modern optimal control theory with a quadratic performance index was used. Implementing this control law required use of a

Kalman filter as the optimal estimator. The extended Kalman filter algorithm was used since the measurement states were non-linear functions of the state vectors (relative distance, velocity and target acceleration). To test the effects of implementation of the increased measurement sensors, two-, four- and six-measurement sensors were assumed to be implemented in the optimal estimator. The designed guidance laws were evaluated and the effect of the implementation of increased measurement sensors was tested. Simulation results revealed that the designed guidance law was successful within the specified scenarios. The effect of implementation of increased measurement sensors generated more information about the state vectors, but as the Kalman filter algorithm became more complex, the estimator performance was not enhanced to the degree expected.

RPT#: AD-A145646 84/03/00 85N11123

REPORT DOCUMENTATION PAGE

1. Recipient's Reference	2. Originator's Reference	3. Further Reference	4. Security Classification of Document						
	AGARD-LS-166	ISBN 92-835-0514-X	UNCLASSIFIED						
5. Originator	Advisory Group for Aerospace Research and Development North Atlantic Treaty Organization 7 rue Ancelle, 92200 Neuilly sur Seine, France								
6. Title	KALMAN FILTER INTEGRATION OF MODERN GUIDANCE AND NAVIGATION SYSTEMS								
7. Presented on	26—27 June 1989 in Delft, The Netherlands, on 29—30 June 1989 in Neubiberg (near Munich), Germany and on 3-4 July 1989 in London, United Kingdom								
8. Author(s)/Editor(s)	Various		9. Date June 1989						
10. Author's/Editor's Address	Various		11. Pages 184						
12. Distribution Statement	This document is distributed in accordance with AGARD policies and regulations, which are outlined on the Outside Back Covers of all AGARD publications.								
13. Keywords/Descriptors									
<table border="0"> <tr> <td>Navigational computers</td> <td>Tracking (position)</td> </tr> <tr> <td>Guidance computers</td> <td>Avionics systems engineering</td> </tr> <tr> <td>Control equipment</td> <td></td> </tr> </table>				Navigational computers	Tracking (position)	Guidance computers	Avionics systems engineering	Control equipment	
Navigational computers	Tracking (position)								
Guidance computers	Avionics systems engineering								
Control equipment									
14. Abstract									
<p>The integration of modern guidance and navigation systems is usually performed with a sub-optimal implementation of the Kalman filter. The most difficult problem is how to develop that sub-optimal implementation when considering system modelling, algorithm design and real hardware non-linearities. This lecture series brings together a group of speakers with outstanding practical experience in the design of integrated systems, providing the audience with the principles, insights and mechanisms of real, current-day system synthesis approaches and giving the overall background necessary for synthesizing future practical guidance and navigation systems. Two of the lectures deal with the synthesis of solutions to tracking problems. The remainder of the lectures deal with the integration of avionics systems.</p> <p>This Lecture Series, sponsored by the Guidance and Control Panel of AGARD, has been implemented by the Consultant and Exchange Programme.</p>									

<p>AGARD Lecture Series No.166 Advisory Group for Aerospace Research and Development, NATO KALMAN FILTER INTEGRATION OF MODERN GUIDANCE AND NAVIGATIONAL SYSTEMS Published June 1989 184 pages</p> <p>The integration of modern guidance and navigation systems is usually performed with a sub-optimal implementation of the Kalman filter. The most difficult problem is how to develop that sub-optimal implementation when considering system modelling, algorithm design and real hardware non-linearities. This lecture series brings together a group of speakers with outstanding practical experience in the design of</p> <p>P.T.O</p>	<p>AGARD-LS-166</p> <p>Navigation computers Guidance computers Control equipment Tracking (position) Avionics systems engineering</p>	<p>AGARD Lecture Series No.166 Advisory Group for Aerospace Research and Development, NATO KALMAN FILTER INTEGRATION OF MODERN GUIDANCE AND NAVIGATIONAL SYSTEMS Published June 1989 184 pages</p> <p>The integration of modern guidance and navigation systems is usually performed with a sub-optimal implementation of the Kalman filter. The most difficult problem is how to develop that sub-optimal implementation when considering system modelling, algorithm design and real hardware non-linearities. This lecture series brings together a group of speakers with outstanding practical experience in the design of</p> <p>P.T.O</p>	<p>AGARD-LS-166</p> <p>Navigation computers Guidance computers Control equipment Tracking (position) Avionics systems engineering</p>
<p>AGARD Lecture Series No.166 Advisory Group for Aerospace Research and Development, NATO KALMAN FILTER INTEGRATION OF MODERN GUIDANCE AND NAVIGATIONAL SYSTEMS Published June 1989 184 pages</p> <p>The integration of modern guidance and navigation systems is usually performed with a sub-optimal implementation of the Kalman filter. The most difficult problem is how to develop that sub-optimal implementation when considering system modelling, algorithm design and real hardware non-linearities. This lecture series brings together a group of speakers with outstanding practical experience in the design of</p> <p>P.T.O</p>	<p>AGARD-LS-166</p> <p>Navigation computers Guidance computers Control equipment Tracking (position) Avionics systems engineering</p>	<p>AGARD Lecture Series No.166 Advisory Group for Aerospace Research and Development, NATO KALMAN FILTER INTEGRATION OF MODERN GUIDANCE AND NAVIGATIONAL SYSTEMS Published June 1989 184 pages</p> <p>The integration of modern guidance and navigation systems is usually performed with a sub-optimal implementation of the Kalman filter. The most difficult problem is how to develop that sub-optimal implementation when considering system modelling, algorithm design and real hardware non-linearities. This lecture series brings together a group of speakers with outstanding practical experience in the design of</p> <p>P.T.O</p>	<p>AGARD-LS-166</p> <p>Navigation computers Guidance computers Control equipment Tracking (position) Avionics systems engineering</p>

<p>integrated systems, providing the audience with the principles, insights and mechanisms of real, current-day system synthesis approaches and giving the overall background necessary for synthesizing future practical guidance and navigation systems. Two of the lectures deal with the synthesis of solutions to tracking problems. The remainder of the lectures deal with the integration of avionics systems.</p> <p>This Lecture Series, sponsored by the Guidance and Control Panel of AGARD, has been implemented by the Consultant and Exchange Programme.</p>	<p>integrated systems, providing the audience with the principles, insights and mechanisms of real, current-day system synthesis approaches and giving the overall background necessary for synthesizing future practical guidance and navigation systems. Two of the lectures deal with the synthesis of solutions to tracking problems. The remainder of the lectures deal with the integration of avionics systems.</p> <p>This Lecture Series, sponsored by the Guidance and Control Panel of AGARD, has been implemented by the Consultant and Exchange Programme.</p>
<p>ISBN 92-835-0514-X</p> <p>integrated systems, providing the audience with the principles, insights and mechanisms of real, current-day system synthesis approaches and giving the overall background necessary for synthesizing future practical guidance and navigation systems. Two of the lectures deal with the synthesis of solutions to tracking problems. The remainder of the lectures deal with the integration of avionics systems.</p> <p>This Lecture Series, sponsored by the Guidance and Control Panel of AGARD, has been implemented by the Consultant and Exchange Programme.</p>	<p>ISBN 92-835-0514-X</p> <p>integrated systems, providing the audience with the principles, insights and mechanisms of real, current-day system synthesis approaches and giving the overall background necessary for synthesizing future practical guidance and navigation systems. Two of the lectures deal with the synthesis of solutions to tracking problems. The remainder of the lectures deal with the integration of avionics systems.</p> <p>This Lecture Series, sponsored by the Guidance and Control Panel of AGARD, has been implemented by the Consultant and Exchange Programme.</p>
<p>ISBN 92-835-0514-X</p>	<p>ISBN 92-835-0514-X</p>

AGARD

NATO  OTAN

7 rue Ancelle - 92200 NEUILLY-SUR-SEINE
FRANCE

Telephone (1)47.38.57.00 - Telex 810 178

**DISTRIBUTION OF UNCLASSIFIED
AGARD PUBLICATIONS**

AGARD does NOT hold stocks of AGARD publications at the above address for general distribution. Initial distribution of AGARD publications is made to AGARD Member Nations through the following National Distribution Centres. Further copies are sometimes available from these Centres, but if not may be purchased in Microfiche or Photocopy form from the Purchase Agencies listed below.

NATIONAL DISTRIBUTION CENTRES

BELGIUM

Coordonnateur AGARD - VSL
Etat-Major de la Force Aérienne
Quartier Reine Elisabeth
Rue d'Evere, 1140 Bruxelles

CANADA

Director Scientific Information Services
Dept of National Defence
Ottawa, Ontario K1A 0K2

DENMARK

Danish
Ved Id
2100 C

FRANCE

O.N.E.
29 Av
92320

GERMANY

Fachr
Physik
Karlar
D-751

GREECE

Hellei
Aircr
Depa
Holai

ICELAND

Direc
c/o Flugrau
Reykjavik

ITALY

Aeronautica Militare
Ufficio del Delegato Nazionale all'AGARD
3 Piazzale Adenauer
00144 Roma/EUR

LUXEMBOURG

See Belgium

NETHERLANDS

Netherlands Delegation to AGARD
National Aerospace Laboratory, NLR
P.O. Box 126
2600 AC Delft

NORWAY

Norwegian Defence Research Establishment
Attn: Biblioteket



National Aeronautics and
Space Administration

Washington, D.C.
20546

**SPECIAL FOURTH CLASS MAIL
BOOK**

Postage and Fees Paid
National Aeronautics and
Space Administration
NASA-461

Official Business
Penalty for Private Use \$300



AGARD

LS 001 AGARDLS166890725S002672D
DEPT OF DEFENSE
DEFENSE TECHNICAL INFORMATION CENTER
DTIC-FDAC
CAMERON STATION BLDG 5
ALEXANDRIA VA 223046145

UNITED STATES

National Aeronautics and Space Administration (NASA)
Langley Research Center
M/S 180
Hampton, Virginia 23665

**THE UNITED STATES NATIONAL DISTRIBUTION CENTRE (NASA) DOES NOT HOLD
STOCKS OF AGARD PUBLICATIONS. AND APPLICATIONS FOR COPIES SHOULD BE MADE
DIRECT TO THE NATIONAL TECHNICAL INFORMATION SERVICE (NTIS) AT THE ADDRESS BELOW.**

PURCHASE AGENCIES

National Technical
Information Service (NTIS)
5285 Port Royal Road
Springfield
Virginia 22161, USA

ESA/Information Retrieval Service
European Space Agency
10, rue Mario Nikis
75015 Paris, France

The British Library
Document Supply Centre
Boston Spa, Wetherby
West Yorkshire LS23 7BQ
England

Requests for microfiche or photocopies of AGARD documents should include the AGARD serial number, title, author or editor, and publication data. Requests to NTIS should include the NASA accession report number. Full bibliographical references and abstracts of AGARD publications are given in the following journals:

Scientific and Technical Aerospace Reports (STAR)
published by NASA Scientific and Technical
Information Branch
NASA Headquarters (NIT-40)
Washington D.C. 20546, USA

Government Reports Announcements (GRA)
published by the National Technical
Information Services, Springfield
Virginia 22161, USA



Printed by Specialised Printing Services Limited
40 Chigwell Lane, Loughton, Essex IG10 3TZ